Upstream process development for cultured red blood cell production

Gallego Murillo, Joan Sebastián

DOI
10.4233/uuid:b4091579-66ea-4401-9277-dffe5a83ab90

Publication date
2023

Document Version
Final published version

Citation (APA)
Gallego Murillo, J. S. (2023). *Upstream process development for cultured red blood cell production*. [Dissertation (TU Delft), Delft University of Technology]. https://doi.org/10.4233/uuid:b4091579-66ea-4401-9277-dffe5a83ab90

UPSTREAM PROCESS DEVELOPMENT FOR CULTURED RED BLOOD CELL PRODUCTION

Joan Sebastián Gallego Murillo

Upstream process development for cultured red blood cell production

Upstream process development for cultured red blood cell production

Dissertation

For the purpose of obtaining the degree of doctor
at Delft University of Technology,
by the authority of the Rector Magnificus prof. dr. ir. T.H.J.J. van der Hagen,
chair of the Board for Doctorates,
to be defended publicly on
Friday 10 November 2023 at 10:00 o'clock

by

Joan Sebastián GALLEGO MURILLO

Master of Science in Life Science & Technology
Delft University of Technology, the Netherlands,

Born in Bogotá, Colombia

This dissertation has been approved by the promotors:

promotor: Prof. dr. ir. L.A.M. van der Wielen
promotor: Prof. dr. S.A. Wahl
promotor: Dr. M.M. von Lindern

Composition of the doctoral committee:

Rector Magnificus	chairperson
Prof. dr. ir. L.A.M. van der Wielen	Delft University of Technology, promotor
Prof. dr. S.A. Wahl	FAU Erlangen-Nürnberg, Germany former Delft University of Technology, promotor
Dr. M.M. von Lindern	Sanquin Research, promotor

Independent members:

Prof. dr. ir. M. Ottens	Delft University of Technology
Prof. dr. J.M.S. Cabral	Instituto Superior Tecnico, University of Lisbon, Portugal
Prof. dr. A.M. Toye	University of Bristol, United Kingdom
Dr. ir. A.J.J. Straathof	Delft University of Technology

Reserve member:

Prof. dr. J.T. Pronk	Delft University of Technology

This work was supported by the ZonMW TAS program (project 116003004), by the Landsteiner Foundation for Bloodtransfusion Research (LSBR project 1239), and by Sanquin Blood Supply grants PPOC17-28 and PPOC119-14.

Keywords:	erythroblast; cultured red blood cells; deferiprone; bioreactor; *ex vivo* erythropoiesis, metabolomics.
Printed by:	Proefschriftspecialist
Copy editing by:	Daniela Carolina García Rojas
Editorial design by:	Daniela Carolina García Rojas
Cover illustration by:	Francisco Viveros Góngora (@vigosketchbook)

Typeset in Libertinus, Nunito, and London Underground Dot Matrix.

ISBN/EAN: 978-94-6384-490-1

Printing of this thesis was financially supported by Sanquin Research.
An electronic version of this dissertation is available at https://repository.tudelft.nl/

"Un deseo por la quietud
es también
el proyecto de un resguardo
frente al movimiento
de eso
que creo que es la vida,
y que sacude y agrieta."

Gloria Susana Esquivel

UPSTREAM PROCESS DEVELOPMENT FOR CULTURED RED BLOOD CELL PRODUCTION

Joan Sebastián Gallego Murillo

Contents

Summary

Production of cultured red blood cells (cRBCs) hold the promise of being a potentially unlimited source of cells that could cover the increasing demand of RBCs for transfusion purposes, while having more control on the quality and safety of the cells compared to the current donor-dependent system. cRBCs could also be used for novel therapies in which cells are used as carriers of therapeutic molecules. Scaling up cRBC manufacture is essential to produce the large number of cells needed for such applications. However, scaling up the current static culture systems for the production of erythroblasts (RBC precursor cells) would be prohibitively labor-intensive, requiring large volumes of medium and a high footprint. The work presented in this thesis aims to develop solutions to some of the key challenges in the scaling up of cRBC manufacture.

Stirred tank bioreactors (STRs) are the standard for the large-scale production of biopharma therapeutics, including monoclonal antibodies and vaccines. Agitation in this type of reactors can reduce the concentration gradients of essential nutrients compared to static culture systems such as culture dishes. STRs also offer active control of critical operating parameters in the culture, such as dissolved oxygen concentration, pH and temperature. We therefore developed a culture protocol for the proliferation and differentiation of erythroblasts in STRs (**Chapter 2**). To define the operating conditions that sustain erythroblast proliferation in STRs, the effect of agitation, aeration strategy, and dissolved oxygen concentration was evaluated using 0.5 L STRs. Using this knowledge, the cultivation process could then be scaled up to 3 L bioreactors.

Erythroblasts lose their replication capacity when transitioning from proliferation to differentiation culture conditions. Thus, efficient proliferation of erythroblasts is essential to produce the large number of cells required for cRBC manufacture. Growing erythroblasts under proliferative conditions is typically performed following a repeated-batch cultivation strategy, in which the culture is diluted every 24 hours with fresh medium to a fixed lower cell concentration. To reduce culture volumes, it is desirable to use higher cell concentrations. However, at increasing cell densities we observe a decrease in growth (**Chapter 3**). The observed growth limitations of erythroblast cultures at high cell densities appeared to be caused by depletion of low molecular weight nutrients (molecular mass <3 kDa) in the spent medium. We quantified consumption rates of amino acids, major contributors to biomass synthesis in proliferating mammalian cell cultures. Although the concentration of some amino

acids decreases considerably over time, supplementation with additional amino acids did not improve growth. Following an untargeted metabolomics approach, we identified multiple pathways that indicate an excess of oxidative stress in erythroblast proliferation cultures.

Perfusion proved to be a successful alternative cultivation strategy to overcome growth limitations due to depletion of nutrient components (Chapter 3). Increasing the maximum cell concentration in erythroblast cultures leads to an increase in the volumetric productivity (number of cells produced per reactor volume per culture time), which decreases the reactor volume needed to produce the same amount of cRBCs. However, large volumes of medium would still be required to sustain those cultures. Currently, the cost of culture medium for erythroid cultures makes cRBC manufacture economically unfeasible. Growth factors and proteins added to the medium are major contributors to the cost of the medium. Holotransferrin, an iron-carrying protein, is the main cost driver in erythroblast differentiation medium. We show that holotransferrin in erythroblast cultures can be replaced by a GMP-compatible iron chelator (deferiprone; Def), bound to ferric ion ($Def_3 \cdot Fe^{3+}$; **Chapter 4**). Addition of $Def_3 \cdot Fe^{3+}$ to the culture medium resulted in similar final cRBC yields of cRBCs during proliferation and differentiation of erythroblast cultures compared to optimal holotransferrin concentrations. During differentiation, $Def_3 \cdot Fe^{3+}$ fully supported enucleation and hemoglobinization. We did not observe toxic effects of $Def_3 \cdot Fe^{3+}$.

Finally, the main conclusions of this thesis are discussed, providing also an overview of the next developments that are required to make the production of cRBCs at large scale technically and economically feasible (**Chapter 5**). A multidisciplinary approach is needed to further reduce media cost, optimize medium composition to improve cell yields, and to improve the bioreactor culture system developed in this work.

Samenvatting

Productie van gekweekte rode bloedcellen (cRBC's) belooft een schier onbeperkte bron van cellen om de toenemende vraag naar RBC's voor transfusiedoeleinden te kunnen dekken, met meer controle over de kwaliteit en veiligheid van het transfusieproduct in vergelijking met het huidige donor afhankelijke systeem. cRBC's kunnen ook worden gebruikt voor nieuwe therapieën waarbij therapeutische moleculen aan RBC worden gekoppeld, of in RBC tot expressie komen. Opschaling van de productie van cRBC's is urgent om het grote aantal cellen te produceren voor dergelijke toepassingen. Het opschalen van statische kweeksystemen voor de productie van erytroblasten (voorlopercellen van RBC's) zou echter te arbeidsintensief zijn, waarbij grote hoeveelheden medium en veel ruimte vereist zouden zijn. Het onderzoek dat in dit proefschrift wordt gepresenteerd, heeft tot doel om efficiente oplossingen te ontwikkelen voor enkele van de uitdagingen van een grootschalige productie van cRBC's.

Geroerde tank-bioreactoren (STR's) zijn de standaard voor grootschalige productie van biologische farmaceutica, waaronder monoklonale antilichamen en vaccins. Door te roeren in dit soort reactoren worden de concentratiegradiënten van essentiële nutrienten verminderd in vergelijking met statische kweeksysteem zoals kweekschalen. STR's bieden ook actieve controle over kritieke bedrijfsparameters in de celproductie, zoals de concentratie van opgeloste zuurstof, pH en temperatuur. We hebben daarom een kweekprotocol ontwikkeld voor de proliferatie en differentiatie van erytroblasten in STR's (**Hoofdstuk 2**). Om de operatiecondities te definiëren die de proliferatie van erytroblasten in STR's het best bevorderen, werd het effect van roeren, beluchtingsstrategie en concentratie van opgeloste zuurstof geëvalueerd in STR's van 0,5 liter. Het kweekproces kon vervolgens worden opgeschaald naar 3 liter bioreactoren.

Erytroblasten verliezen hun vermogen om zich te blijven vermeerderen wanneer ze overgaan van een proliferatie modus naar een differentiatie modus. Daarom is efficiënte proliferatie van erytroblasten essentieel om het grote aantal cellen te produceren dat nodig is voor de productie van cRBC's. Het opkweken van erytroblasten onder proliferatie condities wordt meestal uitgevoerd volgens een repeated -batchkweekstrategie, waarbij de celkweek iedere 24 uur wordt verdund met vers medium tot een vaste

lagere celdichtheid. Bij hogere celdichtheden zagen we een afname van de groei (**Hoofdstuk 3**). De waargenomen groeibeperkingen van erytroblastculturen bij hogere celdichtheid bleken veroorzaakt door uitputting van laag moleculaire voedingsstoffen (molmassa <3 kDa) van gebruikt medium. Aminozuren leveren een belangrijke bijdrage aan de synthese van biomassa in prolifererende zoogdiercelculturen. Kwantificering van aminozuren in het medium, en in de cellen van liet zien dat de concentratie van sommige aminozuren aanzienlijk afneemt in de loop van de tijd. Echter, de proliferatie van erythroblasten verbeterde niet door aanvulling met extra aminozuren. Met behulp van een niet-gerichte metabolomics-benadering hebben we meerdere paden geïdentificeerd die wijzen op een overmaat aan oxidatieve stress in proliferatieculturen van erytroblasten.

Perfusie bleek een succesvolle alternatieve kweekstrategie te zijn om groeibeperkingen door uitputting van mediumcomponenten te overwinnen (Hoofdstuk 3). Het verhogen van de maximale celconcentratie in erytroblastculturen leidt tot een toename van de volumetrische productiviteit (aantal geproduceerde cellen per reactievolumeeenheid per kweektijd), waardoor het benodigde reactorvolume voor dezelfde productie van cRBC's, afneemt. Hierdoor zijn echter nog steeds grote hoeveelheden medium nodig. De kosten van het kweekmedium voor erytroïde culturen maken de productie van cRBC's momenteel nog economisch onhaalbaar. Groeifactoren en eiwitten die aan het medium worden toegevoegd, zijn belangrijke oorzaken voor de hoge kosten van het medium. Holotransferrine, een ijzerdragend eiwit, is de belangrijkste kostenpost in differentiatiemedium. We laten zien dat holotransferrine in erytroblastculturen vervangen kan worden door een klinisch toepasbare ijzerchelator, deferiprone, gebonden aan Fe^{3+} ($Def_3{\cdot}Fe^{3+}$; **Hoofdstuk 4**). Toevoeging van holotransferrine of $Def_3{\cdot}Fe^{3+}$ aan het kweekmedium resulteerde in vergelijkbare eindopbrengsten van cRBC's tijdens proliferatie en differentiatie van erytroblastculturen in vergelijking met optimale concentraties van holotransferrine. Tijdens differentiatie ondersteunde $Def_3{\cdot}Fe^{3+}$ volledige enucleatie en hemoglobinisatie. We hebben geen toxische effecten van $Def_3{\cdot}Fe^{3+}$ waargenomen.

Ten slotte bediscussieer ik de belangrijkste conclusies van dit proefschrift en geef ik een vooruitblik naar de volgende ontwikkelingen om de productie van cRBC's technisch en economisch haalbaar te maken (**Hoofdstuk 5**). Een multidisciplinaire aanpak is nodig om de kosten van het medium verder te verlagen, de samenstelling van het medium te optimaliseren om celopbrengsten te verbeteren, en het ontwikkelde bioreactorkweeksysteem verder te verbeteren.

Resumen

La transfusión de eritrocitos o glóbulos rojos (RBCs, por sus siglas en inglés) es la terapia celular más usada actualmente en aplicaciones clínicas. La producción de glóbulos rojos cultivados (cRBCs) tiene el potencial de ser una fuente ilimitada de células que podría complementar el sistema actual 100% dependiente de donantes. De esta manera, podría cubrir la creciente demanda de glóbulos rojos para transfusión, a la vez que haría posible controlar la calidad y la seguridad del producto final. El uso de cRBCs en aplicaciones clínicas requiere sistemas de producción que sean capaces de generar la gran cantidad de células que son necesarias para transfusiones. Sin embargo, los sistemas actuales desarrollados para el cultivo de eritroblastos (células precursoras de los glóbulos rojos) son en su mayoría en 2D, y para los cuales son necesarios grandes volúmenes de medio de cultivo, extensas áreas de cultivo, y altos costos de mano de obra. Esta tesis tiene como objetivo proponer soluciones a algunos de los retos más relevantes para escalar la producción de cRBCs.

Los biorreactores de tanque agitado se utilizan con frecuencia en la producción a gran escala de productos biofarmacéuticos, como anticuerpos monoclonales y vacunas. La agitación en este tipo de reactores ayuda a reducir la magnitud de los gradientes de concentración de nutrientes esenciales para las células, generando condiciones más homogéneas comparadas con sistemas de cultivo estáticos como placas de Petri. Los biorreactores de tanque agitado también permiten el control de parámetros críticos, como la concentración de oxígeno disuelto, el pH y la temperatura. En esta tesis se ha desarrollado un protocolo de cultivo para la proliferación y diferenciación de eritroblastos en biorreactores de tanque agitado (**Capítulo 2**). Los efectos de la agitación, la estrategia de aireación, y la concentración de oxígeno disuelto fueron evaluados para definir condiciones de operación de biorreactores de 0.5 litros que permiten obtener una proliferación y diferenciación eficiente de eritroblastos. El proceso de cultivo fue escalado a biorreactores de 3 litros usando esta información.

Los eritroblastos pierden su capacidad de replicación en la transición entre las fases de proliferación y diferenciación. Por lo tanto, el desarrollo de un sistema eficiente de proliferación de eritroblastos es fundamental para poder producir el gran número de glóbulos rojos necesarios para una transfusión. Los cultivos de eritroblastos en condiciones proliferativas suelen realizarse siguiendo una estrategia de cultivo por lotes repetidos. A estos cultivos se añade medio fresco al cultivo cada 24 horas, reabasteciendo los nutrientes que han sido consumidos, diluyendo subproductos

metabólicos potencialmente inhibidores, y reduciendo la concentración de células a un valor predefinido. Para reducir los volúmenes de cultivo es conveniente usar concentraciones de células más altas en el proceso. Sin embargo, durante este proyecto se observó que concentraciones altas de células llevan a tasas de replicación más bajas en la fase de proliferación (**Capítulo 3**). Estas limitaciones de replicación en cultivos de eritroblastos a concentraciones celulares elevadas parecen ser causadas por la reducción en la concentración de nutrientes de bajo peso molecular (masa molecuar <3 kDa). Las tasas de consumo de aminoácidos, los cuales contribuyen en gran proporción a la síntesis de biomasas en cultivos de células animales, fueron determinadas para eritroblastos en proliferación. Aunque la concentración de algunos aminoácidos disminuye de manera considerable durante el cultivo, suplementar el medio con dichos aminoácidos no mejoró la tasa de replicación celular. Siguiendo un enfoque metabolómico no dirigido fue posible identificar varias rutas metabólicas que indican un exceso de estrés oxidativo en cultivos de proliferación de eritroblastos.

La perfusión demostró ser una estrategia de cultivo alternativa que permite superar las limitaciones de crecimiento causadas por el agotamiento de nutrientes (Capítulo 3). El aumento de la concentración celular máxima en los cultivos de eritroblastos conduce a un incremento de la productividad volumétrica del proceso (número de células producidas por unidad de volumen de reactor por unidad tiempo de cultivo), lo que disminuye el volumen necesario del reactor para producir la misma cantidad de cRBCs. Sin embargo, seguirían siendo necesarios grandes volúmenes de medio para mantener esos cultivos. Actualmente, el costo del medio para los cultivos eritroides hace que la producción de cRBCs sea económicamente inviable. Los factores de crecimiento y otras proteínas añadidas al medio contribuyen en gran medida al costo del mismo. La holotransferrina, una proteína portadora de hierro, es el principal factor que eleva el costo del medio utilizado durante la fase de diferenciación. Se ha demostrado que la holotransferrina en los cultivos de eritroblastos puede sustituirse por un quelante de hierro (deferiprona; Def) unido al ion férrico ($Def_3 \cdot Fe^{3+}$; **Capítulo 4**). Este quelante es compatible con buenas prácticas de fabricación, un prerrequisito para la producción de cRBCs que puedan ser usados en transfusiones. La adición de $Def_3 \cdot Fe^{3+}$ al medio de cultivo llevó a niveles de producción de células durante cultivos eritroides de proliferación y diferenciación similares a los que se obtienen cuando concentraciones óptimas de holotransferrina son usadas. Durante la diferenciación, células enucleadas y completamente hemoglobinizadas fueron producidas cuando $Def_3 \cdot Fe^{3+}$ se usaba en el medio de diferenciación. No fue observado ningún efecto tóxico causado por la suplementación de $Def_3 \cdot Fe^{3+}$.

Por último, las principales conclusiones de esta tesis son discutidas, proporcionando también una visión general de los desarrollos que aún son necesarios para que la producción de cRBCs a gran escala sea técnica y económicamente viable (**Capítulo 5**). Se necesitará un enfoque multidisciplinar para reducir aún más el costo del medio, optimizar su composición para mejorar el rendimiento celular, y para mejorar el sistema de cultivo en biorreactores de tanque agitado desarrollado en este proyecto.

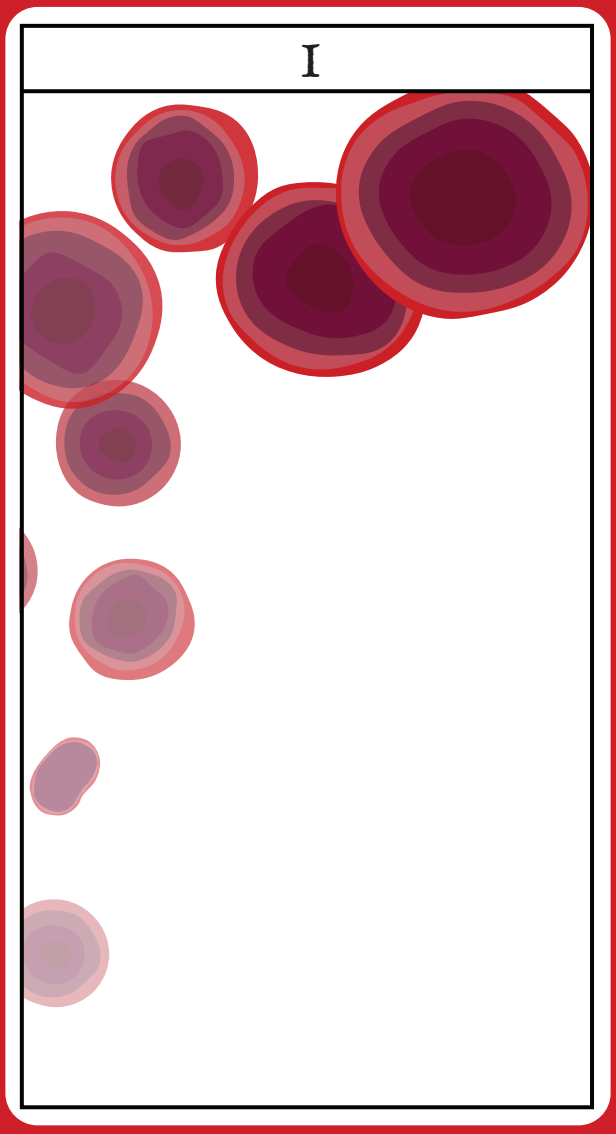
I

Chapter 1

General introduction

1.1. Current transfusion practice and challenges

Erythrocytes or red blood cells (RBCs) are the most abundant cell type in the human body, representing around 84% of the total number of cells of an adult ($2.0\text{-}2.5\times10^{13}$ RBCs) [1]. RBCs deliver oxygen and remove carbon dioxide from tissues. Human RBCs have an average lifespan of about 115-125 days, which translates to a mean production rate of $1.8\text{-}2.5\times10^{6}$ RBCs per second [2–4]. Disturbances like an imbalance in the RBC turnover, RBCs with reduced oxygen transport capacity, or the sudden loss of blood can lead to insufficient oxygenation levels, and subsequent tissue and organ damage.

Blood transfusion is the most used cell therapy. In 2018, 118.5 million blood donations were collected globally. However, availability of blood products is not uniformly distributed, with only 27.5% of global blood donations being collected in low- and lower-middle income countries, which on the other hand represent 48.4% of the world's population [5]. Also in high-income countries, blood shortages are expected to be more frequent in the upcoming years due to an aging population that has an increasing demand for blood transfusion, while the potential donor population is expected to decrease [6–9]. New therapies, such as using RBCs as carriers for targeted drug delivery, may further increase RBC demand [10]. The deficit is aggravated for patients that have been alloimmunized against RBC antigens, as is commonly the case for those who receive frequent RBC transfusions, such as sickle cell disease patients [11–14].

In 2018, 724 000 donations were collected in the Netherlands, of which 403 900 RBC concentrates were obtained and supplied for erythrocyte transfusion purposes [15]. Improved management of surgical procedures combined with a customized transfusion management reduced the need for donor blood over the last years in The Netherlands. Continuous donor recruitment, however, remains crucial. Globalization and an increasing multiculturalism are additional societal factors that lead to the need of having a broad donor base to ensure a safe transfusion practice. The expression frequency of antigens that are part of more than 35 known blood group systems is associated with ethnicity [16]. In a multiethnic society the complexity of co-expressed antigens augments, and it becomes increasingly difficult to find matching blood for patients that depend on regular transfusions [17,18].

Production of cultured red blood cells (cRBCs) from stem cells has been proposed as a means to tackle these and other challenges of the current fully donor-dependent system, such as the inherent difficulties of screening for novel bloodborne diseases, or the demand for transfusion units with fully matched blood group for patients that have developed alloimmunization, or with rare blood groups [19,20]. cRBC manufacture methods are based on *ex vivo* erythroid cultures that mimic the RBC production process

that takes place in the body, also known as erythropoiesis. *Ex vivo* erythroid culture protocols were initially developed to better understand the mechanisms driving the commitment to the erythroid lineage, the morphological changes through terminal differentiation, and the role of growth factors in the erythroid differentiation process, which can be difficult to study with detail in human subjects or in animal models. In addition to its potential for research purposes, production of cRBC at scale represents a potentially unlimited source of RBCs for transfusion purposes, with more control on the quality and safety of the final product. In addition to their use for blood transfusions, cRBCs could also be employed as carriers of biologically active compounds, such as enzymes [21–24], encapsulated drugs [25,26], or biosensors [27].

1.2. *In vivo* erythropoiesis

All blood cells, including red blood cells (erythrocytes), white blood cells (leukocytes), and platelets (thrombocytes), are derived from hematopoietic stem cells (HSC). This process, also known as hematopoiesis, is classically modelled in a hierarchical manner with the HSC as initial state, and with each differentiation stage restricting the number of lineages into which a cell can commit (Figure 1). Although *in vivo* hematopoiesis has been extensively studied in healthy human patients and in patients with blood disorders (e.g. anemia), *ex vivo* cultures have broadened the knowledge on the mechanisms behind HSC differentiation.

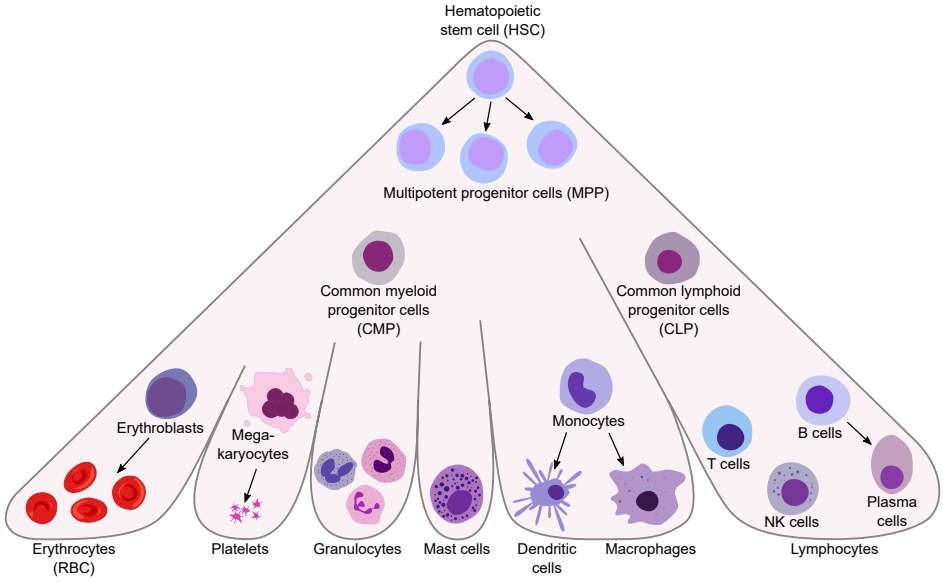

Figure 1.
(See caption on next page)

For the case of red blood cell production (erythropoiesis; Figure 2), the first step is the differentiation of HSC into a multipotent progenitor cell (MPP), which can still give rise to any blood cell, but have less self-renewal capacity than HSC. MPP can then commit into the lymphoid or myeloid lineages, by differentiating into common lymphoid progenitors (CLP) or common myeloid progenitor (CMP) cells, respectively. CMPs can then differentiate further to granulocyte macrophage progenitors (GMP), which can generate granulocytes and monocytes, or to megakaryocyte-erythroid progenitor cells (MEP), which will ultimately lead to the production of RBCs or of platelets. Along this first stage from HSC to MEP, cells display a decrease in the expression of the transmembrane protein CD34.

Commitment of MEP to the erythroid lineage leads to the first erythroid precursor cells, also known as proerythroblasts. Proerythroblasts have an average diameter of 12-20 μm, a large nuclei and open chromatin, and are characterized by low expression levels of glycophorin A (GYPA or CD235a) and high levels of transferrin receptor 1 (TfR1, or CD71) and integrin alpha 4 (CD49d) in their surface. Proerythroblasts differentiate further into basophilic, polychromatophilic, and orthochromatic erythroblasts, successively. Through this process, also known as terminal erythroid differentiation, big morphological changes take place: decrease in cell size, increase in chromatin condensation, and gradual clearance of organelles including ribosomes and mitochondria. This is accompanied by an accumulation of hemoglobin, a decrease in cytoplasmic RNA levels, increase in CD235 expression and gradual loss of CD49d from the cell surface.

Orthochromatic erythroblasts subsequently expel their nuclei, resulting in enucleated reticulocytes, and pyrenocytes (nuclei wrapped in cell membrane). Pyrenocytes are cleared by macrophages present in the bone marrow, while reticulocytes enter the blood stream, where maturation into erythrocytes takes place. In this last stage, clearing of residual organelles and remaining RNA continues, CD71 expression is lost, and further remodeling of the cell membrane takes place, leading to flexible biconcave RBCs [30].

Figure 1. Hematopoietic differentiation model. Hematopoietic stem cells (HSC) differentiate into multipotent progenitor cells (MPP), which then give rise to red blood cells (RBC) or erythrocytes, platelets or thrombocytes, and all white blood cells (including macrophages, lymphocytes, neutrophils, eosinophils, basophils, monocytes, and mast cells). Although hematopoietic differentiation was classically described as a tree-like hierarchy in which HSC differentiate into a discrete number of lineage-restricted progenitor cells, recent studies propose a continuum differentiation model that consider the heterogeneity in the progenitor cell population and the ability of those cells to differentiate into multiple lineages [28,29]. Erythropoiesis (production of red blood cells) is depicted in the most left arm of this scheme.

Distinguishing between the different stages of terminal erythroid differentiation, from proerythroblasts to reticulocytes, can be performed using microscope staining techniques targeting hemoglobin, DNA and RNA (e.g. May Grunwald-Giemsa and benzidine stain), or by flow cytometry using DNA dyes (e.g. DRAQ5, or propidium iodide PI) and measuring the expression level of the surface markers CD71, CD235a and C49d.

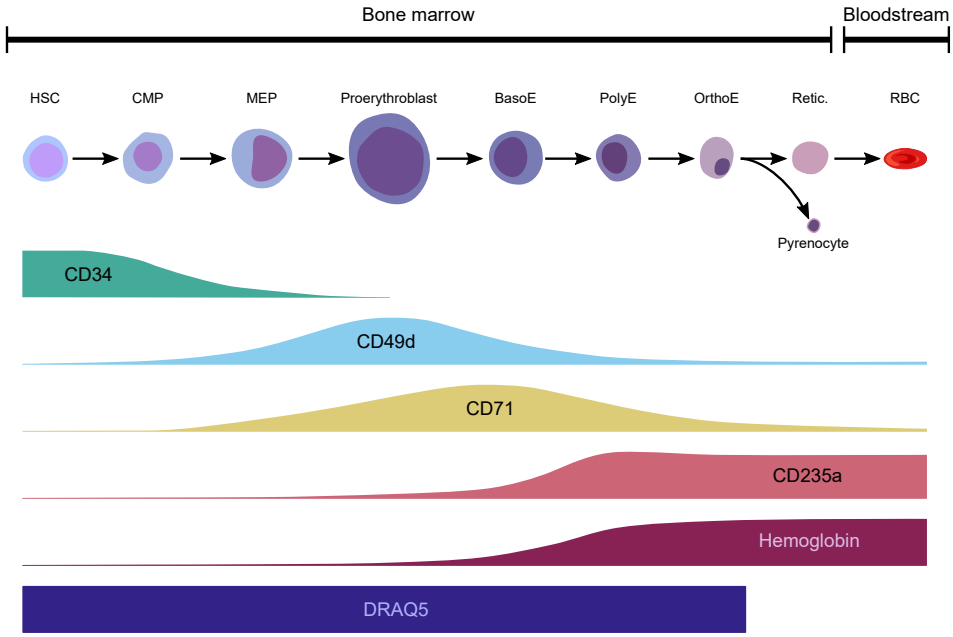

Figure 2. Differentiation of hematopoietic stem cells to erythrocytes. Red blood cell production (erythropoiesis) is a complex multistep process in which hematopoietic stem cells (HSC) differentiate into mature erythrocytes. The first step of this process is the differentiation of HSC into common myeloid progenitor cells (CMP), which can differentiate into erythrocytes, megakaryocytes, and myeloblasts. Further commitment to the erythroid lineage gives rise to megakaryocyte-erythroid progenitor cells (MEP), which can develop into cells fully committed to the erythroid lineage (proerythroblasts). Proerythroblasts follow a terminal differentiation process towards basophilic (BasoE), polychromatophilic (PolyE), and orthochromatic (OrthoE) erythroblasts. During this differentiation process, erythroblasts display a reduction in proliferative capacity, decrease in cell size, increasing hemoglobin content, and chromatic condensation. The erythroblast differentiation process culminates with the egression of the nuclei, giving rise to reticulocytes (Retic) and pyrenocytes (expelled nuclei surrounded by plasma membrane). Reticulocytes complete the maturation process in the bloodstream. The different cellular stages of erythropoiesis can be identified by the expression profile of surface proteins, such as CD34, CD235a, CD71 and CD49d. DRAQ5, a DNA-binding dye, can be used to distinguish between reticulocytes and nucleated cells.

1.2.1. The bone marrow microenvironment

In vivo erythropoiesis in adult humans takes place in the bone marrow, particularly in trabecular bone, comprising a wide variety of supportive stromal cells [31]. These stromal cells create distinct niches in the bone marrow. The high degree of vascularization in the bone marrow ensures the availability of oxygen- and nutrient-rich blood to the cells residing in the bone marrow microenvironment (BMM), the exchange and transport of growth factors, and the removal of waste products. Different stages of the erythroid development take place in specific niches in the BMM. In general, the mostly quiescent stem cells are thought to reside in low oxygen niches close to osteoblasts, while actively dividing progenitors often develop in close contact with mesenchymal stromal cells and perivascular cells [32]. The final differentiation of erythroblasts to reticulocytes occurs in macrophage islands located close to blood vessels [33].

1.2.2. Growth factors during erythropoiesis

A key regulator of erythropoiesis is erythropoietin (Epo), a hormone produced in the kidney and liver, that upon binding to its cognate receptor (EpoR) triggers intracellular signal transduction pathways that ensure survival of the immature erythroid cells [34]. Mouse embryos lacking Epo or the EpoR die around day E13 with a complete lack of definitive erythrocytes [35,36]. Epo production is controlled by oxygenation of the kidney and is increased by low-oxygen levels (hypoxia) or anemia. Under these conditions, Epo serum concentration increases, stimulating the survival and proliferation of erythroblasts, leading to an increase in the production rate of RBCs [37].

Stem cell factor (SCF, Steel factor) is also crucial for erythropoiesis. Mice deficient in SCF or its receptor cKit are born with severe anemia [38,39]. Importantly, Steel-dickie mice, that produce only soluble SCF because they lack the SCF transmembrane domain, are also anemic [40]. Thus, *in vivo* erythropoiesis is dependent on direct interaction with cells that express membrane-bound SCF. Binding of SCF to the tyrosine kinase receptor c-Kit induces a cascade of intracellular signaling pathways that promote cell growth, delay differentiation, and support survival of erythroid progenitor and precursor cells.

Under acute situations in which the *in vivo* steady state erythroid output is insufficient (for example, due to rapid blood loss, and inflammation caused by infections or tissue damage), an increase in RBC production is required to compensate the anemia. This process, known as stress erythropoiesis, requires glucocorticoids. These lipophilic steroid hormones mediate the increase in the proliferation of erythroid progenitor cells during stress erythropoiesis *in vivo* [41].

1.2.3. Iron requirements during erythropoiesis

Efficient hemoglobin synthesis during terminal differentiation is required to produce functional cRBCs that can transport oxygen comparable to native RBCs. A single RBC contains around 300 million hemoglobin molecules, representing 30-35% of the dry weight of the cell. Hemoglobin is comprised of four globin sub-units, each with a single iron-containing heme group. Iron uptake by developing erythroid cells is mainly enabled by transferrin. Iron-loaded transferrin (holo-transferrin), produced *in vivo* by hepatocytes, is internalized into the cell upon binding to the transferrin receptor TfR. Iron is then released and used for heme and ferritin synthesis, while iron-free transferrin (apo-transferrin) and the TfR transfer back to the cell surface.

1.3. *Ex vivo* production of cRBCs

1.3.1. Cell sources

Several cell sources can be used for *ex vivo* erythroid cultures, including primary cells (i.e. derived from living tissue) and immortalized cell lines. Currently, growth of large number of cRBCs works best from primary cell sources. Cord blood [42,43], peripheral blood [44], and bone marrow cells [45,46] are often used as source of primary cells, which can be cultured and committed to the erythroid lineage. Peripheral blood mononuclear cells (PBMCs) can be separated from other blood components including erythrocytes, granulocytes, and plasma by density centrifugation. PBMCs mainly consist of monocytes and lymphocytes, but they also contain a small fraction (~0.17%) of circulating stem cells, characterized by expression of the $CD34^+$ marker protein on the cell surface, that can differentiate into erythroid cells [47]. Using the entire peripheral blood mononuclear cells as starting material leads to higher cRBC yields compared to using a pure $CD34^+$ population as single cell source, due to the positive contribution of $CD14^+$ monocytes/macrophages present in the PBMC pool that produce soluble factors supporting stem cell survival [48,49].

The main advantage of immortalized cell lines as source for cRBC production is the unlimited availability of extremely rare blood group profiles [20]. The currently most promising immortalized cell lines are, firstly, those immortalized by conditional expression of the HPV (human papilloma virus) E6/E7 genes. These include HUDEP, HiDEP and BEL-A lines. These cell lines can generate enucleated reticulocytes, but the inhibition of tumor suppressor genes increases the risk of genetic instability and functionally impaired reticulocytes [50–52]. The second type of cell lines are induced pluripotent stem cells (iPSC). The differentiation of iPSC to embryoid bodies, and subsequently to hematopoietic organoids mimics embryogenesis. Mostly, these

cultures yield large, nucleated, primitive red blood cells with embryonic hemoglobin (HbE) that are not suitable for transfusion purposes [53,54]. However, progress is being made to achieve definitive erythropoiesis yielding enucleated reticulocytes with fetal hemoglobin (HbF).

1.3.2. Current erythroid culture methods

Due to the distinct growth factor requirements of each erythroid development stage, protocols for *ex vivo* erythroid cultures are often divided in two to four stages, with differences in medium composition, concentration of growth factors, and medium refreshment regimes. Control of the transition between erythroblast proliferation and differentiation stages is essential to produce the large amounts of erythroblasts required for efficient cRBC production. Suboptimal culture conditions may result in the spontaneous differentiation of proerythroblasts, which leads to a loss in the proliferation potential of the culture, limiting the production of the large number of cRBCs required for transfusion purposes [55].

Typically, protocols contain an initial expansion phase in which proliferation of the hematopoietic stem cells and the commitment to the erythroid lineage take place in presence of factors that support the stem cell (IL3, SCF, sometimes TPO, IL6, FLT3) and the emerging erythroid cells (Epo, SCF) (Supplementary Table S1). This is followed by a stage of extensive proliferation of the erythroid progenitor and precursor cells. During this stage, cells are reseeded periodically, or when the cell concentration in the culture exceeds a certain limit (e.g. 1-2×10^6 cells/mL). As the cooperative activity of Epo, SCF and glucocorticoids is required for the extensive proliferation of erythroid precursor cells, these factors are added with every medium refreshment. Finally, for the differentiation of the cultured erythroblasts, SCF and glucocorticoids are removed from the medium. In this stage, medium is often supplemented with a higher Epo concentration compared to the expansion stages. Serum or plasma, and insulin-like growth factor (IGF-1 or IGF-2) are also included. Extra iron-loaded transferrin can also be added to support the massive production of hemoglobin during terminal differentiation. In some protocols, an extra culture stage to enhance enucleation efficiency is performed.

A 3-stage protocol was used for the first clinical trial in which cRBCs were transfused to a patient [56]. In this study, hydrocortisone was used in the first 7 days of culture together with SCF, Epo and IL-2. This was followed by a short second stage of 4 days only using SCF and Epo. The majority of the cell number fold increase was observed in the last stage, in presence of Epo alone, lasting 7 days. An overall 61 500-fold increase in cell numbers and high enucleation efficiency (80%) was reached, allowing to produce 1-2 mL of packed cRBCs using only 10^6 $CD34^+$ cells (derived from peripheral blood) as

starting material. The produced cRBCs displayed similar oxygen equilibrium curves, hemoglobin content and deformability as peripheral blood RBCs. Similar 3-stage protocols, omitting addition of glucocorticoids, have been used to produce larger numbers of cRBCs: 3×10^6 cells (~5 mL of packed cRBCs) after $>10^4$ cell number fold change [57], and $>10^{11}$ cRBCs (~10 mL of packed cells) after $>10^5$ fold change using a GMP-compatible protocol [58].

Recently, another GMP-compatible 3-stage culture protocol using PBMCs as cell source was reported, with high yields (10^7-fold erythroblast proliferation level) and high enucleation efficiencies (>90%) [55]. The first stage of this protocol starts with the culture of PBMCs in the presence of Epo, SCF, dexamethasone (Dex) and interleukin 3 (IL3), committing them to erythroid lineage and leading to a proerythroblast-enriched population after 7 days. In the second stage, also known as main expansion phase, proerythroblasts are cultured with Epo, SCF and Dex for up to 21 days, during which cells proliferate massively. Synchronous terminal differentiation of the proliferating erythroblasts is triggered by the removal of SCF and Dex from the medium, the increase of Epo concentrations, and supplementation with human plasma. During this last stage, taking 10-12 days, erythroblasts mature into enucleated reticulocytes that functionally resembled RBCs isolated from peripheral blood in terms of hemoglobin content, deformability, and oxygen binding capacity.

1.3.3. Current media compositions for erythroid cultures

First erythroid culture protocols used culture medium supplemented with serum as source of hormones, growth factors, vitamins, and extra nutrients. As serum composition is poorly defined and is subject to significant batch-to-batch variations, serum replacements are needed for production of cRBCs that could be used for medical purposes. The pioneer work of Iscove et al. and Migliaccio et al. led to the formulation of serum-free culture medium that can support erythroblast proliferation, in which serum was replaced by a combination of Epo, albumin, cholesterol, holotransferrin, insulin, nucleosides, trace elements, and sodium pyruvate [59,60]. However, plasma is still often supplemented during erythroblast differentiation and terminal reticulocyte maturation due to its observed positive effect on enucleation levels and reticulocyte stability [55,61].

Although chemically defined medium represents an important step towards the production of cRBCs for clinical applications, high medium costs still render this process economically unfeasible. Cost analysis of cRBC production performed by Timmins et al. considering the typical cell densities reached in erythroid cultures ($<5\times10^6$ cells/mL) and media costs alone (specifically, only the contribution of the most

expensive supplements: Epo, SCF, albumin, transferrin, insulin) estimate a range of 80 000-90 000 dollars for a single RBC transfusion unit. New media formulations have been developed with lower concentration of expensive molecules, or their replacement by cheaper non-animal-derived components. Olivier et al. developed an erythroid culture protocol in which albumin could be replaced by a combination of a chemically defined mix of lipids, an enhancer of lipid solubility (methyl-β-cyclodextrin), and an antioxidant (6-hydroxy-2,5,7,8-tetramethylchroman-2-carboxylic acid; Trolox) [62]. In this protocol, human transferrin was also replaced by a recombinant version of the protein produced in rice (Optiferrin). The replacement of albumin by polyvinyl alcohol is also an important step forward to a chemically defined, cost-effective media [63–65].

1.4. Culture systems for cRBC production

A single transfusion unit of packed RBCs contains ~2×10^{12} cells in a volume of 250-300 mL[1] [45]. In 2009, Timmins et al. estimated that the production of a single cRBCs transfusion unit would need 660 L of medium, using the typical cell concentrations reported for suspension erythroid cultures [66]. These large medium requirements are evident from the first proof-of-principle human transfusion of cRBCs, in which 13 L of medium were required to produce 1×10^{10} enucleated cells (0.5% of a total transfusion unit), equivalent to 2600 L of media for a full transfusion unit [56]. Although larger numbers of cRBCs have been produced using more efficient erythroid culture protocols (Griffiths et al.: 24 L for 5 mL of packed RBCs [57]; Kupzig et al.: >25 L for 10 mL of packed RBCs [58]), large medium volumes would still be needed (600-1400 L for a single transfusion unit). Thus, the development of efficient and scalable culture systems is required for the large-scale production of cRBCs.

1.4.1. Static suspension culture approaches

Most erythroid culture protocols described in literature are performed in static culture dishes or flasks. Due to the low cost and effort required to set up this type of systems, static cell cultures have been traditionally used as the main research model to study mammalian cell physiology. As hematopoietic cells are non-adhesive, cultures are performed in suspension without the need for a cell detachment method (e.g. trypsin treatment) for cell passaging. This reduces the amount of work required to maintain such cultures compared to adherent cell lines, such as fibroblasts.

[1] This value can be derived from the volume (250-300 mL) and hematocrit (percentage of the total volume occupied by RBCs; 55-80%) of a transfusion unit of packed RBCs, and the mean corpuscular volume of erythrocytes (80-100 fL per cell).

Culture dishes and flasks are maintained in incubators with a controlled temperature, humidity and gas composition. Typically, maintenance of suspension static cultures is performed by periodically measuring the cell concentration in the dish after resuspending the cells settled at the bottom surface, followed by dilution with fresh medium to maintain the culture cell concentration low (usually <2-5×10^6 cells/mL). Because the cultures have to be removed from the incubator for sampling, perturbations in temperature and pH are inevitable, which can affect the growth and viability of the cells [67,68]. Furthermore, due to the lack of mixing and the settling of the cells to the bottom surface, static culture systems can display spatial gradients in the concentration of metabolites, especially under high cell densities and for species with low diffusion rates, or very short life times (e.g. reactive oxygen species) [69]. Although microsensors to monitor local pH, dissolved oxygen and concentrations of nutrients (glucose, lactate) are available, active control of such parameters using measured values at the scale of culture dishes and flasks is challenging.

Liquid height and surface cell concentration (cells per unit of area) are common scaling parameters for dish cultures. Both parameters define the vertical oxygen concentration profile in the dish [70]. Although large culture dishes and flasks are commercially available (up to 500 cm^2 of surface area), scaling the cell production using conventional culture dishes and flasks follows a scale-out approach (multiple "small" units maintained in parallel) rather than a scale-up strategy (a few or a single large culture unit). This results in very labor-intensive processes for media refreshment and final harvesting. It also leads to a high footprint: for conventional culture dishes with an inner diameter of 8.7 cm (surface area = 60 cm^2), each holding 12 mL of culture (liquid height = 2 mm), 33 000-83 000 dishes with a total footprint of 200-500 m^2 would be required to produce a single transfusion unit assuming a cell culture density of 2-5×10^6 cells/mL (surface concentration of 4-10×10^5 cells/cm^2). Multilayered vessels, such as Corning's CellSTACKs and HYPERFlasks, have been developed to increase the surface area available for growth while maintaining a low footprint (up to 40× higher compared to culture flasks). CellSTACKs have been used for the production of >3×10^{10} cRBCs, sufficient to determine the lifespan of cRBCs after an autologous transfusion in a patient [56]. Although multilayered vessels require less incubator space compared to culture dishes to produce the same number of cells, microscopic viewing of the cells to monitor the progress of the culture can be limited, and manipulation of such systems for periodical sampling and final harvest is cumbersome. Furthermore, it is unclear whether cells cultured in these systems are exposed to similar or worse oxygen limitations to those in conventional dishes and flasks.

A strategy to reduce the large surface requirements in static culture systems is to improve the gas transfer to the liquid, allowing to increase the culture volume per plate while ensuring that cells are not exposed to oxygen limitations. This is often done using polydimethylsiloxane (PDMS) dishes and flasks, as it is a material with much higher oxygen and carbon dioxide permeabilities compared to polystyrene (conventional material used for culture dishes) [71]. Recently, a GMP-compatible static erythroid culture protocol using a vessel with a gas-permeable silicone membrane at the base was reported [55]. This culture system (G-Rex; Wilson Wolf Manufacturing; Saint Paul, MN) was reported can support liquid heights of up to 10 cm per cm^2 of surface area, resulting in a 50-fold increase in surface cell density (cells per cm^2) compared to conventional culture dishes. By having a single vessel and the possibility to automate medium refreshment and harvest, the manual work involved in sustaining the culture is reduced [72]. However, scale up is still by surface area, and only limited control on culture conditions can be achieved.

1.4.2. Immobilization strategies

The human bone marrow is an extremely efficient RBC manufacturing system, producing $1.6\text{-}2.2\times10^{11}$ erythrocytes per day in a volume of 1.1-2.1 L [73]. Thus, bioreactor designs mimicking the microenvironment and structure of the bone marrow have been proposed for cRBC production. Housler et al. used a hollow fiber bioreactor consisting of a central compartment where cells reside, perfused by capillaries through which fresh medium and gas (air + CO_2) are supplied, mimicking the *in vivo* perfusion of the bone marrow. Seeded $CD34^+$ HSCs committed to the erythroid lineage, proliferated, and differentiated to enucleated cRBCs, reaching cell densities of up to 8×10^7 cells/mL and 1300-fold proliferation levels [74]. A similar approach using hollow fibers perfusing a porous scaffold in which cells are seeded was used by Allenby et al. [75]. In this system, spatial cell distributions similar to *in vivo* conditions were observed, with a differential localization of proliferating and differentiating erythroid cells, which was correlated with local hypoxic conditions in the scaffold material. Formation of erythroid niches, with erythroblasts associated to macrophages in structures resembling *in vivo* erythroblastic islands, was also found. Although enucleated cRBCs could egress through the hollow fibers, the permeability of the hollow fibers to cRBCs was identified as a bottleneck in this set-up [76]. Moreover, manufacture of the porous scaffolds is technically challenging [77]. Although hollow fiber bioreactor can be a useful model of *in vivo* hematopoiesis, and allow to separate the cells from shear caused by liquid flow and aeration of other culture systems (see following section), scaling up these systems for large scale production of cRBCs can be challenging due to the large gradients observed along and across the fibers [78,79].

1.4.3. Agitated and stirred culture systems

Active mixing allows to overcome some of the problems associated with static cultures, by reducing nutrient, oxygen, and cell concentration gradients in the culture. Several technologies are available for suspension cultures of mammalian cells with different levels of complexity, including roller bottles, shake flasks, rocking bioreactors, spinner flasks, and stirred tank bioreactors. Roller bottles, commonly used to proliferate anchorage-dependent cells, have also been used for HSC and erythroblast cultures [80,81]. In this system, the rotation of the bottle reduces nutrient gradients in the liquid while keeping shear and turbulence low. Although this system is relatively inexpensive, it is volumetrically inefficient, as the maximum liquid volume in each bottle is often only 10-20% of the total vessel volume [82].

Shake flasks are another low-cost mixed culture system, commonly used for the adaptation of adherent cell lines to suspension conditions. Critical parameters for shake flask cultures are the mixing conditions (orbital throw and rpm of the orbital shaker), volume occupancy of the flask, and presence of baffles, as all define the mixing conditions of the liquid and the gas mass transfer rates [83–85]. Temperature control and gas supply are achieved by placing the shaker platform inside an incubator with controlled atmosphere. Currently, shake flasks of up to 6 L of total volume are commercially available, and are often used with a higher working volume compared to roller bottles (30-40% of the flask volume). Shake flasks have been used for erythroid cultures, mainly as a platform to evaluate the effect of mixing conditions on erythroblast proliferation and differentiation [86].

In addition to orbital shaking, liquid cultures can also be agitated using a rocking motion. In this type of bioreactors, cultures are kept in a vessel (often a single-use plastic bag) attached to a device that rocks either back and forth, or in a bi-axial manner, inducing waves in the liquid. Culture bags used in rocking bioreactors can reach volumes of 200 L (maximum working volume = 100 L), and often include pH and dissolved oxygen sensors, gas lines for the aeration of the culture through headspace, and multiple liquid ports for sterile inoculation, sampling, and harvesting. Batch and fed-batch are the common operating modes in rocking cultures, but continuous perfusion can also be implemented in such systems, either using floating cell retention filters or external hollow fiber modules [87,88]. Culture bags of up to 200 L are available, with constant volumetric power input (power per volume, a function of rocking frequency and angle) commonly used as scale-up parameter [89]. Erythroid cultures in 1 L wave bioreactors have been reported, exhibiting low expansion yields compared to static cultures [90]. Culture dishes and flasks on rocking platforms have also been used to evaluate the effect of shear stress on erythroid cultures [91].

Agitation can also be achieved using submerged impellers. The simplest version of such systems is a flask with a suspended magnetic stirrer, also known as spinner flask. This system has a low cost compared to rocking bioreactors, and does not require more equipment than an incubator and a magnetic stirrer platform. Although aeration is still limited by diffusion (incubator's gas must go through the top cap of the flask to the liquid surface), the agitation improves the oxygen transfer to the culture, especially if the spinner flask contains baffles and the impeller is only partially submerged [92]. Spinners include several side arms that can be used for direct pipetting of medium or for harvesting of the culture. However, as the number of ports and compatible probes is limited, spinner flasks have restricted monitoring and control capabilities for key operating parameters (e.g. pH and dissolved oxygen concentration). Spinner flasks have been used for small scale erythroid cultures (<1.5 L) [51,93,94], but larger vessels can reach volumes of up to 36 L. The scale-out potential of such vessels have been demonstrated by Griffiths et al. and Kupzig et al., using multiple 1.5-2.0 L stirred vessels operated in parallel (>24 L total culture volume; fed-batch mode) to produce 5 and 10 mL of packed cRBCs, respectively [57,58]. Macroporous microcarriers have also been used in spinner flask erythroid cultures, with the goal of protecting cells from the turbulence caused by the agitation, while providing cells an environment similar to the spongy bone of the bone marrow [94].

1.4.4. Stirred tank reactors as platform for cRBC production

Stirred tank reactors (STRs) are the most widely used culture system for large scale microbial and mammalian cell culture process. Agitation in this type of bioreactors is performed by the rotation of one or multiple impellers. Stainless-steel or glass STRs are the standard for (large scale) microbial and mammalian cell culture. These systems provide multiple liquid in- and outlets that can be used for the inoculation of the reactor, sampling of the culture, addition of medium and other liquids (feeds, antifoam), and harvest. Aeration is typically performed using a submerged sparger, although aeration via a continuous gas flow through the headspace may be sufficient for low cell concentration cultures in small STRs (high surface-area-to-volume ratio). To ensure aseptic conditions during the cultivation process, stainless-steel STRs are either autoclaved or sterilized using steam-in-place systems, depending on the vessel volume. Reactors of up to 25 000 L have been successfully designed and used for mammalian cell cultures for production of monoclonal antibodies [95]. Cleaning of the vessel and any stainless-steel piping is also required between reactor runs. Due to the challenges of validating cleaning and sterilization procedures, and the cost and time requirements to perform those operations in processes following good manufacturing practices (GMP) guidelines, single-use bioreactors have become a popular alternative in industry. By having pre-sterilized single-use vessels that are discarded and replaced between runs, the

agility of the process can be increased, replacing the cleaning, sterilization, and validation times of stainless-steel STRs by the shorter installation times of single-use STRs [96].

Stirred bioreactors have been used for the culture of hematopoietic cells for almost 30 years [97]. Although small scale STRs (≤15 mL) have also been successfully used for cRBCs, the used conditions vary broadly with respect to medium composition, cell density, oxygenation, agitation conditions, and nutrient feeding strategy, making a direct comparison to other cultivation systems and conditions challenging [98–101].

Ratcliffe et al. used 15 mL ambr® STRs (Sartorius Stedim; Germany) for the expansion of umbilical cord $CD34^+$-derived HSCs, and observed 6 cumulative population doublings after 10 days of culture without media exchange, which could be increased to 8 doublings in 14 days of culture if media was fully changed every 2 days [100]. This culture protocol was further optimized by Bayley et al., showing that ~4000-fold change (12 doublings) could be reached after 24 days of culture, with a final enucleation efficiency of up to ~80%. The media refreshment strategy was a critical parameter to achieve high cell yields, and was further studied by Glen et al. also in ambr® STRs but in cultures with a short time-span (up to 60 h) [102]. More recently, Han et al. followed a design-of-experiments (DOE) approach to select optimal inoculation conditions and operating parameters to support erythroblast expansion and differentiation in the ambr® system [98]. However, expansion of early erythroblast cultures could not be sustained at any of the screened conditions. Lee et al. showed that erythroblast expansion could be scaled up to a 500 mL STR, albeit using an immortalized erythroblast cell line with overexpression of an anti-apoptotic gene (BCL-XL) and with very low enucleation efficiency [99]. Although commercial companies such as Rubius Therapeutics have filed patents for cRBC production in STRs of up to 200 L, no public data on the performance of such reactors is available apart from the low cell concentrations being used (0.1-2.0×10^6 cells/mL) [103,104].

1.5. Challenges and constraints for high-cell density cRBC cultivation

Any bioreactor system to be used for cRBC production must support cultivation conditions that are adequate for the efficient proliferation and differentiation of erythroblasts. To ensure that those conditions are fulfilled, adequate nutrient and oxygen availability is required, while controlling operating parameters that may negatively impact the growth and viability of the culture (e.g. turbulence and shear stress). Knowing the physical constraints for each stage during erythropoiesis would help to define operating windows for key parameters of bioreactor design and operation, such as mixing conditions, feeding and aeration rates.

1.5.1. Hydrodynamic forces: shear stress and turbulence

Mammalian cells are generally assumed to be highly sensitive to hydrodynamic forces. The principle behind this assumption is that mammalian cells are relatively big cells that lack cell walls and therefore are not able to resist mechanical deformation [105]. Although mechanical stress has been linked to regulation of cell cycle, decrease in proliferation and culture viability, its effects appear to be strongly cell-type specific [106–108]. It is relevant to note that assumptions of shear sensitivity can also lead to a sub-optimal process design for bioreactor operation in which low liquid velocities are preferred, which can lead to mixing problems and oxygen limitations in agitated systems at large scale. Thus, defining the optimal hydrodynamic conditions that support erythroid cultures is a requirement for the design of a scalable culture system.

Hydrodynamic conditions in the bone marrow microenvironment, dominated by slow perfusion of nutrients and low fluid shear stress (0.29 ± 0.27 Pa in sinusoidal capillaries), are different to those of STRs in which complex patterns of fluid flow take place [109,110]. However, turbulent mechanical conditions in a bioreactor may activate similar mechano-sensing processes as *in vivo*. How exactly cells in general are able to sense mechanical stress has been an open question for a long time. Relatively recently discovered mechanosensitive channels Piezo1 and Piezo2 shed light on the mechanism of mechanosensing in the animal kingdom [111]. Although the exact working mechanism is yet to be fully understood, its expression is strikingly widespread among different tissues and even different species. Piezo1 is expressed also on erythroblasts, both in the bone marrow and in *ex vivo* cultures [55,112]. Chemical induction of Piezo1 activity in cultured reticulocytes leads to a delay in maturation (i.e. delay in the loss of CD71 expression, and reduced deformability) [113]. More recently, the activation of Piezo1 on erythroblasts cultured in shake flasks was described, directly affecting the proliferation and differentiation dynamics [86]. Studies in STRs have shown that the different stages of erythroid cultures have distinct sensitivity to shear stress. Immature erythroid cells responded to shear stress with reduced viability and increased cell fragility, whereas cultures of more mature cells were robust and showed a linear increase in enucleation through the range of tested stirring speeds [98]. In addition to the effects of shear present in the culture system, it has been described that shear induced by the circulation through tubing using a peristaltic pump can induce changes (morphological, and at protein level) in cultured reticulocytes associated to a more mature state [114], agreeing with the observed maturation of cultured reticulocytes into biconcave cells in the circulation of transfused mice [58].

1.5.2. Oxygen availability

The effect of low oxygen concentration in the body (systemic hypoxia) on the production level of RBCs is an extensively studied phenomenon. This adaptation is mediated by hypoxia-inducible factors (HIFs), leading to an increase of Epo synthesis in the kidney, and a subsequent Epo-mediated upregulation of erythroid proliferation [115]. However, the direct effect at the cellular level of oxygen concentration on HSCs and erythroid precursor cells is less clear. Measuring the oxygen concentration in the bone marrow microenvironment where erythroblast proliferation and differentiation takes place is challenging. However, new experimental techniques using microscopy and phosphorescent probes have allowed to map the oxygen concentration landscape in the bone marrow. Beyond the cortical bone layer, the bone marrow is characterized by a low oxygen concentration (average oxygen tension of 52 mmHg; equivalent to $C_{O_2,sat}$ = 2.68 mg O_2/L; see Supplementary Information) [116], and by large oxygen concentration between the sinusoidal micro-vessels (carrying oxygen-rich blood) and the extravascular regions [117]. Direct measurements of oxygen concentrations in the bone marrow microenvironment indicate oxygen tensions of 13-20 mmHg ($C_{O_2,sat}$ = 0.67-1.03 mg O_2/L), much lower than arterial oxygen levels [118]. The role of oxygen gradients on the differential localization of HSCs in the bone marrow has been described, with proliferating HSCs preferentially localized close to the sinusoidal capillaries, while quiescent HSC tend to locate in low-oxygen regions far away from blood vessels [119–121]. A similar localization pattern has been observed for erythroblasts, with erythroblasts migrating towards the sinusoids as maturation progresses [122].

Ex vivo erythroid cultures have offered a way to study the role of oxygen concentration on erythropoiesis. A positive effect of low oxygen concentrations on erythroid maturation and enucleation has been reported [123–126]. In these studies, the controlled parameter is the oxygen concentration in the gas phase. Typically, hypoxic conditions are evaluated using an oxygen molar fraction (y_{O_2}) of 5% instead of the standard 21%. At 37 °C and 1 atm of pressure, this would be equivalent to oxygen tension value of 38 and 160 mmHg, and saturation concentration of oxygen (in water) of 1.96 and 6.90 mg O_2/L, respectively. However, under such conditions it is difficult to determine (and control) the local oxygen concentrations to which cells are exposed. In such diffusion-driven system in which cells localize at the bottom of the dish while the oxygen transfer from the gas phase occurs at the top of the liquid layer, there are significant oxygen concentration gradients. Local oxygen concentrations around the cells will be a function of cell confluence and liquid height, making the direct comparison between experiments challenging if those variables are not reported [70,71,127].

Erythroid culture bioreactors in which the dissolved oxygen concentration is measured and actively controlled allow to quantify the effect of oxygen levels on the different erythroid development stages; however, data is scarce. Bayley et al. reported a negative impact of high dissolved oxygen levels ($C_{O_2}/C_{O_2,sat} > 50\%$) on enucleation level during erythroblast differentiation in stirred tank bioreactors, but no effect on cell proliferation [101]. Using a similar bioreactor set-up, Han et al. observed a more complex effect of dissolved oxygen concentration on enucleation and final cell (reticulocyte) yield, in which low oxygen levels led to a positive or negative response on enucleation depending on the value of other process parameters (pH and temperature) [98].

1.5.3. Media composition and nutrient availability

Together with sufficient oxygen availability, ensuring sufficient levels of nutrients and minimizing the accumulation of toxic metabolic byproducts during culture is required for cell survival and proliferation. Glucose, often the most abundant metabolite in media formulations for cell culture (e.g. 25 mM in Iscove's Modified Dulbecco's Medium; IMDM), is rapidly taken up by proliferating mammalian cells. Although part of the glucose is diverted to the pentose phosphate pathway, the majority is used via glycolysis to produce pyruvate, which, instead of entering the tricarboxylic acid (TCA) cycle to be fully oxidated, is converted into lactate [128]. This phenomenon of high glycolytic flux relative to respiration in mammalian cells, even when sufficient oxygen is available, is also known as aerobic glycolysis or the Warburg effect. Although it can be seen as wasteful metabolism in terms of moles of ATP produced per consumed mole of glucose, aerobic glycolysis in mammalian cells seems to support rapid proliferation of mammalian cells [129].

Glutamine, the most abundant amino acid in plasma and in culture medium, is also rapidly consumed by proliferating mammalian cells [130–132]. Glutamine can be used as a precursor of TCA cycle intermediates via glutaminolysis. In this pathway, glutamine is first converted to glutamate, followed by the conversion to α-ketoglutarate, each step releasing an ammonium ion. Glutamine can also be used as carbon and nitrogen source for the synthesis of other non-essential amino acids, and for *de novo* purine and pyrimidine biosynthesis [133]. The commitment of HSCs to the erythroid lineage has been shown to be dependent on glutamine uptake and its usage for nucleotide synthesis rather than as a TCA cycle precursor [134].

Although both glucose and glutamine contribute to the majority of the cell energy requirements of cultured mammalian cells, all other amino acids included in culture media are major mass contributors for biomass synthesis, being sources of carbon and nitrogen not only for proteins but also for all other biomass building blocks (RNA, DNA,

lipids) [135,136]. During erythroid differentiation, erythroblasts display an increase in uptake rates of amino acids to support the production of the α- and β- globin chains of hemoglobin [137]. Glycine is also rapidly consumed in erythroblast cultures, as it is directly required for heme synthesis: for one heme group, 8 glycine molecules are required [138]. Thus, to produce the ~3×10^8 hemoglobin molecules present in a single RBC, each containing 4 heme groups, ~1.2 pg of glycine are required. Although glycine is a non-essential amino acid, insufficient uptake of glycine by erythroblasts leads to a decrease in heme synthesis during differentiation both *in vivo* and in *ex vivo* erythroid cultures [139].

Sufficient lipid availability is also required during erythroid culture. The first reported serum-free culture medium for erythroid culture, known as HEMA^{def}, required non-delipidated albumin and cholesterol supplementation to support the proliferation of early erythroid progenitor cells at levels comparable to those observed in medium using fetal bovine serum [60,140]. Lipid composition and metabolism show significant changes during erythroid development [141]. Lipid requirements are also dynamic during erythroid cultures: cholesterol is required for erythroblast proliferation, as insufficient cholesterol uptake and cholesterol biosynthesis lead to lower cell yields in erythroblast cultures. By contrast, cholesterol synthesis is downregulated during erythroblast differentiation, and low cholesterol levels may be required during erythroid differentiation to ensure efficient erythroblast maturation and enucleation [142]. Interestingly, Bernecker et al. showed that cRBCs have lower cholesterol content compared to native RBCs and reticulocytes [143]. This deficiency, which can affect membrane resistance to osmotic shock, is partially recovered by supplementation with cholesterol-rich lipids in the culture media. Other lipids present in plasma are also required to sustain erythroid cultures. The effect of lipid supplementation on erythroid cultures is dependent on the lipid mix being used, affecting the time from the PBMC stage until peak cell growth, and final erythroblast yields [144]. Compared to commercially available lipid mixes, specific lipoprotein fractions from human plasma appear to be more effective to increase the yield of erythroid progenitor cells and of erythroblasts [145]. Together, this suggests the existence of optimal lipid levels and profiles for the different stages of erythroid cultures.

The importance of other metabolites in erythroid cultures has been less studied. Analysis of metabolite transporters in the surface of cells during erythroid differentiation have revealed a high expression of the riboflavin (vitamin B_2) transporters RFVT1/2, suggesting an increase in the uptake requirements of this nutrient in erythroid progenitor cells and proerythroblasts compared to HSCs and late erythroblasts [146]. Folate (vitamin B_9) and cobalamin (vitamin B_{12}) deficiency also affect erythropoiesis, leading *in vivo* to an ineffective erythroblast differentiation, to the production of large

reticulocytes and RBCs, and to megaloblastic anemia. Lack of folate or cobalamine can cause an imbalance in the levels of the methionine-homocysteine cycle intermediate tetrahydrofolate (THF), which is involved in purine and pyrimidine synthesis [147].

1.5.4. Inhibitory metabolic byproducts

Lactate and ammonium are the major waste products in mammalian cell cultures. The concentrations of both species have a direct effect on cell proliferation [148]. Apart from being accumulated due to the breakdown of glutamine and other amino acids, ammonium can also be produced due to chemical decomposition of glutamine in the medium, but to a much lower extent in serum-free medium [149]. Ammonium leads to cell growth inhibition, and to cell necrosis at high concentrations (50 mM) [150]. Proposed mechanisms of ammonium toxicity in cell cultures are the competition of NH_4^+ with K^+ in transmembrane transporter proteins, and a generalized acidification of the cytosol [151]. High ammonium concentrations can also inhibit enzymes involved in glutamine catabolic pathways feeding the TCA cycle, such as glutamine dehydrogenase and aspartate aminotransferase [152]. Tolerance to ammonium is cell-line dependent, with GI50 (concentration resulting in a 50% inhibition of cell growth) typically between 1 and 4 mM [148,153,154]. Some cell lines have shown very high tolerance to ammonium, with GI50 > 8 mM [152,155–157].

Compared to ammonium, mammalian cells tolerate higher lactate concentrations, typically with a GI50 ranging between 20 and 60 mM [148,153,154]. Part of the toxic effect seems to be due the increase in osmolarity at those concentrations. Lactate accumulation also leads to a decrease in extracellular pH, if pH is not actively controlled during culture [158]. Interestingly, very high lactate levels can also inhibit lactate dehydrogenase activity, potentially leading to a redox imbalance due to an impaired regeneration of NAD^+ and an accumulation of NADH [152]. A complex interactive effect of lactate and ammonium has been described, in which lactate can decrease ammonium toxicity [154]. Feeding strategies that allow to have reduced glucose concentrations during culture can be used to minimize lactate accumulation [159]. Similar strategies can be used to reduce ammonium production by controlling glutamine concentration [155].

Data on lactate and ammonium production during erythroid cultures is limited and difficult to compare due to difference in culture protocols, cell sources and cultivation methods. Ratcliffe et al. reported ammonium concentrations of up to 1.5 mM in microbioreactor cultures without medium dilution, with lactate concentration ranging between 1.1 and 11.2 mM [100]. Similar lactate and ammonium concentrations were observed by Han et al. (<11.3 mM and <4 mM, respectively) [98]. Bayley et al.

measured up to 12 mM of lactate in their cultures, but ammonium was below the detection limit (<0.3 mM). They also described a superadditive inhibitory effect of lactate and ammonium [101]. Production rates for both byproducts were also estimated by Lee et al. for an immortalized cell line (0.218-0.293 pmol/cell/h for lactate, and 0.015-0.023 pmol/cell/h for ammonium), and by Sivalingam et al. for an hiPSC clone (0.475 and 0.038 pmol/cell/h for lactate and ammonium, respectively) [93,99]. The main mechanism of growth inhibition by lactate in hematopoietic cultures seems to be due to the decrease in pH associated to lactate accumulation, with a mild inhibition (up to 25%) at concentrations >30 mM that could be explained by the increase in osmolarity [160]. An increase in erythroid differentiation at lactate concentrations of up to 10 mM has also been described, potentially associated with an increase in oxidative stress levels in the culture [161].

Although lactate and ammonia are the most studied toxic metabolic byproducts in mammalian cell cultures, novel inhibitory metabolites have been recently identified by following metabolomics approaches. Mulukutla et al. identified a set of 9 metabolites involved in amino acid metabolism (either as byproducts or as intermediates) that are accumulated during CHO cell cultures causing growth inhibition [162]. The concentration of these metabolites could be lowered by using feeding strategies that reduced the effective concentration and uptake rates of specific amino acids during culture, and by genetic engineering to increase the expression level of specific enzymes involved in the catabolic pathways of those amino acids [163]. Accumulation of byproducts of tryptophan and branched-chain amino acid metabolism, polyamine synthesis, and nicotinate metabolism at levels that can inhibit cell growth was also observed in CHO and HEK293 cell cultures [164]. For an overview of such novel inhibitory metabolites, the reviews by Pereira et al. and Coulet et al. are suggested [165,166].

Such novel inhibitors could be involved in the growth limitations observed by Bayley et al. in erythroblast cultures. Although accumulation of lactate, ammonia and inhibitory cytokines like TGF-β was observed in those cultures, final titers did not reach inhibitory levels that could explain the observed decrease in growth rate after 13-16 h from cell inoculation in fresh medium [101].

1.6. Scope of this thesis

The aim of this thesis is to develop a safe and economic process for the production of transfusion-ready cRBCs, focusing on the erythroblast proliferation and differentiation culture stages. Based on the literature review (this chapter), the following challenges for the cost-effective manufacture of cRBC were identified:

- Lack of a clear quantification of the effect of relevant operating parameters (e.g. stirring speed, and oxygen concentration) on erythroblast cultures, which is required for the scale up of the process.
- Growth inhibition in erythroblast proliferation cultures limits the maximum cell densities that can be used during the process, leading to large culture volumes and medium requirements.
- The usage of expensive growth factors and other proteins leads to high culture medium costs.

To achieve the goal of this work, these challenges are addressed by combining experimental and computational approaches at multiple culture scales.

One of the main requirements for cRBC production is the development of a scalable bioreactor culture system, due to the large number of cells needed to meet even a small fraction of the demand for transfusion-ready RBCs. We explored the use of stirred tank bioreactors for erythroblast cultures, focusing on the effect of dissolved oxygen and agitation on cell proliferation and differentiation. Knowing the effect of these two parameters on erythroid cultures is critical, as mixing and oxygen mass transfer may become limiting in large bioreactors when scaling up the process (**Chapter 2**).

The metabolome of animal cell lines commonly used in biopharmaceutical processes, especially for the production of monoclonal antibodies, has been extensively studied. However, available metabolic data of erythroid cultures is limited. We studied the metabolism of cultured erythroblasts, with the aim of identifying putative growth inhibitors, and increasing the productivity of the culture (**Chapter 3**).

Erythroblast cultures requires culture medium containing expensive proteins that make the production of cRBC economically unfeasible. The replacement of such proteins with other low-cost molecules that display the same functionality during culture is a potential solution to reduce the cost of the process. Replacement of transferrin, a protein that binds and transport the iron required for the hemoglobinization of cRBCs, with an iron chelator in erythroid cultures was evaluated (**Chapter 4**).

1.7. References

1. Sender, R.; Fuchs, S.; Milo, R. Revised Estimates for the Number of Human and Bacteria Cells in the Body. *PLOS Biol.* **2016**, *14*, e1002533, doi:10.1371/journal.pbio.1002533.

2. Higgins, J.M. Red Blood Cell Population Dynamics. *Clin. Lab. Med.* **2015**, *35*, 43–57, doi:10.1016/j.cll.2014.10.002.

3. Shrestha, R.P.; Horowitz, J.; Hollot, C.V.; Germain, M.J.; Widness, J.A.; Mock, D.M.; Veng-Pedersen, P.; Chait, Y. Models for the Red Blood Cell Lifespan. *J. Pharmacokinet. Pharmacodyn.* **2016**, *43*, 259–274, doi:10.1007/s10928-016-9470-4.

4. Zhang, H.-D.; Ma, Y.-J.; Liu, Q.-F.; Ye, T.-Z.; Meng, F.-Y.; Zhou, Y.-W.; Yu, G.-P.; Yang, J.-P.; Jiang, H.; Wang, Q.-S.; et al. Human Erythrocyte Lifespan Measured by Levitt's CO Breath Test with Newly Developed Automatic Instrument. *J. Breath Res.* **2018**, *12*, 036003, doi:10.1088/1752-7163/aaacf1.

5. World Health Organization *Action Framework to Advance Universal Access to Safe, Effective and Quality-Assured Blood Products 2020–2023*; World Health Organization, **2020**; ISBN 978-92-4-000038-4.

6. Greinacher, A.; Weitmann, K.; Lebsa, A.; Alpen, U.; Gloger, D.; Stangenberg, W.; Kiefel, V.; Hoffmann, W. A Population-Based Longitudinal Study on the Implications of Demographics on Future Blood Supply. *Transfusion (Paris)* **2016**, *56*, 2986–2994, doi:10.1111/trf.13814.

7. Eichler, H.; Feyer, A.K.; Weitmann, K.; Hoffmann, W.; Henseler, O.; Opitz, A.; Patek, A.; Hans, D.N.; Schönborn, L.; Greinacher, A. Population-Based Analysis of the Impact of Demographics on the Current and Future Blood Supply in the Saarland. *Transfus. Med. Hemotherapy* **2021**, *48*, 175–182, doi:10.1159/000512645.

8. Oliveira, E.M. de; Reis, I.A. What Are the Perspectives for Blood Donations and Blood Component Transfusion Worldwide? A Systematic Review of Time Series Studies. *Sao Paulo Med. J.* **2020**, *138*, 54–59, doi:10.1590/1516-3180.2019.0415.R1.06112019.

9. Liu, W.-J.; Chen, Y.-Y.; Hsu, L.-I.; Chen, J.-W.; Wei, S.-T.; Hou, S.-M. An Imbalance in Blood Collection and Demand Is Anticipated to Occur in the near Future in Taiwan. *J. Formos. Med. Assoc.* **2021**, doi:10.1016/j.jfma.2021.07.027.

10. Bush, L.M.; Healy, C.P.; Javdan, S.B.; Emmons, J.C.; Deans, T.L. Biological Cells as Therapeutic Delivery Vehicles. *Trends Pharmacol. Sci.* **2021**, *42*, 106–118, doi:10.1016/j.tips.2020.11.008.

11. Conrath, S.; Vantilcke, V.; Parisot, M.; Maire, F.; Selles, P.; Elenga, N. Increased Prevalence of Alloimmunization in Sickle Cell Disease? Should We Restore Blood Donation in French Guiana? *Front. Med.* **2021**, *8*, doi:10.3389/fmed.2021.681549.

12. Vichinsky, E.P. Current Issues with Blood Transfusions in Sickle Cell Disease. *Semin. Hematol.* **2001**, *38*, 14–22, doi:10.1016/s0037-1963(01)90056-3.

13. Tormey, C.A.; Hendrickson, J.E. Transfusion-Related Red Blood Cell Alloantibodies: Induction and Consequences. *Blood* **2019**, *133*, 1821–1830, doi:10.1182/blood-2018-08-833962.

14. Zalpuri, S.; Zwaginga, J.J.; le Cessie, S.; Elshuis, J.; Schonewille, H.; van der Bom, J.G. Red-Blood-Cell Alloimmunization and Number of Red-Blood-Cell Transfusions. *Vox Sang.* **2012**, *102*, 144–149, doi:10.1111/j.1423-0410.2011.01517.x.

15. Sanquin Blood Supply Foundation Sanquin Annual Report 2018. **2019**.

16. Daniels, G. *Human Blood Groups*; 3rd ed.; Wiley-Blackwell, **2013**; ISBN 978-1-118-49362-5.

17. Klinkenberg, E.F.; Huis In't Veld, E.M.J.; de Wit, P.D.; van Dongen, A.; Daams, J.G.; de Kort, W.L.A.M.; Fransen, M.P. Blood Donation Barriers and Facilitators of Sub-Saharan African Migrants and Minorities in Western High-income Countries: A Systematic Review of the Literature. *Transfus. Med. Oxf. Engl.* **2019**, *29*, 28–41, doi:10.1111/tme.12517.

18. Vichinsky, E.P.; Earles, A.; Johnson, R.A.; Hoag, M.S.; Williams, A.; Lubin, B. Alloimmunization in Sickle Cell Anemia and Transfusion of Racially Unmatched Blood. *N. Engl. J. Med.* **1990**, *322*, 1617–1621, doi:10.1056/NEJM199006073222301.

19. Pellegrin, S.; Severn, C.E.; Toye, A.M. Towards Manufactured Red Blood Cells for the Treatment of Inherited Anemia. *Haematologica* **2021**, doi:10.3324/haematol.2020.268847.

20. Peyrard, T.; Bardiaux, L.; Krause, C.; Kobari, L.; Lapillonne, H.; Andreu, G.; Douay, L. Banking of Pluripotent Adult Stem Cells as an Unlimited Source for Red Blood Cell Production: Potential Applications for Alloimmunized Patients and Rare Blood Challenges. *Transfus. Med. Rev.* **2011**, *25*, 206–216, doi:10.1016/j.tmrv.2011.01.002.

21. Bax, B.E.; Bain, M.D.; Fairbanks, L.D.; Webster, A.D.B.; Ind, P.W.; Hershfield, M.S.; Chalmers, R.A. A 9-Yr Evaluation of Carrier Erythrocyte Encapsulated Adenosine Deaminase (ADA) Therapy in a Patient with Adult-Type ADA Deficiency. *Eur. J. Haematol.* **2007**, *79*, 338–348, doi:10.1111/j.1600-0609.2007.00927.x.

22. Beutler, E.; Dale, G.L.; Guinto, D.E.; Kuhl, W. Enzyme Replacement Therapy in Gaucher's Disease: Preliminary Clinical Trial of a New Enzyme Preparation. *Proc. Natl. Acad. Sci.* **1977**, *74*, 4620–4623, doi:10.1073/pnas.74.10.4620.

23. Levene, M.; Bain, M.D.; Moran, N.F.; Nirmalananthan, N.; Poulton, J.; Scarpelli, M.; Filosto, M.; Mandel, H.; MacKinnon, A.D.; Fairbanks, L.; et al. Safety and Efficacy of Erythrocyte Encapsulated Thymidine Phosphorylase in Mitochondrial Neurogastrointestinal Encephalomyopathy. *J. Clin. Med.* **2019**, *8*, 457, doi:10.3390/jcm8040457.

24. Meinders, M.; Shoemark, D.; Dobbe, J.G.G.; Streekstra, G.J.; Frayne, J.; Toye, A.M. Expression and Retention of Thymidine Phosphorylase in Cultured Reticulocytes as a Novel Treatment for MNGIE. *Mol. Ther. Methods Clin. Dev.* **2020**, *17*, 822–830, doi:10.1016/j.omtm.2020.03.029.

25. Del C. Batlle, A.M.; Bustos, N.L.; Stella, A.M.; Wider, E.A.; Conti, H.A.; Mendez, A. Enzyme Replacement Therapy in Porphyrias—IV. First Successful Human Clinical Trial of δ-Aminolevulinate Dehydratase-Loaded Erythrocyte Ghosts. *Int. J. Biochem.* **1983**, *15*, 1261–1265, doi:10.1016/0020-711X(83)90216-1.

26. Hammel, P.; Fabienne, P.; Mineur, L.; Metges, J.-P.; Andre, T.; De La Fouchardiere, C.; Louvet, C.; El Hajbi, F.; Faroux, R.; Guimbaud, R.; et al. Erythrocyte-Encapsulated Asparaginase (Eryaspase) Combined with Chemotherapy in Second-Line Treatment of Advanced Pancreatic Cancer: An Open-Label, Randomized Phase IIb Trial. *Eur. J. Cancer* **2020**, *124*, 91–101, doi:10.1016/j.ejca.2019.10.020.

27. Ritter, S.C.; Milanick, M.A.; Meissner, K.E. Encapsulation of FITC to Monitor Extracellular PH: A Step towards the Development of Red Blood Cells as Circulating Blood Analyte Biosensors. *Biomed. Opt. Express* **2011**, *2*, 2012–2021, doi:10.1364/BOE.2.002012.

28. Zhang, Y.; Huang, Y.; Hu, L.; Cheng, T. New Insights into Human Hematopoietic Stem and Progenitor Cells via Single-Cell Omics. *Stem Cell Rev. Rep.* **2022**, *18*, 1322–1336, doi:10.1007/s12015-022-10330-2.

29. Cheng, H.; Zheng, Z.; Cheng, T. New Paradigms on Hematopoietic Stem Cell Differentiation. *Protein Cell* **2020**, *11*, 34–44, doi:10.1007/s13238-019-0633-0.

30. Ovchynnikova, E.; Aglialoro, F.; von Lindern, M.; van den Akker, E. The Shape Shifting Story of Reticulocyte Maturation. *Front. Physiol.* **2018**, *9*, doi:10.3389/fphys.2018.00829.

31. Comazzetto, S.; Shen, B.; Morrison, S.J. Niches That Regulate Stem Cells and Hematopoiesis in Adult Bone Marrow. *Dev. Cell* **2021**, *56*, 1848–1860, doi:10.1016/j.devcel.2021.05.018.

32. Kandarakov, O.; Belyavsky, A.; Semenova, E. Bone Marrow Niches of Hematopoietic Stem and Progenitor Cells. *Int. J. Mol. Sci.* **2022**, *23*, 4462, doi:10.3390/ijms23084462.

33. Li, W.; Guo, R.; Song, Y.; Jiang, Z. Erythroblastic Island Macrophages Shape Normal Erythropoiesis and Drive Associated Disorders in Erythroid Hematopoietic Diseases. *Front. Cell Dev. Biol.* **2021**, *8*, doi:10.3389/fcell.2020.613885.

34. Watowich, S.S. The Erythropoietin Receptor: Molecular Structure and Hematopoietic Signaling Pathways. *J. Investig. Med. Off. Publ. Am. Fed. Clin. Res.* **2011**, *59*, 1067–1072, doi:10.231/JIM.0b013e31820fb28c.

35. Wu, H.; Liu, X.; Jaenisch, R.; Lodish, H.F. Generation of Committed Erythroid BFU-E and CFU-E Progenitors Does Not Require Erythropoietin or the Erythropoietin Receptor. *Cell* **1995**, *83*, 59–67, doi:10.1016/0092-8674(95)90234-1.

36. Lin, C.S.; Lim, S.K.; D'Agati, V.; Costantini, F. Differential Effects of an Erythropoietin Receptor Gene Disruption on Primitive and Definitive Erythropoiesis. *Genes Dev.* **1996**, *10*, 154–164, doi:10.1101/gad.10.2.154.

37. Paulson, R.F.; Hariharan, S.; Little, J.A. Stress Erythropoiesis: Definitions and Models for Its Study. *Exp. Hematol.* **2020**, *89*, 43-54.e2, doi:10.1016/j.exphem.2020.07.011.

38. Huang, E.; Nocka, K.; Beier, D.R.; Chu, T.Y.; Buck, J.; Lahm, H.W.; Wellner, D.; Leder, P.; Besmer, P. The Hematopoietic Growth Factor KL Is Encoded by the Sl Locus and Is the Ligand of the C-Kit Receptor, the Gene Product of the W Locus. *Cell* **1990**, *63*, 225–233, doi:10.1016/0092-8674(90)90303-v.

39. Zsebo, K.M.; Williams, D.A.; Geissler, E.N.; Broudy, V.C.; Martin, F.H.; Atkins, H.L.; Hsu, R.-Y.; Birkett, N.C.; Okino, K.H.; Murdock, D.C.; et al. Stem Cell Factor Is Encoded at the SI Locus of the Mouse and Is the Ligand for the C-Kit Tyrosine Kinase Receptor. *Cell* **1990**, *63*, 213–224, doi:10.1016/0092-8674(90)90302-U.

40. Brannan, C.I.; Lyman, S.D.; Williams, D.E.; Eisenman, J.; Anderson, D.M.; Cosman, D.; Bedell, M.A.; Jenkins, N.A.; Copeland, N.G. Steel-Dickie Mutation Encodes a c-Kit Ligand Lacking Transmembrane and Cytoplasmic Domains. *Proc. Natl. Acad. Sci. U. S. A.* **1991**, *88*, 4671–4674, doi:10.1073/pnas.88.11.4671.

41. Bauer, A.; Tronche, F.; Wessely, O.; Kellendonk, C.; Reichardt, H.M.; Steinlein, P.; Schütz, G.; Beug, H. The Glucocorticoid Receptor Is Required for Stress Erythropoiesis. *Genes Dev.* **1999**, *13*, 2996–3002, doi:10.1101/gad.13.22.2996.

42. Miharada, K.; Hiroyama, T.; Sudo, K.; Nagasawa, T.; Nakamura, Y. Efficient Enucleation of Erythroblasts Differentiated in Vitro from Hematopoietic Stem and Progenitor Cells. *Nat. Biotechnol.* **2006**, *24*, 1255–1256, doi:10.1038/nbt1245.

43. Neildez-Nguyen, T.M.A.; Wajcman, H.; Marden, M.C.; Bensidhoum, M.; Moncollin, V.; Giarratana, M.-C.; Kobari, L.; Thierry, D.; Douay, L. Human Erythroid Cells Produced Ex Vivo at Large Scale Differentiate into Red Blood Cells in Vivo. *Nat. Biotechnol.* **2002**, *20*, 467–472, doi:10.1038/nbt0502-467.

44. Migliaccio, G.; Di Pietro, R.; di Giacomo, V.; Di Baldassarre, A.; Migliaccio, A.R.; Maccioni, L.; Galanello, R.; Papayannopoulou, T. In Vitro Mass Production of Human Erythroid Cells from the Blood of Normal Donors and of Thalassemic Patients. *Blood Cells. Mol. Dis.* **2002**, *28*, 169–180, doi:10.1006/bcmd.2002.0502.

45. Giarratana, M.-C.; Kobari, L.; Lapillonne, H.; Chalmers, D.; Kiger, L.; Cynober, T.; Marden, M.C.; Wajcman, H.; Douay, L. Ex Vivo Generation of Fully Mature Human Red Blood Cells from Hematopoietic Stem Cells. *Nat. Biotechnol.* **2005**, *23*, 69–74, doi:10.1038/nbt1047.

46. Panzenböck, B.; Bartunek, P.; Mapara, M.Y.; Zenke, M. Growth and Differentiation of Human Stem Cell Factor/Erythropoietin-Dependent Erythroid Progenitor Cells In Vitro. *Blood* **1998**, *92*, 3658–3668, doi:10.1182/blood.V92.10.3658.

47. Jobin, C.; Cloutier, M.; Simard, C.; Néron, S. Heterogeneity of in Vitro–Cultured CD34+ Cells Isolated from Peripheral Blood. *Cytotherapy* **2015**, *17*, 1472–1484, doi:10.1016/j.jcyt.2015.05.006.

48. van den Akker, E.; Satchwell, T.J.; Pellegrin, S.; Daniels, G.; Toye, A.M. The Majority of the in Vitro Erythroid Expansion Potential Resides in CD34(-) Cells, Outweighing the Contribution of CD34(+) Cells and Significantly Increasing the Erythroblast Yield from Peripheral Blood Samples. *Haematologica* **2010**, *95*, 1594–1598, doi:10.3324/haematol.2009.019828.

49. Heideveld, E.; Masiello, F.; Marra, M.; Esteghamat, F.; Yağcı, N.; von Lindern, M.; Migliaccio, A.R.F.; van den Akker, E. CD14+ Cells from Peripheral Blood Positively Regulate Hematopoietic Stem and Progenitor Cell Survival Resulting in Increased Erythroid Yield. *Haematologica* **2015**, *100*, 1396–1406, doi:10.3324/haematol.2015.125492.

50. Daniels, D.E.; Downes, D.J.; Ferrer-Vicens, I.; Ferguson, D.C.J.; Singleton, B.K.; Wilson, M.C.; Trakarnsanga, K.; Kurita, R.; Nakamura, Y.; Anstee, D.J.; et al. Comparing the Two Leading Erythroid Lines BEL-A and HUDEP-2. *Haematologica* **2020**, *105*, e389–e394, doi:10.3324/haematol.2019.229211.

51. Trakarnsanga, K.; Griffiths, R.E.; Wilson, M.C.; Blair, A.; Satchwell, T.J.; Meinders, M.; Cogan, N.; Kupzig, S.; Kurita, R.; Nakamura, Y.; et al. An Immortalized Adult Human Erythroid Line Facilitates Sustainable and Scalable Generation of Functional Red Cells. *Nat. Commun.* **2017**, *8*, 14750, doi:10.1038/ncomms14750.

52. Kurita, R.; Suda, N.; Sudo, K.; Miharada, K.; Hiroyama, T.; Miyoshi, H.; Tani, K.; Nakamura, Y. Establishment of Immortalized Human Erythroid Progenitor Cell Lines Able to Produce Enucleated Red Blood Cells. *PLOS ONE* **2013**, *8*, e59890, doi:10.1371/journal.pone.0059890.

53. Ebrahimi, M.; Forouzesh, M.; Raoufi, S.; Ramazii, M.; Ghaedrahmati, F.; Farzaneh, M. Differentiation of Human Induced Pluripotent Stem Cells into Erythroid Cells. *Stem Cell Res. Ther.* **2020**, *11*, 1–13, doi:10.1186/s13287-020-01998-9.

54. Lim, Z.R.; Vassilev, S.; Leong, Y.W.; Hang, J.W.; Rénia, L.; Malleret, B.; Oh, S.K.-W. Industrially Compatible Transfusable IPSC-Derived RBCs: Progress, Challenges and Prospective Solutions. *Int. J. Mol. Sci.* **2021**, *22*, 9808, doi:10.3390/ijms22189808.

55. Heshusius, S.; Heideveld, E.; Burger, P.; Thiel-Valkhof, M.; Sellink, E.; Varga, E.; Ovchynnikova, E.; Visser, A.; Martens, J.H.A.; von Lindern, M.; et al. Large-Scale in Vitro Production of Red Blood Cells from Human Peripheral Blood Mononuclear Cells. *Blood Adv.* **2019**, *3*, 3337–3350, doi:10.1182/bloodadvances.2019000689.

56. Giarratana, M.-C.; Rouard, H.; Dumont, A.; Kiger, L.; Safeukui, I.; Le Pennec, P.-Y.; François, S.; Trugnan, G.; Peyrard, T.; Marie, T.; et al. Proof of Principle for Transfusion of in Vitro–Generated Red Blood Cells. *Blood* **2011**, *118*, 5071–5079, doi:10.1182/blood-2011-06-362038.

57. Griffiths, R.E.; Kupzig, S.; Cogan, N.; Mankelow, T.J.; Betin, V.M.S.; Trakarnsanga, K.; Massey, E.J.; Lane, J.D.; Parsons, S.F.; Anstee, D.J. Maturing Reticulocytes Internalize Plasma Membrane in Glycophorin A–Containing Vesicles That Fuse with Autophagosomes before Exocytosis. *Blood* **2012**, *119*, 6296–6306, doi:10.1182/blood-2011-09-376475.

58. Kupzig, S.; Parsons, S.F.; Curnow, E.; Anstee, D.J.; Blair, A. Superior Survival of Ex Vivo Cultured Human Reticulocytes Following Transfusion into Mice. *Haematologica* **2017**, *102*, 476–483, doi:10.3324/haematol.2016.154443.

59. Iscove, N.N.; Guilbert, L.J.; Weyman, C. Complete Replacement of Serum in Primary Cultures of Erythropoietin-Dependent Red Cell Precursors (CFU-E) by Albumin, Transferrin, Iron, Unsaturated Fatty Acid, Lecithin and Cholesterol. *Exp. Cell Res.* **1980**, *126*, 121–126, doi:10.1016/0014-4827(80)90476-0.

60. Migliaccio, G.; Migliaccio, A.R. Cloning of Human Erythroid Progenitors (BFU-E) in the Absence of Fetal Bovine Serum. *Br. J. Haematol.* **1987**, *67*, 129–133, doi:10.1111/j.1365-2141.1987.00129.x.

61. Boccacci, Y.; Dumont, N.; Doyon, Y.; Laganière, J. Accessory-Cell-Free Differentiation of Hematopoietic Stem and Progenitor Cells into Mature Red Blood Cells. *bioRxiv* **2022**, doi:10.1101/2022.09.14.507311.

62. Olivier, E.N.; Zhang, S.; Yan, Z.; Suzuka, S.; Roberts, K.; Wang, K.; Bouhassira, E.E. PSC-RED and MNC-RED: Albumin-Free and Low-Transferrin Robust Erythroid Differentiation Protocols to Produce Human Enucleated Red Blood Cells. *Exp. Hematol.* **2019**, *75*, 31-52. e15, doi:10.1016/j.exphem.2019.05.006.

63. Wilkinson, A.C.; Ishida, R.; Nakauchi, H.; Yamazaki, S. Long-Term Ex Vivo Expansion of Mouse Hematopoietic Stem Cells. *Nat. Protoc.* **2020**, *15*, 628–648, doi:10.1038/s41596-019-0263-2.

64. Sudo, K.; Yamazaki, S.; Wilkinson, A.C.; Nakauchi, H.; Nakamura, Y. Polyvinyl Alcohol Hydrolysis Rate and Molecular Weight Influence Human and Murine HSC Activity Ex Vivo. *Stem Cell Res.* **2021**, *56*, 102531, doi:10.1016/j.scr.2021.102531.

65. Sakurai, M.; Ishitsuka, K.; Ito, R.; Wilkinson, A.C.; Kimura, T.; Mizutani, E.; Nishikii, H.; Sudo, K.; Becker, H.J.; Takemoto, H.; et al. Chemically Defined Cytokine-Free Expansion of Human Haematopoietic Stem Cells. *Nature* **2023**, *615*, 127–133, doi:10.1038/s41586-023-05739-9.

66. Timmins, N.E.; Nielsen, L.K. Manufactured RBC — Rivers of Blood, or an Oasis in the Desert? *Biotechnol. Adv.* **2011**, *29*, 661–666, doi:10.1016/j.biotechadv.2011.05.002.

67. Taylor, A.C. Responses of Cells to pH Changes in the Medium. *J. Cell Biol.* **1962**, *15*, 201–209, doi:10.1083/jcb.15.2.201.

68. Neutelings, T.; Lambert, C.A.; Nusgens, B.V.; Colige, A.C. Effects of Mild Cold Shock (25°C) Followed by Warming Up at 37°C on the Cellular Stress Response. *PLOS ONE* **2013**, *8*, e69687, doi:10.1371/journal.pone.0069687.

69. Kieninger, J.; Weltin, A.; Flamm, H.; Urban, G.A. Microsensor Systems for Cell Metabolism – from 2D Culture to Organ-on-Chip. *Lab. Chip* **2018**, *18*, 1274–1291, doi:10.1039/C7LC00942A.

70. Place, T.L.; Domann, F.E.; Case, A.J. Limitations of Oxygen Delivery to Cells in Culture: An Underappreciated Problem in Basic and Translational Research. *Free Radic. Biol. Med.* **2017**, *113*, 311–322, doi:10.1016/j.freeradbiomed.2017.10.003.

71. Tse, H.M.; Gardner, G.; Dominguez-Bendala, J.; Fraker, C.A. The Importance of Proper Oxygenation in 3D Culture. *Front. Bioeng. Biotechnol.* **2021**, *9*, 241, doi:10.3389/fbioe.2021.634403.

72. Bajgain, P.; Mucharla, R.; Wilson, J.; Welch, D.; Anurathapan, U.; Liang, B.; Lu, X.; Ripple, K.; Centanni, J.M.; Hall, C.; et al. Optimizing the Production of Suspension Cells Using the G-Rex "M" Series. *Mol. Ther. Methods Clin. Dev.* **2014**, *1*, 14015, doi:10.1038/mtm.2014.15.

73. Nombela-Arrieta, C.; Manz, M.G. Quantification and Three-Dimensional Microanatomical Organization of the Bone Marrow. *Blood Adv.* **2017**, *1*, 407–416, doi:10.1182/bloodadvances.2016003194.

74. Housler, G.J.; Miki, T.; Schmelzer, E.; Pekor, C.; Zhang, X.; Kang, L.; Voskinarian-Berse, V.; Abbot, S.; Zeilinger, K.; Gerlach, J.C. Compartmental Hollow Fiber Capillary Membrane-Based Bioreactor Technology for in Vitro Studies on Red Blood Cell Lineage Direction of Hematopoietic Stem Cells. *Tissue Eng. Part C Methods* **2012**, *18*, 133–142, doi:10.1089/ten.TEC.2011.0305.

75. Allenby, M.C.; Panoskaltsis, N.; Tahlawi, A.; Dos Santos, S.B.; Mantalaris, A. Dynamic Human Erythropoiesis in a Three-Dimensional Perfusion Bone Marrow Biomimicry. *Biomaterials* **2019**, *188*, 24–37, doi:10.1016/j.biomaterials.2018.08.020.

76. Misener, R.; Allenby, M.C.; Fuentes-Garí, M.; Gupta, K.; Wiggins, T.; Panoskaltsis, N.; Pistikopoulos, E.N.; Mantalaris, A. Stem Cell Biomanufacturing under Uncertainty: A Case Study in Optimizing Red Blood Cell Production. *AIChE J.* **2017**, doi:10.1002/aic.16042.

77. Misener, R.; Fuentes Garí, M.; Rende, M.; Velliou, E.; Panoskaltsis, N.; Pistikopoulos, E.N.; Mantalaris, A. Global Superstructure Optimisation of Red Blood Cell Production in a Parallelised Hollow Fibre Bioreactor. *Comput. Chem. Eng.* **2014**, *71*, 532–553, doi:10.1016/j.compchemeng.2014.10.004.

78. Piret, J.M.; Devens, D.A.; Cooney, C.L. Nutrient and Metabolite Gradients in Mammalian Cell Hollow Fiber Bioreactors. *Can. J. Chem. Eng.* **1991**, *69*, 421–428, doi:10.1002/cjce.5450690204.

79. Mohebbi-Kalhori, D.; Behzadmehr, A.; Doillon, C.J.; Hadjizadeh, A. Computational Modeling of Adherent Cell Growth in a Hollow-Fiber Membrane Bioreactor for Large-Scale 3-D Bone Tissue Engineering. *J. Artif. Organs* **2012**, *15*, 250–265, doi:10.1007/s10047-012-0649-1.

80. Zhang, Y.; Wang, C.; Wang, L.; Shen, B.; Guan, X.; Tian, J.; Ren, Z.; Ding, X.; Ma, Y.; Dai, W.; et al. Large-Scale Ex Vivo Generation of Human Red Blood Cells from Cord Blood CD34+ Cells. *Stem Cells Transl. Med.* **2017**, *6*, 1698–1709, doi:10.1002/sctm.17-0057.

81. Andrade-Zaldívar, H.; Kalixto-Sánchez, M.A.; de la Rosa, A.P.B.; De León-Rodríguez, A. Expansion of Human Hematopoietic Cells from Umbilical Cord Blood Using Roller Bottles in CO2 and CO2-Free Atmosphere. *Stem Cells Dev.* **2011**, *20*, 593–598, doi:10.1089/scd.2010.0236.

82. Jagschies, G.; Lindskog, E.; Łącki, K.; Galliher, P. *Biopharmaceutical Processing: Development, Design, and Implementation of Manufacturing Processes*; Elsevier, **2018**; ISBN 978-0-08-100623-8.

83. Platas, O.B.; Sandig, V.; Pörtner, R.; Zeng, A.-P. Evaluation of Process Parameters in Shake Flasks for Mammalian Cell Culture. *BMC Proc.* **2013**, *7*, P17, doi:10.1186/1753-6561-7-S6-P17.

84. Azizan, A.; Büchs, J. Three-Dimensional (3D) Evaluation of Liquid Distribution in Shake Flask Using an Optical Fluorescence Technique. *J. Biol. Eng.* **2017**, *11*, 1–9, doi:10.1186/s13036-017-0070-7.

85. Zhang, H.; Williams-Dalson, W.; Keshavarz-Moore, E.; Shamlou, P.A. Computational-Fluid-Dynamics (CFD) Analysis of Mixing and Gas–Liquid Mass Transfer in Shake Flasks. *Biotechnol. Appl. Biochem.* **2005**, *41*, 1–8, doi:10.1042/BA20040082.

86. Aglialoro, F.; Abay, A.; Yagci, N.; Rab, M.A.E.; Kaestner, L.; van Wijk, R.; von Lindern, M.; van den Akker, E. Mechanical Stress Induces Ca2+-Dependent Signal Transduction in Erythroblasts and Modulates Erythropoiesis. *Int. J. Mol. Sci.* **2021**, *22*, doi:10.3390/ijms22020955.

87. Ohashi, R.; Singh, V.; Hamel, J.-F.P. Perfusion Cell Culture in Disposable Bioreactors. In *Animal Cell Technology: From Target to Market: Proceedings of the 17th ESACT Meeting Tylösand, Sweden, June 10–14, 2001*; Lindner-Olsson, E., Chatzissavidou, N., Lüllau, E., Eds.; ESACT Proceedings; Springer Netherlands: Dordrecht, **2001**; pp. 403–409 ISBN 978-94-010-0369-8.

88. Clincke, M.-F.; Mölleryd, C.; Zhang, Y.; Lindskog, E.; Walsh, K.; Chotteau, V. Very High Density of CHO Cells in Perfusion by ATF or TFF in WAVE Bioreactor™. Part I. Effect of the Cell Density on the Process. *Biotechnol. Prog.* **2013**, *29*, 754–767, doi:10.1002/btpr.1704.

89. Svay, K.; Urrea, C.; Shamlou, P.A.; Zhang, H. Computational Fluid Dynamics Analysis of Mixing and Gas–Liquid Mass Transfer in Wave Bag Bioreactor. *Biotechnol. Prog.* **2020**, *36*, e3049, doi:10.1002/btpr.3049.

90. Timmins, N.E.; Athanasas, S.; Günther, M.; Buntine, P.; Nielsen, L.K. Ultra-High-Yield Manufacture of Red Blood Cells from Hematopoietic Stem Cells. *Tissue Eng. Part C Methods* **2011**, *17*, 1131–1137, doi:10.1089/ten.tec.2011.0207.

91. Boehm, D.; Murphy, W.G.; Al-Rubeai, M. The Effect of Mild Agitation on in Vitro Erythroid Development. *J. Immunol. Methods* **2010**, *360*, 20–29, doi:10.1016/j.jim.2010.05.007.

92. Annathur, G.V.; Pierce, J.L.; Combs, R.G.; Rathore, A.S.; Banerjee, A.; Steinmeyer, D.E. Improvements in Spinner-Flask Designs for Insect-Cell Suspension Culture. *Biotechnol. Appl. Biochem.* **2003**, *38*, 15–18, doi:10.1042/BA20030001.

93. Sivalingam, J.; SuE, Y.; Lim, Z.R.; Lam, A.T.L.; Lee, A.P.; Lim, H.L.; Chen, H.Y.; Tan, H.K.; Warrier, T.; Hang, J.W.; et al. A Scalable Suspension Platform for Generating High-Density Cultures of Universal Red Blood Cells from Human Induced Pluripotent Stem Cells. *Stem Cell Rep.* **2020**, *16*, 182–197, doi:10.1016/j.stemcr.2020.11.008.

94. Lee, E.; Han, S.Y.; Choi, H.S.; Chun, B.; Hwang, B.; Baek, E.J. Red Blood Cell Generation by Three-Dimensional Aggregate Cultivation of Late Erythroblasts. *Tissue Eng. Part A* **2015**, *21*, 817–828, doi:10.1089/ten.tea.2014.0325.

95. Farid, S.S. Process Economics of Industrial Monoclonal Antibody Manufacture. *J. Chromatogr. B* **2007**, *848*, 8–18, doi:10.1016/j.jchromb.2006.07.037.

96. Lopes, A.G. Single-Use in the Biopharmaceutical Industry: A Review of Current Technology Impact, Challenges and Limitations. *Food Bioprod. Process.* **2015**, *93*, 98–114, doi:10.1016/j.fbp.2013.12.002.

97. Collins, P.C.; Nielsen, L.K.; Patel, S.D.; Papoutsakis, E.T.; Miller, W.M. Characterization of Hematopoietic Cell Expansion, Oxygen Uptake, and Glycolysis in a Controlled, Stirred-Tank Bioreactor System. *Biotechnol. Prog.* **1998**, *14*, 466–472, doi:10.1021/bp980032e.

98. Han, S.Y.; Lee, E.M.; Lee, J.; Lee, H.; Kwon, A.M.; Ryu, K.Y.; Choi, W.-S.; Baek, E.J. Red Cell Manufacturing Using Parallel Stirred-Tank Bioreactors at the Final Stages of Differentiation Enhances Reticulocyte Maturation. *Biotechnol. Bioeng.* **2021**, *118*, doi:https://doi.org/10.1002/bit.27691.

99. Lee, E.; Lim, Z.R.; Chen, H.-Y.; Yang, B.X.; Lam, A.T.-L.; Chen, A.K.-L.; Sivalingam, J.; Reuveny, S.; Loh, Y.-H.; Oh, S.K.-W. Defined Serum-Free Medium for Bioreactor Culture of an Immortalized Human Erythroblast Cell Line. *Biotechnol. J.* **2018**, *13*, e1700567, doi:10.1002/biot.201700567.

100. Ratcliffe, E.; Glen, K.E.; Workman, V.L.; Stacey, A.J.; Thomas, R.J. A Novel Automated Bioreactor for Scalable Process Optimisation of Haematopoietic Stem Cell Culture. *J. Biotechnol.* **2012**, *161*, 387–390, doi:10.1016/j.jbiotec.2012.06.025.

101. Bayley, R.; Ahmed, F.; Glen, K.; McCall, M.; Stacey, A.; Thomas, R. The Productivity Limit of Manufacturing Blood Cell Therapy in Scalable Stirred Bioreactors. *J. Tissue Eng. Regen. Med.* **2017**, *12*, e368-e378, doi:10.1002/term.2337.

102. Glen, K.E.; Cheeseman, E.A.; Stacey, A.J.; Thomas, R.J. A Mechanistic Model of Erythroblast Growth Inhibition Providing a Framework for Optimisation of Cell Therapy Manufacturing. *Biochem. Eng. J.* **2018**, *133*, 28–38, doi:10.1016/j.bej.2018.01.033.

103. Law, B.; Gilbert, A.B. Methods of Generating Enucleated Erythroid Cells Using Myo-Inositol. Patent US 2020/0370016 A1, **2021**.

104. Rubius Therapeutics Rubius Therapeutics Reports Fourth Quarter and Full-Year 2018 Financial Results with Business Updates - Rubius Therapeutics Available online: https://ir.rubiustx.com/news-releases/news-release-details/rubius-therapeutics-reports-fourth-quarter-and-full-year-2018/ (accessed on 5 July 2021).

105. Hu, W.; Berdugo, C.; Chalmers, J.J. The Potential of Hydrodynamic Damage to Animal Cells of Industrial Relevance: Current Understanding. *Cytotechnology* **2011**, *63*, 445–460, doi:10.1007/s10616-011-9368-3.

106. Lee, H.J.; Ewere, A.; Diaz, M.F.; Wenzel, P.L. TAZ Responds to Fluid Shear Stress to Regulate the Cell Cycle. *Cell Cycle Georget. Tex* **2018**, *17*, 147–153, doi:10.1080/15384101.2017.1404209.

107. Shi, J.; Wu, B.; Li, S.; Song, J.; Song, B.; Lu, W.F. Shear Stress Analysis and Its Effects on Cell Viability and Cell Proliferation in Drop-on-Demand Bioprinting. *Biomed. Phys. Eng. Express* **2018**, *4*, 045028, doi:10.1088/2057-1976/aac946.

108. Ma, N.; Koelling, K.W.; Chalmers, J.J. Fabrication and Use of a Transient Contractional Flow Device to Quantify the Sensitivity of Mammalian and Insect Cells to Hydrodynamic Forces. *Biotechnol. Bioeng.* **2002**, *80*, 428–437, doi:10.1002/bit.10387.

109. Bixel, M.G.; Kusumbe, A.P.; Ramasamy, S.K.; Sivaraj, K.K.; Butz, S.; Vestweber, D.; Adams, Ralf.H. Flow Dynamics and HSPC Homing in Bone Marrow Microvessels. *Cell Rep.* **2017**, *18*, 1804–1816, doi:10.1016/j.celrep.2017.01.042.

110. Mazo, I.B.; Gutierrez-Ramos, J.-C.; Frenette, P.S.; Hynes, R.O.; Wagner, D.D.; von Andrian, U.H. Hematopoietic Progenitor Cell Rolling in Bone Marrow Microvessels: Parallel Contributions by Endothelial Selectins and Vascular Cell Adhesion Molecule 1. *J. Exp. Med.* **1998**, *188*, 465–474, doi:10.1084/jem.188.3.465.

111. Coste, B.; Mathur, J.; Schmidt, M.; Earley, T.J.; Ranade, S.; Petrus, M.J.; Dubin, A.E.; Patapoutian, A. Piezo1 and Piezo2 Are Essential Components of Distinct Mechanically Activated Cation Channels. *Science* **2010**, *330*, 55–60, doi:10.1126/science.1193270.

112. Andolfo, I.; Alper, S.L.; De Franceschi, L.; Auriemma, C.; Russo, R.; De Falco, L.; Vallefuoco, F.; Esposito, M.R.; Vandorpe, D.H.; Shmukler, B.E.; et al. Multiple Clinical Forms of Dehydrated Hereditary Stomatocytosis Arise from Mutations in PIEZO1. *Blood* **2013**, *121*, 3925–3935, S1-12, doi:10.1182/blood-2013-02-482489.

113. Moura, P.L.; Hawley, B.R.; Dobbe, J.G.G.; Streekstra, G.J.; Rab, M.A.E.; Bianchi, P.; van Wijk, R.; Toye, A.M.; Satchwell, T.J. PIEZO1 Gain-of-Function Mutations Delay Reticulocyte Maturation in Hereditary Xerocytosis. *Haematologica* **2020**, *105*, e268–e271, doi:10.3324/haematol.2019.231159.

114. Moura, P.L.; Hawley, B.R.; Mankelow, T.J.; Griffiths, R.E.; Dobbe, J.G.G.; Streekstra, G.J.; Anstee, D.J.; Satchwell, T.J.; Toye, A.M. Non-Muscle Myosin II Drives Vesicle Loss during Human Reticulocyte Maturation. *Haematologica* **2018**, *103*, 1997–2007, doi:10.3324/haematol.2018.199083.

115. Haase, V.H. Regulation of Erythropoiesis by Hypoxia-Inducible Factors. *Blood Rev.* **2013**, *27*, 41–53, doi:10.1016/j.blre.2012.12.003.

116. Ishikawa, Y.; Ito, T. Kinetics of Hemopoietic Stem Cells in a Hypoxic Culture. *Eur. J. Haematol.* **1988**, *40*, 126–129, doi:10.1111/j.1600-0609.1988.tb00808.x.

117. Chow, D.C.; Wenning, L.A.; Miller, W.M.; Papoutsakis, E.T. Modeling PO2 Distributions in the Bone Marrow Hematopoietic Compartment. I. Krogh's Model. *Biophys. J.* **2001**, *81*, 675–684, doi:10.1016/S0006-3495(01)75732-3.

118. Spencer, J.A.; Ferraro, F.; Roussakis, E.; Klein, A.; Wu, J.; Runnels, J.M.; Zaher, W.; Mortensen, L.J.; Alt, C.; Turcotte, R.; et al. Direct Measurement of Local Oxygen Concentration in the Bone Marrow of Live Animals. *Nature* **2014**, *508*, 269–273, doi:10.1038/nature13034.

119. Parmar, K.; Mauch, P.; Vergilio, J.-A.; Sackstein, R.; Down, J.D. Distribution of Hematopoietic Stem Cells in the Bone Marrow According to Regional Hypoxia. *Proc. Natl. Acad. Sci. U. S. A.* **2007**, *104*, 5431–5436, doi:10.1073/pnas.0701152104.

120. Nombela-Arrieta, C.; Pivarnik, G.; Winkel, B.; Canty, K.J.; Harley, B.; Mahoney, J.E.; Park, S.-Y.; Lu, J.; Protopopov, A.; Silberstein, L.E. Quantitative Imaging of Hematopoietic Stem and Progenitor Cell Localization and Hypoxic Status in the Bone Marrow Microenvironment. *Nat. Cell Biol.* **2013**, *15*, 533–543, doi:10.1038/ncb2730.

121. Acar, M.; Kocherlakota, K.S.; Murphy, M.M.; Peyer, J.G.; Oguro, H.; Inra, C.N.; Jaiyeola, C.; Zhao, Z.; Luby-Phelps, K.; Morrison, S.J. Deep Imaging of Bone Marrow Shows Non-Dividing Stem Cells Are Mainly Perisinusoidal. *Nature* **2015**, *526*, 126–130, doi:10.1038/nature15250.

122. Yokoyama, T.; Etoh, T.; Kitagawa, H.; Tsukahara, S.; Kannan, Y. Migration of Erythroblastic Islands toward the Sinusoid as Erythroid Maturation Proceeds in Rat Bone Marrow. *J. Vet. Med. Sci.* **2003**, *65*, 449–452, doi:10.1292/jvms.65.449.

123. Vlaski, M.; Lafarge, X.; Chevaleyre, J.; Duchez, P.; Boiron, J.-M.; Ivanovic, Z. Low Oxygen Concentration as a General Physiologic Regulator of Erythropoiesis beyond the EPO-Related Downstream Tuning and a Tool for the Optimization of Red Blood Cell Production Ex Vivo. *Exp. Hematol.* **2009**, *37*, 573–584, doi:10.1016/j.exphem.2009.01.007.

124. Bapat, A.; Schippel, N.; Shi, X.; Jasbi, P.; Gu, H.; Kala, M.; Sertil, A.; Sharma, S. Hypoxia Promotes Erythroid Differentiation through the Development of Progenitors and Proerythroblasts. *Exp. Hematol.* **2021**, *97*, 32-46.e35, doi:10.1016/j.exphem.2021.02.012.

125. Simionato, G.; Rabe, A.; Gallego-Murillo, J.S.; van der Zwaan, C.; Hoogendijk, A.J.; van den Biggelaar, M.; Minetti, G.; Bogdanova, A.; Mairbäurl, H.; Wagner, C.; et al. In Vitro Erythropoiesis at Different PO2 Induces Adaptations That Are Independent of Prior Systemic Exposure to Hypoxia. *Cells* **2022**, *11*, 1082, doi:10.3390/cells11071082.

126. Goto, T.; Ubukawa, K.; Kobayashi, I.; Sugawara, K.; Asanuma, K.; Sasaki, Y.; Guo, Y.-M.; Takahashi, N.; Sawada, K.; Wakui, H.; et al. ATP Produced by Anaerobic Glycolysis Is Essential for Enucleation of Human Erythroblasts. *Exp. Hematol.* **2019**, *72*, 14-26.e1, doi:10.1016/j.exphem.2019.02.004.

127. Peniche Silva, C.J.; Liebsch, G.; Meier, R.J.; Gutbrod, M.S.; Balmayor, E.R.; van Griensven, M. A New Non-Invasive Technique for Measuring 3D-Oxygen Gradients in Wells During Mammalian Cell Culture. *Front. Bioeng. Biotechnol.* **2020**, doi:10.3389/fbioe.2020.00595.

128. Young, J.D. Metabolic Flux Rewiring in Mammalian Cell Cultures. *Curr. Opin. Biotechnol.* **2013**, *24*, doi:10.1016/j.copbio.2013.04.016.

129. Luengo, A.; Li, Z.; Gui, D.Y.; Sullivan, L.B.; Zagorulya, M.; Do, B.T.; Ferreira, R.; Naamati, A.; Ali, A.; Lewis, C.A.; et al. Increased Demand for NAD+ Relative to ATP Drives Aerobic Glycolysis. *Mol. Cell* **2021**, *81*, 691-707.e6, doi:10.1016/j.molcel.2020.12.012.

130. Cynober, L.A. Plasma Amino Acid Levels with a Note on Membrane Transport: Characteristics, Regulation, and Metabolic Significance. *Nutr. Burbank Los Angel. Cty. Calif* **2002**, *18*, 761–766, doi:10.1016/s0899-9007(02)00780-3.

131. McMenamy, R.H.; Lund, C.C.; Oncley, J.L. Unbound Amino Acid Concentrations in Human Blood Plasmas. *J. Clin. Invest.* **1957**, *36*, 1672–1679, doi:10.1172/JCI103568.

132. Zielke, H.R.; Sumbilla, C.M.; Zielke, C.L.; Tildon, J.T.; Ozand, P.T. Glutamine Metabolism by Cultured Mammalian Cells. In Proceedings of the Glutamine Metabolism in Mammalian Tissues; Häussinger, D., Sies, H., Eds.; Springer: Berlin, Heidelberg, **1984**; pp. 247–254.

133. Yoo, H.C.; Yu, Y.C.; Sung, Y.; Han, J.M. Glutamine Reliance in Cell Metabolism. *Exp. Mol. Med.* **2020**, *52*, 1496–1516, doi:10.1038/s12276-020-00504-8.

134. Oburoglu, L.; Tardito, S.; Fritz, V.; de Barros, S.C.; Merida, P.; Craveiro, M.; Mamede, J.; Cretenet, G.; Mongellaz, C.; An, X.; et al. Glucose and Glutamine Metabolism Regulate Human Hematopoietic Stem Cell Lineage Specification. *Cell Stem Cell* **2014**, *15*, 169–184, doi:10.1016/j.stem.2014.06.002.

135. Fan, J.; Kamphorst, J.J.; Mathew, R.; Chung, M.K.; White, E.; Shlomi, T.; Rabinowitz, J.D. Glutamine-Driven Oxidative Phosphorylation Is a Major ATP Source in Transformed Mammalian Cells in Both Normoxia and Hypoxia. *Mol. Syst. Biol.* **2013**, *9*, 712, doi:10.1038/msb.2013.65.

136. Hosios, A.M.; Hecht, V.C.; Danai, L.V.; Johnson, M.O.; Rathmell, J.C.; Steinhauser, M.L.; Manalis, S.R.; Vander Heiden, M.G. Amino Acids Rather than Glucose Account for the Majority of Cell Mass in Proliferating Mammalian Cells. *Dev. Cell* **2016**, *36*, 540–549, doi:10.1016/j.devcel.2016.02.012.

137. Chung, J.; Bauer, D.E.; Ghamari, A.; Nizzi, C.P.; Deck, K.M.; Kingsley, P.D.; Yien, Y.Y.; Huston, N.C.; Chen, C.; Schultz, I.J.; et al. The MTORC1/4E-BP Pathway Coordinates Hemoglobin Production with L-Leucine Availability. *Sci. Signal.* **2015**, *8*, ra34, doi:10.1126/scisignal.aaa5903.

138. Wittenberg, J.; Shemin, D. The Location in Protoporphyrin of the Carbon Atoms Derived from the Alpha-Carbon Atom of Glycine. *J. Biol. Chem.* **1950**, *185*, 103–116, doi: 10.1016/S0021-9258(18)56398-5.

139. Garcia-Santos, D.; Schranzhofer, M.; Bergeron, R.; Sheftel, A.D.; Ponka, P. Extracellular Glycine Is Necessary for Optimal Hemoglobinization of Erythroid Cells. *Haematologica* **2017**, *102*, 1314–1323, doi:10.3324/haematol.2016.155671.

140. Stewart, S.; Zhu, B.; Axelrad, A. A "Serum-Free" Medium for the Production of Erythropoietic Bursts by Murine Bone Marrow Cells. *Exp. Hematol.* **1984**, *12*, 309–318, PMID:6723823.

141. Huang, N.-J.; Lin, Y.-C.; Lin, C.-Y.; Pishesha, N.; Lewis, C.A.; Freinkman, E.; Farquharson, C.; Millán, J.L.; Lodish, H. Enhanced Phosphocholine Metabolism Is Essential for Terminal Erythropoiesis. *Blood* **2018**, *131*, 2955–2966, doi:10.1182/blood-2018-03-838516.

142. Lu, Z.; Huang, L.; Li, Y.; Xu, Y.; Zhang, R.; Zhou, Q.; Sun, Q.; Lu, Y.; Chen, J.; Shen, Y.; et al. Fine-Tuning of Cholesterol Homeostasis Controls Erythroid Differentiation. *Adv. Sci.* **2022**, *9*, 2102669, doi:10.1002/advs.202102669.

143. Bernecker, C.; Köfeler, H.; Pabst, G.; Trötzmüller, M.; Kolb, D.; Strohmayer, K.; Trajanoski, S.; Holzapfel, G.A.; Schlenke, P.; Dorn, I. Cholesterol Deficiency Causes Impaired Osmotic Stability of Cultured Red Blood Cells. *Front. Physiol.* **2019**, *10*, doi:10.3389/fphys.2019.01529.

144. Migliaccio, G.; Sanchez, M.; Masiello, F.; Tirelli, V.; Varricchio, L.; Whitsett, C.; Migliaccio, A.R. Humanized Culture Medium for Clinical Expansion of Human Erythroblasts. *Cell Transplant.* **2010**, *19*, 453–469, doi:10.3727/096368909X485049.

145. Zingariello, M.; Bardelli, C.; Sancillo, L.; Ciaffoni, F.; Genova, M.L.; Girelli, G.; Migliaccio, A.R. Dexamethasone Predisposes Human Erythroblasts Toward Impaired Lipid Metabolism and Renders Their Ex Vivo Expansion Highly Dependent on Plasma Lipoproteins. *Front. Physiol.* **2019**, *10*, 281, doi:10.3389/fphys.2019.00281.

146. Justus, D.; Yan, H.; Hale, J.; Blanc, L.; Bitaudeau, F.; Petit, V.; Kinet, S.; Sitbon, M.; Taylor, N.; Narla, M. Evaluating Metabolic Regulation of Human Erythropoiesis By Profiling Nutrient Transporter Expression. *Blood* **2019**, *134*, 342, doi:10.1182/blood-2019-124380.

147. Koury, M.J.; Ponka, P. New Insights into Erythroipoiesis: The Roles of Folate, Vitamin B12, and Iron. *Annu. Rev. Nutr.* **2004**, *24*, 105–131, doi:10.1146/annurev.nutr.24.012003.132306.

148. Ozturk, S.S.; Riley, M.R.; Palsson, B.O. Effects of Ammonia and Lactate on Hybridoma Growth, Metabolism, and Antibody Production. *Biotechnol. Bioeng.* **1992**, *39*, 418–431, doi:10.1002/bit.260390408.

149. Lin, A.; Agrawal, P. Glutamine Decomposition in DMEM: Effect of PH and Serum Concentration. *Biotechnol. Lett.* **1988**, *10*, 695–698, doi:10.1007/BF01025284.

150. Singh, R.P.; Al-Rubeai, M.; Gregory, C.D.; Emery, A.N. Cell Death in Bioreactors: A Role for Apoptosis. *Biotechnol. Bioeng.* **1994**, *44*, 720–726, doi:10.1002/bit.260440608.

151. Schneider, M.; Marison, I.W.; von Stockar, U. The Importance of Ammonia in Mammalian Cell Culture. *J. Biotechnol.* **1996**, *46*, 161–185, doi:10.1016/0168-1656(95)00196-4.

152. Lao, M.-S.; Toth, D. Effects of Ammonium and Lactate on Growth and Metabolism of a Recombinant Chinese Hamster Ovary Cell Culture. *Biotechnol. Prog.* **1997**, *13*, 688–691, doi:10.1021/bp9602360.

153. Cruz, H.J.; Freitas, C.M.; Alves, P.M.; Moreira, J.L.; Carrondo, M.J.T. Effects of Ammonia and Lactate on Growth, Metabolism, and Productivity of BHK Cells. *Enzyme Microb. Technol.* **2000**, *27*, 43–52, doi:10.1016/S0141-0229(00)00151-4.

154. Hassell, T.; Gleave, S.; Butler, M. Growth Inhibition in Animal Cell Culture. The Effect of Lactate and Ammonia. *Appl. Biochem. Biotechnol.* **1991**, *30*, 29–41, doi:10.1007/BF02922022.

155. Glacken, M.W.; Fleischaker, R.J.; Sinskey, A.J. Reduction of Waste Product Excretion via Nutrient Control: Possible Strategies for Maximizing Product and Cell Yields on Serum in Cultures of Mammalian Cells. *Biotechnol. Bioeng.* **1986**, *28*, 1376–1389, doi:10.1002/bit.260280912.

156. Hansen, H.A.; Emborg, C. Influence of Ammonium on Growth, Metabolism, and Productivity of a Continuous Suspension Chinese Hamster Ovary Cell Culture. *Biotechnol. Prog.* **1994**, *10*, 121–124, doi:10.1021/bp00025a014.

157. Yang, M.; Butler, M. Effects of Ammonia on CHO Cell Growth, Erythropoietin Production, and Glycosylation. *Biotechnol. Bioeng.* **2000**, *68*, 370–380, doi:10.1002/(SICI)1097-0290(20000520)68:4<370::AID-BIT2>3.0.CO;2-K.

158. Michl, J.; Park, K.C.; Swietach, P. Evidence-Based Guidelines for Controlling PH in Mammalian Live-Cell Culture Systems. *Commun. Biol.* **2019**, *2*, 1–12, doi:10.1038/s42003-019-0393-7.

159. Konakovsky, V.; Clemens, C.; Müller, M.M.; Bechmann, J.; Berger, M.; Schlatter, S.; Herwig, C. Metabolic Control in Mammalian Fed-Batch Cell Cultures for Reduced Lactic Acid Accumulation and Improved Process Robustness. *Bioengineering* **2016**, *3*, 5, doi:10.3390/bioengineering3010005.

160. Patel, S.D.; Papoutsakis, E.T.; Winter, J.N.; Miller, W.M. The Lactate Issue Revisited: Novel Feeding Protocols To Examine Inhibition of Cell Proliferation and Glucose Metabolism in Hematopoietic Cell Cultures. *Biotechnol. Prog.* **2000**, *16*, 885–892, doi:10.1021/bp000080a.

161. Luo, S.-T.; Zhang, D.-M.; Qin, Q.; Lu, L.; Luo, M.; Guo, F.-C.; Shi, H.-S.; Jiang, L.; Shao, B.; Li, M.; et al. The Promotion of Erythropoiesis via the Regulation of Reactive Oxygen Species by Lactic Acid. *Sci. Rep.* **2017**, *7*, 38105, doi:10.1038/srep38105.

162. Mulukutla, B.C.; Kale, J.; Kalomeris, T.; Jacobs, M.; Hiller, G.W. Identification and Control of Novel Growth Inhibitors in Fed-Batch Cultures of Chinese Hamster Ovary Cells. *Biotechnol. Bioeng.* **2017**, *114*, 1779–1790, doi:10.1002/bit.26313.

163. Mulukutla, B.C.; Mitchell, J.; Geoffroy, P.; Harrington, C.; Krishnan, M.; Kalomeris, T.; Morris, C.; Zhang, L.; Pegman, P.; Hiller, G.W. Metabolic Engineering of Chinese Hamster Ovary Cells towards Reduced Biosynthesis and Accumulation of Novel Growth Inhibitors in Fed-Batch Cultures. *Metab. Eng.* **2019**, *54*, 54–68, doi:10.1016/j.ymben.2019.03.001.

164. Kuang, B.; Dhara, V.G.; Hoang, D.; Jenkins, J.; Ladiwala, P.; Tan, Y.; Shaffer, S.A.; Galbraith, S.C.; Betenbaugh, M.J.; Yoon, S. Identification of Novel Inhibitory Metabolites and Impact Verification on Growth and Protein Synthesis in Mammalian Cells. *Metab. Eng. Commun.* **2021**, *13*, e00182, doi:10.1016/j.mec.2021.e00182.

165. Pereira, S.; Kildegaard, H.F.; Andersen, M.R. Impact of CHO Metabolism on Cell Growth and Protein Production: An Overview of Toxic and Inhibiting Metabolites and Nutrients. *Biotechnol. J.* **2018**, *13*, e1700499, doi:10.1002/biot.201700499.

166. Coulet, M.; Kepp, O.; Kroemer, G.; Basmaciogullari, S. Metabolic Profiling of CHO Cells during the Production of Biotherapeutics. *Cells* **2022**, *11*, 1929, doi:10.3390/cells11121929.

167. Sander, R. Compilation of Henry's Law Constants (Version 4.0) for Water as Solvent. *Atmospheric Chem. Phys.* **2015**, *15*, 4399–4981, doi:10.5194/acp-15-4399-2015.

168. Zander, R. Oxygen Solubility in Normal Human Blood. In *Oxygen Transport to Tissue*; Kovách, A.G.B., Dóra, E., Kessler, M., Silver, I.A., Eds.; Pergamon, **1981**; pp. 331–332 ISBN 978-0-08-027346-4.

169. Christmas, K.M.; Bassingthwaighte, J.B. Equations for O2 and CO2 Solubilities in Saline and Plasma: Combining Temperature and Density Dependences. *J. Appl. Physiol.* **2017**, *122*, 1313–1320, doi:10.1152/japplphysiol.01124.2016.

170. von Lindern, M.; Zauner, W.; Mellitzer, G.; Steinlein, P.; Fritsch, G.; Huber, K.; Löwenberg, B.; Beug, H. The Glucocorticoid Receptor Cooperates with the Erythropoietin Receptor and C-Kit to Enhance and Sustain Proliferation of Erythroid Progenitors in Vitro. *Blood* **1999**, *94*, 550–559, doi:10.1182/blood.V94.2.550.

171. Carlile, G.W.; Smith, D.H.; Wiedmann, M. Caspase-3 Has a Nonapoptotic Function in Erythroid Maturation. *Blood* **2004**, *103*, 4310–4316, doi:10.1182/blood-2003-09-3362.

172. Leberbauer, C.; Boulmé, F.; Unfried, G.; Huber, J.; Beug, H.; Müllner, E.W. Different Steroids Co-Regulate Long-Term Expansion versus Terminal Differentiation in Primary Human Erythroid Progenitors. *Blood* **2005**, *105*, 85–94, doi:10.1182/blood-2004-03-1002.

173. Olivier, E.N.; Qiu, C.; Velho, M.; Hirsch, R.E.; Bouhassira, E.E. Large-Scale Production of Embryonic Red Blood Cells from Human Embryonic Stem Cells. *Exp. Hematol.* **2006**, *34*, 1635–1642, doi:10.1016/j.exphem.2006.07.003.

174. Cheung, J.O.P.; Casals-Pascual, C.; Roberts, D.J.; Watt, S.M. A Small-Scale Serum-Free Liquid Cell Culture Model of Erythropoiesis to Assess the Effects of Exogenous Factors. *J. Immunol. Methods* **2007**, *319*, 104–117, doi:10.1016/j.jim.2006.11.002.

175. Dorn, I.; Lazar-Karsten, P.; Boie, S.; Ribbat, J.; Hartwig, D.; Driller, B.; Kirchner, H.; Schlenke, P. In Vitro Proliferation and Differentiation of Human CD34+ Cells from Peripheral Blood into Mature Red Blood Cells with Two Different Cell Culture Systems. *Transfusion (Paris)* **2008**, *48*, 1122–1132, doi:10.1111/j.1537-2995.2008.01653.x.

2.8. Supplementary information

2.8.1. Comparing *in vivo* and *ex vivo* oxygen concentrations

Multiple parameters are used to describe oxygen content in tissues and in blood, and a good understanding on the relationship between these values is required to translate parameters typically measured *in vivo* and static culture systems (e.g. culture dishes) to operating conditions that are measured and controlled in a bioreactor setting. The first of such variables is the dissolved oxygen concentration in a liquid (C_{O_2}), which is the amount of oxygen (in mass or molar basis) dissolved per unit of liquid volume (typical units: mg O_2/L or μmol O_2/L). The dissolved oxygen concentration can also be expressed as a percentage of the saturation concentration of oxygen in the liquid, a key parameter measured in stirred tank bioreactors. The saturation concentration ($C_{O_2,sat}$; same units as C_{O_2}) will be a function of the composition of the gas that is in equilibrium with the liquid, temperature and pressure. Typically, this relationship can be described using Henry's law:

$$C_{O_2,sat} = H\, p_{O_2}$$

Where H is the Henry coefficient of oxygen, which is highly dependent on the temperature of the system and total concentration of solutes in the liquid. p_{O_2} is the partial pressure of oxygen in the gas phase, which can be calculated from the total gas pressure (P_G) and the molar fraction of oxygen in the gas (y_{O_2}):

$$p_{O_2} = y_{O_2}\, P_G$$

At physiological temperature (37 °C), the Henry coefficient for oxygen on pure water is $H_{O_2,w} = 1.03 \times 10^{-3}$ mol O_2/L/atm (=32.9 mg O_2/L/atm) [167]. Thus, at atmospheric oxygen concentration ($y_{O_2} = 0.2095$) and sea level pressure ($P_G = 1\ \text{atm} = 760\ \text{mmHg} = 101325\ \text{Pa}$), the solubility of oxygen in water is 6.90 mg O_2/L.

Oxygen content in blood is typically reported in volumetric terms: mL of oxygen gas at normal conditions (293.15 K; 1 atm) per mL of blood. Oxygen in blood is present in two forms: dissolved in the liquid phase, and tightly bound to the hemoglobin present inside RBCs. Oxygen can be dissolved in both the plasma and RBC fractions of blood, each having a different oxygen solubility concentration. The Henry coefficients of oxygen on plasma and the intracellular space of RBCs at physiological conditions (37 °C) are 0.0217 and 0.0354 mL/mL/atm, respectively [168,169]. Thus, for an average human adult with an RBC volumetric fraction (hematocrit) of 45%, $H_{O_2,blood}$ is

0.03 mL/mL/atm (=39.24 mg O_2/L/atm) at 37 °C, slightly higher than pure water. This value is also known as the solubility coefficient of oxygen in blood. Dissolved oxygen concentrations in blood and tissue are commonly measured using polarographic electrodes, and are reported as oxygen tension values (p_{O_2}, in mmHg), which can then be converted to mass or volumetric concentrations using the Henry coefficient. In arterial blood, average oxygen tension is 100 mmHg, equivalent to 5.16 mg O_2/L.

Dissolved oxygen represents a small fraction of the total oxygen content in blood, with most oxygen being present bound to hemoglobin. A single hemoglobin molecule can bind to four oxygen molecules, meaning that each gram of fully saturated hemoglobin carries 1.38 mg O_2 (or 1.39 mL O_2/g Hb), a value known as hemoglobin oxygen carrying capacity. This would represent a hemoglobin-bound oxygen content in blood of 287 mg O_2/L (= 200 mL O_2/L blood) for the average blood hemoglobin content in adult humans (145 g Hb/L), around 30× higher than the dissolved oxygen content in blood, and ~98% of the total oxygen blood content. The Hb-bound oxygen concentration is also a function of the fraction of total hemoglobin that is saturated with oxygen, also known as oxygen saturation (S_{O_2}), typically between 97 and 100%. S_{O_2} is highly dependent on the dissolved oxygen concentration in blood. This dependency is described by the oxygen association/dissociation curve.

Supplementary Table S1. Reported culture protocols for the production of cultured red blood cells.

Reference	Cell source	Culture protocol	Culture time	Basal medium	Media supplementations in each stage
von Lindern et al. (1999) [170]	Mononuclear cells from umbilical cord blood, bone marrow, and peripheral blood.	2-stage	*Stage 1:* 5-30 days *Stage 2:* 14 days	CFU-E medium (DMEM supplemented with FCS, holotransferrin, mercaptoethanol, detoxified BSA, sodium bicarbonate, TGFα, estradiol)	*Stage 1:* Epo (0.5 U/mL), SCF (100 ng/mL), dex (0.5 μM) *Stage 2:* Epo (0.5 U/mL)
Migliaccio et al. (2002) [44]	$CD34^+$ cells isolated from aduzlt PBMCs	2-stage	*Stage 1:* 7-25 days *Stage 2:* 5 days	IMDM	*Stage 1:* FBS (20%), SCF (10 ng/mL), Epo (1 U/mL), IL-3 (1 ng/mL), dex (1 μM), estradiol (1 μM) *Stage 2:* FCS (20%), Epo (1 U/mL), insulin (10 ng/mL)
Neildez-Nguyen et al. (2002) [43]	$CD34^+$ cells isolated from umbilical cord blood	3-stage	*Stage 1:* 7 days *Stage 2:* 7 days *Stage 3:* 10 days	Long term marrow culture medium (LCM; prepared as IMDM supplemented with folic acid, L-glutamine, heparin, hydrocortisone, myoinositol, and monothioglycerol) plus BSA, transferrin, ferrous sulfate, ferric nitrate, insulin, soybean lecithin and cholesterol.	*Stage 1:* Flt3-L (50 ng/mL), Tpo (100 ng/mL), SCF (100 ng/mL) *Stage 2:* SCF (50 ng/mL), Epo (3 U/mL), IFG-1 (50 ng/mL) *Stage 3:* Epo (3 U/mL), IFG-1 (50 ng/mL)
Carlile et al. (2004) [171]	$CD34^+$ cells isolated from PBMCs	4-stage	*Stage 1:* 3 days *Stage 2:* 4 days *Stage 3:* 2 days *Stage 4:* 7 days	QBSF-60	*Stage 1:* IL-3 (10 ng/mL), SCF (10 ng/mL) *Stage 2:* IL-3 (10 ng/mL), SCF (10 ng/mL), Epo (2 U/mL) *Stage 3:* SCF (10 ng/mL), Epo (2 U/mL) *Stage 4:* Epo (2 U/mL)
Giarratana et al. (2005) [45]	$CD34^+$ cells isolated from bone marrow, peripheral blood, and umbilical cord blood	3-stage	*Stage 1:* 8 days *Stage 2:* 3 days *Stage 3:* 10 days	LCM supplemented with BSA, transferrin, ferrous sulfate, ferric nitrate and insulin.	*Stage 1:* hydrocortisone (1 μM), SCF (100 ng/mL), IL-3 (5 ng/mL), Epo (3 U/mL) *Stage 2:* coculture on an adherent stromal layer, Epo (3 U/mL). *Stage 3:* coculture on an adherent stromal layer without cytokines.
Leberbauer et al. (2005) [172]	Umbilical cord blood	2-stage	*Stage 1:* 14 days *Stage 2:* 6 days	StemSpan (IMDM supplemented with BSA, insulin, transferrin, and 2-β-mercapto-ethanol)	*Stage 1:* Epo (2 U/mL), Dex (1 μM), IGF-1 (40 ng/mL), SCF (100 ng/mL), cholesterol-rich lipid mix (40 μg/mL) *Stage 2:* Epo (10 U/mL), insulin (10 ng/mL), ZK (3 μM), transferrin (1 mg/mL), human serum (3%)

Reference	Cell source	Culture protocol	Culture time	Basal medium	Media supplementations in each stage
Miharada et al. (2006) [42]	$CD34^+$ cells isolated from umbilical cord blood	4-stage	*Stage 1:* 6 days *Stage 2:* 4 days *Stage 3:* 6 days *Stage 4:* 4 days	Stages 1-3: StemSpan supplemented with plasma protein fraction, lipids (α-tocopherol, linoleic acid, cholesterol), sodium selenite, transferrin, insulin, ethanolamine, and 2-mercaptoethanol. Stage 4: IMDM supplemented with plasma protein fraction, D-mannitol, adenine, and Na2HPO4.	*Stage 1:* SCF (50 ng/mL), EPO (6 U/mL), IL-3 (10 ng/mL), VEGF (10 ng/mL), IGF-2 (250 ng/mL) *Stage 2:* SCF (50 ng/mL), Epo (6 U/mL) *Stage 3:* (50 ng/mL), Epo (2 U/mL). *Stage 4:* mifepristone (1 μM)
Olivier et al. (2006) [173]	Human H1 embryonic stem cells	5-stage	*Stage 1:* 15 days *Stage 2:* 7 days *Stage 3:* 7 days *Stage 4:* 3 days *Stage 5:* 7 days	Stage 1: DMEM supplemented with FBS and non-essential amino acids/ Stages 2-5: StemSpan	*Stage 2:* hydrocortisone (1 μM), IL-3 (13 ng/mL), BMP-4 (13 ng/mL), Flt-3L (33 ng/mL), SCF (100 ng/mL), Epo (2.7 U/mL) *Stage 3:* hydrocortisone (1 μM), IL-3 (13 ng/mL), BMP-4 (13 ng/mL), SCF (40 ng/mL), Epo (3.3 U/mL) *Stage 4:* coculture on an adherent stromal layer, Epo (3 U/mL), hemin (25 μM) *Stage 5:* coculture on an adherent stromal layer, hemin (25 μM)
Cheung et al. (2007) [174]	$CD34^+$ cells isolated from umbilical cord blood	1-stage (only proliferation)	*Stage 1:* 14 days	StemBioA	*Stage 1:* IL-3 (20 ng/mL), IL-6 (100 ng/mL), SCF (100 ng/mL), Epo (1 U/mL)
Dorn et al. (2008) [175]	$CD34^+$ cells isolated from adult PBMCs	2-stage	*Stage 1:* 8 days *Stage 2:* 8 days	DMEM supplemented with BSA, sodium bicarbonate, β-mercaptoethanol, and transferrin.	*Stage 1:* Epo (1 U/mL), SCF (100 ng/mL), IGF-1 (40 ng/mL), dex (1 μM), β-estradiol (1 μM) *Stage 2:* Epo (1 U/mL), insulin (1 μg/mL)
van den Akker et al. (2010) [48]	PBMCs	3-stage	*Stage 1:* 5-6 days *Stage 2:* 8-9 days *Stage 3:* 7 days	StemSpan	*Stage 1:* SCF (100 ng/mL), Epo (2 U/mL), dex (1 μM), IGF-1 (40 ng/mL), IL-3, cholesterol-rich lipids (40 μg/mL) *Stage 2:* SCF (100 ng/mL), Epo (2 U/mL), dex (1 μM), IGF-1 (40 ng/mL), cholesterol-rich lipids (40 μg/mL) *Stage 3:* Epo (10 U/mL), insulin (10 μg/mL), human plasma (3%), T3 (1 μM), IGF-1 (40 μg/mL), holotransferrin (500 μg/mL)

Reference	Cell source	Culture protocol	Culture time	Basal medium	Media supplementations in each stage
Giarratana et al. (2011) [56]	$CD34^+$ cells isolated from adult PBMCs	3-stage	*Stage 1:* 7 days *Stage 2:* 4 days *Stage 3:* 7-17 days	IMDM supplemented with plasma, transferrin, insulin, and heparin	*Stage 1:* SCF (100 ng/mL), IL-3 (5 ng/mL), Epo (3 U/mL), hydrocortisone (10 μM) *Stage 2:* SCF (100 ng/mL), Epo (3 U/mL) *Stage 3:* Epo (3 U/mL)
Griffiths et al. (2012) [57]	$CD34^+$ cells isolated from adult PBMCs	3-stage	*Stage 1:* 8 days *Stage 2:* 3 days *Stage 3:* 20 days	IMDM supplemented with serum, FBS, insulin, heparin, and transferrin	*Stage 1:* SCF (10 ng/mL), IL-3 (1 ng/mL), Epo (3 U/mL). *Stage 2:* SCF (10 ng/mL), Epo (3 U/mL), extra transferrin (final conc.: 1000 μg/mL) *Stage 3:* Epo (3 U/mL), extra transferrin (final conc.: 1000 μg/mL)
Kupzig et al. (2017) [58]	$CD34^+$ cells isolated from adult PBMCs or from cord blood	3-stage	*Stage 1:* 10 days *Stage 2:* 3 days *Stage 3:* 7 days	IMDM supplemented with serum, HSA, insulin, heparin, and transferrin	*Stage 1:* SCF (10 ng/mL), IL-3 (1 ng/mL), Epo (3 U/mL). *Stage 2:* SCF (10 ng/mL), Epo (3 U/mL) *Stage 3:* Epo (3 U/mL)
Zhang et al. (2017) [80]	$CD34^+$ cells isolated from umbilical cord blood	4-stage	*Stage 1:* 5 days *Stage 2:* 6 days *Stage 3:* 5 days *Stage 4:* 2 days	IMDM supplemented with putrescine, selenium, insulin, transferrin and folic acid	*Stage 1:* SCF (100 ng/mL), Flt-3L (100 ng/mL), TPO (50 ng/mL) *Stage 2:* SCF (100 ng/mL), Epo (6 U/mL), IL-3 (20 ng/mL), Flt-3L (100 ng/mL), GM-CSF (15 ng/mL) *Stage 3:* SCF (100 ng/mL), Epo (6 U/mL), IL-3 (10 ng/mL), Flt-3L (50 ng/mL) *Stage 4:* SCF (100 ng/mL), Epo (6 U/mL)
Heshusius et al. (2019) [55]	PBMCs	3-stage	*Stage 1:* 6 days *Stage 2:* 15-25 days *Stage 3:* 12 days	Cellquin (IMDM supplemented with HSA, pyruvate, cholesterol, L-α-Phosphatidylcholine, oleic acid, nucleosides, trace elements, insulin, transferrin, and HSA)	*Stage 1:* Epo (2 U/mL), SCF (100 ng/mL), dex (1 μM), IL-3 (1 ng/mL) *Stage 2:* Epo (2 U/mL), SCF (100 ng/mL), dex (1 μM) *Stage 3:* Epo (10 U/mL), human plasma (5%), transferrin (final conc.: 1000 μg/mL), heparin (5 U/mL)

Abbreviations: BEL-A: Bristol Erythroid Line Adult; BMP-4: bone morphogenetic protein 4; BSA: bovine serum albumin; Dex: dexamethasone; DMEM: Dulbecco's Modified Eagle Medium; Epo: erythropoietin; FBS: fetal bovine serum; FCS: fetal calf serum; Flt-3L: FMS-like tyrosine kinase 3 ligand; GM-CSF: granulocyte-macrophage colony-stimulating factor; HSA: human serum albumin; IFG-1: insulin-like growth factor 1; IGF-2: insulin-like growth factor 2; IL-3: interleukin-3; IMDM: Iscove's modified Dulbecco's medium; PBMCs: peripheral blood mononuclear cells; SCF: stem cell factor; T3: thyroid hormone; TGF- α: transforming growth factor alpha; Tpo: thrombopoetin; VEGF: vascular endothelial growth factor; ZK: Dex antagonist ZK112993.

II

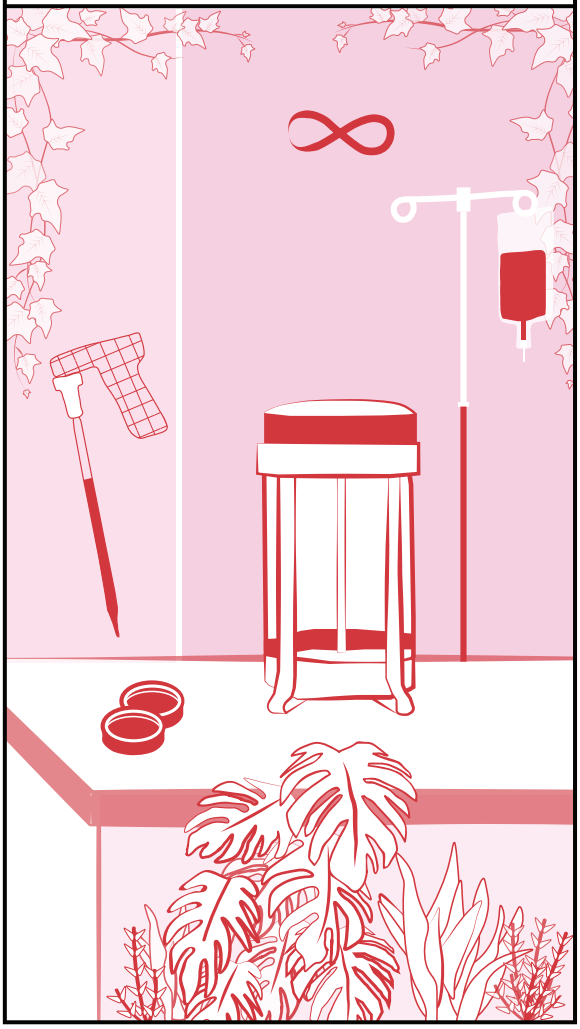

Chapter 2

Expansion and differentiation of *ex vivo* cultured erythroblasts in scalable stirred bioreactors

This chapter has been published in Biotechnology and Bioengineering, Wiley Periodicals LLC. 2022; 119:3096–3116. DOI: 10.1002/bit.28193

Joan Sebastián Gallego Murillo | Giulia Iacono | Luuk A. M. van der Wielen | Emile van den Akker | Marieke von Lindern | Sebastian Aljoscha Wahl

Abstract

Transfusion of donor-derived red blood cells (RBCs) is the most common form of cell therapy. Production of transfusion-ready cultured RBCs (cRBCs) is a promising replacement for the current fully donor-dependent therapy. A single transfusion unit, however, contains 2×10^{12} RBC, which requires large scale production. Here we scale-up cRBC production from static cultures of erythroblasts to 3 L stirred tank bioreactors, and identify the effect of operating conditions on the efficiency of the process. Oxygen requirement of proliferating erythroblasts (0.55-2.01 pg/cell/h) required sparging of air to maintain the dissolved oxygen concentration at the tested setpoint (2.88 mg O_2/L). Erythroblasts could be cultured at dissolved oxygen concentrations as low as 0.7 O_2 mg/mL without negative impact on proliferation, viability or differentiation dynamics. Stirring speeds of up to 600 rpm supported erythroblast proliferation, while 1800 rpm led to a transient halt in growth and accelerated differentiation followed by a recovery after 5 days of culture. Erythroblasts differentiated in bioreactors, with final enucleation levels and hemoglobin content similar to parallel cultures under static conditions.

2.1. Introduction

Blood transfusion is the most common cell therapy to this date. Worldwide about 120 million blood donations, each containing 2×10^{12} red blood cells (RBC), are collected yearly. Nevertheless, availability of blood products for transfusion purposes is not uniformly distributed, with current shortages localized mostly in low-income countries [1]. Globalization and an increasing multiethnicity are societal factors that prompt for a larger, more diverse blood supply to ensure a safe transfusion practice [2,3]. Currently, over 360 blood group antigens are known, being part of more than 35 known blood group systems [4]. Finally, donor-dependent transfusion products harbor a risk for novel bloodborne pathogens that escape current screening programs.

Production of cultured red blood cells (cRBCs) represents a potentially unlimited source of RBCs for transfusion purposes, offering a better control on the quality and safety of the final product. Fully matched cRBCs could be used for patients that have developed alloimmunization or with rare blood groups [5,6]. Furthermore, cRBCs loaded with therapeutics or engineered to present antigens in their surface could be used as a highly efficient drug-delivery system [3,7–9].

Our current *ex vivo* RBC culture protocol starts with peripheral blood mononuclear cells (PBMC) and the commitment of $CD34^+$ hematopoietic stem cells (HSCs) in this fraction to the erythroid lineage, which is characterized by high expression of the transferrin receptor (CD71). Subsequently, erythroblasts expressing glycophorin A ($CD235a^{dim}$), integrin-α4 ($CD49d^{dim\text{-}to\text{-}high}$) and transferrin receptor 1 ($CD71^{high}$) are expanded in presence of erythropoietin (Epo) plus stem cell factor (SCF) and glucocorticoids [10,11]. The addition of SCF and glucocorticoids arrests differentiation and transiently enables renewal divisions of erythroblasts and expansion of a homogeneous erythroblast culture. Withdrawal of glucocorticoids and SCF allows for synchronous differentiation [12,13].

Erythroid cells are commonly cultured in static dishes or flasks, in which spatial inhomogeneities in nutrient concentrations occur due to settling of cells to the bottom surface. Moreover, this cultivation system is susceptible to mass transfer limitations as transfer of oxygen to the culture is fully diffusion-dependent [14–16]. This type of culture systems would culminate in impractical numbers of dishes/flasks (currently about 9 000 - 12 000 T175 flasks for a single transfusion unit) [17,18].

The use of a static culture system in which oxygen transfer is facilitated by a gas-permeable membrane at the bottom of the vessel enabled a 50-fold increase in surface cell density (cells per cm^2) compared to culture dishes [10]. Nevertheless, scale up of this culture protocol is still by area, and limited control on culture conditions can be performed.

Cultivation systems mimicking the microstructure and microenvironment of the bone marrow (BM) niche were developed for cRBC production. Hollow fiber bioreactors enable tissue-like cell concentrations with continuous perfusion of fresh nutrients and dissolved oxygen [19,20]. Microcarriers and porous scaffolds are used, both under static [21,22] and agitated conditions [23]. These biomimetic systems support high erythroblast cell densities. However, scale-up is hampered by gradients in nutrient concentrations along and across hollow fibers [24,25] or inside microcarriers [26,27].

Active agitation of RBC cultures increases nutrient homogeneity and oxygen transfer. This includes roller bottles [28], rocking motion bioreactors [29,30], shake flasks [31,32], and spinner flasks [32–35]. Stirred tank reactors (STRs) additionally allow for online monitoring and control of process parameters such as pH, dissolved oxygen and nutrient concentrations. STRs are commonly used for suspension cultures of different mammalian cells such as CHO, HEK293, hybridoma or Vero cell lines [36–38], reaching volumes of up to ~20 000 L at an industrial scale [39]. This type of reactors can be combined with cell retention systems, such as spin filters or external filtration systems, allowing for continuous culture processes with higher cell densities [40,41].

For cRBCs, small scale STRs (15-500 mL) were used to explore the effects of several operating parameters [42–44]. Some studies reported a large increase in cell numbers, but the conditions that were used varied widely with respect to medium composition, cell density, oxygenation, agitation (impeller type, speed), and nutrient feeding strategy along the different culture stages [42,45]. In most of these cultures, expansion of the cell population was accompanied by differentiation. Erythroblasts undergo major changes during differentiation including reduction of mitochondria, and the change of an actin-based cytoskeleton to a spectrin/ankyrin-based cytoskeleton [46]. Here, we applied defined bioreactor conditions that discriminate between expansion during transient renewal of erythroblasts, and subsequent differentiation to enucleated reticulocytes.

Shear stress is a relevant parameter in scale-up [47]. The impact of shear stress on cultures seems to be cell-line dependent, affecting cell growth, viability, morphology, protein glycosylation, and differentiation fate [48–51]. Shear stress in rocking culture plates or upon orbital shaking in Erlenmeyer flasks reduced erythroblast viability and accelerated erythroid differentiation [29,31]. Enhanced differentiation is in agreement with increased enucleation and reduced cell proliferation reported for STRs [42,45]. The effect of shear stress on erythroblasts may be mediated, at least partially, by the mechanosensitive channel Piezo1, which activates multiple calcium-dependent signaling transduction cascades including the Calcineurin-NFAT pathway, the modulation of STAT5 and ERK signaling, and inside-out integrin activation [31,52,53].

Sparging can also represent a significant source of shear in bioreactor cultures, i.e. due to bubble formation, rise and burst [54–56]. The negative effect of turbulence can be aggravated when higher stirring speeds and gas flow rates are needed upon scale-up to keep the cultures well-mixed with adequate oxygen supply [57]. Nevertheless, it is still unclear if the observed negative effect of sparging on cell cultures is due to the mechanical forces generated during bubble coalescence and breakup, or by biochemical interactions between cells and air bubbles [58–60].

Oxygen availability is a critical parameter in mammalian cell cultures. Cell cultures are often performed under dissolved oxygen (dO_2) concentrations that are higher than those *in vivo*, potentially leading to an increase in oxidative stress, decrease in growth rate, acceleration of cell differentiation, and increase in apoptosis [61]. *In vivo*, erythroblasts are exposed to the hypoxic conditions of the extravascular bone marrow (BM) niche, with a mean oxygen partial pressure of 13.3 mmHg (range: 4.8-21.1 mmHg; [62]), equivalent to a dO_2 concentration of 0.6 mg O_2/L (range: 0.2-0.9 mg O_2/L), or a 8% (range: 3%-13%) of saturation in equilibrium with air (1 atm, 37 °C).

Low oxygen pressure in static culture conditions accelerated erythroblast differentiation, increased hemoglobin levels and the enucleation rates, and increased the expression of the hypoxia-inducible factor 1α (HIF1α) [63,64]. Vlaski et al. also reported accelerated erythroid differentiation, but an increased cell yield in the first culture stage, using gas oxygen concentrations as low as 1.5% [65]. However, it is difficult to predict the local dO_2 concentrations to which cells are exposed in the culture dishes used for these experiments, as static culture systems often display dO_2 gradients [15]. In contrast, a more homogeneous dO_2 concentration can be monitored and controlled in STR cultivations using in-line oxygen measurements. The effect of dO_2 on enucleation and cell yields in STR erythroid cultures depends on other process parameters such as pH, temperature and shear [42].

Oxygen requirements of erythroid cultures are dynamic during the maturation process, with cells switching between oxidative phosphorylation (OXPHOS) and glycolysis [66]. Although oxygen requirements of mature RBCs are well known, there is limited data for erythroid precursors at specific developmental stages. Oxygen consumption rates for erythroblast have been estimated in Seahorse assays, ranging between 0.26 and 1.66 pg/cell/h [67–69]. Erythroblast oxygen requirements in STR cultures range between 0.06 and 0.21 pg/cell/h (cell-specific oxygen consumption rate; q_{O2}), and go as low as 0.01-0.05 pg/cell/h in the later stages of differentiation [45].

In the present study, we report the implementation of our cRBC culture protocol in stirred tank reactors. As oxygen availability was identified as a critical parameter controlling the yields of cRBCs, we estimated the oxygen requirements of erythroblasts

during their transient renewal phase, and evaluated the effect of dissolved oxygen and stirring speed on cell yields during erythroblast expansion and differentiation in this culture system. Based on appropriate culture conditions identified in 0.5 L STRs, we were able to scale up to 3 L STRs, maintaining the same proliferation and differentiation efficiency. To our knowledge, this is the first report of erythroid cultivation in STR bioreactors at >1 L scale, and taking the differentiation stage into account.

2.2. Materials and Methods

2.2.1. Cell culture

Human adult peripheral blood mononuclear cells (PBMCs) were purified by density centrifugation using Ficoll-Paque (density = 1.077 g/mL; 600g, 30 min; GE Healthcare, USA). Informed written consent was given by donors for the use of waste material for research purposes, and was checked by Sanquin's NVT Committee (approval file number NVT0258; 2012) in accordance with the Declaration of Helsinki and the Sanquin Ethical Advisory Board. RBCs were cultured from PBMCs as previously described [10], with minor modifications: nucleosides and trace elements were omitted; cholesterol, oleic acid, and L-α-phosphatidylcholine were replaced by a defined lipid mix (1:1000; Sigma-Aldrich cat#L0288, USA). Expansion cultures were supplemented with erythropoietin (Epo; 1 IU/mL; EPREX®; Janssen-Cilag, The Netherlands), human stem cell factor (hSCF; 50 ng/mL, produced in HEK293T cells), dexamethasone (Dex; 1 µmol/L; Sigma-Aldrich), and interleukin-3 (IL-3; 1 ng/mL, first day only; Stemcell Technologies, Canada). Cell density was maintained between 0.7-2×10^6 cells/mL by daily feeding with fresh expansion medium (either increasing the liquid volume with the addition of fresh medium, or keeping the liquid volume constant by harvesting a fraction of the culture and adding a respective volume of fresh medium).

To induce differentiation, cells were washed and reseeded at 1×10^6 cells/mL in Cellquin medium supplemented with Epo (5 IU/mL), 5% Omniplasma (Octapharma GmbH, Germany), human plasma-derived holotransferrin (1 mg/mL; Sanquin, The Netherlands), and heparin (5 U/mL; LEO Pharma A/S, Denmark). Cells were kept in culture for 11 days, without medium refreshment, until fully differentiated, in either stirred bioreactors or in culture dishes.

2.2.2. Bioreactor and reference culture conditions

All cultivations were performed on either autoclavable (MiniBio 500 mL, or 2 L single wall; glass) or single-use (AppliFlex 0.5 L, or AppliFlex 3.0 L; plastic) stirred bioreactors (Applikon Biotechnology B.V., The Netherlands). For expansion cultures, PBMC-derived erythroblast cultures of at least 150 mL, with a density of 0.7-0.9×10^6 cells/mL were seeded in bioreactors. With the usual seeding methods of PBMC, the required

amount was reached between day 8 and 10. In presence of SCF and dexamethasone, the differentiation stage of the cells remained similar independent of the cultivation duration. The cell concentration was measured every 24 h, and partial media refreshment was performed if the measured cell density was >1.2×10^6 cells/mL, diluting the cell culture to 0.7×10^6 cells/mL. For differentiation cultures, cells were seeded at 1×10^6 cells/mL and cultured without medium additions.

Process control was established using PIMS Lucullus (Securecell AG, Switzerland). Cultures were agitated using a marine impeller (down-pumping) at defined stirring speeds. pH was measured using an AppliSens pH+ probe (AppliSens, The Netherlands) and kept at 7.5 by sparging CO_2 (acid), as culture medium is carbonate-buffered (34.3 mM dissolved $NaHCO_3$). pH probe drift was corrected by recalibration every 2 days using an off-line pH measurement. Dissolved oxygen (dO_2) concentration was monitored using a polarographic probe (AppliSens), and was controlled by sparging pure air using a porous sparger (average pore size = 15 µm). dO_2 values are reported as the percentage relative to the oxygen saturation concentration in water at equilibrium with air (1 atm, 37 °C; 100% = 7.20 mg O_2/L).

Unless indicated otherwise, 0.5 L STR cultures were performed keeping the working volume constant at 300 mL, with a stirring speed of 200 rpm using a marine impeller of diameter 2.8 cm. A constant headspace flow of N_2 (100 mL/min) was used during the whole cultivation to strip excess CO_2 or O_2 from the culture.

Static dish cultures (at 37 °C, air + 5% CO_2 atmosphere) were used in parallel as reference for all tested conditions, with the same inoculum, growth media and seeding/feeding regime performed as in the bioreactors. The dishes surface was 60.1 cm^2, containing 12 mL of medium (liquid height = 2 mm).

2.2.3. Cell characterization

2.2.3.1. Cell count and viability

Cell density was measured in triplicate using an electrical current exclusion method at a size range of 7.5-15 µm and 5-15 µm in expansion and differentiation cultures, respectively (CASY Model TCC; OLS OMNI Life Science, Germany; or Z2 Coulter Counter; Beckman Coulter, USA). Population fold change (FC) was calculated in reference to cell numbers at the start of the growth experiments: $\mathrm{FC} = N(t_i)/N(t_0)$. Viability was determined using a hemocytometer and a dye exclusion method (Trypan Blue; Sigma-Aldrich).

2.2.3.2. Differentiation and viability measurements using flow cytometry

About 200 000 cells were stained in HEPES buffer + 0.5% BSA (30 min, 4 °C), measured using an BD FACSCanto™ II or Accuri C6 flow cytometer (BD Biosciences), gated

against specific isotypes, and analyzed using FlowJo™ (version 10.3). Antibodies or reagents used were: (i) CD235a-PE (1:2500 dilution; OriGene cat#DM066R), CD49d-BV421 (1:100 dilution; BD-Biosciences cat#565277), DRAQ7 (live/dead stain; 1:200 dilution; ThermoFischer Scientific cat#D15106); (ii) CD235a-PE (1:2500 dilution; OriGene cat#DM066R), CD71-APC (1:200 dilution; Miltenyi cat#130-099-219); (iv) PI (live/dead stain; 1:2000 dilution; Invitrogen cat#P3566); (v) AnnexinV-FITC (1:1000 dilution; BioLegend cat#640906), DRAQ7 (live/dead stain; 1:200 dilution; ThermoFischer Scientific cat#D15106); (vi) DRAQ5 (nuclear stain; 1:2500 dilution; abcam cat# ab108410). Stainings with panels (iv), (v) and (vi) were performed 10 minutes before analysis without intermediate washing steps.

2.2.3.3. Cell morphology and hemoglobin content

Cell pellets (2.5×10^6 cells, after centrifugation for 5 min at 600g) were washed with PBS, resuspended in PBS + 5% HSA, and smeared onto microscope slides. Slides were left to air overnight, stained with Hemacolor® Rapid Staining (Sigma-Aldrich), mounted with Entellan® (Merck, Germany), and examined by bright field microscopy (Leica DM5500B; Leica Microsystems, Germany). Hemoglobin content was determined using *o*-phenylenediamine as previously described [70].

2.2.3.4. Lactate and ammonium measurements

Cell culture samples were taken daily before and after medium refreshment. After centrifugation (600g, 5 min), the supernatant was snap frozen in liquid nitrogen and stored at -80 °C until further analysis. Upon thawing, lactate concentrations were measured using a RAPIDlab 1265 blood analyzer (enzymatic amperometric biosensor; Siemens Healthineers, Germany). Ammonium concentration was determined via an enzymatic spectrophotometric assay (Sigma- Aldrich cat#AA0100). Average daily growth rate (μ_{max}), doubling time (τ), and the cell-specific metabolite consumption or production rates (q_{lac}, q_{NH4}) were calculated as described in Supplementary Methods.

2.2.3.5. Oxygen consumption rate determination

For the determination of the oxygen consumption rate of proliferating erythroblast, bioreactor cultures were run at 200 rpm, with no sparging (no active pH or dO_2 control), and with a fixed overhead flow of 100 mL/min air + 5% CO_2 as only source of oxygen. pH was continuously monitored, and passively controlled by the equilibrium between CO_2 in the overhead and the sodium bicarbonate present in the culture medium (pH variation between 7.2 and 7.7 during the cultivation). The cell-specific consumption rate of oxygen (q_{O2}) for each day of culture was determined by the dynamic method, fitting the measured dO_2 data as described in Supplementary Methods and using the experimentally determined mass transfer coefficient of the system (k_La = 0.82 1/h) at the culture conditions.

2.2.4. Statistical analysis

Statistical analyses were performed using unpaired two-tailed two-sample equal-variance Student's *t*-test. All data in figures represent the mean ± the standard deviation of the measurements. The number of replicates is n=3 for all experiments, unless indicated.

2.3. Results

2.3.1. Oxygen consumption by proliferating erythroblasts

To determine the feasibility of erythroblast proliferation in stirred tank bioreactors (STRs), day 9 PBMC-derived erythroblast cultures were seeded in a 2 L STR (working volume = 1 L). Cells were cultured with a stirring speed of 50 rpm (marine impeller; tip speed = 118 mm/s), with air diffusion from the headspace as the sole source of oxygen for the cell culture, similarly to aeration in static culture dishes and orbital shaking [10,31]. We observed complete depletion of oxygen after 6-12 hours in the bioreactor culture, followed by a decrease in cell growth and viability compared to a parallel culture in dishes, albeit only after 24 hours (Figures 1A-C; representative experiment). Continuous sparging of air + 5% CO_2 caused excessive foam production, with cell debris accumulating in foam (data not shown). Proliferation and viability were restored to levels similar or better compared to those of static cultures when headspace aeration was complemented with sparging triggered when the measured dissolved oxygen (dO_2) concentration was lower than 2.88 mg O_2/L (equivalent to 40% of saturation with air; a setpoint typically used in STR mammalian cell cultures; [71–73]) (Figures 1B-C). No foaming was observed under these conditions.

The results prompted to measure the oxygen consumption, for which smaller culture volumes were used (in standardized 0.5 L bioreactors) with headspace aeration (100 mL/min of air + 5% CO_2) and an increased stirring speed (200 rpm; marine impeller; tip speed = 293 mm/s). Day 9 expansion cultures, established from PBMCs, were measured throughout 6 subsequent days of proliferation. Cell numbers were assessed daily, and cultures were diluted with fresh medium, transiently increasing the oxygen concentration (Figures 1D-E). A wide variation of dO_2 was observed, going from as high as 100% of saturation after medium refreshment, to as low as 10% when high cell concentrations were reached. Oxygen was not limiting in these cultures, due to the higher mass transfer coefficient (k_La = 0.82 1/h), and the lower total oxygen demand because of the lower culture volume. The cell-specific oxygen consumption rate (q_{O2}) was calculated for 5 independent cultures at distinct days (Supplementary Methods) and decreased from 2.01±0.53 at the start of the experiment (day 9 of culture) to 0.55±0.24 pg/cell/h 6 days later (Figure 1F; Supplementary Figure S1). The decrease in

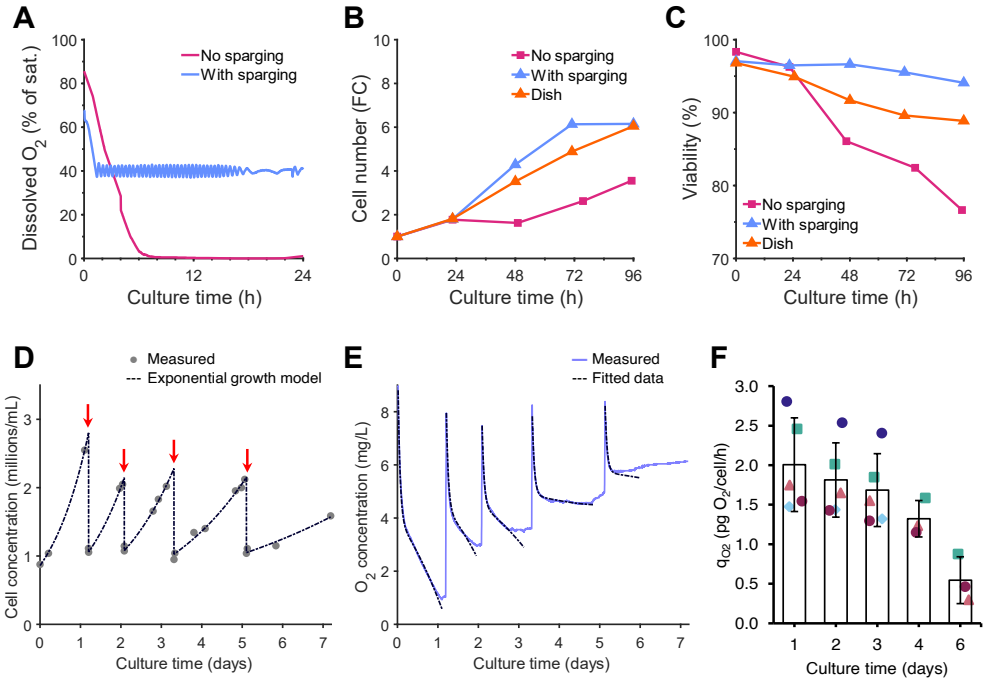

Figure 1. Oxygen can be limiting for erythroblast proliferation in stirred tank bioreactors when headspace aeration is used as sole O_2 source. A-C: Erythroblasts were expanded from PBMCs for 9 days, and subsequently seeded in culture dishes (orange line) or in a 1.5 L STR (working volume: 1 L; stirring speed: 50 rpm; marine down-pumping impeller, diameter: 4.5 cm; 37 °C), in which oxygen was provided by gas flow (air + 5% CO_2) in the headspace (0.3 L/min; purple line, no sparging), or by intermittent sparging triggered at <40% dissolved oxygen (dO_2: % of the oxygen saturation concentration at the culture conditions; blue line), while pH (~7.20) was maintained by bicarbonate-buffered medium in equilibrium with the headspace gas. **(A)** Dissolved oxygen concentration in the culture was measured continuously. **(B)** Erythroblast cell concentration was monitored daily, with medium refreshment if the measured cell concentration was >1.2×10^6 cells/mL. Fold change (FC) in cell number was calculated relative to the number of erythroblasts at the start of culture. **(C)** Culture viability was determined using a trypan blue dye exclusion method. **D-F**: To determine the oxygen requirements of proliferating erythroblasts, day 9 cells were inoculated in 0.5 L STRs (working volume: 300 mL; stirring speed: 200 rpm; marine down-pumping impeller, diameter: 2.8 cm), with a headspace flow of 100 mL/min (air + 5% CO_2) as only source of oxygen for the culture. **(D)** A constant growth rate was fitted for each time interval between consecutive medium refreshment events. **(E)** The drop of dissolved oxygen after each medium refreshment was used to estimate the cell-specific oxygen consumption rate (q_{O_2}) for each time interval, using the experimentally determined mass transfer coefficient (k_La) of 0.82 1/h (see Supplementary Methods). **(F)** The average cell-specific oxygen consumption rate, q_{O_2}, during erythroblast expansion was calculated as the mean of at 5 independent bioreactor runs (time intervals for which the q_{O_2} was calculated for each run available in Supplementary Figure S1). Panels A-E show data for a representative reactor run.

oxygen consumption mirrored a decrease in cell proliferation (Figure 1D). It was shown earlier that cultures undergo limited spontaneous differentiation (as measured in the increase of $CD235a^+/CD71^{low}$ cells), reducing the expansion rate of the erythroblast population [10]. Moreover, differentiating erythroblasts require less oxygen [45]. Such enhanced spontaneous differentiation of erythroblasts could explain both the reduced proliferation and decreased oxygen consumption.

Although headspace aeration can ensure oxygen availability in 0.5 L bioreactor cultures, a faster aeration system will be required to ensure sufficient O_2 supply in cultures with increased volume or higher cell density. Additionally, due to the limited transfer rate, the dissolved oxygen level cannot be controlled well using headspace aeration only (i.e. long response times), which makes the evaluation of the effect of specific dO_2 concentrations on erythroblast cultures challenging.

2.3.2. Controlled aeration supports erythroblast expansion in stirred tank bioreactors

To improve the dO_2 control in 0.5 L bioreactors, we used intermittent sparging of air, combined with a continuous headspace flow of nitrogen (100 mL N_2/min) to strip excess O_2 from the culture and drive dO_2 to the desired setpoint (40% dO_2) (Supplementary Figure S2A). Intermittent sparging of CO_2 controlled the pH (=7.5; Supplementary Figure S2B).

Day 9 PBMC-derived erythroblast cultures were seeded in the bioreactors at an initial cell concentration of 0.7×10^6 cells/mL (Figure 2A). Erythroblasts seeded in culture dishes were cultured in parallel using similar medium refreshment conditions as reference.

The growth profile was comparable between bioreactor and static cultures, showing a 750-fold increase in cell number after 10 days of culture (resp. day 9 to day 18 counting from PBMC isolation and seeding; Figure 2B). No significant difference was found between the viability of bioreactor and dish cultures (day 10 PI^- events: 92.9%±1.1% in bioreactors, 94.5%±0.4% in culture dishes; Figure 2C). Flow cytometry indicated that most cells were committed to the erythroid lineage at the start of the bioreactor culture (<10% $CD235a^-/CD71^-$ cells; >70% $CD235a^+$; Figure 2D; gating strategy available in Supplementary Figure S3). Although sustained proliferation of $CD235a^+/CD49d^+/CD71^{high}$ erythroblasts can be maintained in presence of EPO, hSCF and dexamethasone, some spontaneous differentiation can take place, initially leading to an increase in $CD235a^+$ cells, and a subsequent gradual decrease of CD49d and CD71 expression. Both in bioreactors and dishes the percentage of $CD235a^+/CD71^{low}$ and $CD235a^+/CD49d^-$ cells was maintained lower than 10% during the whole cultivation (Figures 2D-E). During the last 5 days of the experiment (day 14-19 after seeding PBMCs), the mean

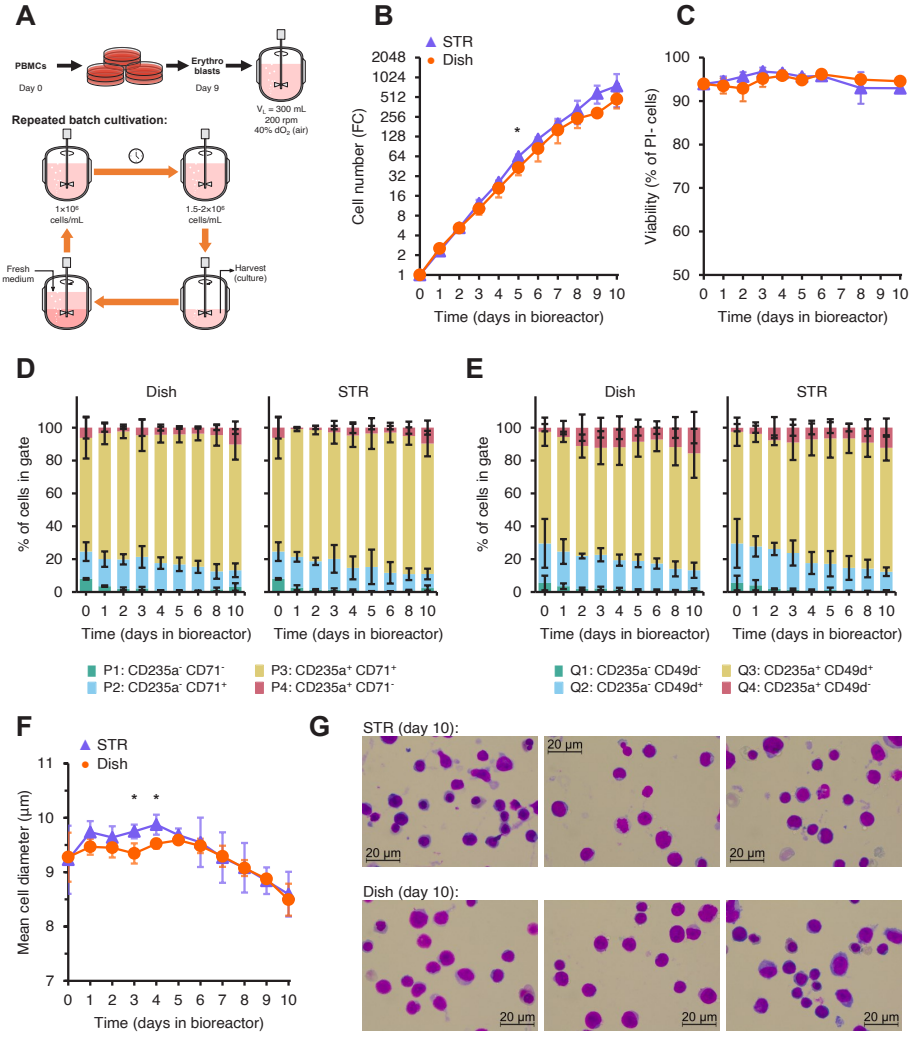

Figure 2. Efficient expansion of erythroblasts can be achieved in stirred tank bioreactors. Erythroblasts were expanded from PBMCs for 9 days, and subsequently seeded in culture dishes (orange lines) or STRs (blue lines) at a starting cell concentration of 0.7×10^6 cells/mL. STRs were run with a constant N_2 headspace flow to fully control dO_2 and pH. **(A)** Cells were cultured using a sequential batch feeding strategy: medium was refreshed when the cell concentration (measured daily) was $>1.2\times10^6$ cells/mL. **(B)** Cell concentration during 10 days of expansion (fold change (FC) compared to start of the culture). **(C-E)** Cells were stained with propidium iodide (PI; the percentage of PI^- cells indicate the % of viable cells) **(C)**, and with CD235a plus CD71 **(D)**, or CD235a plus CD49d **(E)** (gating strategy available in Supplementary Figure S3). **(F)** Mean cell diameter (of cells >5 µm) was measured daily. **(G)** Cytospin cell morphology by May-Grünwald-Giemsa (Pappenheim) staining of cultures after 10 days of expansion. All data is displayed as mean ± SD (error bars; n=3 reactor runs / donors). Significance is shown for the comparison with dish cultures (unpaired two-tailed two-sample equal-variance Student's *t*-test; $^*p<0.05$, $^{**}p<0.01$, $^{***}p<0.001$, not displayed if difference is not significant).

cell diameter gradually decreased (Figure 2F). Staining with AnnexinV and DRAQ7 indicated only a low percentage of apoptotic or dead cells (Supplementary Figure S3D), whereas cytospins indicated a large portion of cells with condensed nuclei (Figure 2G), indicative of spontaneous differentiation. Thus, spontaneous differentiation, rather than decreased viability, reduced the proliferative capacity of day 17-19 cultures. Importantly, this was similar between static cultures and cells cultured in bioreactors.

2.3.3. Effect of dO_2 concentration on erythroblast expansion cultures

Standard mammalian cell culture conditions are mostly hyperoxic compared to their native *in vivo* niche, potentially leading to oxidative stress and impaired growth [61]. The 40% dO_2 used in our initial experiments, equivalent to 2.88 mg O_2/mL, is 5-fold higher than the oxygen concentration in the bone marrow compartment in which erythroblast proliferation and differentiation takes place (0.6 mg O_2/mL; [62]). Therefore, we tested whether BM-mimicking oxygen concentrations also supported erythroblast expansion. Bioreactor cultures at 10% dO_2 (0.72 mg O_2/L) showed comparable cell yields to dish conditions (Figure 3A), while requiring lower volumes of sparged air compared to 40% dO_2 (Supplementary Figure S4A). A continuous decrease of growth rate, from 0.78±0.19 1/day to 0.45±0.05 1/day after 8 days of culture, was observed in bioreactor cultures at 10% dO_2. By contrast, in hyperoxic bioreactor cultures (dO_2 = 40%) the growth rate was stable at ~0.78 1/day for the first 5 days of culture, followed by a decrease to 0.38±0.12 1/day at day 8 of cultivation (Figure 3B; growth rates calculated using cell counts available in Supplementary Figure S4C).

Figure 3. Low dissolved oxygen concentration support erythroblast expansion. Erythroblasts were expanded from PBMCs for 9 days, and subsequently seeded in culture dishes (orange line) or STRs (100 mL/min N_2 headspace flow) at a starting cell concentration of 0.7×10^6 cells/mL. Dissolved oxygen was controlled by air sparging when below the targeted setpoint (10% (purple line) or 40% (blue line), equivalent to 0.72 and 2.88 mg O_2/L respectively), and by stripping of excess oxygen using 100 mL/min N_2 headspace flow. **(A)** Cell concentration monitored for 8 days of culture, with medium refreshment when the measured cell concentration (daily) was $>1.2\times10^6$ cells/mL. Fold change (FC) in cell number was calculated using the number of erythroblasts at the start of culture. **(B)** Growth rate was calculated for each day using the total biomass concentration (μm^3 of total cell volume per mL of culture) assuming exponential growth between consecutive media refreshment events. **(C)** Mean cell diameter was measured daily. **(D-E)** Cells were stained with CD235a plus CD71 **(D)**, or CD235a plus CD49d **(E)**. **(F)** Cell-specific lactate production rate ($q_{lac,vol}$) calculated using growth rate data and measured extracellular lactate concentrations (see Supplementary Methods). All data is displayed as mean ± SD (error bars; n=3 reactor runs / donors, unless indicated otherwise). Significance is shown for the comparison with dish cultures (unpaired two-tailed two-sample equal-variance Student's *t*-test; $^*p<0.05$, $^{**}p<0.01$, $^{***}p<0.001$, not displayed if difference is not significant). Growth rates and q_{lac} calculated using cell counts available in Supplementary Figure S4.

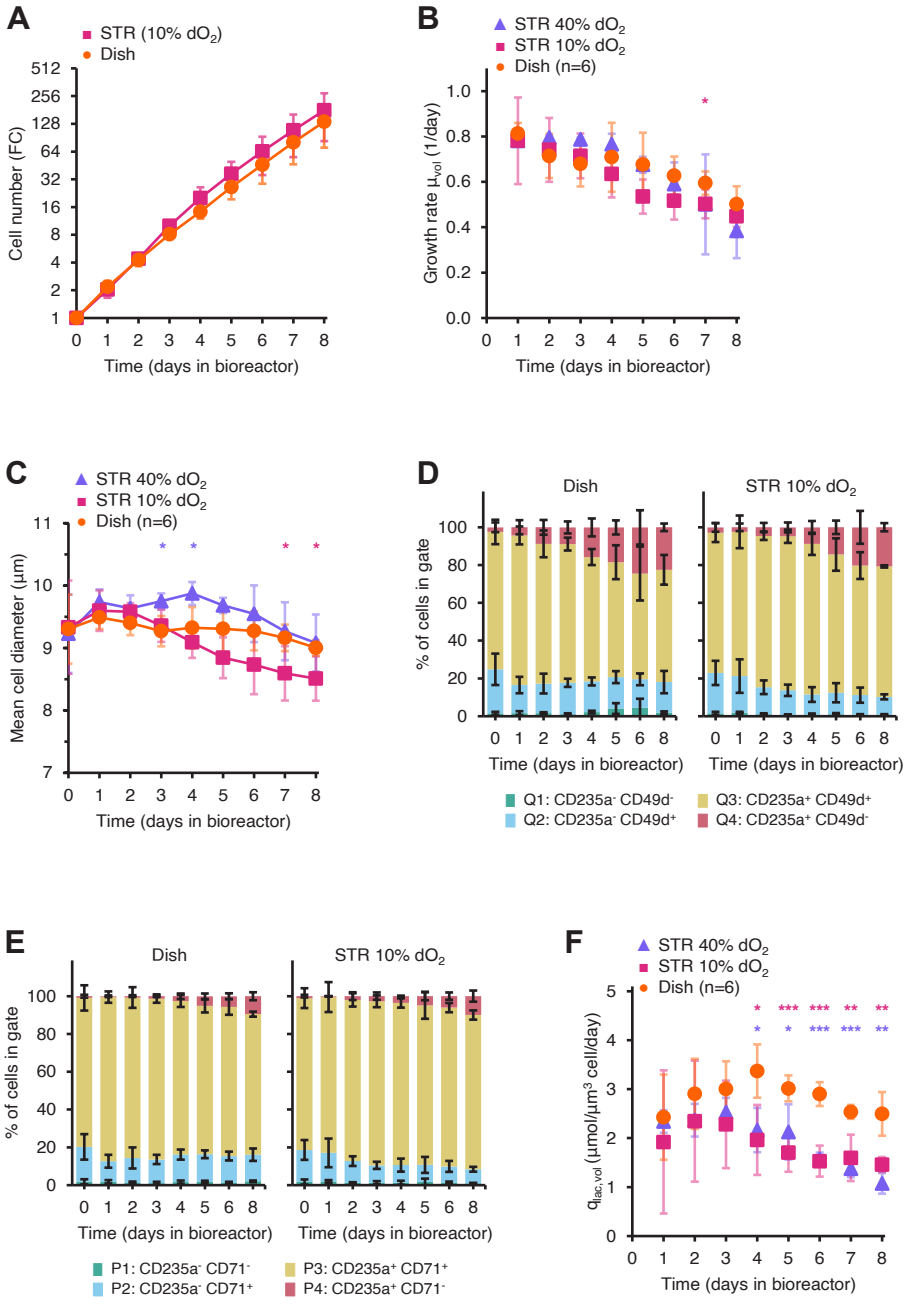

Figure 3.
(See caption on previous page)

Cell size also decreased faster during the culture period at 10% dO_2 (Figure 3C). This may indicate partial differentiation within the population of $CD235a^+/CD71^+/CD49d^+$ population, or a reduced protein synthesis at this lower O_2 concentration [74]. Although the percentage of $CD235a^+/CD49d^-/CD71^{low}$ cells increased during culture, this was similar between bioreactors at 10% dO_2 and standard static cultures (Figure 3D-E). Lactate, typically produced by aerobic glycolysis and glutaminolysis, may negatively influence erythroblast growth and viability. Extracellular lactate concentrations were typically <6 mM during culture in bioreactors or culture dishes (Supplementary Figure S2E). Nevertheless, a consistently lower cell-specific lactate production rate ($q_{lac,vol}$) was observed in bioreactor conditions both at 10 and 40% dO_2, compared to culture dishes (>20% reduction; Figure 3F; $q_{lac,counts}$ available in Supplementary Figure S4D), suggesting a higher rate of aerobic glycolysis in static cultures. The q_{lac} values decreased after 4 days of culture in both bioreactors and dish cultures to the same extent, which may be due to the concurrent reduction in growth rate. In addition to lactate, ammonia is a common inhibitor of cell proliferation. The ammonia production, however, was similar in bioreactor runs at 10% or 40% dO_2 and in standard dish cultures (Supplementary Figure S4B,E).

Although a 10% dO_2 setpoint is closer to the physiological oxygen concentrations in which erythroblasts proliferate *in vivo*, we conclude that the lower dO_2 does not alter growth or spontaneous differentiation compared to a 40% dO_2 setpoint.

2.3.4. Shear stress affects erythroblast proliferation during expansion cultures

Shear stress is another critical parameter in mammalian cell cultures. It can have a negative effect on growth and viability [75], whereas insufficient stirring speeds leads to inadequate mixing and aeration when scaling up [57]. To evaluate the effect of stirring speed on erythroblast proliferation, erythroblasts were inoculated in 0.5 L bioreactors, and the impeller speed was increased from 200 rpm to 600 rpm (tip speed = 880 mm/s) and 1800 rpm (tip speed = 2640 mm/s). After 6 days of culture, a 87.2±2.7-fold change in cell number was observed in the 600 rpm cultivations (Figure 4A), similar to the growth levels previously observed at 200 rpm and in static cultures. By contrast, an agitation speed of 1800 rpm reduced proliferation during the first 4 days of culture, which, however, recovered to values comparable to those observed at 600 rpm after 6 days of culture (Figure 4B).

The increase in stirring speed to 600 rpm did not enhance spontaneous differentiation, with only 12.1±2.8% cells in the most differentiated $CD235^+$ $CD49d^-$ compartment at day 6. At 1800 rpm, however, CD49d expression decreased in the first 3 days of culture,

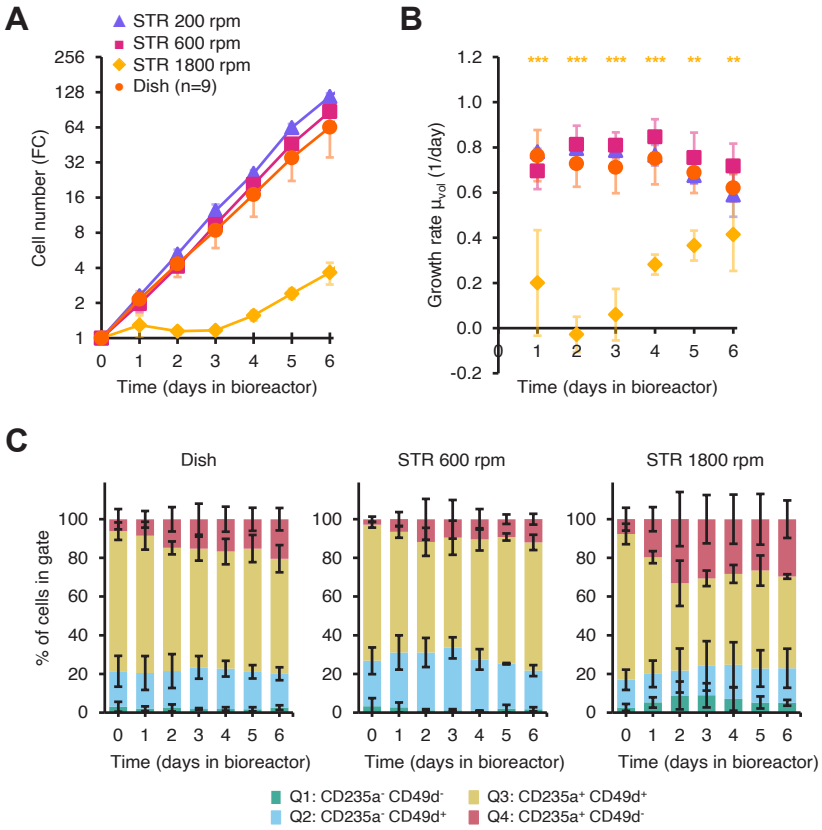

Figure 4. High stirring speeds can sustain erythroblast expansion. Erythroblasts were expanded from PBMCs for 9 days, and subsequently seeded in culture dishes (orange line) or STRs (dO_2: 40% controlled by sparging of air; 100 mL/min N_2 headspace flow) at a starting cell concentration of 0.7×10^6 cells/mL, under agitation at 200 (blue line), 600 (purple line) or 1800 rpm (yellow line). **(A)** Cells were maintained between 0.7 and 1.5×10^6 cells/mL by dilution with fresh medium. Cumulative cell numbers were calculated and represented as fold change (FC) compared to the start of the experiment. **(B)** Growth rate for each day was calculated assuming exponential growth between consecutive media refreshment events. **(C)** Cells were stained with CD235a plus CD49d to evaluate the progression of spontaneous differentiation during culture. All data is displayed as mean ± SD (error bars; n=3 reactor runs / donors, unless indicated otherwise). Significance is shown for the comparison with dish cultures (unpaired two-tailed two-sample equal-variance Student's *t*-test; $^*p<0.05$, $^{**}p<0.01$, $^{***}p<0.001$, not displayed if difference is not significant).

stabilizing in the following days (Figure 4C). Cell cycle progression was not affected by the stirring speed (Supplementary Figure S5).

2.3.5. Terminal differentiation of erythroblast cultures in biore actors

We validated that erythroblasts expanded in bioreactors could be differentiated as standard static cultures throughout all conditions (data not shown). To examine terminal differentiation in bioreactors, day 10 PBMC-derived erythroblast cultures were seeded in differentiation medium at a starting cell concentration of 1.5×10^6 cells/mL, both in bioreactors and culture dishes (Figure 5A). Bioreactors were controlled with the same conditions as in the reference expansion phase (40% dO_2, pH 7.5, 200 rpm, 37 °C). During the first 3 days of differentiation, cell numbers increased in both systems. Simultaneously, sparging was required to maintain dO_2 at 40% (Supplementary Figure S6). This was followed by a cell cycle arrest in both static and bioreactor conditions. Bioreactor cultures showed a gradual decrease in cell numbers until the end of culture, while cell numbers in static conditions remained similar (Figure 5B). Concurrently, the dO_2 concentration increased in absence of sparging after 4 days of culture. A similar decrease in cell numbers was also observed for differentiating erythroblasts subjected to orbital shaking compared to static controls (manuscript in preparation). Here, the decrease was shown to originate from a disintegration of stiff pyrenocytes, whereas the number of enucleated and more flexible reticulocytes remained constant.

Differentiation was evident from a decrease in mean cell diameter in bioreactors and culture dishes (Figure 5C) with a concomitant loss of CD49d and CD71 expression (Figure 5D-E). Hemoglobin accumulation and enucleation efficiency was also similar

Figure 5. Erythroblast differentiation can be achieved in stirred tank bioreactors. Erythroblasts were expanded from PBMCs for 10 days, and subsequently seeded in differentiation medium at a starting cell concentration of 1×10^6 cells/mL. **(A)** Cells were transferred to culture dishes or STRs and kept in culture for 11 subsequent days without medium refreshment. **(B)** Cell concentration during 11 days of differentiation in STRs (blue symbols) and dishes (orange symbols). **(C)** Mean cell diameter was measured daily. **(D-E)** Cells were stained with CD235a plus CD49d **(D)**, or CD235a plus CD71 **(E)**, and percentages in each quadrant are shown. **(F)** Enucleation percentage of erythroid cells was calculated from the forward scatter and DRAQ5 staining. $DRAQ5^-$ cell numbers (reticulocytes, R) were divided by the sum of small $DRAQ5^+$ events (nuclei, N + reticulocytes, R). **(G)** Hemoglobin was measured in arbitrary units (a.u.) and the intracellular hemoglobin concentration was calculated using the total cell volume. **(H)** Representative cytospin cell morphology by May-Grünwald-Giemsa (Pappenheim) staining of bioreactor cultures during differentiation. All data is displayed as mean ± SD (error bars; n=3 reactor runs / donors). Significance is shown for the comparison with dish cultures (unpaired two-tailed two-sample equal-variance Student's *t*-test; $^*p<0.05$, $^{**}p<0.01$, $^{***}p<0.001$, not displayed if difference is not significant).

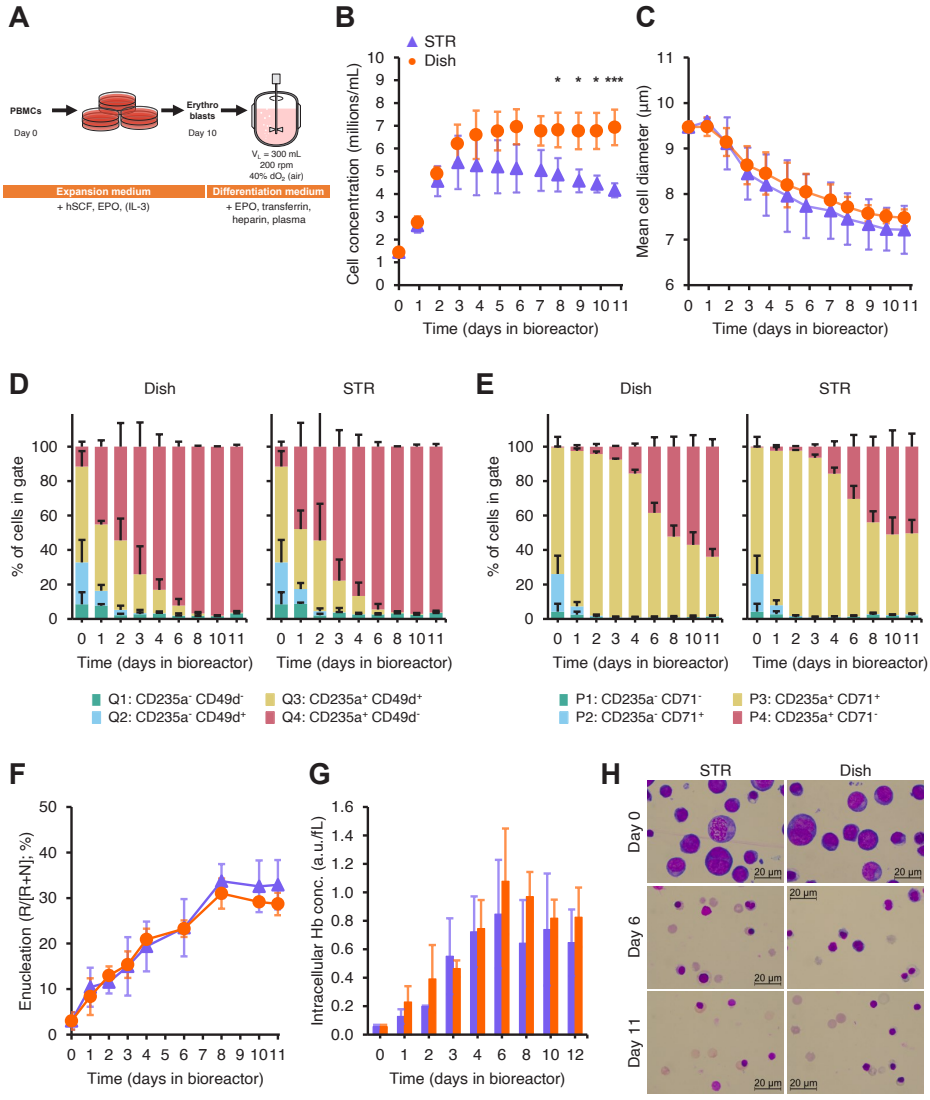

Figure 5.
(See caption on previous page)

in static and stirred bioreactors (Figure 5F-G). Presence of enucleated cells and egressed nuclei was confirmed by cytospins (Figure 5H). In conclusion, erythroblast differentiation could also be supported in our stirred bioreactor systems, reaching similar levels of enucleation to those of culture dishes, albeit with slightly lower cell yields.

2.3.6. Expansion cultures can be scaled up to 3L bioreactors

Knowing the boundaries of cultured erythroblast in STRs enabled us to scale-up from 300 mL cultures in 500 mL STRs to larger volumes. Day 8 erythroblasts cultures from PBMCs were seeded at a density of 0.7×10^6 cells/mL in a 500 mL STR (initial culture volume = 100-150 mL), and cell density was adjusted daily to 0.7×10^6 cells/mL by adding more medium. When the volume surpassed 400 mL, cells were transferred to a 3 L STR (minimum working volume = 800 mL), operated with a tip speed similar to that tested in 0.5 L bioreactors (300 mm/s; single down-pumping marine impeller; diameter = 5 cm; 115 rpm). Medium was added to maintain cell density until a total volume of 2.5 L was reached. Subsequently, the total volume was maintained at 2.5 L and excess cells were removed (Figure 6A-B). The cell cultures proliferated exponentially for 9 subsequent days achieving an average 196-fold increase in the 3L STR, and 234-fold under static conditions (Figure 6C). Interestingly, the variation between 3 cultures was smaller in the STR (range: 112-280-fold) compared to the same cultures expanded in dishes (range: 51-462-fold). After 9 days of culture, there was no difference in viability or differentiation stage of the cells (Figure 6D-E; Supplementary Figure S7A). Similar to the 300 mL cultures, lactate production in 2.5 L STRs was lower compared to static conditions (Supplementary Figure S7B).

Figure 6. Scale-up of erythroblast expansion to 3 L stirred tank bioreactors. Erythroblasts were expanded from PBMCs for 8 days, and subsequently seeded in culture dishes or 0.5 L stirred tank bioreactors (starting volume: 100-200 mL) at a starting cell concentration of 0.7×10^6 cells/mL. **(A)** Cells were kept in culture following a fed batch feeding strategy in which medium was refreshed if the measured cell concentration (daily) was $>1.2\times10^6$ cells/mL. Upon reaching a total number of >400 million cells, the culture was transferred to a 3.0 L bioreactor (starting volume: 800 mL; 115 rpm with marine down-pumping impeller, diameter: 5.0 cm), which was progressively filled by daily medium additions. **(B)** Culture volume in the bioreactor for an exemplary run. Transition from the 0.5 L to the 3 L reactor was performed at day 3 of culture (red arrow). Upon filling of the 3 L reactor (blue arrow), excess cells were harvested daily to keep a working volume of 2.5-2.7 L. **(C)** Erythroblast cell concentration was monitored for 9 days of culture. Fold change (FC) in cell number was calculated relative to erythroblast numbers at the start of culture. The same preculture was seeded in parallel in the STR and in a dish. **(D-E)** Cells were stained with AnnexinV (apoptosis staining) and DRAQ7 (cell impermeable DNA stain) **(D)**, or CD235a plus CD49d (erythroid differentiation markers). Percentage of cells in each quadrant is included. **(E)**. All data is displayed as mean ± SD (error bars; n=3 reactor runs / donors).

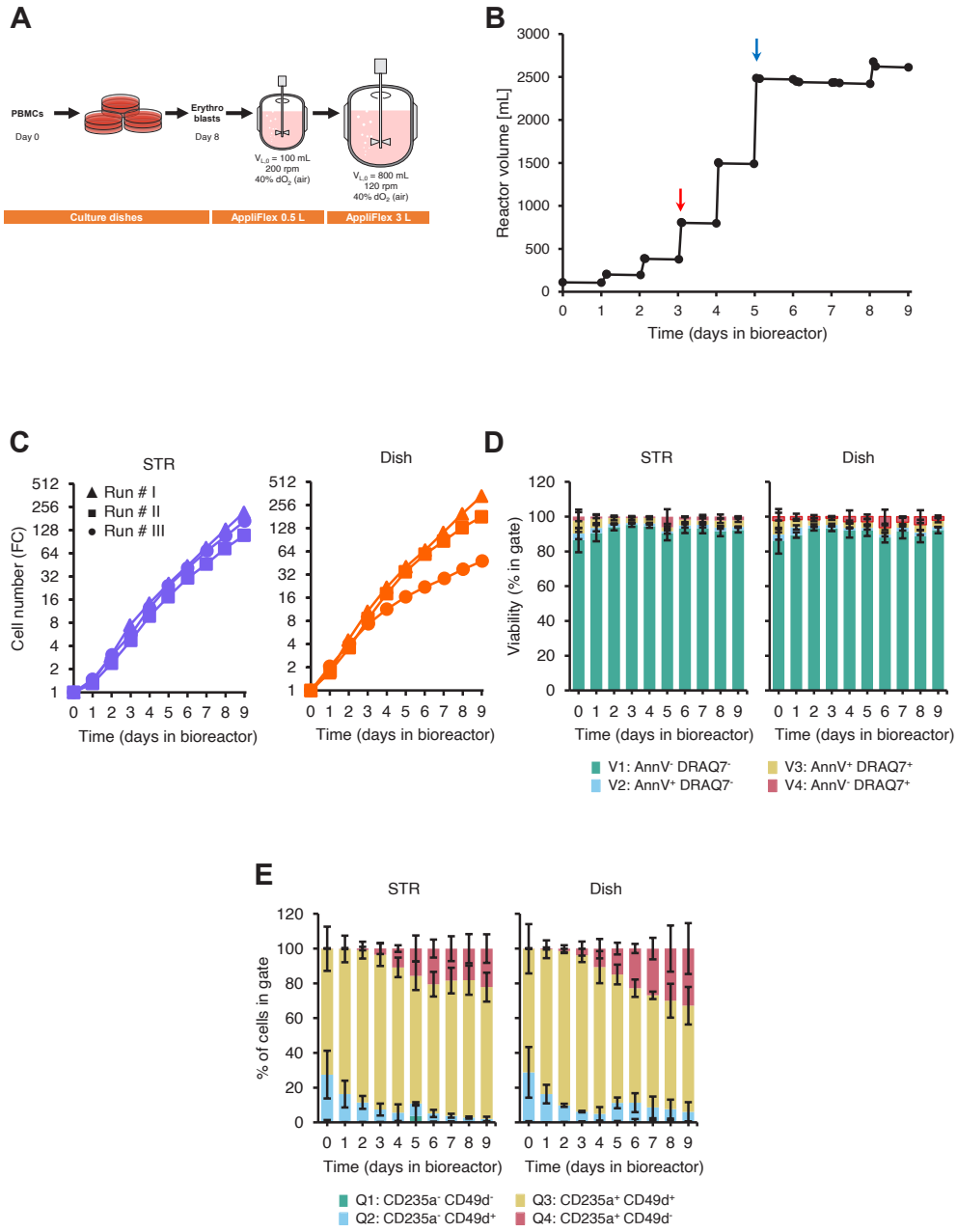

Figure 6.
(See caption on previous page)

2.4. Discussion

Efficient cRBC production requires the transition from static culture systems to scalable cultivation platforms. We established the process conditions (oxygen and agitation) required for effective expansion and differentiation of erythroblast cultures in STRs. Oxygen availability was critical during expansion of erythroblast cultures, whereas the requirement for oxygen decreased during terminal differentiation. Stirring speeds required for a homogeneous distribution of cells in the bioreactor did not affect cell growth or differentiation. Only much elevated stirring speeds led to a temporary cell growth arrest and an acceleration in spontaneous erythroblast differentiation. Within the operating boundaries established in this study, the STR culture volume could be scaled up from 300 mL to 2500 mL. Whereas static cultures show some variation in their expansion potential, STR cultures proved to be more reproducible, which adds to the reliability of the process.

2.4.1. Oxygen requirements of erythroblast in culture

Using a combination of headspace N_2 gas flow and intermittent air allowed us to tightly control dO_2 in our bioreactor cultures. While low dO_2 setpoints can reduce the overall sparging requirements of the culture and are closer to the *in vivo* hematopoietic niche, no significant improvement on growth, lactate accumulation or spontaneous differentiation was observed in our experiments when the dO_2 setpoint was decreased from 40% to 10%. Although oxygen concentration setpoints lower than 10% dO_2 may enhance proliferation, maintaining a constant dO_2 <10% in our set-up is technically challenging due to the noise in dO_2 readings and the oscillations caused by the discrete sparging events. This could be addressed by using oxygen probes with lower response times or with aeration strategies in which gas composition is adjusted based on the dO_2 measurements, avoiding large oxygen concentration peaks during sparging. Studying the effect of lower and fluctuating dO_2 concentrations can provide further information on the potential challenges that could be faced in the large bioreactors required for the production of the required number of cRBCs for a single transfusion unit, in which oxygen and nutrient gradients are difficult to avoid, and the risk of having oxygen-limited regions is higher [76,77].

The oxygen requirements of erythroblasts decreased during culture, from 2.01 to 0.55 pg/cell/h, and increasingly less during terminal differentiation. These values explain the fast decrease in dO_2 concentration in the initial 2 L bioreactor experiments, in which the k_La (0.27 1/h; headspace aeration only) could only support theoretical early erythroblast concentrations of $<0.97\times10^6$ cells/mL. Seahorse assays, used to quantify glycolysis and mitochondrial oxidative phosphorylation of cells by measuring oxygen

consumption rates and extracellular acidization rates, have been reported for cultured erythroblasts. However, these assays are performed with low cell numbers and using medium with a composition different to that used for culture, potentially resulting in q_{O2} values not representative of the culture conditions [78]. Bayle et al. reported much lower q_{O2} values for their bioreactor cultures, decreasing from 0.063 pg/cell/h for early erythroblasts to 0.017 pg/cell/h in the later stages of differentiation [45]. A similar decrease in oxygen requirements during erythroid differentiation was described by Browne et al., from 2.84 to 0.13 pg/cell/h for proerythroblasts and reticulocytes, respectively [79]. This decrease in oxygen requirement could be a result of mitophagy at terminal stages of erythroblast differentiation decreasing mitochondria numbers and marking the shift to anaerobic metabolism as occurring in RBCs [80–82]. Differences between our measured q_{O2} values and those previously reported could be explained by differences in the differentiation status of erythroid cells used at the start of the bioreactor cultures, culture medium composition or oxygen concentration [83]. Of note, our values are in agreement with measured oxygen uptake rates of other human cell lines (0.4-6.2 pg O_2/cell/h; [84]). We suggest using continuous dO_2 measurements and the dynamic method to estimate q_{O2} in erythroid cultures, as other methods such as using offgas data are difficult to implement due to the low oxygen consumption rates of mammalian cell cultures [85].

In this study, we used (intermittent) air sparging, together with a constant headspace nitrogen gas flow to enable a fast control of dissolved oxygen and pH levels. Although the constant nitrogen flow leads to stripping of oxygen from the liquid, which was compensated by additional sparging, cell growth was similar to that observed in the reference static cultures in dishes. Furthermore, this strategy did not lead to significant foaming in the 0.5 L nor the 3 L bioreactor cultures (note that the medium has a low protein content; 0.1% w/w of albumin). This strategy can probably be applied for larger bioreactor cultures as well, especially when enriching the aeration with pure oxygen [86]. Although dissolved CO_2 levels in bioreactor cultures (pCO_2 = 10-40 mmHg; data not shown) were similar to those under physiological conditions, CO_2 accumulation may represent a challenge for further scale up or at higher cell density cultures, for which CO_2 stripping via sparging will become more relevant [87,88].

Foaming due to excessive sparging can negatively affect the process' performance by aggregation of expensive growth factors and other proteins in the foam layer [59,89], and an increased risk for the sterility of the process during a putative foam-out event [90]. In case significant foaming appears, antifoams could be applied. Nevertheless, care has to be taken as there are reports that these reagents negatively affect mass transfer and cell growth [91–93]. For example, pluronic F68, a non-silicone-based copolymer

antifoaming agent, reduces attachment of cells to rising gas bubbles, minimizing their exposure to bubble bursting [94–97]. However, effects of pluronics on cell strength and stiffness, cell aggregation, and membrane trafficking processes have been described previously [97–100]. For erythroid cultures, pluronics can reduce enucleation efficiency and potentially increase RBC aggregation [45,101]. Other antifoam agents such as those based on silicone polymers can be problematic, as they can negatively affect equipment, decrease the efficiency of downstream steps, and have a toxic effect upon injection in patients [102,103].

Antifoam addition has minimal effects on protecting cells to high gas entrance velocities, a major contributor of sparging-induced shear [56,104]. Thus, we suggest the usage of spargers with larger pore sizes for larger scale bioreactor erythroid cultures to reduce the impact of high shear caused by bubble formation and detachment from the sparger. Even more promising is to replace sparging by a membrane gas exchanger, although cells could be exposed to new shear due to the continuous recirculation through the system. Furthermore, the cultivation system gets much more complex and the cost of the process increases [105].

2.4.2. Erythroid expansion cultures are robust to high stirring speeds

This study shows that erythroblast expansion cultures can withstand agitation speeds of up to 600 rpm (tip speed = 880 mm/s), without negatively affecting growth, viability or the differentiation stage of the cells. Surprisingly, very high stirring speeds (1800 rpm) led to a temporary arrest in growth, followed by a recovery after 5-6 days, accompanied by an acceleration in erythroid differentiation as reported previously for erythroid cultures in flasks under orbital shaking [31]. This recovery in growth could be explained by an adaptation of culture cells to these turbulent conditions, or by the selection of erythroblast cells more tolerant to agitation during the first days of culture. A more thorough characterization of this adaptation on not only the erythroblast transcriptome but also at the lipidomic and metabolomic level will need to be performed to identify (signaling) pathways triggered by this mechanical stress, the nature of the adaptative response (e.g. membrane composition remodeling), and to determine the mechanism under which erythroid differentiation is promoted under these conditions.

Interestingly, other studies have reported less tolerance of erythroblast cultures to agitation. Increased apoptosis, acceleration of erythroid differentiation, and lower enucleation levels have been observed in a gyro-rocker bioreactor at low orbital speeds (20 rpm) [29]. Bayley et al. also observed a decrease in proliferation in stirred bioreactors compared to static cultures, although no significance difference on growth was observed between stirring speeds of 300 and 450 rpm (tip speeds = 180 and 270

mm/s, respectively) [45]. Han et al. observed a dependence on the inoculum age to agitation tolerance, with proerythroblast and basophilic erythroblast cultures showing a quick decrease in growth and viability in microbioreactors agitated at 300 rpm (tip speed = 180 mm/s), while more mature cells (day 12 after $CD34^+$ isolation and start of culture), could tolerate the same conditions [42]. However, it is difficult to directly compare the hydrodynamic conditions between these reports, partly due to differences in the culture set-up but also due to a lack of consensus on which mixing parameter (rpm, tip speed, volumetric power input) is more appropriate to do this comparison, which together co-define the dynamic shear stress experienced by cells. Local turbulent energy dissipation rate (EDR) has been suggested as an alternative parameter to define optimal ranges of agitation for mammalian cell culture [106]. Supporting the relevance of energy dissipation rate, it has been recently reported that turbulence and not shear stress is critical for large scale platelet production [107]. Estimates of EDR in STRs could be useful to rationally drive the scale-up of the process, ensuring limited exposure of erythroblast to excessive hydrodynamic forces.

Although the effect of shear stress and EDR can be evaluated in STRs by varying the agitation rate, changes in stirring speed also affect the mass transfer rate between the gas and liquid phases, impacting the aeration requirements to control dO_2 and pH at the defined setpoints. This, in turn, can influence the exposure of cells to high local O_2 (and CO_2, if pH is controlled with this gas) concentrations and to high EDR regions due to bubble bursting phenomena [59]. A full uncoupling of agitation and aeration is challenging, as other aeration strategies such as using submerged oxygen-permeable membranes, can also lead to undesired effect such as very high local O_2 concentrations [108–110].

2.4.3. Quantification of metabolite consumption/production rates in erythroid culture

We observed a decrease in erythroblast proliferation during expansion cultures, with growth rates as low as ~0.3 1/day at the end of the cultures. Growth limitations in erythroblast batch and fed-batch cultures has been previously reported, but the origin of this limitation has not been identified yet [45,111]. Here we report lactate and ammonium concentrations below 6 and 0.6 mM respectively, which are lower than typical growth-inhibiting concentrations for other animal cell lines [112–114]. Interestingly, we measured lactate production rates (q_{lac}) of 0.5-2.5 pmol/cell/day, significantly lower than those reported for other erythroid cultures (3-12 pmol/cell/day; [32,43,45,115]). Dissolved oxygen concentration in the bioreactor did not have a significant effect on q_{lac}, but static cultures consistently showed higher rates in later days of culture. Oxygen limitations caused by low oxygen concentrations (<10% dO_2) in the bottom of culture dishes could lead to an increase in anaerobic glycolysis

rates in erythroblasts cultured under static conditions, leading to the observed lactate production [116]. Even at the measured low concentrations, lactate can potentially induce activation of erythroid-related genes such as STAT5, affecting erythroid differentiation dynamics [117]. Strategies to limit lactate production in culture could be implemented, such as feeding profiles that limit glucose concentrations during culture.

2.4.4. Outlook

A 200-fold expansion per PBMC already takes place in the first 8 days of culture (before reactor inoculation), still performed under static conditions in culture dishes [10], resulting in an overall 200×750 = 150 000-fold expansion after 10 days of culture in the bioreactor. The high cell yields in this first culture stage are partly due to the positive contribution of $CD14^+$ monocytes/macrophages present in the PBMC pool by the production of soluble factors that support erythroblast expansion [118,119]. Full translation of our protocol to STRs would require defining operating conditions that would support HSC proliferation and macrophages in the first days of culture.

While we could scale-up erythroblast expansion cultures from dishes to 0.5 L and 3.0 L bioreactors, the large number of cells required for a single cRBC transfusion unit would still require prohibitively large STRs. Perfusion approaches can be used to increase cell concentrations, leading to a significant footprint reduction compared to fed-batch processes, and potentially to a lower production cost if the perfusion rate and perfusion media composition is sufficiently optimized [120,121]. Perfusion processes also support a more stable culture environment and cell metabolism, by continuously removing inhibitory metabolic byproducts (e.g. lactate and ammonia) and ensuring sufficient nutrient levels during culture [122,123]. The cell-retention strategies required for perfusion could also be of value to perform the required medium changes when transitioning from proliferation to differentiation in culture, where removal of hSCF is needed for efficient maturation and enucleation. We expect our quantitative physiological data and observations on the effect of bioreactor operating parameters to be relevant for the further scale-up of erythroblast proliferation and differentiation bioreactor cultures, and the optimization of feeding regimes with the aim to achieve a cost-effective cRBC production process.

2.5. Abbreviations

BM	Bone marrow
BSA	Bovine serum albumin
CD235a	Glycophorin A
CD49d	Integrin alpha 4
CD71	Transferrin receptor 1
cRBC	Cultured red blood cell
Dex	Dexamethasone
EDR	Energy dissipation rate
Epo	Erythropoietin
EpoR	Erythropoietin receptor
FC	Fold change
HEPES	4-(2-hydroxyethyl)-1-piperazineethanesulfonic acid
HIF1α	Hypoxia-inducible factor 1, alpha subunit
HSA	Human serum albumin
HSC	Hematopoietic stem cell
hSCF	Human stem cell factor
NFATC2	Nuclear factor of activated T-cells 2
OXPHOS	Oxidative phosphorylation
PBMC	Peripheral blood mononuclear cell
PBS	Phosphate-buffered saline
PI	Propidium iodide
RBC	Red blood cell
rpm	Revolutions per minute
SCF	Stem cell factor
STAT5	Signal transducer and activator of transcription 5A
STR	Stirred tank reactor
TCA	Tricarboxylic acid

2.6. List of symbols

V_L	Volume of culture (units: L)
C_N	Cell concentration (units: cells/mL of culture)
C_V	Biomass concentration (units: μm^3 of cells/mL of culture)
N	Total number of cells (units: cells)
μ	Growth rate (units = 1/day). Can be calculated using cell counts (μ_{counts}) or biomass concentration (μ_{vol})
τ	Doubling time (units = day).
$k_L a$	Overall volumetric mass transfer coefficient of the system for oxygen, recalculated to a liquid-side mass transfer oxygen composition gradient (units = 1/h)

C_{O_2}	Concentration of dissolved oxygen in the liquid (units: mg O_2/L)
$C_{O_2}^{sat}$	Concentration of saturation for oxygen in the liquid (units: mg O_2/L)
dO_2	Dissolved oxygen concentration as percentage of the saturation concentration at the defined conditions (37 °C, 1 atm, air; units = %)
q_{O_2}	Cell-specific consumption rate of oxygen (units = pg O_2/cell/day)
q_{lac}	Cell-specific production rate of lactate. Can be calculated using cell counts ($q_{lac,counts}$; units = mol lactate/cell/day) or biomass concentration ($q_{lac,vol}$; units = mol lactate/μm^3 cell/day)
q_{NH_4}	Cell-specific production rate of ammonium. Can be calculated using cell counts ($q_{NH_4,counts}$; units = mol NH_4^+/cell/day) or biomass concentration ($q_{NH_4,vol}$; units = mol NH_4^+/μm^3 cell/day)
C_{lac}	Extracellular lactate concentration (units: mol lactate/L)
C_{NH_4}	Extracellular ammonium concentration (units: mol NH_4^+/L)

2.7. Acknowledgments

We thank Queralt Farràs Costa and Víctor Puig I Laborda (Department of Biotechnology, Faculty of Applied Sciences, Delft University of Technology; Delft; The Netherlands) for their assistance on the determination of oxygen consumption rates. We also thank Yi Song, Dirk Geerts and Rob Kerste (Department of Biotechnology, Faculty of Applied Sciences, Delft University of Technology; Delft; The Netherlands) for their support on setting up the 0.5 L bioreactors. We thank Nurcan Yağcı (Sanquin Research) who performed PBMC isolation and precultures. We thank Marten Hansen (Laboratory for Cell Therapies, Sanquin) for the support on setting up the 3 L bioreactors. We thank Tom van Arragon and Cristina Bernal Martínez (Applikon Biotechnology; Delft; The Netherlands) for technical help and advice on bioreactor cultures.

2.8. Author contribution

J.S.G.M. performed the experiments; J.S.G.M., E.v.d.A., A.W., and M.v.L. designed the experiments, analyzed the data, and wrote the manuscript; G.I. and L.v.d.W contributed to data analysis and writing of the manuscript.

2.9. References

1. World Health Organization *Guidance on Centralization of Blood Donation Testing and Processing*; World Health Organization, **2021**; ISBN 978-92-4-002082-5.

2. Klinkenberg, E.F.; Huis In't Veld, E.M.J.; de Wit, P.D.; van Dongen, A.; Daams, J.G.; de Kort, W.L.A.M.; Fransen, M.P. Blood Donation Barriers and Facilitators of Sub-Saharan African Migrants and Minorities in Western High-income Countries: A Systematic Review of the Literature. *Transfus. Med. Oxf. Engl.* **2019**, *29*, 28–41, doi:10.1111/tme.12517.

3. Vichinsky, E.P.; Earles, A.; Johnson, R.A.; Hoag, M.S.; Williams, A.; Lubin, B. Alloimmunization in Sickle Cell Anemia and Transfusion of Racially Unmatched Blood. *N. Engl. J. Med.* **1990**, *322*, 1617–1621, doi:10.1056/NEJM199006073222301.

4. Daniels, G. *Human Blood Groups*; 3rd ed.; Wiley-Blackwell, **2013**; ISBN 978-1-118-49362-5.

5. Pellegrin, S.; Severn, C.E.; Toye, A.M. Towards Manufactured Red Blood Cells for the Treatment of Inherited Anemia. *Haematologica* **2021**, doi:10.3324/haematol.2020.268847.

6. Peyrard, T.; Bardiaux, L.; Krause, C.; Kobari, L.; Lapillonne, H.; Andreu, G.; Douay, L. Banking of Pluripotent Adult Stem Cells as an Unlimited Source for Red Blood Cell Production: Potential Applications for Alloimmunized Patients and Rare Blood Challenges. *Transfus. Med. Rev.* **2011**, *25*, 206–216, doi:10.1016/j.tmrv.2011.01.002.

7. Koleva, L.; Bovt, E.; Ataullakhanov, F.; Sinauridze, E. Erythrocytes as Carriers: From Drug Delivery to Biosensors. *Pharmaceutics* **2020**, *12*, E276, doi:10.3390/pharmaceutics12030276.

8. Sun, X.; Han, X.; Xu, L.; Gao, M.; Xu, J.; Yang, R.; Liu, Z. Surface-Engineering of Red Blood Cells as Artificial Antigen Presenting Cells Promising for Cancer Immunotherapy. *Small Weinh. Bergstr. Ger.* **2017**, *13*, doi:10.1002/smll.201701864.

9. Zhang, X.; Luo, M.; Dastagir, S.R.; Nixon, M.; Khamhoung, A.; Schmidt, A.; Lee, A.; Subbiah, N.; McLaughlin, D.C.; Moore, C.L.; et al. Engineered Red Blood Cells as an Off-the-Shelf Allogeneic Anti-Tumor Therapeutic. *Nat. Commun.* **2021**, *12*, 2637, doi:10.1038/s41467-021-22898-3.

10. Heshusius, S.; Heideveld, E.; Burger, P.; Thiel-Valkhof, M.; Sellink, E.; Varga, E.; Ovchynnikova, E.; Visser, A.; Martens, J.H.A.; von Lindern, M.; et al. Large-Scale in Vitro Production of Red Blood Cells from Human Peripheral Blood Mononuclear Cells. *Blood Adv.* **2019**, *3*, 3337–3350, doi:10.1182/bloodadvances.2019000689.

11. Migliaccio, G.; Di Pietro, R.; di Giacomo, V.; Di Baldassarre, A.; Migliaccio, A.R.; Maccioni, L.; Galanello, R.; Papayannopoulou, T. In Vitro Mass Production of Human Erythroid Cells from the Blood of Normal Donors and of Thalassemic Patients. *Blood Cells. Mol. Dis.* **2002**, *28*, 169–180, doi:10.1006/bcmd.2002.0502.

12. Leberbauer, C.; Boulmé, F.; Unfried, G.; Huber, J.; Beug, H.; Müllner, E.W. Different Steroids Co-Regulate Long-Term Expansion versus Terminal Differentiation in Primary Human Erythroid Progenitors. *Blood* **2005**, *105*, 85–94, doi:10.1182/blood-2004-03-1002.

13. von Lindern, M.; Zauner, W.; Mellitzer, G.; Steinlein, P.; Fritsch, G.; Huber, K.; Löwenberg, B.; Beug, H. The Glucocorticoid Receptor Cooperates with the Erythropoietin Receptor and C-Kit to Enhance and Sustain Proliferation of Erythroid Progenitors in Vitro. *Blood* **1999**, *94*, 550–559, doi:10.1182/blood.V94.2.550.

14. Peniche Silva, C.J.; Liebsch, G.; Meier, R.J.; Gutbrod, M.S.; Balmayor, E.R.; van Griensven, M. A New Non-Invasive Technique for Measuring 3D-Oxygen Gradients in Wells During Mammalian Cell Culture. *Front. Bioeng. Biotechnol.* **2020**, doi:10.3389/fbioe.2020.00595.

15. Place, T.L.; Domann, F.E.; Case, A.J. Limitations of Oxygen Delivery to Cells in Culture: An Underappreciated Problem in Basic and Translational Research. *Free Radic. Biol. Med.* **2017**, *113*, 311–322, doi:10.1016/j.freeradbiomed.2017.10.003.

16. Sugiura, S.; Sakai, Y.; Nakazawa, K.; Kanamori, T. Superior Oxygen and Glucose Supply in Perfusion Cell Cultures Compared to Static Cell Cultures Demonstrated by Simulations Using the Finite Element Method. *Biomicrofluidics* **2011**, *5*, 022202, doi:10.1063/1.3589910.

17. Timmins, N.E.; Nielsen, L.K. Blood Cell Manufacture: Current Methods and Future Challenges. *Trends Biotechnol.* **2009**, *27*, 415–422, doi:10.1016/j.tibtech.2009.03.008.

18. Timmins, N.E.; Nielsen, L.K. Manufactured RBC — Rivers of Blood, or an Oasis in the Desert? *Biotechnol. Adv.* **2011**, *29*, 661–666, doi:10.1016/j.biotechadv.2011.05.002.

19. Allenby, M.C.; Panoskaltsis, N.; Tahlawi, A.; Dos Santos, S.B.; Mantalaris, A. Dynamic Human Erythropoiesis in a Three-Dimensional Perfusion Bone Marrow Biomimicry. *Biomaterials* **2019**, *188*, 24–37, doi:10.1016/j.biomaterials.2018.08.020.

20. Housler, G.J.; Miki, T.; Schmelzer, E.; Pekor, C.; Zhang, X.; Kang, L.; Voskinarian-Berse, V.; Abbot, S.; Zeilinger, K.; Gerlach, J.C. Compartmental Hollow Fiber Capillary Membrane-Based Bioreactor Technology for in Vitro Studies on Red Blood Cell Lineage Direction of Hematopoietic Stem Cells. *Tissue Eng. Part C Methods* **2012**, *18*, 133–142, doi:10.1089/ten.TEC.2011.0305.

21. Severn, C.E.; Macedo, H.; Eagle, M.J.; Rooney, P.; Mantalaris, A.; Toye, A.M. Polyurethane Scaffolds Seeded with CD34(+) Cells Maintain Early Stem Cells Whilst Also Facilitating Prolonged Egress of Haematopoietic Progenitors. *Sci. Rep.* **2016**, *6*, 32149, doi:10.1038/srep32149.

22. Severn, C.E.; Eissa, A.M.; Langford, C.R.; Parker, A.; Walker, M.; Dobbe, J.G.G.; Streekstra, G.J.; Cameron, N.R.; Toye, A.M. Ex Vivo Culture of Adult CD34+ Stem Cells Using Functional Highly Porous Polymer Scaffolds to Establish Biomimicry of the Bone Marrow Niche. *Biomaterials* **2019**, *225*, 119533, doi:10.1016/j.biomaterials.2019.119533.

23. Lee, E.; Han, S.Y.; Choi, H.S.; Chun, B.; Hwang, B.; Baek, E.J. Red Blood Cell Generation by Three-Dimensional Aggregate Cultivation of Late Erythroblasts. *Tissue Eng. Part A* **2015**, *21*, 817–828, doi:10.1089/ten.tea.2014.0325.

24. Mohebbi-Kalhori, D.; Behzadmehr, A.; Doillon, C.J.; Hadjizadeh, A. Computational Modeling of Adherent Cell Growth in a Hollow-Fiber Membrane Bioreactor for Large-Scale 3-D Bone Tissue Engineering. *J. Artif. Organs* **2012**, *15*, 250–265, doi:10.1007/s10047-012-0649-1.

25. Piret, J.M.; Devens, D.A.; Cooney, C.L. Nutrient and Metabolite Gradients in Mammalian Cell Hollow Fiber Bioreactors. *Can. J. Chem. Eng.* **1991**, *69*, 421–428, doi:10.1002/cjce.5450690204.

26. Preissmann, A.; Wiesmann, R.; Buchholz, R.; Werner, R.G.; Noé, W. Investigations on Oxygen Limitations of Adherent Cells Growing on Macroporous Microcarriers. *Cytotechnology* **1997**, *24*, 121–134, doi:10.1023/A:1007973924865.

27. Yu, P. Numerical Simulation on Oxygen Transfer in a Porous Scaffold for Animal Cell Culture. *Int. J. Heat Mass Transf.* **2012**, *55*, 4043–4052, doi:10.1016/j.ijheatmasstransfer.2012.03.046.

28. Zhang, Y.; Wang, C.; Wang, L.; Shen, B.; Guan, X.; Tian, J.; Ren, Z.; Ding, X.; Ma, Y.; Dai, W.; et al. Large-Scale Ex Vivo Generation of Human Red Blood Cells from Cord Blood CD34+ Cells. *Stem Cells Transl. Med.* **2017**, *6*, 1698–1709, doi:10.1002/sctm.17-0057.

29. Boehm, D.; Murphy, W.G.; Al-Rubeai, M. The Effect of Mild Agitation on in Vitro Erythroid Development. *J. Immunol. Methods* **2010**, *360*, 20–29, doi:10.1016/j.jim.2010.05.007.

30. Timmins, N.E.; Athanasas, S.; Günther, M.; Buntine, P.; Nielsen, L.K. Ultra-High-Yield Manufacture of Red Blood Cells from Hematopoietic Stem Cells. *Tissue Eng. Part C Methods* **2011**, *17*, 1131–1137, doi:10.1089/ten.tec.2011.0207.

31. Aglialoro, F.; Abay, A.; Yagci, N.; Rab, M.A.E.; Kaestner, L.; van Wijk, R.; von Lindern, M.; van den Akker, E. Mechanical Stress Induces Ca2+-Dependent Signal Transduction in Erythroblasts and Modulates Erythropoiesis. *Int. J. Mol. Sci.* **2021**, *22*, doi:10.3390/ijms22020955.

32. Sivalingam, J.; SuE, Y.; Lim, Z.R.; Lam, A.T.L.; Lee, A.P.; Lim, H.L.; Chen, H.Y.; Tan, H.K.; Warrier, T.; Hang, J.W.; et al. A Scalable Suspension Platform for Generating High-Density Cultures of Universal Red Blood Cells from Human Induced Pluripotent Stem Cells. *Stem Cell Rep.* **2020**, *16*, 182–197, doi:10.1016/j.stemcr.2020.11.008.

33. Griffiths, R.E.; Kupzig, S.; Cogan, N.; Mankelow, T.J.; Betin, V.M.S.; Trakarnsanga, K.; Massey, E.J.; Lane, J.D.; Parsons, S.F.; Anstee, D.J. Maturing Reticulocytes Internalize Plasma Membrane in Glycophorin A–Containing Vesicles That Fuse with Autophagosomes before Exocytosis. *Blood* **2012**, *119*, 6296–6306, doi:10.1182/blood-2011-09-376475.

34. Kupzig, S.; Parsons, S.F.; Curnow, E.; Anstee, D.J.; Blair, A. Superior Survival of Ex Vivo Cultured Human Reticulocytes Following Transfusion into Mice. *Haematologica* **2017**, *102*, 476–483, doi:10.3324/haematol.2016.154443.

35. Trakarnsanga, K.; Griffiths, R.E.; Wilson, M.C.; Blair, A.; Satchwell, T.J.; Meinders, M.; Cogan, N.; Kupzig, S.; Kurita, R.; Nakamura, Y.; et al. An Immortalized Adult Human Erythroid Line Facilitates Sustainable and Scalable Generation of Functional Red Cells. *Nat. Commun.* **2017**, *8*, 14750, doi:10.1038/ncomms14750.

36. Chu, L.; Robinson, D.K. Industrial Choices for Protein Production by Large-Scale Cell Culture. *Curr. Opin. Biotechnol.* **2001**, *12*, 180–187, doi:10.1016/S0958-1669(00)00197-X.

37. Rodrigues, M.E.; Costa, A.R.; Henriques, M.; Azeredo, J.; Oliveira, R. Technological Progresses in Monoclonal Antibody Production Systems. *Biotechnol. Prog.* **2010**, *26*, 332–351, doi:10.1002/btpr.348.

38. Tapia, F.; Vázquez-Ramírez, D.; Genzel, Y.; Reichl, U. Bioreactors for High Cell Density and Continuous Multi-Stage Cultivations: Options for Process Intensification in Cell Culture-Based Viral Vaccine Production. *Appl. Microbiol. Biotechnol.* **2016**, *100*, 2121–2132, doi:10.1007/s00253-015-7267-9.

39. Farid, S.S. Process Economics of Industrial Monoclonal Antibody Manufacture. *J. Chromatogr. B* **2007**, *848*, 8–18, doi:10.1016/j.jchromb.2006.07.037.

40. Avgerinos, G.C.; Drapeau, D.; Socolow, J.S.; Mao, J.; Hsiao, K.; Broeze, R.J. Spin Filter Perfusion System for High Density Cell Culture: Production of Recombinant Urinary Type Plasminogen Activator in CHO Cells. *Bio/Technology* **1990**, *8*, 54–58, doi:10.1038/nbt0190-54.

41. Karst, D.J.; Serra, E.; Villiger, T.K.; Soos, M.; Morbidelli, M. Characterization and Comparison of ATF and TFF in Stirred Bioreactors for Continuous Mammalian Cell Culture Processes. *Biochem. Eng. J.* **2016**, *110*, 17–26, doi:10.1016/j.bej.2016.02.003.

42. Han, S.Y.; Lee, E.M.; Lee, J.; Lee, H.; Kwon, A.M.; Ryu, K.Y.; Choi, W.-S.; Baek, E.J. Red Cell Manufacturing Using Parallel Stirred-Tank Bioreactors at the Final Stages of Differentiation Enhances Reticulocyte Maturation. *Biotechnol. Bioeng.* **2021**, *118*, doi:https://doi.org/10.1002/bit.27691.

43. Lee, E.; Lim, Z.R.; Chen, H.-Y.; Yang, B.X.; Lam, A.T.-L.; Chen, A.K.-L.; Sivalingam, J.; Reuveny, S.; Loh, Y.-H.; Oh, S.K.-W. Defined Serum-Free Medium for Bioreactor Culture of an Immortalized Human Erythroblast Cell Line. *Biotechnol. J.* **2018**, *13*, e1700567, doi:10.1002/biot.201700567.

44. Ratcliffe, E.; Glen, K.E.; Workman, V.L.; Stacey, A.J.; Thomas, R.J. A Novel Automated Bioreactor for Scalable Process Optimisation of Haematopoietic Stem Cell Culture. *J. Biotechnol.* **2012**, *161*, 387–390, doi:10.1016/j.jbiotec.2012.06.025.

45. Bayley, R.; Ahmed, F.; Glen, K.; McCall, M.; Stacey, A.; Thomas, R. The Productivity Limit of Manufacturing Blood Cell Therapy in Scalable Stirred Bioreactors. *J. Tissue Eng. Regen. Med.* **2017**, doi:10.1002/term.2337.

46. Chen, K.; Liu, J.; Heck, S.; Chasis, J.A.; An, X.; Mohandas, N. Resolving the Distinct Stages in Erythroid Differentiation Based on Dynamic Changes in Membrane Protein Expression during Erythropoiesis. *Proc. Natl. Acad. Sci. U. S. A.* **2009**, *106*, 17413–17418, doi:10.1073/pnas.0909296106.

47. Sieblist, C.; Jenzsch, M.; Pohlscheidt, M. Equipment Characterization to Mitigate Risks during Transfers of Cell Culture Manufacturing Processes. *Cytotechnology* **2016**, *68*, 1381–1401, doi:10.1007/s10616-015-9899-0.

48. Godoy-Silva, R.; Chalmers, J.J.; Casnocha, S.A.; Bass, L.A.; Ma, N. Physiological Responses of CHO Cells to Repetitive Hydrodynamic Stress. *Biotechnol. Bioeng.* **2009**, *103*, 1103–1117, doi:10.1002/bit.22339.

49. Kretzmer, G.; Schügerl, K. Response of Mammalian Cells to Shear Stress. *Appl. Microbiol. Biotechnol.* **1991**, *34*, 613–616, doi:10.1007/BF00167909.

50. Wolfe, R.P.; Ahsan, T. Shear Stress during Early Embryonic Stem Cell Differentiation Promotes Hematopoietic and Endothelial Phenotypes. *Biotechnol. Bioeng.* **2013**, *110*, 1231–1242, doi:10.1002/bit.24782.

51. Wu, S.-C. Influence of Hydrodynamic Shear Stress on Microcarrier-Attached Cell Growth: Cell Line Dependency and Surfactant Protection. *Bioprocess Eng.* **1999**, *21*, 201–206, doi:10.1007/s004490050663.

52. Aglialoro, F.; Hofsink, N.; Hofman, M.; Brandhorst, N.; van den Akker, E. Inside Out Integrin Activation Mediated by PIEZO1 Signaling in Erythroblasts. *Front. Physiol.* **2020**, *11*, 958, doi:10.3389/fphys.2020.00958.

53. Caulier, A.; Jankovsky, N.; Demont, Y.; Ouled-Haddou, H.; Demagny, J.; Guitton, C.; Merlusca, L.; Lebon, D.; Vong, P.; Aubry, A.; et al. PIEZO1 Activation Delays Erythroid Differentiation of Normal and Hereditary Xerocytosis-Derived Human Progenitor Cells. *Haematologica* **2020**, *105*, 610–622, doi:10.3324/haematol.2019.218503.

54. Murhammer, D.W.; Goochee, C.F. Sparged Animal Cell Bioreactors: Mechanism of Cell Damage and Pluronic F-68 Protection. *Biotechnol. Prog.* **1990**, *6*, 391–397, doi:10.1021/bp00005a012.

55. Villiger, T.K.; Morbidelli, M.; Soos, M. Experimental Determination of Maximum Effective Hydrodynamic Stress in Multiphase Flow Using Shear Sensitive Aggregates. *AIChE J.* **2015**, *61*, 1735–1744, doi:10.1002/aic.14753.

56. Zhu, Y.; Cuenca, J.V.; Zhou, W.; Varma, A. NS0 Cell Damage by High Gas Velocity Sparging in Protein-Free and Cholesterol-Free Cultures. *Biotechnol. Bioeng.* **2008**, *101*, 751–760, doi:10.1002/bit.21950.

57. Xing, Z.; Kenty, B.M.; Li, Z.J.; Lee, S.S. Scale-up Analysis for a CHO Cell Culture Process in Large-Scale Bioreactors. *Biotechnol. Bioeng.* **2009**, *103*, 733–746, doi:10.1002/bit.22287.

58. Sobolewski, P.; Kandel, J.; Klinger, A.L.; Eckmann, D.M. Air Bubble Contact with Endothelial Cells in Vitro Induces Calcium Influx and IP3-Dependent Release of Calcium Stores. *Am. J. Physiol. - Cell Physiol.* **2011**, *301*, C679–C686, doi:10.1152/ajpcell.00046.2011.

59. Walls, P.L.L.; McRae, O.; Natarajan, V.; Johnson, C.; Antoniou, C.; Bird, J.C. Quantifying the Potential for Bursting Bubbles to Damage Suspended Cells. *Sci. Rep.* **2017**, *7*, 1–9, doi:10.1038/s41598-017-14531-5.

60. Walsh, C.; Ovenden, N.; Stride, E.; Cheema, U. Quantification of Cell-Bubble Interactions in a 3D Engineered Tissue Phantom. *Sci. Rep.* **2017**, *7*, 6331, doi:10.1038/s41598-017-06678-y.

61. Mas-Bargues, C.; Sanz-Ros, J.; Román-Domínguez, A.; Inglés, M.; Gimeno-Mallench, L.; El Alami, M.; Viña-Almunia, J.; Gambini, J.; Viña, J.; Borrás, C. Relevance of Oxygen Concentration in Stem Cell Culture for Regenerative Medicine. *Int. J. Mol. Sci.* **2019**, *20*, 1195, doi:10.3390/ijms20051195.

62. Spencer, J.A.; Ferraro, F.; Roussakis, E.; Klein, A.; Wu, J.; Runnels, J.M.; Zaher, W.; Mortensen, L.J.; Alt, C.; Turcotte, R.; et al. Direct Measurement of Local Oxygen Concentration in the Bone Marrow of Live Animals. *Nature* **2014**, *508*, 269–273, doi:10.1038/nature13034.

63. Bapat, A.; Schippel, N.; Shi, X.; Jasbi, P.; Gu, H.; Kala, M.; Sertil, A.; Sharma, S. Hypoxia Promotes Erythroid Differentiation through the Development of Progenitors and Proerythroblasts. *Exp. Hematol.* **2021**, *97*, 32-46.e35, doi:10.1016/j.exphem.2021.02.012.

64. Goto, T.; Ubukawa, K.; Kobayashi, I.; Sugawara, K.; Asanuma, K.; Sasaki, Y.; Guo, Y.-M.; Takahashi, N.; Sawada, K.; Wakui, H.; et al. ATP Produced by Anaerobic Glycolysis Is Essential for Enucleation of Human Erythroblasts. *Exp. Hematol.* **2019**, *72*, 14-26.e1, doi:10.1016/j.exphem.2019.02.004.

65. Vlaski, M.; Lafarge, X.; Chevaleyre, J.; Duchez, P.; Boiron, J.-M.; Ivanovic, Z. Low Oxygen Concentration as a General Physiologic Regulator of Erythropoiesis beyond the EPO-Related Downstream Tuning and a Tool for the Optimization of Red Blood Cell Production Ex Vivo. *Exp. Hematol.* **2009**, *37*, 573–584, doi:10.1016/j.exphem.2009.01.007.

66. Richard, A.; Vallin, E.; Romestaing, C.; Roussel, D.; Gandrillon, O.; Gonin-Giraud, S. Erythroid Differentiation Displays a Peak of Energy Consumption Concomitant with Glycolytic Metabolism Rearrangements. *PLOS ONE* **2019**, *14*, e0221472, doi:10.1371/journal.pone.0221472.

67. Caielli, S.; Cardenas, J.; de Jesus, A.A.; Baisch, J.; Walters, L.; Blanck, J.P.; Balasubramanian, P.; Stagnar, C.; Ohouo, M.; Hong, S.; et al. Erythroid Mitochondrial Retention Triggers Myeloid-Dependent Type I Interferon in Human SLE. *Cell* **2021**, *184*, 4464-4479.e19, doi:10.1016/j.cell.2021.07.021.

68. Gonzalez-Menendez, P.; Romano, M.; Yan, H.; Deshmukh, R.; Papoin, J.; Oburoglu, L.; Daumur, M.; Dumé, A.-S.; Phadke, I.; Mongellaz, C.; et al. An IDH1-Vitamin C Crosstalk Drives Human Erythroid Development by Inhibiting pro-Oxidant Mitochondrial Metabolism. *Cell Rep.* **2021**, *34*, 108723, doi:10.1016/j.celrep.2021.108723.

69. Jensen, E.L.; Gonzalez-Ibanez, A.M.; Mendoza, P.; Ruiz, L.M.; Riedel, C.A.; Simon, F.; Schuringa, J.J.; Elorza, A.A. Copper Deficiency-Induced Anemia Is Caused by a Mitochondrial Metabolic Reprograming in Erythropoietic Cells. *Metallomics* **2019**, *11*, 282–290, doi:10.1039/c8mt00224j.

70. Bakker, W.J.; Blázquez-Domingo, M.; Kolbus, A.; Besooyen, J.; Steinlein, P.; Beug, H.; Coffer, P.J.; Löwenberg, B.; von Lindern, M.; van Dijk, T.B. FoxO3a Regulates Erythroid Differentiation and Induces BTG1, an Activator of Protein Arginine Methyl Transferase 1. *J. Cell Biol.* **2004**, *164*, 175–184, doi:10.1083/jcb.200307056.

71. Jan, D.C.H.; Petch, D.A.; Huzel, N.; Butler, M. The Effect of Dissolved Oxygen on the Metabolic Profile of a Murine Hybridoma Grown in Serum-Free Medium in Continuous Culture. *Biotechnol. Bioeng.* **1997**, *54*, 153–164, doi:10.1002/(SICI)1097-0290(19970420)54:2<153::AID-BIT7>3.0.CO;2-K.

72. Ozturk, S.S.; Palsson, B.O. Effect of Medium Osmolarity on Hybridoma Growth, Metabolism, and Antibody Production. *Biotechnol. Bioeng.* **1991**, *37*, 989–993, doi:10.1002/bit.260371015.

73. Restelli, V.; Wang, M.-D.; Huzel, N.; Ethier, M.; Perreault, H.; Butler, M. The Effect of Dissolved Oxygen on the Production and the Glycosylation Profile of Recombinant Human Erythropoietin Produced from CHO Cells. *Biotechnol. Bioeng.* **2006**, *94*, 481–494, doi:10.1002/bit.20875.

74. Brugarolas, J.; Lei, K.; Hurley, R.L.; Manning, B.D.; Reiling, J.H.; Hafen, E.; Witters, L.A.; Ellisen, L.W.; Kaelin, W.G. Regulation of MTOR Function in Response to Hypoxia by REDD1 and the TSC1/TSC2 Tumor Suppressor Complex. *Genes Dev.* **2004**, *18*, 2893–2904, doi:10.1101/gad.1256804.

75. Neunstoecklin, B.; Stettler, M.; Solacroup, T.; Broly, H.; Morbidelli, M.; Soos, M. Determination of the Maximum Operating Range of Hydrodynamic Stress in Mammalian Cell Culture. *J. Biotechnol.* **2015**, *194*, 100–109, doi:10.1016/j.jbiotec.2014.12.003.

76. Anane, E.; Knudsen, I.M.; Wilson, G.C. Scale-down Cultivation in Mammalian Cell Bioreactors—The Effect of Bioreactor Mixing Time on the Response of CHO Cells to Dissolved Oxygen Gradients. *Biochem. Eng. J.* **2021**, *166*, 107870, doi:10.1016/j.bej.2020.107870.

77. Serrato, J.A.; Palomares, L.A.; Meneses-Acosta, A.; Ramírez, O.T. Heterogeneous Conditions in Dissolved Oxygen Affect N-Glycosylation but Not Productivity of a Monoclonal Antibody in Hybridoma Cultures. *Biotechnol. Bioeng.* **2004**, *88*, 176–188, doi:10.1002/bit.20232.

78. van der Windt, G.J.W.; Chang, C.-H.; Pearce, E.L. Measuring Bioenergetics in T Cells Using a Seahorse Extracellular Flux Analyzer. *Curr. Protoc. Immunol.* **2016**, *113*, 3.16B.1-3.16B.14, doi:10.1002/0471142735.im0316bs113.

79. Browne, S.M.; Daud, H.; Murphy, W.G.; Al-Rubeai, M. Measuring Dissolved Oxygen to Track Erythroid Differentiation of Hematopoietic Progenitor Cells in Culture. *J. Biotechnol.* **2014**, *187*, 135–138, doi:10.1016/j.jbiotec.2014.07.433.

80. Barde, I.; Rauwel, B.; Marin-Florez, R.M.; Corsinotti, A.; Laurenti, E.; Verp, S.; Offner, S.; Marquis, J.; Kapopoulou, A.; Vanicek, J.; et al. A KRAB/KAP1-MiRNA Cascade Regulates Erythropoiesis through Stage-Specific Control of Mitophagy. *Science* **2013**, *340*, 350–353, doi:10.1126/science.1232398.

81. Chen, M.; Sandoval, H.; Wang, J. Selective Mitochondrial Autophagy during Erythroid Maturation. *Autophagy* **2008**, *4*, 926–928, doi:10.4161/auto.6716.

82. Sandoval, H.; Thiagarajan, P.; Dasgupta, S.K.; Schumacher, A.; Prchal, J.T.; Chen, M.; Wang, J. Essential Role for Nix in Autophagic Maturation of Erythroid Cells. *Nature* **2008**, *454*, 232–235, doi:10.1038/nature07006.

83. Moradi, F.; Moffatt, C.; Stuart, J.A. The Effect of Oxygen and Micronutrient Composition of Cell Growth Media on Cancer Cell Bioenergetics and Mitochondrial Networks. *Biomolecules* **2021**, *11*, 1177, doi:10.3390/biom11081177.

84. Wagner, B.A.; Venkataraman, S.; Buettner, G.R. The Rate of Oxygen Utilization by Cells. *Free Radic. Biol. Med.* **2011**, *51*, 700–712, doi:10.1016/j.freeradbiomed.2011.05.024.

85. Singh, V. On-Line Measurement of Oxygen Uptake in Cell Culture Using the Dynamic Method. *Biotechnol. Bioeng.* **1996**, *52*, 443–448, doi:10.1002/(SICI)1097-0290(19961105)52:3<443::AID-BIT12>3.0.CO;2-K.

86. Varley, J.; Brown, A.K.; Boyd, J.W.R.; Dodd, P.W.; Gallagher, S. Dynamic Multi-Point Measurement of Foam Behaviour for a Continuous Fermentation over a Range of Key Process Variables. *Biochem. Eng. J.* **2004**, *20*, 61–72, doi:10.1016/j.bej.2004.02.012.

87. Pattison, R.N.; Swamy, J.; Mendenhall, B.; Hwang, C.; Frohlich, B.T. Measurement and Control of Dissolved Carbon Dioxide in Mammalian Cell Culture Processes Using an in Situ Fiber Optic Chemical Sensor. *Biotechnol. Prog.* **2000**, *16*, 769–774, doi:10.1021/bp000089c.

88. Xing, Z.; Lewis, A.M.; Borys, M.C.; Li, Z.J. A Carbon Dioxide Stripping Model for Mammalian Cell Culture in Manufacturing Scale Bioreactors. *Biotechnol. Bioeng.* **2017**, *114*, 1184–1194, doi:10.1002/bit.26232.

89. Xiao, Y.; Konermann, L. Protein Structural Dynamics at the Gas/Water Interface Examined by Hydrogen Exchange Mass Spectrometry. *Protein Sci. Publ. Protein Soc.* **2015**, *24*, 1247–1256, doi:10.1002/pro.2680.

90. Vardar-Sukan, F. Foaming and Its Control in Bioprocesses. In *Recent Advances in Biotechnology*; Vardar-Sukan, F., Sukan, Ş.S., Eds.; NATO ASI Series; Springer Netherlands: Dordrecht, **1992**; pp. 113–146 ISBN 978-94-011-2468-3.

91. Al-Masry, W.A. Effects of Antifoam and Scale-up on Operation of Bioreactors. *Chem. Eng. Process. Process Intensif.* **1999**, *38*, 197–201, doi:10.1016/S0255-2701(99)00014-8.

92. Routledge, S.J.; Poyner, D.R.; Bill, R.M. Antifoams: The Overlooked Additive? *Pharm. Bioprocess.* **2014**, *2*, 103–106, doi:10.2217/PBP.14.5.

93. Velugula-Yellela, S.R.; Williams, A.; Trunfio, N.; Hsu, C.; Chavez, B.; Yoon, S.; Agarabi, C. Impact of Media and Antifoam Selection on Monoclonal Antibody Production and Quality Using a High Throughput Micro-bioreactor System. *Biotechnol. Prog.* **2018**, *34*, 262–270, doi:10.1002/btpr.2575.

94. Chattopadhyay, D.; Rathman, J.F.; Chalmers, J.J. The Protective Effect of Specific Medium Additives with Respect to Bubble Rupture. *Biotechnol. Bioeng.* **1995**, *45*, 473–480, doi:10.1002/bit.260450603.

95. Jordan, M.; Eppenberger, H.M.; Sucker, H.; Widmer, F.; Einsele, A. Interactions between Animal Cells and Gas Bubbles: The Influence of Serum and Pluronic F68 on the Physical Properties of the Bubble Surface. *Biotechnol. Bioeng.* **1994**, *43*, doi:10.1002/bit.260430603.

96. Ma, N.; Chalmers, J.J.; Auniņs, J.G.; Zhou, W.; Xie, L. Quantitative Studies of Cell-Bubble Interactions and Cell Damage at Different Pluronic F-68 and Cell Concentrations. *Biotechnol. Prog.* **2004**, *20*, 1183–1191, doi:10.1021/bp0342405.

97. Tharmalingam, T.; Ghebeh, H.; Wuerz, T.; Butler, M. Pluronic Enhances the Robustness and Reduces the Cell Attachment of Mammalian Cells. *Mol. Biotechnol.* **2008**, *39*, 167–177, doi:10.1007/s12033-008-9045-8.

98. Guzniczak, E.; Jimenez, M.; Irwin, M.; Otto, O.; Willoughby, N.; Bridle, H. Impact of Poloxamer 188 (Pluronic F-68) Additive on Cell Mechanical Properties, Quantification by Real-Time Deformability Cytometry. *Biomicrofluidics* **2018**, *12*, 044118, doi:10.1063/1.5040316.

99. Sahay, G.; Batrakova, E.V.; Kabanov, A.V. Different Internalization Pathways of Polymeric Micelles and Unimers and Their Effects on Vesicular Transport. *Bioconjug. Chem.* **2008**, *19*, 2023–2029, doi:10.1021/bc8002315.

100. Zhang, Z.; al-Rubeai, M.; Thomas, C.R. Effect of Pluronic F-68 on the Mechanical Properties of Mammalian Cells. *Enzyme Microb. Technol.* **1992**, *14*, 980–983, doi:10.1016/0141-0229(92)90081-x.

101. Armstrong, J.K.; Meiselman, H.J.; Wenby, R.B.; Fisher, T.C. Modulation of Red Blood Cell Aggregation and Blood Viscosity by the Covalent Attachment of Pluronic Copolymers. *Biorheology* **2001**, *38*, 239–247, PMID:11381178.

102. Harington, J.S. A Study of the Chemical Composition and Potential Hazards of an Antifoam Substance Used in Intracardiac Surgery. *Thorax* **1961**, *16*, 120–127, doi:10.1136/thx.16.2.120

103. McGregor, W.C.; Weaver, J.F.; Tansey, S.P. Antifoam Effects on Ultrafiltration. *Biotechnol. Bioeng.* **1988**, *31*, 385–389, doi:10.1002/bit.260310416.

104. Chaudhary, G.; Luo, R.; George, M.; Tescione, L.; Khetan, A.; Lin, H. Understanding the Effect of High Gas Entrance Velocity on Chinese Hamster Ovary (CHO) Cell Culture Performance and Its Implications on Bioreactor Scale-up and Sparger Design. *Biotechnol. Bioeng.* **2020**, *117*, 1684–1695, doi:10.1002/bit.27314.

105. Wang, S.; Godfrey, S.; Ravikrishnan, J.; Lin, H.; Vogel, J.; Coffman, J. Shear Contributions to Cell Culture Performance and Product Recovery in ATF and TFF Perfusion Systems. *J. Biotechnol.* **2017**, *246*, 52–60, doi:10.1016/j.jbiotec.2017.01.020.

106. Chalmers, J.J. Mixing, Aeration and Cell Damage, 30+ Years Later: What We Learned, How It Affected the Cell Culture Industry and What We Would like to Know More About. *Curr. Opin. Chem. Eng.* **2015**, *10*, 94–102, doi:10.1016/j.coche.2015.09.005.

107. Ito, Y.; Nakamura, S.; Sugimoto, N.; Shigemori, T.; Kato, Y.; Ohno, M.; Sakuma, S.; Ito, K.; Kumon, H.; Hirose, H.; et al. Turbulence Activates Platelet Biogenesis to Enable Clinical Scale Ex Vivo Production. *Cell* **2018**, *174*, 636-648.e18, doi:10.1016/j.cell.2018.06.011.

108. Aunins, J.G.; Henzler, H.-J. Aeration in Cell Culture Bioreactors. In *Biotechnology Set*; John Wiley & Sons, Ltd, **2001**; pp. 219–281 ISBN 978-3-527-62099-9.

109. Côté, P.; Bersillon, J.-L.; Huyard, A. Bubble-Free Aeration Using Membranes: Mass Transfer Analysis. *J. Membr. Sci.* **1989**, *47*, 91–106, doi:10.1016/S0376-7388(00)80862-5.

110. Emery, A.N.; Jan, D.C.-H.; Al-Rueai, M. Oxygenation of Intensive Cell-Culture System. *Appl. Microbiol. Biotechnol.* **1995**, *43*, 1028–1033, doi:10.1007/BF00166920.

111. Glen, K.E.; Cheeseman, E.A.; Stacey, A.J.; Thomas, R.J. A Mechanistic Model of Erythroblast Growth Inhibition Providing a Framework for Optimisation of Cell Therapy Manufacturing. *Biochem. Eng. J.* **2018**, *133*, 28–38, doi:10.1016/j.bej.2018.01.033.

112. Cruz, H.J.; Freitas, C.M.; Alves, P.M.; Moreira, J.L.; Carrondo, M.J.T. Effects of Ammonia and Lactate on Growth, Metabolism, and Productivity of BHK Cells. *Enzyme Microb. Technol.* **2000**, *27*, 43–52, doi:10.1016/S0141-0229(00)00151-4.

113. Hassell, T.; Gleave, S.; Butler, M. Growth Inhibition in Animal Cell Culture. The Effect of Lactate and Ammonia. *Appl. Biochem. Biotechnol.* **1991**, *30*, 29–41, doi:10.1007/BF02922022.

114. Ozturk, S.S.; Riley, M.R.; Palsson, B.O. Effects of Ammonia and Lactate on Hybridoma Growth, Metabolism, and Antibody Production. *Biotechnol. Bioeng.* **1992**, *39*, 418–431, doi:10.1002/bit.260390408.

115. Patel, S.D.; Papoutsakis, E.T.; Winter, J.N.; Miller, W.M. The Lactate Issue Revisited: Novel Feeding Protocols To Examine Inhibition of Cell Proliferation and Glucose Metabolism in Hematopoietic Cell Cultures. *Biotechnol. Prog.* **2000**, *16*, 885–892, doi:10.1021/bp000080a.

116. Al-Ani, A.; Toms, D.; Kondro, D.; Thundathil, J.; Yu, Y.; Ungrin, M. Oxygenation in Cell Culture: Critical Parameters for Reproducibility Are Routinely Not Reported. *PLoS ONE* **2018**, *13*, e0204269, doi:10.1371/journal.pone.0204269.

117. Luo, S.-T.; Zhang, D.-M.; Qin, Q.; Lu, L.; Luo, M.; Guo, F.-C.; Shi, H.-S.; Jiang, L.; Shao, B.; Li, M.; et al. The Promotion of Erythropoiesis via the Regulation of Reactive Oxygen Species by Lactic Acid. *Sci. Rep.* **2017**, *7*, 38105, doi:10.1038/srep38105.

118. van den Akker, E.; Satchwell, T.J.; Pellegrin, S.; Daniels, G.; Toye, A.M. The Majority of the in Vitro Erythroid Expansion Potential Resides in CD34(-) Cells, Outweighing the Contribution of CD34(+) Cells and Significantly Increasing the Erythroblast Yield from Peripheral Blood Samples. *Haematologica* **2010**, *95*, 1594–1598, doi:10.3324/haematol.2009.019828.

119. Heideveld, E.; Masiello, F.; Marra, M.; Esteghamat, F.; Yağcı, N.; von Lindern, M.; Migliaccio, A.R.F.; van den Akker, E. CD14+ Cells from Peripheral Blood Positively Regulate Hematopoietic Stem and Progenitor Cell Survival Resulting in Increased Erythroid Yield. *Haematologica* **2015**, *100*, 1396–1406, doi:10.3324/haematol.2015.125492.

120. Pollock, J.; Ho, S.V.; Farid, S.S. Fed-Batch and Perfusion Culture Processes: Economic, Environmental, and Operational Feasibility under Uncertainty. *Biotechnol. Bioeng.* **2013**, *110*, 206–219, doi:10.1002/bit.24608.

121. Xu, S.; Gavin, J.; Jiang, R.; Chen, H. Bioreactor Productivity and Media Cost Comparison for Different Intensified Cell Culture Processes. *Biotechnol. Prog.* **2017**, *33*, 867–878, doi:10.1002/btpr.2415.

122. Walther, J.; Lu, J.; Hollenbach, M.; Yu, M.; Hwang, C.; McLarty, J.; Brower, K. Perfusion Cell Culture Decreases Process and Product Heterogeneity in a Head-to-Head Comparison With Fed-Batch. *Biotechnol. J.* **2019**, *14*, 1700733, doi:10.1002/biot.201700733.

123. Zamani, L.; Lundqvist, M.; Zhang, Y.; Aberg, M.; Edfors, F.; Bidkhori, G.; Lindahl, A.; Mie, A.; Mardinoglu, A.; Field, R.; et al. High Cell Density Perfusion Culture Has a Maintained Exoproteome and Metabolome. *Biotechnol. J.* **2018**, doi:10.1002/biot.201800036.

124. Shuler, M.L.; Kargi, F. *Bioprocess Engineering: Basic Concepts*; Prentice-Hall international series in the physical and chemical engineering sciences; 2nd Edition.; Prentice Hall, **2002**; ISBN 978-0-13-478215-7.

125. Bandyopadhyay, B.; Humphrey, A.E.; Taguchi, H. Dynamic Measurement of the Volumetric Oxygen Transfer Coefficient in Fermentation Systems. *Biotechnol. Bioeng.* **1967**, *9*, 533–544, doi:10.1002/bit.260090408.

126. Tribe, L.A.; Briens, C.L.; Margaritis, A. Determination of the Volumetric Mass Transfer Coefficient (k(L)a) Using the Dynamic "Gas out-Gas in" Method: Analysis of Errors Caused by Dissolved Oxygen Probes. *Biotechnol. Bioeng.* **1995**, *46*, 388–392, doi:10.1002/bit.260460412.

2.10. Supplementary methods

2.10.1. Cell cycle state measurements using flow cytometry

About 1×10^6 cells were centrifuged (5 min, 600g), washed with ice-cold PBS, fixed with 5 mL of ice-cold methanol, and stored at -20 °C until analysis. From this suspension, 200 000 fixed cells were centrifuged (10 min, 1200g), washed with ice-cold PBS, resuspended in FxCycle™ PI/RNase staining solution (Invitrogen), incubated in the dark (10 min, 20 °C), and analyzed using an Accuri C6 flow cytometer (BD Biosciences). Calculation of the percentages of cells in G0/G1, S, and G2/M phase was done using FlowJo™ using the Watson Pragmatic algorithm set to the following parameters: G1 peak range = 300 000 – 600 000; G1 peak CV = unconstrained; G2 peak = unconstrained; G2 peak CV = G1 peak CV.

2.10.2. Calculation of kinetic parameters

Growth rate and doubling time

For the expansion of erythroblasts, cells were cultured following a sequential batch feeding strategy in which medium was refreshed if the cell concentration (determined daily) was $>1.2\times10^6$ cells/mL. This leads to cell and metabolite concentrations over time as displayed in Supplementary Figure S2C-F. We assumed that cells followed exponential growth at a constant rate (μ; 1/day) between consecutive dilution events:

$$\frac{d\,(C_N\,V_L)}{dt} = \mu_{\text{counts}}\,C_N\,V_L$$

where C_N is the concentration of cells (in cells/mL), V_L is the volume of culture (in mL), and t is the time of culture (in days).

The maximum growth rate was estimated for each time interval between dilutions, using the measured cell concentration post- medium refreshment (t_{i-1}) and after overnight growth (t_i), assuming no change in culture volume between both timepoints (i.e. evaporation):

$$\mu_{\text{counts}} = \frac{\ln\left(\frac{C_N(t_i)}{C_N(t_{i-1})}\right)}{t_i - t_{i-1}}$$

As cell size decrease is characteristic of erythropoiesis, the total volume of cells per unit of volume of culture (C_V; μm^3 of cells per mL of culture) was also used as proxy for total biomass concentration. With this biomass concentration, we calculated a growth rate that takes into account the progressive decrease in cell size during culture (μ_{vol}; 1/day):

$$\mu_{\text{vol}} = \frac{\ln\left(\frac{C_V(t_i)}{C_V(t_{i-1})}\right)}{t_i - t_{i-1}}$$

For both μ_{counts} and μ_{vol}, only data of cells with a diameter larger than 7.5 or 5 µm was used, respectively. Doubling time was calculated as:

$$\tau = \frac{\ln 2}{\mu}$$

Cell-specific consumption and production rates of metabolites

Cell-specific consumption/production rates of metabolites were assumed to be constant between consecutive medium refreshment events, and were calculated using metabolite concentration data and the calculated growth rate:

$$\frac{d\,(C_{\text{lac}}\,V_L)}{dt} = q_{\text{lac,counts}}\,C_N\,V_L$$

For instance, the cell-specific production rate of lactate ($q_{\text{lac,counts}}$; mol lactate/cell/day) was calculated as:

$$q_{\text{lac,counts}}(t_i) = \mu_{\text{counts}}(t_i)\frac{C_{\text{lac}}(t_i) - C_{\text{lac}}(t_{i-1})}{C_N(t_i) - C_N(t_{i-1})}$$

where $C_{\text{lac}}(t_i)$ is the measured supernatant concentration of lactate (in mol/mL) at timepoint t_i. Rates were also calculated using the total biomass concentration (e.g. $q_{\text{lac,vol}}$; mol lactate/ µm^3 cell/day).

Cell-specific oxygen consumption rate

For the determination of the cell-specific oxygen consumption rate (q_{O_2}; mol O_2/cell/h), dissolved oxygen data between consecutive medium refreshments (~24 h intervals) was fitted to a black box model assuming a constant growth rate and q_{O_2} in the analyzed time interval:

$$\frac{d\,(C_{O_2}\,V_L)}{dt} = k_L a\,\left(C_{O_2}^{\text{sat}} - C_{O_2}\right)V_L - q_{O_2}C_N V_L$$

where V_L is the culture volume (in L), $C_{O_2}^{\text{sat}}$ is the saturation oxygen concentration for the culture conditions (7.2 mg O_2/L = 0.225 mmol O_2/L using air + 5% CO_2 at atmospheric pressure and 37 °C), C_{O_2} is the dissolved oxygen concentration in the culture (in mol/L, calculated as $C_{O_2} = \text{dO}_2 \times C_{O_2}^{\text{sat}}$), and $k_L a$ is the overall volumetric mass transfer coefficient of the system recalculated to a liquid-side mass transfer oxygen composition gradient (with a being the specific interfacial area = m^2 interfacial area/m^3 liquid volume) [124]. The cell concentration C_N (cells/L) was calculated for all timepoints of each day using the estimated growth rate:

$$C_N(t) = C_{N,0}\,e^{\mu_{\text{count}}\,t}$$

The value of q_{O_2} for each day was calculated by iteratively solving the differential equation describing C_{O_2} was and fitting to each 24 h interval of dO_2 measurements. The value of the overall mass transfer coefficient of the system ($k_L a$) was determined experimentally for the culture conditions (using water, with equal working volume, temperature and pressure) with the dynamic method: oxygen was purged from the liquid by nitrogen sparging until reaching a dO_2<0.5%, followed by a constant flow of air in the headspace of 100 mL/min until close to saturation (dO_2>90%). The value of $k_L a$ was estimated by fitting of the same black box model to the measured dO_2 data, with $q_{O_2} = 0$ [125,126].

2.11. Supplementary figures

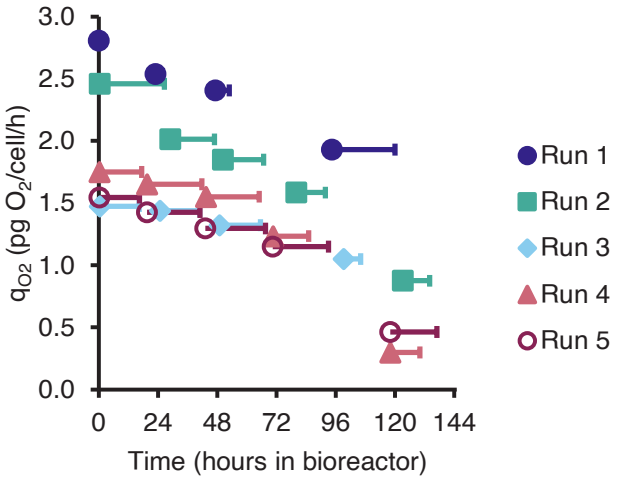

Supplementary Figure S1. Quantification of oxygen requirements of expanding erythroblasts. Erythroblasts were expanded from PBMCs for 9 days, and subsequently seeded in 500 mL stirred tank bioreactors (working volume = 300 mL; stirring speed = 200 rpm; marine down-pumping impeller with diameter = 2.8 cm) at a starting cell concentration of 0.7×10^6 cells/mL. A headspace flow of 100 mL/min (air + 5% CO_2) as only source of oxygen for the culture. Cell-specific oxygen consumption rates (q_{O2}) was determined via the dynamic method, using the drop of dO_2 after each dilution event and the calculated growth rate between consecutive medium refreshment events (see Supplementary Methods). Length of the bars depict the time interval used for the fitting of the oxygen mass balance model.

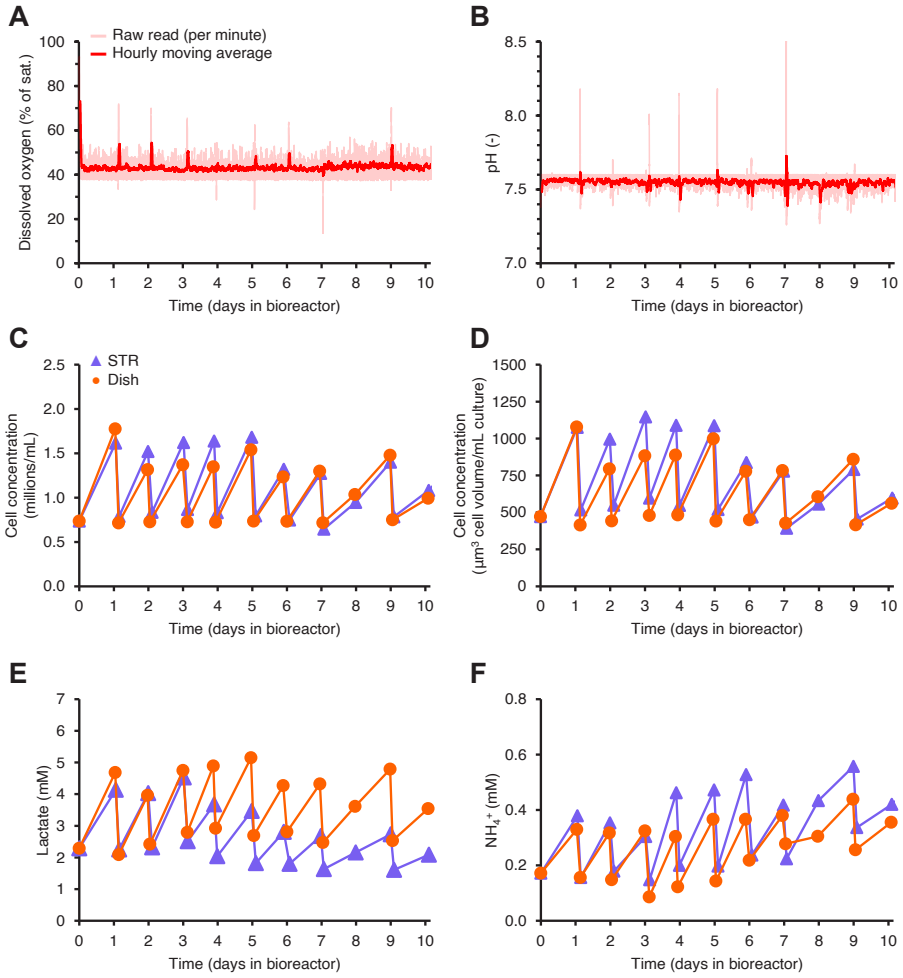

Supplementary Figure S2. Expansion of erythroblasts in stirred tank bioreactors. Erythroblasts were expanded from PBMCs for 9 days, and subsequently seeded in culture dishes or STRs (working volume = 300 mL; stirring speed = 200 rpm; marine down-pumping impeller with diameter = 2.8 cm; 100 mL/min N_2 headspace flow) at a starting cell concentration of 0.7×10^6 cells/mL. **(A)** dO_2 concentration was continuously measured and controlled at 40% (equivalent to 2.8 mg O_2/L) by sparging of air. **(B)** pH was continuously measured and controlled at 7.5 by sparging of CO_2. **(C)** Cell concentration was measured daily during 10 days of expansion. Cells were cultured following a sequential batch feeding strategy in which medium was refreshed if the daily measured cell concentration was $>1.2\times10^6$ cells/mL. **(D)** Total biomass concentration was calculated using the total cell volume (cells with diameter >5 µm) per mL of culture. **(E-F)** Extracellular lactate and ammonia concentrations were measured daily before and after medium refreshment. All data is displayed for a representative reactor run, using the same donor for both bioreactor and dish cultures.

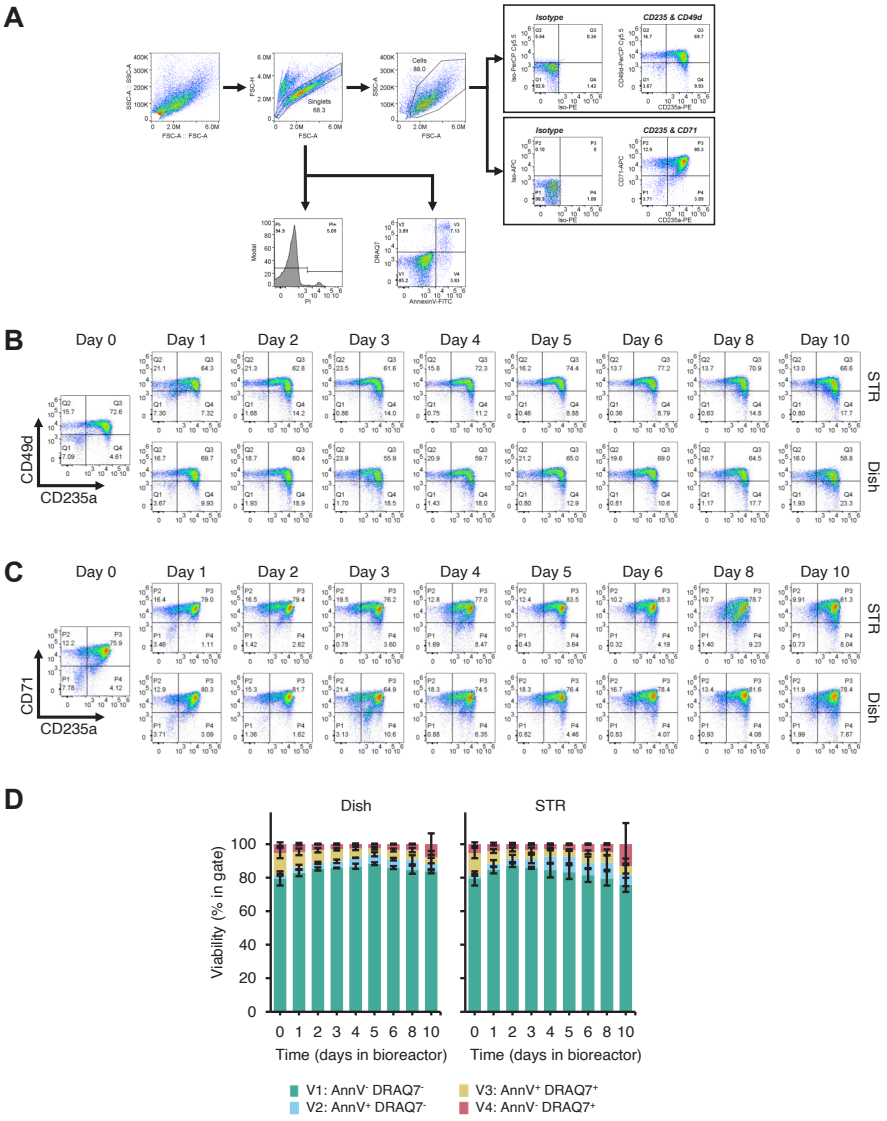

Supplementary Figure S3. Erythroid cell surface marker expression and viability in erythroblasts expanded in stirred tank bioreactors. Erythroblasts were expanded from PBMCs for 9 days, and subsequently seeded in culture dishes or STRs (working volume = 300 mL; stirring speed = 200 rpm; marine down-pumping impeller with diameter = 2.8 cm; 100 mL/min N_2 headspace flow) at a starting cell concentration of 0.7×10^6 cells/mL. **(A)** Gating strategy to evaluate the differentiation level of cultured erythroblasts. Single events were gated (FSC-A vs. FSC-H), followed by gating of cells (FSC vs SSC). Cells were stained for CD235a/CD71 or CD235a/CD49d, with gates defined based on appropriate IgG isotype controls. **(B-C)** Representative density plots indicating the expression of the cell surface markers CD71, CD235 and CD49d after 10 days of culture. **(D)** Cells were also stained with AnnexinV (apoptosis staining) and DRAQ7 (cell impermeable DNA stain); data displayed as mean ± SD (error bars; n=3 reactor runs / donors).

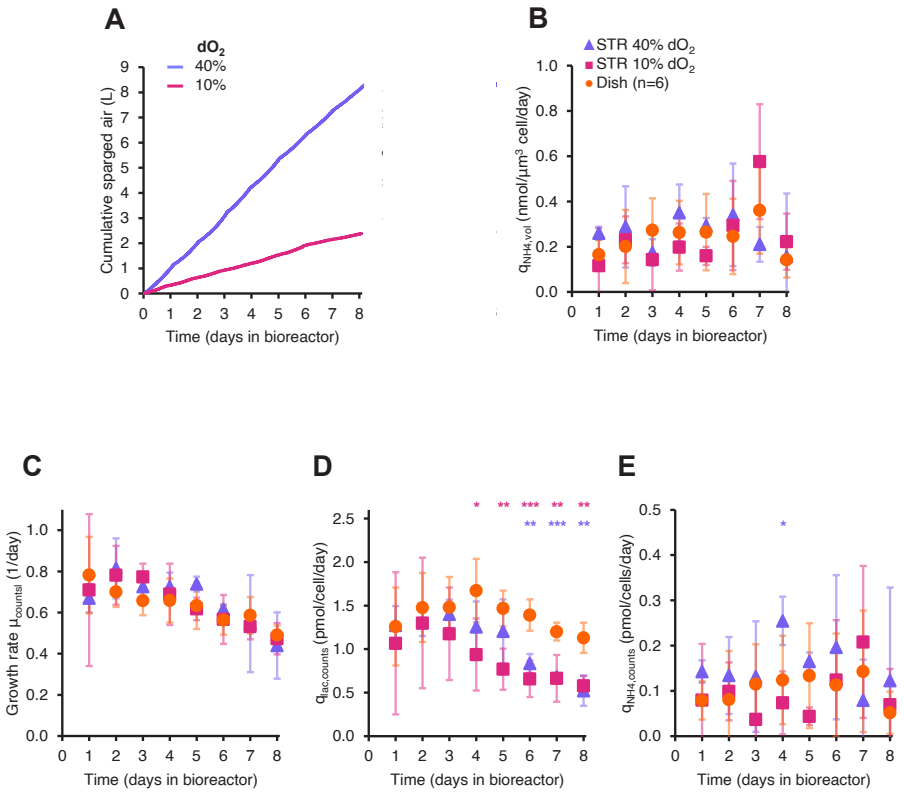

Supplementary Figure S4. Lower dissolved oxygen setpoints lead to lower sparging requirements. Erythroblasts were expanded from PBMCs for 9 days, and subsequently seeded in culture dishes or STRs (working volume = 300 mL; 200 rpm; pH=7.5; 100 mL/min N_2 headspace flow) at a starting cell concentration of 0.7×10^6 cells/mL. Dissolved oxygen was controlled by means of air sparging when below the targeted setpoint (10% of 40%, equivalent to 0.72 and 2.88 mg O_2/L respectively), and by stripping of excess oxygen using 100 mL/min N_2 headspace flow. **(A)** Cumulative volume of air sparged through the culture for representative reactor runs. **(B)** Cell-specific ammonium production rate ($q_{NH4,vol}$) calculated using growth rate data and measured extracellular lactate concentrations before and after each medium refreshment (see Supplementary Methods). **(C-E)** Rates were also calculated using the total cell concentration (cells per mL of culture). All data in panels **B-E** is displayed as mean ± SD (error bars; n=3 reactor runs / donors, unless indicated otherwise). Significance is shown for the comparison with dish cultures (unpaired two-tailed two-sample equal-variance Student's *t*-test; *p<0.05, **p<0.01, ***p<0.001, not displayed if difference is not significant).

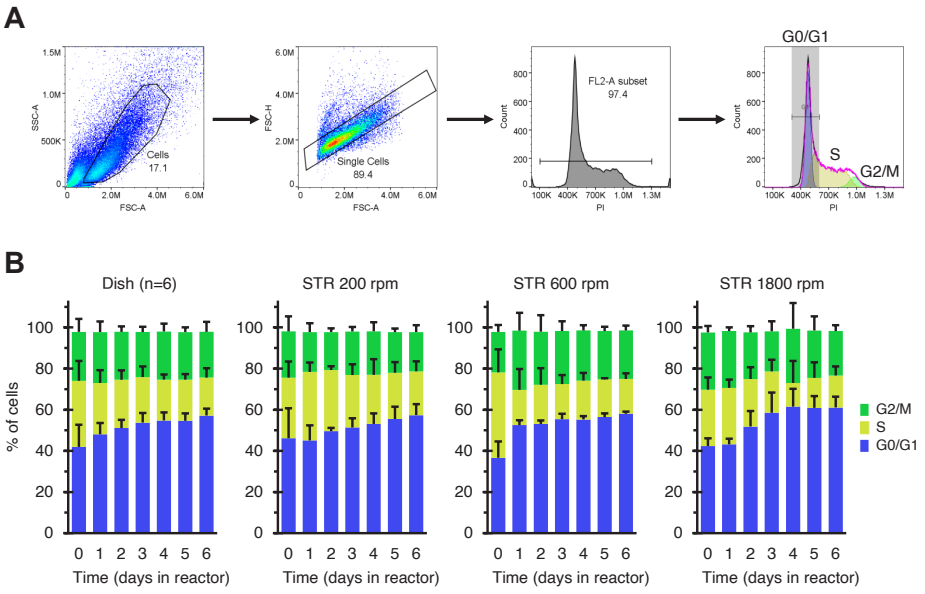

Supplementary Figure S5. Effect of stirring speed on cell cycle of cultured erythroblasts. Erythroblasts were expanded from PBMCs for 9 days, and subsequently seeded in culture dishes or STRs (working volume = 300 mL; marine down-pumping impeller with diameter = 2.8 cm; dO_2=40% controlled by sparging of air; pH=7.5 controlled by sparging of CO_2; 100 mL/min N_2 headspace flow) at a starting cell concentration of 0.7×10^6 cells/mL, under agitation at 200, 600 or 1800 rpm. **(A)** Gating strategy to evaluate the fraction of fixed cells in the G0/G1, S, or G2/M cell cycle stages. Cells were gated (FSC vs SSC), followed by gating of single events (FSC-A vs. FSC-H). Background in the PI channel was discarded, followed by fitting using the Watson Pragmatic algorithm. **(B)** Fraction of cells in the G0/G1, S, and G2/M cell cycle phases in bioreactor and static cultures. All data is displayed as mean ± SD (error bars; n=3 reactor runs / donors, unless indicated otherwise).

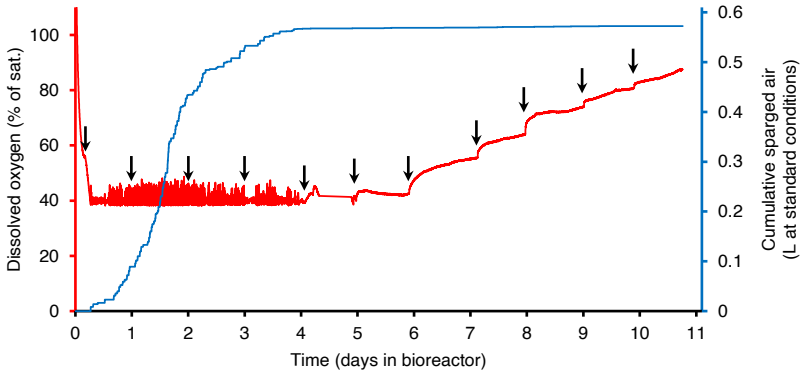

Supplementary Figure S6. Oxygen requirements decrease during erythroblast differentiation. Erythroblasts were expanded from PBMCs for 10 days, and subsequently seeded in differentiation medium at a starting cell concentration of 1×10^6 cells/mL. Cells were then transferred to culture dishes or STRs in culture dishes or STRs (working volume = 300 mL; stirring speed = 200 rpm; pH = 7.5) and kept in culture for 11 days without medium refreshment. Dissolved oxygen was measured continuously during the culture (red line; left axis). Air + 5% CO_2 was sparged only when dO_2 was <40%. Cumulative sparged air volume is also displayed (blue line; right axis). When taking samples (indicated with arrows), air was used to purge the sampling circuit, leading to an increase in the dO_2 concentration.

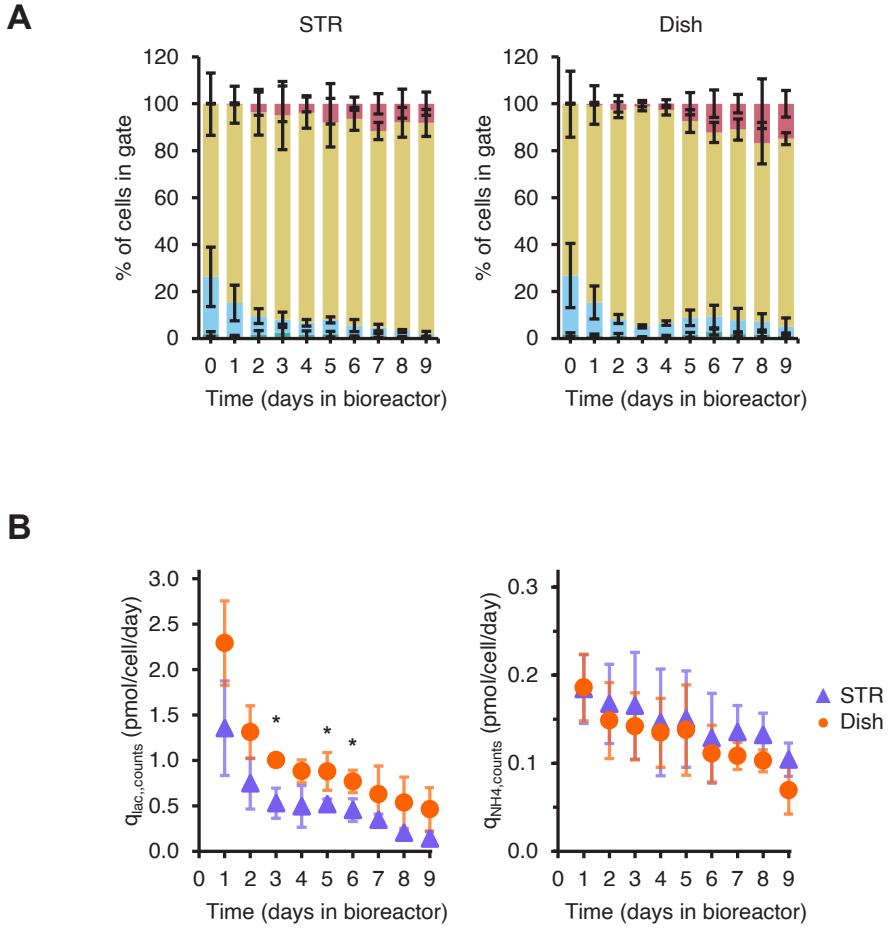

Supplementary Figure S7. Expression of the erythroid surface markers (CD235a, CD71) and production rates of toxic metabolites (lactate, ammonia) in erythroblasts cultured in 3 L stirred tank bioreactors. Erythroblasts were expanded from PBMCs for 8 days, and subsequently seeded in culture dishes or 0.5 L stirred tank bioreactors at a starting cell concentration of 0.7-0.9×10^6 cells/mL. Cells were kept in culture following a fed batch feeding strategy in which medium was refreshed if the measured cell concentration (daily) was >1.2×10^6 cells/mL. Upon reaching a total number of >400 million cells, the culture was transferred to a 3.0 L bioreactor which was progressively filled by daily medium additions. **(A)** Cells were stained CD235a plus CD71 (erythroid differentiation markers). **(B)** Cell-specific production rates of lactate and ammonia calculated from the total cell counts, and extracellular metabolite concentrations. All data is displayed as mean ± SD (error bars; n=3 reactor runs / donors). Significance is shown for the comparison with dish cultures (unpaired two-tailed two-sample equal-variance Student's *t*-test; **p*<0.05, ***p*<0.01, ****p*<0.001, not displayed if difference is not significant).

III

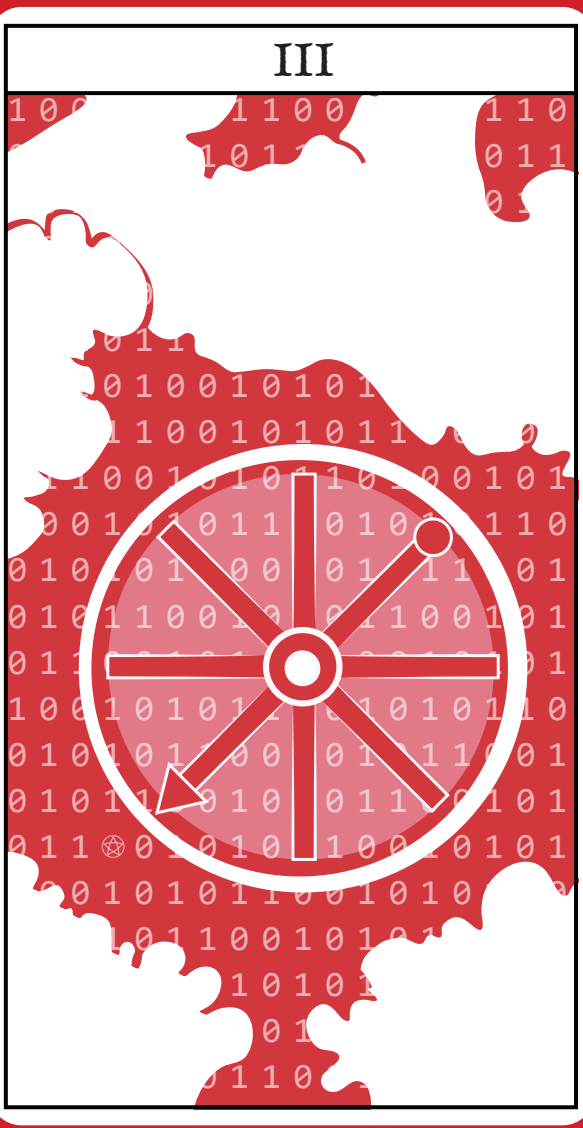

Chapter 3

Metabolic profiling of cultured erythroblast for the production of transfusion-ready cultured red blood cells

Joan Sebastián Gallego-Murillo | Ingeborg van Lakwijk | Nurcan Yağcı | Julie A. Reisz | Angelo D'Alessandro | Luuk A. M. van der Wielen | Emile van den Akker | Aljoscha Wahl | Marieke von Lindern

Abstract

Transfusion-ready red blood cells (RBCs) can be cultured *ex vivo* from hematopoietic progenitors. Currently, however, a cultured RBC transfusion unit cannot be produced at competitive costs. Large volumes of medium are required to maintain a maximum erythroblast cell density of 1-2×10^6 cells/mL during the proliferation culture stage. To identify the origin of the cell density limitation we compared the growth support of fresh, spent, and treated media, and we performed metabolomic studies. Media that were exposed to an increasing concentration of erythroblasts displayed a proportional decrease in their ability to support erythroblast proliferation. With a 1:1 combination with fresh medium, the growth was restored for all treated media. Separation of both fresh and spent media with a 3 kDa cut-off, and subsequent recombination of the two fractions, indicated that exhaustion of the small molecular weight fraction (<3 kDa) was responsible for the growth limitation. We performed targeted and untargeted metabolomics analysis, for both the intra- and extracellular compartments, following seeding in fresh medium (12, 24, 36 h). After 36 h of culture, we observed degradation of nucleosides, depletion of amino acids, and a decrease in intermediates of the glutathione-ascorbate, ɣ-glutamyl and cysteine-methionine cycles. The latter compounds suggested accumulated oxidative stress in high density erythroblast cultures. Elimination of nucleosides from the medium led to a lower accumulation of purine salvage intermediates, and a 30% increase in cell productivity.

3.1. Introduction

Production of cultured RBCs (cRBCs) has great potential as an additional source of transfusion-ready RBCs, particularly to increase the availability of RBCs with rare blood group phenotypes [1–3]. Starting from iPSC- or blood-derived hematopoietic stem cells, erythroblasts can be produced in large numbers, followed by differentiation into mature, hemoglobinized, enucleated cRBCs that resemble peripheral blood reticulocytes [4,5]. Expansion of erythroblast cultures requires the growth factors erythropoietin (Epo), stem cell factor (SCF), and glucocorticoid hormones. Substitution of SCF and glucocorticoids by omniplasma, together with an increase in Epo levels, induces synchronous differentiation to mature RBCs [6–8].

A single transfusion unit contains 2×10^{12} mature RBCs. To reach this high number of cells, a robust increase in cell numbers is needed during the expansion phase of the cultures. Currently, erythroblast cultures are kept at low cell concentrations ($<2\times10^{6}$ cells/mL), through daily dilutions with fresh medium. Addition of fresh culture medium lowers the cell concentration, but also replenishes nutrients and growth factors, and dilutes potential inhibitory metabolites and cytokines produced by the proliferating cells [9–11].

Growth limitations have been observed in high cell density erythroblast cultures ($3\text{-}5\times10^{6}$ cells/mL) after less than 20 h of inoculation in fresh medium, suggesting either a quick depletion of essential nutrients or growth factors, or the fast accumulation of inhibitory cytokines or metabolic byproducts [12]. Supplementation of culture medium with nutrients such as glucose, amino acids, and vitamins, or with growth factors (Epo, SCF) does not result in a significant difference in proliferation rate. A significant accumulation of the inhibitory cytokine TFG-β has been detected (>1 ng/mL). Nevertheless, this compound alone only leads to moderate decrease in growth rate (<10%) [12].

Mathematical models fitted to the observed growth limitations in erythroblast cultures indicated an optimized medium refreshment frequency and reduced medium requirements in repeated batch cultivation strategy [13]. However, the requirement of frequent fresh medium addition, combined with the high cost of media, still leads to non-competitive high production costs [14,15].

Growth inhibition is commonly observed in batch and fed-batch cultures of industrially relevant animal cell lines. Accumulation of lactate and ammonium are the most common cause of growth inhibition [16]. Under substrate-excess conditions, rapidly proliferating cell cultures heavily rely on glycolysis, leading to the accumulation of

lactate, which can lead to toxic effects due to an increase in osmolarity and decrease in pH . Ammonium, mainly produced as a byproduct of glutamine catabolism, is also a common cause of growth inhibition [17,21]. Although accumulation of lactate and ammonium is observed in erythroblast cultures, the concentrations are well below growth inhibitory levels [12,22–26].

Unbiased approaches using untargeted metabolomics in mammalian cell cultures have identified novel metabolic byproducts associated with growth inhibition [27]. In particular, an increase in levels of growth-inhibitory intermediates of amino acid catabolism, and impaired oxidative stress control in Chinese hamster ovary (CHO) cell cultures were reported [28,29]. Reducing the production of these inhibitors by metabolic engineering and modifications in the medium composition have led to significant improvements in cell yields, as well as in quality and titer of the final product, typically monoclonal antibodies [30–32].

To achieve cost-effective production of cRBCs, the culture conditions must be optimized for high cell density cultures. In the present work, we aim to identify the origins of the observed limitations of cell concentrations in erythroblast cultures. This knowledge will enable us to propose strategies at both feeding regime and media composition level to surpass current limitations. We quantified the cell density limitations in the erythroblast proliferation phase of our erythroid culture system, identified the limit in the cell productivity (produced cells per mL of fresh medium per unit of time), and demonstrated that perfusion of fresh medium in a stirred tank bioreactor setup allows for higher erythroblast cell concentrations. The observed erythroblast growth limitation is caused mainly by small molecules (<3 kDa) present in the culture supernatant. Metabolic profiling of erythroblasts at low and high cell densities identified metabolic pathways that indicate excessive oxidative stress in the culture.

3.2. Materials and Methods

3.2.1. Erythroblast cell culture

Blood from healthy volunteer donors was collected and peripheral blood mononuclear cells (PBMCs) were purified by density centrifugation using Ficoll-Paque (density = 1.077 g/mL; 600g, 30 min; GE Healthcare; USA). Informed written consent was given by donors to give approval for research purposes, and was checked by Sanquin's NVT Committee (approval file number NVT0258; 2012) in accordance with the Declaration of Helsinki and the Sanquin Ethical Advisory Council.

Erythroblast were cultured from PBMCs as previously described (Heshusius et al.,

2019), with minor modifications in the expansion medium (Cellquin) composition: trace elements were omitted; cholesterol, oleic acid, and L-α-phosphatidylcholine were replaced by a defined lipid mix (1:1000; Sigma-Aldrich cat#L0288; USA). In short, PBMCs were cultured in the presence of human stem cell factor (hSCF; 100 ng/mL, produced in-house with HEK293T cells), erythropoietin (Epo; 2 IU/mL; EPREX®; Janssen-Cilag; Netherlands), dexamethasone (Dex; 1 µmol/L; Sigma-Aldrich), and interleukin-3 (IL-3; 1 ng/mL, first day only; Stemcell Technologies; Canada). After 7 days, a pro-erythroblast population ($CD235a^{low}/CD71^{+}/CD49^{+}$) was obtained, and was kept in culture at a cell concentration of $0.7\text{-}2\times10^{6}$ cells/mL by daily feeding with fresh expansion medium prior to culture experiments. For cultures without nucleosides, medium without adenosine, guanosine, thymidine, cytidine, uracil, 2'-deoxyadenosine, 2'-deoxycytidine, and 2'-deoxyguanosine was used.

Cell concentration was determined using an electric current exclusion method with a size cutoff of 7.5 µm (CASY Model TCC, OLS OMNI Life Science, Germany; or Z2 Coulter Counter, Beckman Coulter, USA). Viability was determined using a hemocytometer and a dye exclusion method (Trypan Blue; Sigma).

3.2.2. Targeted profiling of culture supernatant

Measurement of amino acid concentrations in supernatant samples was determined via gas chromatography-mass spectrometry (GC-MS) and isotope dilution mass spectrometry (IDMS), as previously described [33]. Briefly, culture samples were spun down (600g, 5 min), and the supernatant was freeze dried, reconstituted and derivatized using acetonitrile and N-tert-Butyldimethylsilyl-N-methyltrifluoroacetamide (MTBSTFA), and subsequently analyzed by GC-MS. IDMS for amino acid quantification was performed using a U-^{13}C-labelled cell extract as an internal standard mix.

For quantification of extracellular Epo and hSCF concentrations, erythroblasts cultures were performed in proliferation medium with 2 IU/mL Epo (EPREX®; Janssen-Cilag; Netherlands) and 100 ng/mL hSCF (BioLegend cat#573908; USA). Supernatant samples were snap frozen, and stored at -80 °C until measurement. After thawing on ice, samples were analyzed via sandwich enzyme-linked immunosorbent assays (ELISA; ab211647 and ab176109, Abcam; USA).

The average q-rates for amino acids and growth factors were calculated with Equation 1, where q_i is the cell-specific consumption (>0) or production (<0) rate for the component i, $C_{i,t}$ and $C_{i,t+1}$ are the measured concentrations of component i at the evaluated timepoints (t and $t+1$), and $C_{X,t}$ and $C_{X,t+1}$ are the measured cell concentrations at the same timepoints. The average growth rate μ in that same time

interval was calculated using Equation 2.

$$q_i = \mu \cdot \frac{C_{i,t+1} - C_{i,t}}{C_{X,t+1} - C_{X,t}} \quad \text{Equation (1)}$$

$$\mu = \frac{\ln(C_{X,t+1}) - \ln(C_{X,t})}{t+1 \; - \; t} \quad \text{Equation (2)}$$

3.2.3. Bioreactor perfusion culture

The perfusion bioreactor culture was performed in a 500 mL glass bioreactor (MiniBio; Applikon Biotechnology; Netherlands) with a working volume of 250 mL. A day 9 cell culture from PBMCs was seeded in the bioreactor at an initial cell concentration of 1×10^6 cells/mL. Agitation was performed using a down-pumping marine impeller (100 rpm; diameter = 2.8 cm). Dissolved oxygen concentration was maintained at 2.9 mg/L (40% of the oxygen saturation concentration in water at equilibrium with air at 1 atm and 37 °C) by sparging with air, and pH was controlled at 7.4 by sparging with CO_2.

Cell retention in the bioreactor was performed using an acoustic settler (BioSep 1 L; Applikon Biotechnology) run without recirculation and using a cyclic backflushing mode, as described before [34,35], set to the following parameters: ON time = 5-15 min, OFF time = 10-15 s, power = 3 W. The volumetric perfusion rate was adjusted daily based on the cell counting data to obtain an average cell-specific perfusion rate (CSPR) of 500 pL/cell/day, equivalent to the fresh medium utilization rate in the repeated batch cultivation method with half medium refreshment every 24 h.

3.2.4. Spent medium analysis and fractionation

Erythroblasts were expanded from PBMCs for 11 days and subsequently seeded in fresh medium at cell concentrations between 1 and 15×10^6 cells/mL, as indicated. Cells were cultured for 16 h, and spun down (600g, 5 min). Spent medium was filtrated (0.22 µm), snap frozen in liquid nitrogen, and stored at -80 °C until further use. Upon thawing, day 9 erythroblasts were washed, resuspended in fresh medium, spent medium or a 1:1 (vol) combination of both, and cultured for 48 h without medium refreshment.

For medium fractionation experiments, fresh or spent medium was filtrated using an Amicon Ultra-15 3 kDa centrifugal filter, following manufacturer's protocol (Millipore Merck; Germany), resulting in a filtrate and retentate fractions. Day 9 erythroblasts were seeded in combinations of retentate and filtrate of fresh or spent medium, as indicated.

3.2.5. Spent medium supplementation

The effect of spent medium supplementation with specific fractions of IMDM was evaluated using previously prepared solutions with respective IMDM components. For basal IMDM (bIMDM), a solution containing 1.49 mM $CaCl_2$, 0.81 mM $MgSO_4$, 4.43 mM KCl, 36 mM $NaHCO_3$, 77.1 mM NaCl, 1.04 mM NaH_2PO_4, 0.75 µM KNO_3, 25 mM HEPES, and 25 mM D-glucose was prepared with demineralized water. For selenite supplementation, Na_2SeO_3 was added to bIMDM to a final concentration of 0.1 µM (bIMDM+Se).

To test the effect of amino acid supplementation, bIMDM was supplemented with essential amino acids only (bIMDM+EAA), or with both essential and non-essential amino acids (bIMDM+EAA+NEAA). Amino acids in the prepared media were at 2× the concentration in commercial IMDM, so when combining 1:1 with spent medium any depleted amino acid would be restored to the levels originally present in IMDM. Final concentrations of essential amino acids in bIMDM+EAA and bIMDM+EAA+NEAA were 1.6 mM L-lysine, 0.93 mM L-tyrosine, 0.58 mM L-cystine, 0.8 mM L-arginine, 0.4 mM L-histidine, 1.6 mM L-isoleucine, 0.4 mM L-methionine, 0.8 mM L-phenylalanine, 1.6 mM L-leucine, 1.6 mM L-threonine, 0.16 mM L-tryptophan, 1.6 mM L-valine, and 4.0 mM L-glutamine. For non-essential amino acids, final concentrations in bIMDM+EAA+NEAA were 0.8 mM L-serine, 0.45 mM L-aspartate, 0.69 mM L-proline, 0.8 mM glycine, 0.38 mM L-asparagine, 0.56 mM L-alanine, and 1.0 mM L-glutamate.

Similarly, bIMDM was supplemented with vitamins (bIMDM+Vit) to have final concentrations 2× higher relative to commercial IMDM. For this, MEM vitamin mix (ThermoFisher cat#11120052), biotin and vitamin B12 were added to bIMDM to final concentrations as follows: 8 mg/L nicotinamide, 8 mg/L cholin chloride, 8 mg/L Ca-D-pantothenate, 8 mg/L pyridoxal HCl, 8 mg/L thiamine HCl, 0.8 mg/L riboflavin, 8 mg/L folic acid, 16 mg/L myo-inositol, 26 µg/L biotin, and 26 µg/L vitamin B12.

Epo, hSCF and Dex were added to the final media combinations (e.g. 1:1 spent medium and bIMDM) to have final concentrations of 2 IU/mL, 100 ng/mL and 1 µM, respectively.

3.2.6. Extra- and intracellular untargeted UHPLC-MS metabolomics

Day 11 erythroblasts of three independent donors were washed twice with phosphate-buffered saline (PBS), resuspended in fresh medium, and cultured for 36 h under static conditions without medium refreshment. Samples containing 3×10^6 cells were spun down (600g, 5 min, 4 °C), and both cell pellet and supernatant were snap frozen in liquid nitrogen and stored at -80 °C until extraction. Metabolite extraction was performed

using an ice-cold methanol:acetonitrile:water buffer (5:3:2) by vortexing for 30 minutes at 4 °C. Analyses were performed using a Vanquish UHPLC system (Thermo Fischer Scientific; USA) coupled online to a Q Exactive mass spectrometer, as previously described [36]. Metabolite assignment was performed using MAVEN [37].

Data cleaning was performed in three stages: (i) pre-filtering of metabolites that did not show significant differences in peak areas (Student *t*-test, $p>0.05$) at any condition or timepoint compared to blank samples, (ii) missing value imputation (missing values replaced by 1/5 of the smallest positive value in the original dataset), and (iii) filtering based on the quality control (QC) samples (if a metabolite showed a relative standard deviation >25% in the QC samples, it is not considered for further analysis).

For analysis of metabolomics data, principal component analysis (PCA) was performed using the peak area data for each annotated metabolite after glog transformation and mean-centering. *k*-means clustering was performed using the *ComplexHeatmap* R package [38], using the *clustree* and *factoextra* packages to determine the optimal number of clusters [39].

For functional analysis, metabolites were first mapped to the Human Metabolome Database (HMDB). Metabolite-set quantitative enrichment analysis (MSQEA) and pathway quantitative enrichment analysis (PQEA) of the complete set of metabolites and of individual *k*-means clusters were performed using MetaboAnalystR v3 (package version 3.0.3 amap_0.8-18) [40,41], and a metabolite set library derived from the Small Molecule Pathway Database [42,43]. All R code used to process and analyze the metabolomics data is available at request.

3.2.7. Mathematical modelling of growth inhibition

Erythroblast growth inhibition was modelled using kinetic unstructured unsegregated mathematical models described with a set of three ordinary differential equations (culture volume, cell concentration, and non-dimensionalized inhibitor concentration). Detailed equations for the growth models and for the simulations of bioreactor cultures under different feeding regimes are available in Supplementary Methods.

3.3. Results

3.3.1. Limited production of cultured erythroblast is independent of growth factor availability

To determine the cell production capacity of Cellquin medium, erythroblasts cultured from PBMC of two independent donors were inoculated in fresh medium at three different starting cell densities (1, 3 and 5×10^6 cells/mL). The cultures were performed

for 48 h without medium addition or refreshment. All conditions resulted in lower proliferation levels compared to those predicted by an exponential growth model fitted to the first 12 h of growth (Figure 1A). The deviation from exponential growth was larger and took place earlier for high cell density cultures (Figure 1B). The growth rate fitted to the first 12 h of culture ranged from a doubling time of 17.4 h for cultures seeded at 1.3×10^6 cells/mL to 34.6 h for cultures seeded at 5.2×10^6 cells/mL (Table 1). This indicates that medium conditions rapidly become rate limiting at increased cell densities (<12 h after start of the culture).

To determine whether depletion of the growth factors Epo or SCF could explain the observed growth limitations, erythroblasts from three different donors were seeded at 1×10^6 cells/mL in fresh medium supplemented with hSCF and Epo, and cultured for 2 days without any medium refreshment. Less than 25% Epo and 50-80% of the initial hSCF was depleted at day 2 (Figure 1C-D). Assuming that depletion occurred mainly through internalization of ligand with its cognate receptor, Epo and hSCF cell-specific consumption rates (q_{Epo}, q_{hSCF}) were calculated for each donor using the calculated average growth rate between day 0 and 2 (Table 2).

To determine whether periodical replenishment of growth factors would improve cell growth, erythroblasts seeded at cell concentrations between 0.3 and 2×10^6 cells/mL were kept in culture for 4 days with daily addition of fresh hSCF and Epo (100 ng/mL and 2 IU/mL, respectively). After 2 days, growth in low cell density cultures slowed down, while high cell density cultures reached a cell concentration plateau (Supplementary Figure S1). Total number of cells produced per mL of medium relative to the start of the culture peaked at 5-6×10^6 cells/mL for inoculation densities of 1-2×10^6 cells/mL (Figure 1E; growth curves in Supplementary Figure S1).

These observations suggest that growth factor depletion is not the origin of the growth decrease observed in batch cultures. Rather, there is a growth-linked depletion of one or more essential nutrients or the accumulation of toxic byproducts during the batch culture, as if often observed for other bioprocesses [44]. This suggests that other medium feeding strategies are required for erythroblast cultures. Therefore, cultivation using perfusion was used to increase nutrient supply and removal of inhibitory metabolites accumulated during culture.

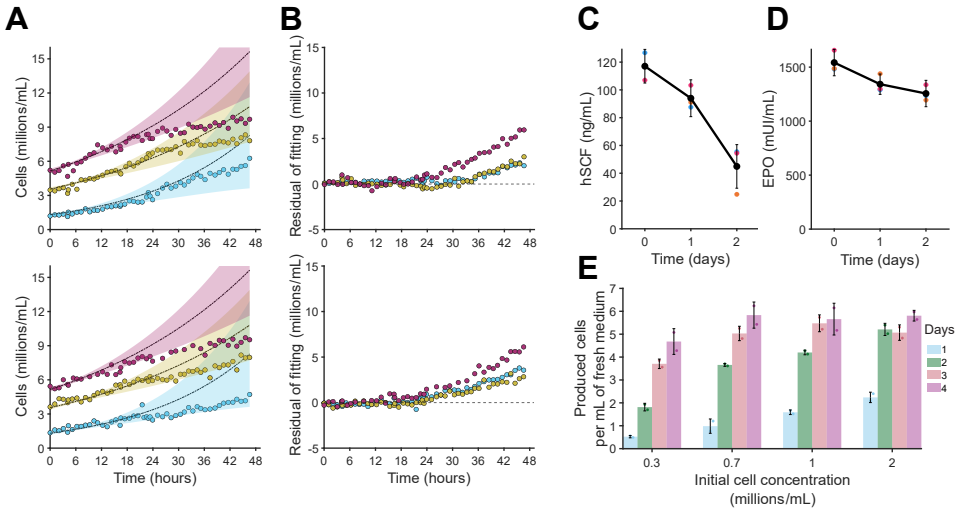

Figure 1. Growth limitations and maximal cell productivity in cultured proliferating erythroblasts. (A-B). PBMC-derived day 10 erythroblasts from two independent donors were inoculated in fresh proliferation medium at different starting cell densities (1, 3 and 5×10^6 cells/mL), and cultured for 2 days without addition of fresh medium (batch culture), with hourly measurements of cell concentration. An exponential growth model, shown as black dotted lines, was fitted for each starting cell density to the first 12 hours of cell culture of both donors (fitted parameters: growth rate μ, and initial cell concentration C_0; value of fitted parameters available in Table 1). Shaded areas indicate the upper and lower 95% prediction bounds for the the fitted model (determined with MATLAB *predint* function) **(A)**. The difference between measured cell concentration and predictions of the exponential growth model was calculated through the complete culture time (**B**; colors match panel A). **(C-D)** Depletion levels of hSCF and Epo were determined in batch erythroblast cultures (3 independent donors) inoculated with a starting cell density of $1.0\text{-}1.5\times10^6$ cells/mL. Colors indicate independent cultures, the black line indicates the average. Calculated growth rates and cell-specific consumption rates of both growth factors for each donor are available in Table 2. **(E)** Maximum cell productivity (produced number of cells per mL of culture, calculated as the difference in cell concentration relative to the start of the culture) was determined for 4-day batch cultures inoculated at 0.3, 0.7, 1 and 2×10^6 cells/mL using erythroblasts derived from 2 independent donors (growth curves available in Supplementary Figure 1). Error bars are displayed as standard deviations of measurements (n=3).

	μ (1/h)	C_0 (×10⁶/mL)
●	0.0398 (0.0231 – 0.0564)	1.30 (1.18 – 1.42)
●	0.0224 (0.0128 – 0.0321)	3.57 (3.39 – 3.74)
●	0.0200 (0.0126 – 0.0274)	5.20 (5.01 – 5.39)

Table 1. Fitted parameters of exponential growth model to erythroblast cultures at different starting cell concentrations. PBMC-derived day 10 erythroblasts from two independent donors were inoculated in fresh proliferation medium at different starting cell densities (1, 3 and 5×10^6 cells/mL), and cultured for 2 days without addition of fresh medium (batch culture), with hourly measurements of cell concentration. Growth rate (μ) and initial cell density (C_0) of an exponential growth model were fitted to the first 12 hours of cell concentration measurements. Parameter values that minimized the sum of square errors are reported, together with 95% confidence bounds.

Donor	μ (1/h)	$-q_{EPO}$ (UI/cell/h; $\times10^{-9}$)	$-q_{hSCF}$ (ng/cell/h; $\times10^{-6}$)
1	0.0230	-1.81	-0.52
2	0.0258	-2.17	-0.69
3	0.0247	-2.45	-0.41

Table 2. Cell-specific consumption rates of Epo and hSCF during erythroblast proliferation cultures. Extracellular Epo and hSCF was measured for erythroblast of three independent donors cultured for 2 days without medium refreshment with an initial cell density of $1.0\text{-}1.5\times10^6$ cells/mL. Overall average growth rate μ, and cell-specific consumption rates (q-rates) of hSCF and EPO were calculated for the two days of culture.

3.3.2. Perfusion bioreactor increases erythroblast cell density

Oxygen may be limiting in erythroid cultures in dishes and agitated bioreactors [26]. However, limitations in cell productivity in batch erythroblast cultures are consistent with previous observations in erythroid stirred tank bioreactor cultivations in which oxygen, a potentially limiting substrate in static cultures, was sufficiently provided [12]. To determine which cultivation strategies can ensure sufficient nutrient availability, and decrease toxic byproducts, we modeled erythroblast proliferation bioreactor cultures under different feeding regimes: (i) batch, (ii) fed batch with constant feed rate (FB_{const}), (iii) fed batch with exponentially increasing feeding (FB_{exp}), (iv) perfusion with a constant perfusion rate ($PERF_{const}$), and (v) perfusion at a fixed cell-specific perfusion rate ($PERF_{CSPR}$) (Figure 2A).

For these simulations, we used the kinetic model previously reported by Glen et al., in which erythroblast growth limitation, either via media exhaustion or toxification, was dependent on cell growth [45]. This model also includes an inhibition decay mechanism. A simplified model (only with growth-dependent inhibition, and using a different dose-response model; Hill equation) was fitted to the same cell concentration experimental data reported by Glen et al. for erythroblast cultures with different medium refreshment regimes, and was also used for bioreactor culture simulations (model details available in Supplementary Methods).

A 1 L culture with 1×10^6 cells/mL was used as starting condition for all scenarios, and the optimized feeding parameters for each culture strategy were determined to minimize the overall medium consumption while reaching a total yield of 30×10^9 cells after 4 days of culture. All evaluated feeding regimes led to higher cell densities (Figure 2Ai) and yield (Figure 2Aii) compared to conventional batch culture mode in which cultures do not receive fresh medium. Both fed-batch alternatives (FB_{const}, FB_{exp}) and CSPR-based perfusion ($PERF_{CSPR}$) led to similar medium consumption levels, but the medium additions used in fed-batch cultures require a bioreactor working volume of 8 L at the end of the culture (Figure 2Aiii,iv). For FB_{exp}, a negative exponential factor was found to be optimal, equivalent to fast feeding in the first days of culture, followed by slow feeding at the end of the cultivation. Under constant CSPR perfusion, maximal inhibition in cell growth rate was <20% during the 4 days of culture, while for fed-batch the growth was reduced by >50% (Figure 2Av). Similar values for the optimized parameters of each feeding regime were obtained for both evaluated models (Supplementary Figure S2, Supplementary Table S1).

To validate whether CSPR-based perfusion allows for higher cell concentrations under our own cell culture conditions, day 9 erythroblast cultures were seeded in a 500 mL STR (working volume = 250 mL) at an initial cell concentration of 1×10^6 cells/mL. Fresh medium was continuously perfused into the bioreactor, and cells were retained using an acoustic filtration system (Figure 2B-C). An average daily CSPR of 500 pL/cell/day was used (daily perfusion rates available in Supplementary Figure S3), equivalent to the medium requirements of culture dishes seeded at the same initial concentration and with half medium refreshment every day. After 5 days of culture, cultures in the perfused bioreactor reached a cell concentration of 10.1×10^6 cells/mL (Figure 2D), with similar overall cell number fold change compared to static cultures in dishes under a repeated batch feeding regime (daily reseeding at 1×10^6 cells/mL with fresh medium) (Figure 2E). Perfused and batch-fed cultures were equally viable and able to differentiate to mature RBC (data not shown). A culture dish kept without medium addition (batch mode) showed a decrease in growth after 3 days of culture (similar to data shown in Supplementary Figure S1). The higher cell yield in the perfusion computational model compared to our bioreactor culture can be explained by differences in the culture protocol (i.e. cell source and media composition) used in our experimental models and by Glen et al [45].

Thus, experimental data confirmed increased erythroblast concentrations in a fixed culture volume that can be achieved by a perfusion feeding approach. The observations highlight that the cause of the growth limitation in erythroblast proliferation cultures can be mitigated by the supply of fresh nutrients and/or removal of toxic byproducts produced during growth.

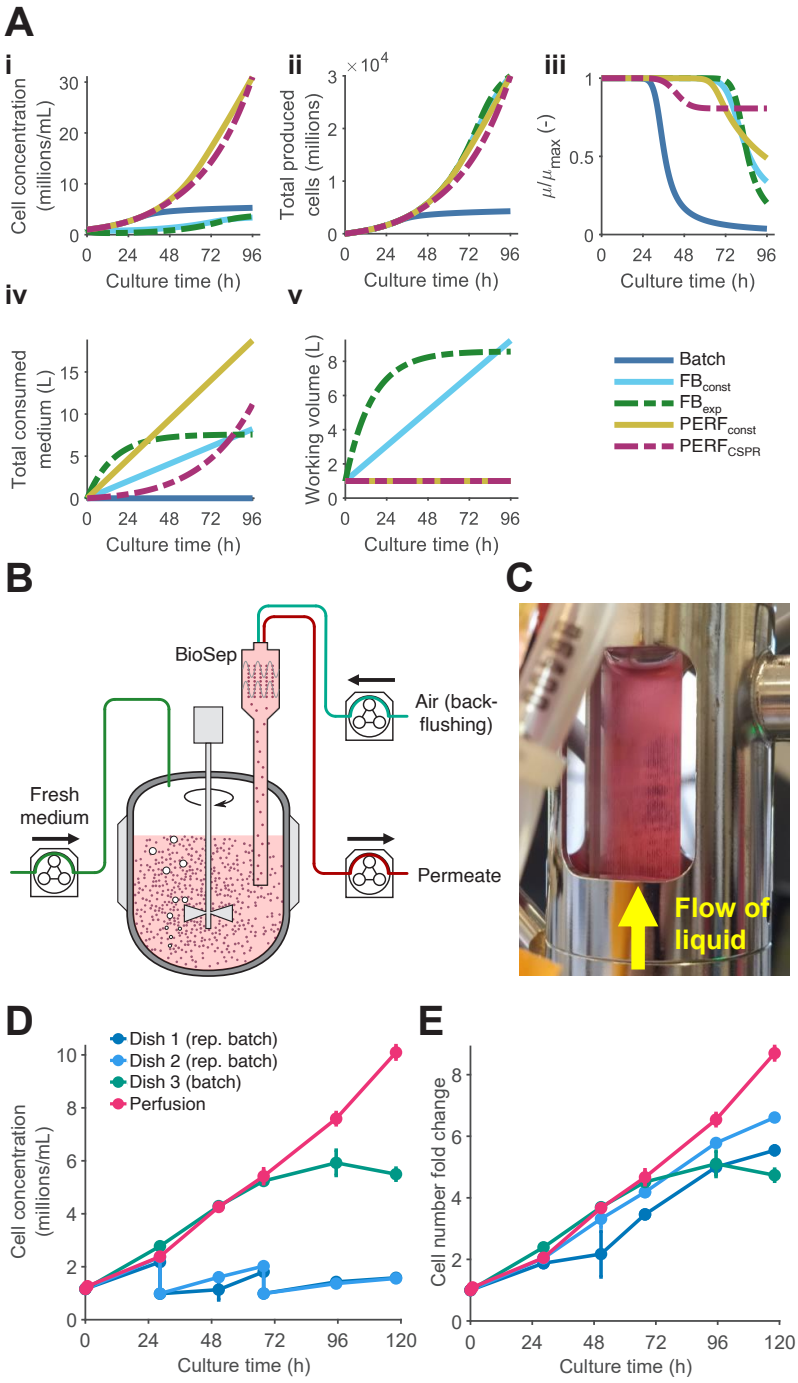

Figure 2.
(See caption on next page)

Figure 2. Perfusion allows to surpass cell-density limitations in erythroblast proliferation cultures. (A) Bioreactor cultures with different feeding strategies (batch, fed batch with constant feed rate FB_{const}, fed batch with exponentially increasing feed FB_{exp}, perfusion at a constant rate $PERF_{const}$, perfusion at a constant cell-specific perfusion rate $PERF_{CSPR}$) were simulated, using a kinetic growth model for erythroblast proliferation including a putative inhibitor produced in a growth-dependent manner. Except for batch mode, the feeding parameters of each feeding regime were optimized to achieve a production of 30×10^9 cells in 4 days in a 1 L bioreactor inoculated at a starting cell concentration of 1×10^6 cells/mL, minimizing the medium volume requirements. Cell concentration **(Ai)**, total produced cells **(Aii)**, magnitude of the growth inhibition (calculated as the ratio of the instantaneous growth rate μ and the maximum growth rate μ_{max} ; **Aiii**), total volume of medium consumed **(Aiv)**, and reactor working volume (**Av**) are displayed. Equations used for the growth model and for the bioreactor simulations are available in Supplementary Methods. **(B)** Day 9 erythroblasts were cultured in a 0.5 L stirred tank bioreactor (working volume = 250 mL) with perfusion, using an acoustic cell retention device (Applikon BioSep), operated semi-continuously, with cycles of permeate liquid flow and cell backflushing using air. **(C)** In this system, cells are retained in the cuvette by sound waves against the upward movement of liquid. Cells can be seen as vertical lines in the separation chamber. **(D-E)** Erythroblast concentration **(D)** and fold-change increase of erythroblast numbers **(E)** in a 5 day culture in a stirred tank bioreactor using an average cell-specific perfusion rate of 500 pL/cell/day (red line), and in culture dishes following either a batch strategy without feeding (green line) or a repeated batch strategy in which the erythroblast concentration was restricted to $<2\times10^6$ by dilution with fresh medium (blue lines). The calculated optimal parameters for the different feeding regimes are available in Supplementary Table S1. Perfusion rates during the complete bioreactor run are available in Supplementary Figure S2.

3.3.3. Exhaustion of small molecules impairs erythroblast proliferation

During perfusion, fresh growth factors and metabolites were fed to the reactor, while potential toxic metabolites were removed from the bioreactor due to the continuous medium exchange. We next determined whether growth decrease was caused by the depletion of an essential nutrient or the accumulation of a toxic byproduct (metabolite or protein) in culture medium. Spent media with increasing levels of cell production were generated by seeding erythroblasts overnight (16 h) in fresh medium at concentrations between 1 and 15×10^6 cells/mL. Supernatant (sterile filtrated; 0.2 µm) was supplemented with fresh growth factors (Epo, hSCF, and dexamethasone) and used to culture an independent batch of erythroblasts at identical, low cell concentration (0.7×10^6 cells/mL). The fresh cultures all doubled in the first 24 h, but the cell yield significantly decreased in the next 24 h when seeded in spent medium derived from overnight exposure to $>5\times10^6$ cells/mL (Figure 3A). The proliferation of fresh cells was increasingly inhibited when media were pre-exposed to higher erythroblast concentrations. Dilution of spent media with fresh medium (1:1) did not shift this correlation between proliferation of fresh cells and the number of cells used in pre-exposure, but recovered cell proliferation for all conditions (Figure 3B). This suggests that the decrease in cell proliferation rates at high cell density is caused by nutrient depletion rather than the production of a toxic byproduct.

Erythroblast culture media contains small molecular weight nutrients (e.g. glucose, amino acids, vitamins, trace elements), proteins (albumin, transferrin, insulin), and lipids. To determine which fraction of medium components is depleted, both fresh and

Figure 3. Small molecules (<3 kDa) contribute the most to the observed growth inhibition in erythroblast batch cultures. (A-B) Spent medium was generated culturing erythroblasts for 16 h at different starting cell concentrations ($1\text{-}15\times10^6$ cells/mL). Either only spent medium **(A)** or a 1:1 mix of spent and fresh media **(B)** was used to seed fresh erythroblasts, which were cultured for 2 days without any media addition (batch cultivation). **(C)** Fresh (F) and spent (S) media were fractionated via ultrafiltration (size threshold: 3 kDa). Erythroblasts were inoculated in different combinations of the flowthrough (<3 kDa) and retentate (>3 kDa) of both media. Cell number fold change after 2 days of culture without refreshment in the reconstituted media is displayed. **(D)** Effect of supplementing spent medium with solutions containing specific components present in Iscove's Modified Dulbecco's Medium (IMDM) on erythroblast proliferation level. Basal IMDM (bIMDM), only containing glucose and the inorganic salts present in full IMDM, was used as background solution to which other IMDM components were added (sodium selenite, Se; essential amino acids, EAA; non-essential amino acids, NEAA; vitamins, Vit). Cell number fold change for erythroblasts inoculated after 2 days of culture is displayed. All data are displayed as mean ± SD (error bars; $n = 9$ donors for panels A and B, $n = 4$ for panel C, $n = 4$ for panel D). Significance levels were calculated using paired two-tailed Student's t-test (ns for non-significant, * for $p < 0.05$, ** for $p < 0.01$, *** for $p < 0.005$).

spent medium (from 15×10^6 cells/mL cultures) were filtered through a 3 kDa cutoff filter. The retentate and flow-through fractions from fresh (F) and spent (S) medium were recombined, and used for cultures of erythroblasts inoculated at 0.7×10^6 cells/mL with addition of fresh growth factors.

The control recombination of retentate and flow-through fractions of fresh medium resulted in similar cell proliferation compared to the unfractionated medium. Unfractionated and recombined spent medium also resulted in similarly reduced cell proliferation (Figure 3C). Importantly, cell growth was restored when erythroblasts were seeded in spent medium retentate combined with flow-through from fresh medium (F<3kDa + S>3kDa). In contrast, cell growth was reduced when erythroblasts

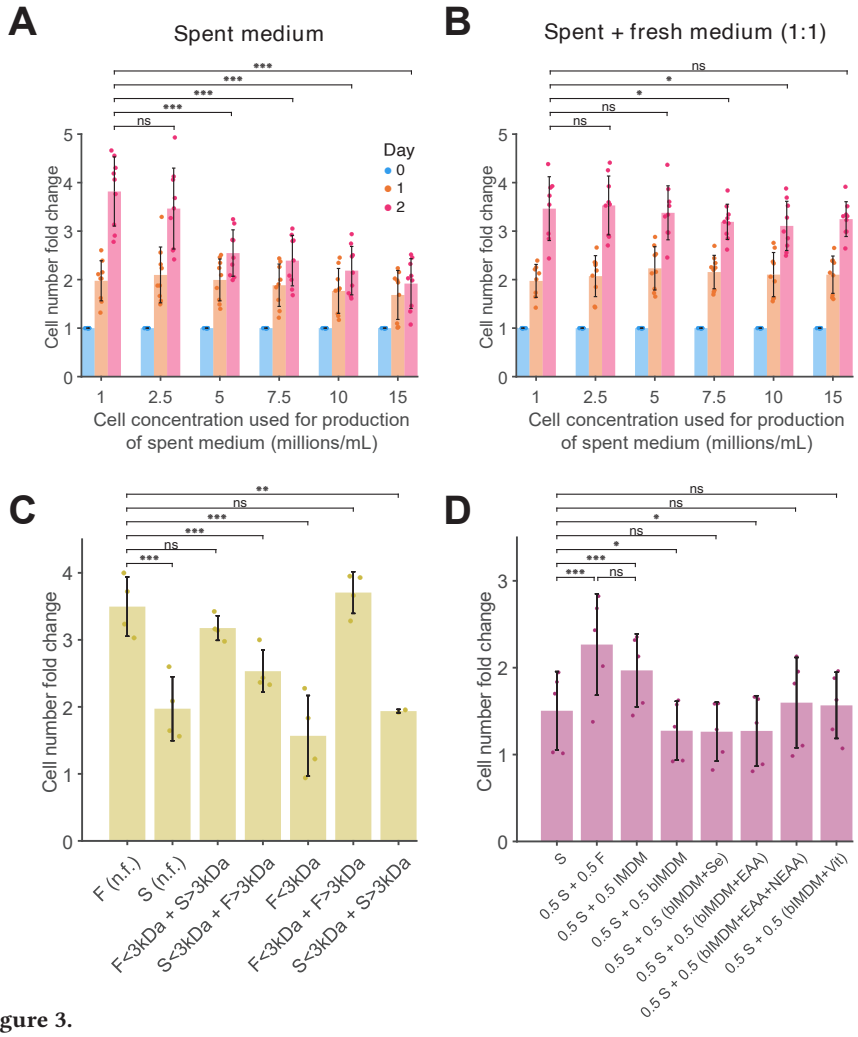

Figure 3.
(See caption on previous page)

were seeded in fresh medium retentate and spent medium flow-through (S<3kDa +F>3kDa). Furthermore, small molecules from fresh medium alone (F<3kDa only) were not sufficient to restore growth. These results suggest that exhaustion of small molecules <3 kDa contributed to the growth limitation in erythroblast batch cultures.

To identify putative depleted small molecules, the spent medium was supplemented with key components of the basal medium IMDM, including essential and non-essential amino acids (EAA and NEAA, respectively), vitamins, and sodium selenite. A minor increase in growth was observed with the addition of non-essential amino acids and vitamins. However, no single condition led to a full recovery of erythroblast proliferation to levels observed in fresh medium (Figure 3D). Thus, we need to investigate the kinetics of medium exhaustion.

3.3.4. Metabolic profiles of media during erythroblast culture

To get a dynamic view of medium nutrients and intermediate metabolites during culture, an untargeted metabolic profiling was performed for the extra- and intra-cellular compartments of the culture. Day 9 erythroblasts cultured from three independent donors were seeded in fresh medium at 0.7 and 2×10^6 cells/mL and cultured for 12, 24 and 36 h. Both cell pellets and supernatant were processed for untargeted metabolome analysis by mass spectrometry.

Analysis of supernatant samples resulted in 93 significantly detected, unique peaks in at least 50% of all samples. Differentially detected nutrients and metabolites were determined by comparison to blank samples run before and after the analysis. Metabolites that showed high variation (relative standard deviation RSD >25%) in quality control samples were not considered for further analysis (Supplementary Figure S5). Principal component analysis (PCA) of extracellular metabolite data showed that independent biological replicates (donors) of a specific time point were closer to each other than samples taken at distinct time points. The first two components described 88% of the total variance (PC1 = 75%, PC2 = 12%; Figure 4A). The clustering of samples seems dependent on time and initial culture density. Central carbon metabolism intermediates and nucleosides largely contribute to PC1 (Figure 4B). Hypoxanthine, an intermediate in purine degradation, displayed the strongest loading (absolute value) for PC2.

For a comprehensive overview of the common and discriminating metabolite profiles, the nutrients and metabolites were visualized using *k*-means clustering (k=5) (Figure 4C-D; see Supplementary Figure 6 for the determination of the optimal number of clusters).

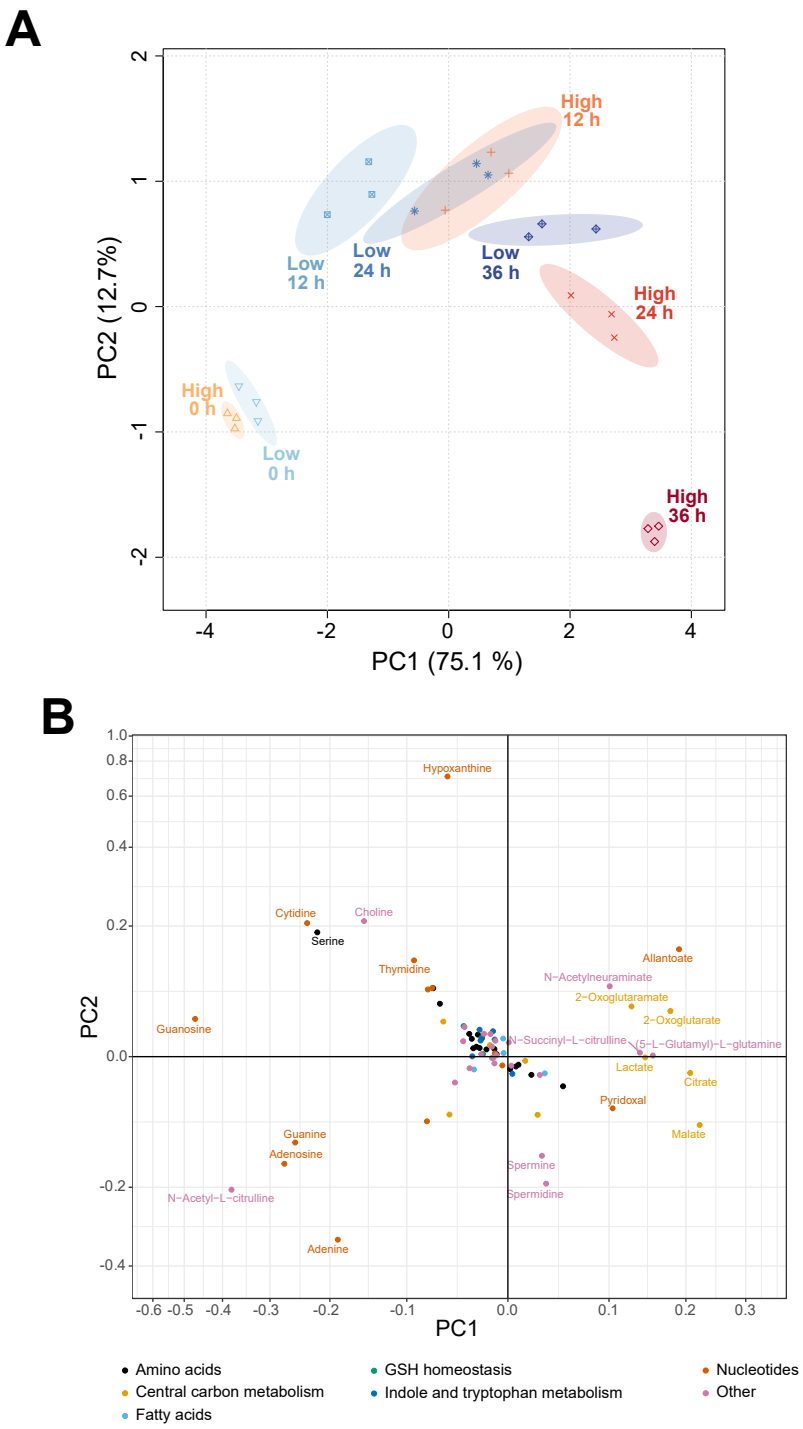

Figure 4.

(Continues in next page)

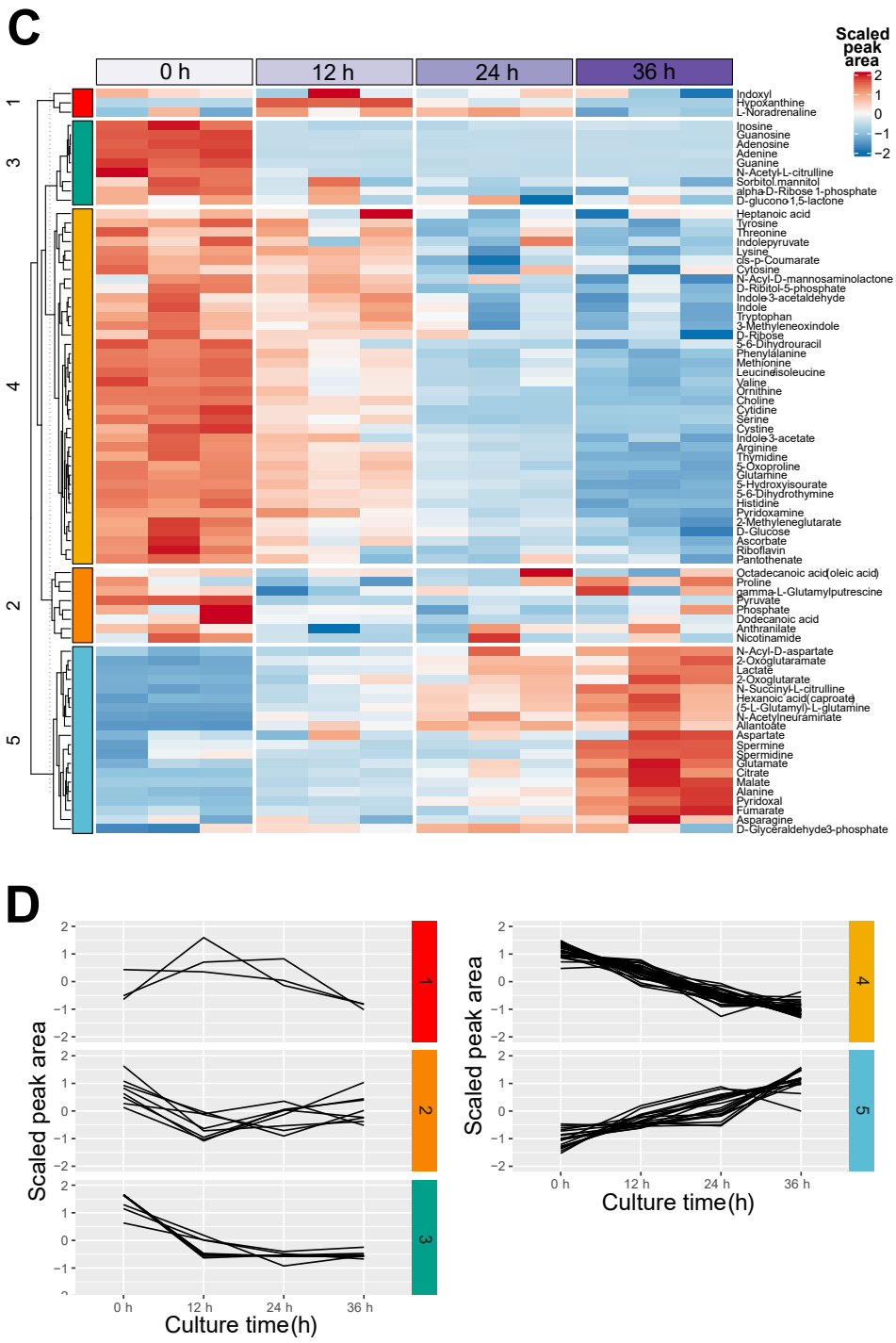

Figure 4.

(Continues in next page)

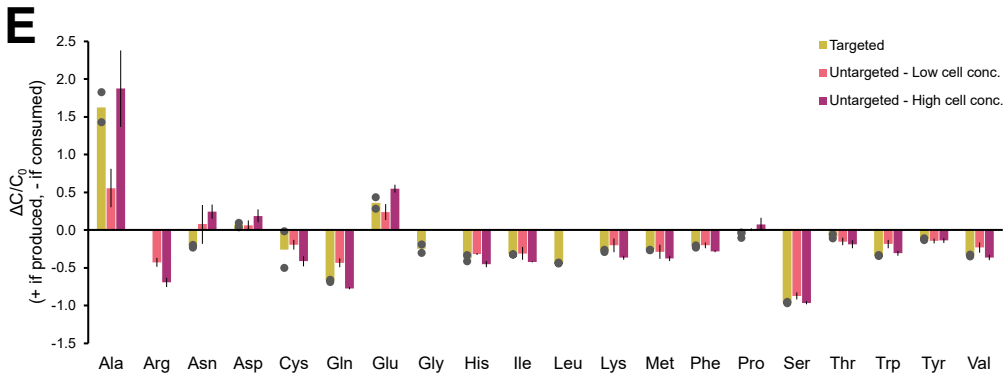

Figure 4. Exo-metabolomics of erythroblast batch cultures. (A-D) Erythroblasts from three independent donors were expanded from PBMCs for 11 days, subsequently inoculated in fresh proliferation medium at a low (0.7×10^6 cells/mL) or high (2.0×10^6 cells/mL) cell concentration, and cultured without medium refreshment for 36 h. Supernatant samples taken at 0, 12, 24, and 36 h were analyzed by untargeted UHPLC-MS metabolomics. **(A)** After removal of non-informative metabolites, and normalization (glog transformation + mean centering) of the peak area, principal component analysis (PCA) was performed. **(B)** Biplot with the loadings of all metabolites for the first two principal components (PC1, PC2). Only metabolites with loadings > 0.1 are labelled. **(C)** Heat map of metabolite peak areas for the high cell density cultures. **(D)** Metabolites were *k*-means clustered, resulting in five groups of metabolites displaying similar trends over the timeseries (cluster 1, *n*=3 metabolites; cluster 2, *n*=9; cluster 3, *n*=38; cluster 4. *n*=8; cluster 5, *n*=20). **(E)** Validation of the amino acid consumption levels observed in the untargeted metabolomics analysis was performed via quantitative determination of amino acid concentrations by GC-MS and IDMS. Erythroblast from two donors were cultured in fresh medium for 2 days. Amino acid concentrations were measured at the beginning (C_0) and end of the culture (C) (data available in Supplementary Table S2). Relative change in amino acid levels is calculated as $\Delta C/C_0 = (C - C_0)/C_0$ (>0 if produced, <0 if consumed), using the measured concentration from targeted metabolomics, or raw peak area for the untargeted data. For the latter, no data is available for glycine (it could not be measured with the used analytical platform). Data in panel E for is displayed as mean ± range of the measurements for targeted data ($n=2$), and as mean ± standard deviation for untargeted data ($n=3$).

Most metabolites showed a monotonic decrease in extracellular concentration with culture time (cluster 4). Some metabolites displayed a transient accumulation (cluster 1) or transient depletion (cluster 2) phase. Multiple intermediates of the TCA cycle (e.g. 2-oxoglutarate, malate, and fumarate) accumulated in the medium (cluster 5). In contrast, nucleoside concentrations rapidly decreased (e.g, guanosine and adenosine; cluster 3).

Amino acids also decreased rapidly in the supernatant (cluster 4), except for aspartate, glutamate, and alanine that accumulated during culture (cluster 5). Amino acids are major contributors to protein synthesis and consequently proliferation [46]. Only

serine, a non-essential amino acid, displayed full depletion after 36 h of culture, both for low and high cell density cultures.

For amino acids, the relative changes determined by untargeted metabolomics were additionally confirmed by targeted measurements. Cells from two independent donors were seeded at 1×10^6 cells/mL, and cultured for 2 days (final cell concentration = 3×10^6 cells/mL). Supernatant samples were analyzed with internal standards using GC-MS (Figure 4E; absolute concentrations available in Supplementary Table S2). Glutamine, the most abundant amino acids in fresh medium, was rapidly consumed (overall cell-specific consumption rate of 283-314 nmol/million cells/day; Supplementary Table S3), reaching a consumption level of 67% at the end of culture.

3.3.5. The intracellular erythroblast metabolome

Samples for intracellular metabolite measurements were collected parallel to the medium samples. Similar to the exometabolome, the principal component analysis shows dependence with culture time, although with larger dispersion between biological replicates (Figure 5A-B). The composition of the metabolome of cells cultured at low concentration for 12 or 24 h overlapped with erythroblasts inoculated at high density for 12 h both in PC1 and PC2. Also the subsequent samples (36 h low density and 24 h high density) show similarities. Cells cultured for 36 h at high density are distant from other measurement timepoints.

Using *k*-means clustering (k=5), the main profiles were identified. Clusters 1 and 2 represent metabolites that are rapidly depleted, including some amino acids (serine, arginine, lysine) and adenine/adenosine (Figure 5C-D). Cluster 3 represents metabolites that stay constant for 24 h but display accelerated decrease in intracellular levels at 36 h. These include glucose, ribose, glutamine and pyrimidines. Clusters 4 and 5 contain metabolites that initially increase in concentration, but are reduced again after 36 h in culture. These include mono- and diphosphate nucleosides and intermediates of the Krebs cycle.

The prominent depletion of amino acids both in medium and in cells suggests that this could be an inhibiting factor. Supplementation with amino acids, however, did not recover proliferation of erythroblasts in exhausted medium (Figure 3D). Thus, the depletion of amino acids likely contributes to the observed erythroblast growth limitations, but other factors play a role as well.

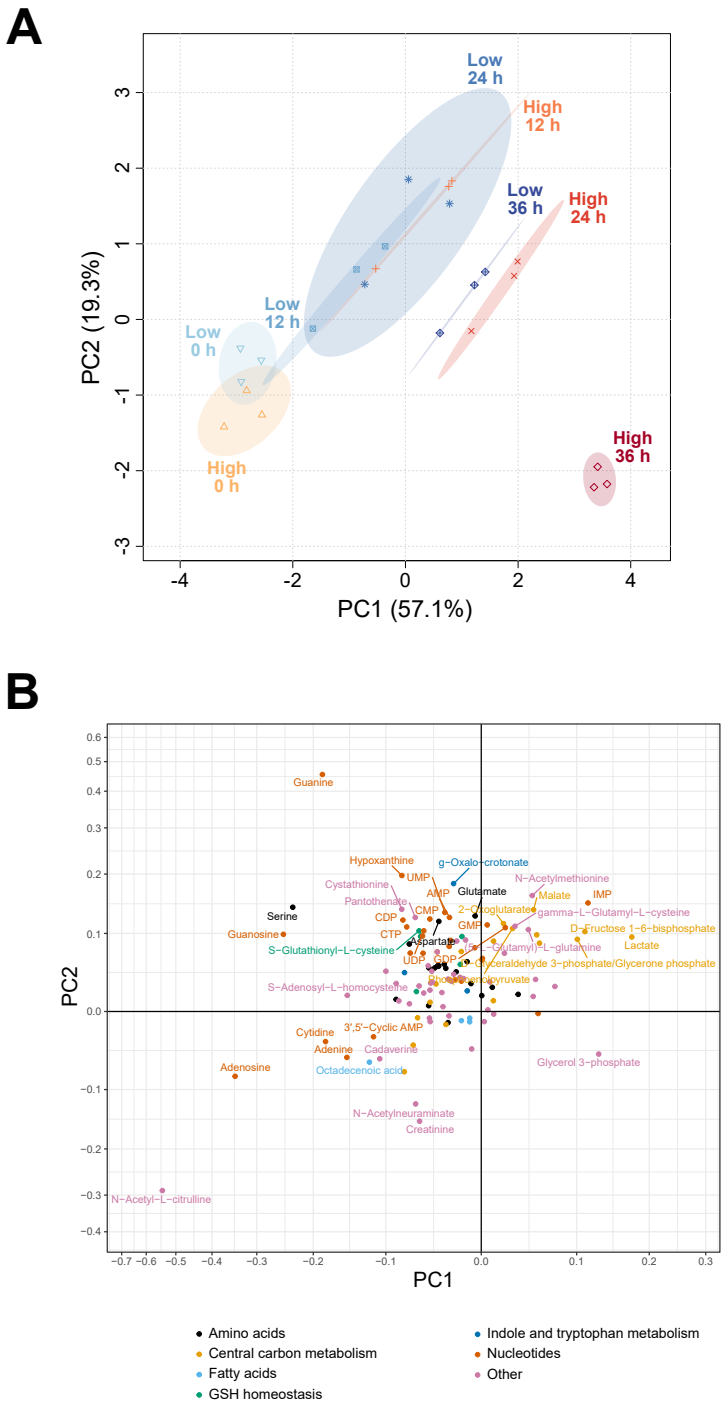

Figure 5.

(Continues in next page)

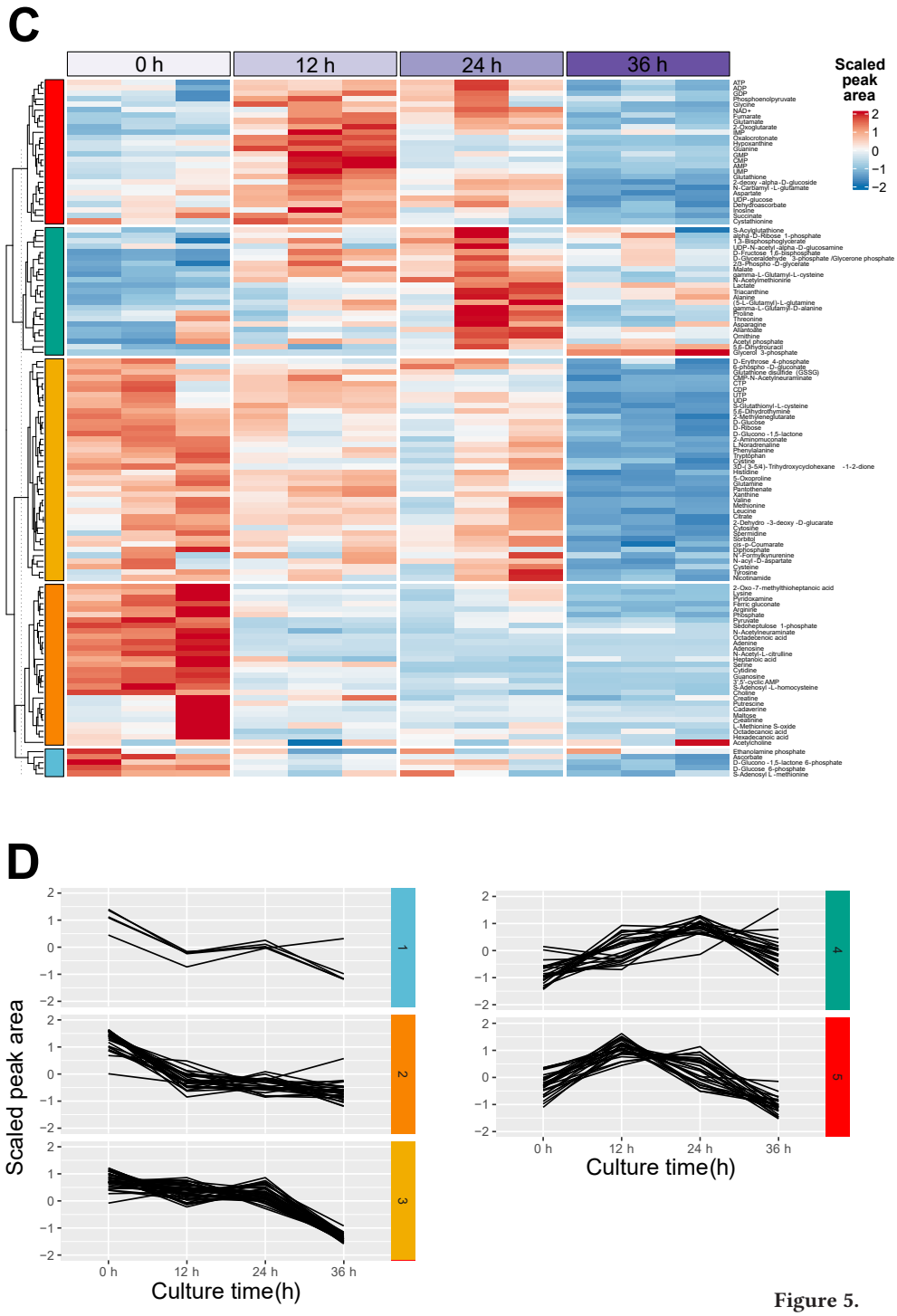

Figure 5.

(See caption on next page)

3.3.6. Redundancy of nucleosides and deoxynucleosides in culture medium

To better understand the implications of metabolites that increase or decrease over time, pathway-based analysis was applied, i.e. analyzing metabolites not as individual features but as members of specific metabolite groups and pathways [47–49]. Particularly, metabolite set quantitative enrichment analysis (MSQEA) was performed on the extracellular metabolome data of high cell density cultures, which revealed an enrichment of purine metabolism in all timepoints relative to the start of the culture (Supplementary Figure S7). Purine metabolism comprises *de novo* biosynthesis from ribose 5-phosphate via phosphoribosyl pyrophosphate, purine salvage, and purine degradation [50,51]. In cultured erythroblasts, a net depletion of adenosine and guanosine was observed both intra- and extracellularly (Figure 6A). This was accompanied by a transient accumulation of most intermediates of the purine degradation pathway.

Hypoxanthine can be recycled to IMP or be further metabolized into xanthine and urate by the enzymatic action of xanthine oxidase, with hydrogen peroxide or superoxide ions as byproducts [52]. Although human cells lack the urate oxidase enzyme, accumulation of allantoate was observed extracellularly in the first 12 h of culture, while displaying a peak of intracellular levels after 24 h followed by a decrease in the following 12 h. The oxidation of urate into allantotate produces again 2 hydrogen peroxide molecules.

When nucleosides/deoxynucleosides were not added to the medium, hypoxanthine did not increase, as expected (Figure 6B). Allantoate, however, still increased to 70% of the levels observed in presence of additional nucleosides. This implies that allantoate is a metabolic byproduct of proliferating erythroblasts, possibly due to a high RNA turnover. The intracellular levels of ATP, ADP and AMP appeared independent of the addition of nucleosides.

To evaluate the long-term effect of the removal of nucleosides from the medium on cell growth, erythroblasts were cultured in medium with or without added nucleosides/deoxynucleosides, with daily addition of fresh medium. Better growth is observed under medium without exogenous nucleosides in the first 5 days of culture (Figure 6C).

Figure 5. Statistical analysis of intracellular metabolomics in erythroblast proliferation cultures. Erythroblasts from three independent donors were expanded from PBMCs for 11 days, subsequently inoculated in fresh proliferation medium at a low (0.7×10^6 cells/mL) or high (2.0×10^6 cells/mL) cell concentration, and cultured without medium refreshment for 36 h. In parallel to the supernatant samples used for Figure 4, cell pellets were taken at 0, 12, 24, and 36 h. Intracellular metabolites were extracted using methanol and acetonitrile. Principal component analysis was performed using the normalized peak area data (**A**, score plot; **B**, loadings biplot). **(C)** Metabolites were clustered in 5 groups using *k*-means clustering performed over the high cell density culture peak area data (cluster 1, *n*=5 metabolites; cluster 2, *n*=29; cluster 3, *n*=40; cluster 4, *n*=23; cluster 5, *n*=26). **(D)** Metabolite peak area trends for each cluster.

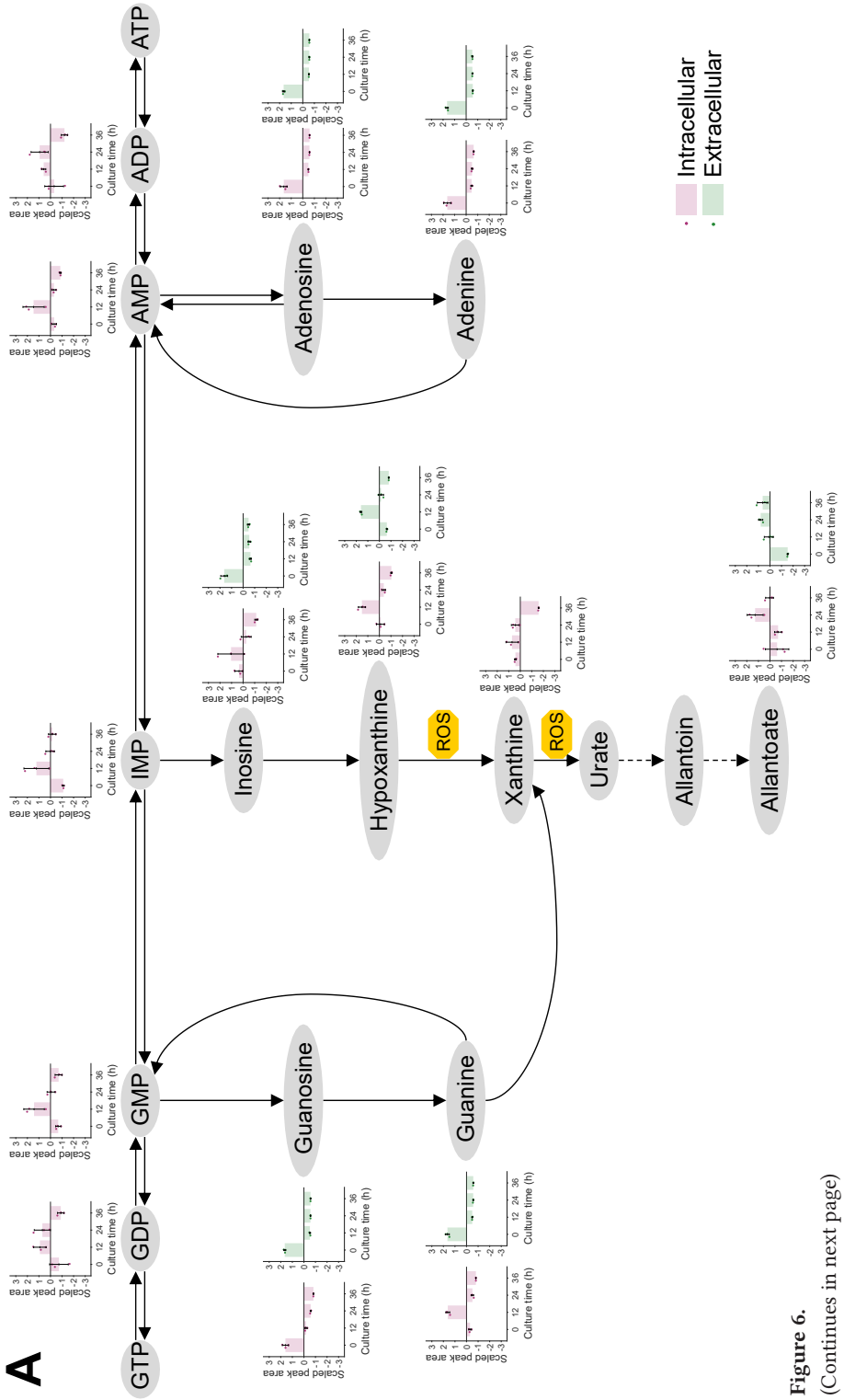

Figure 6.
(Continues in next page)

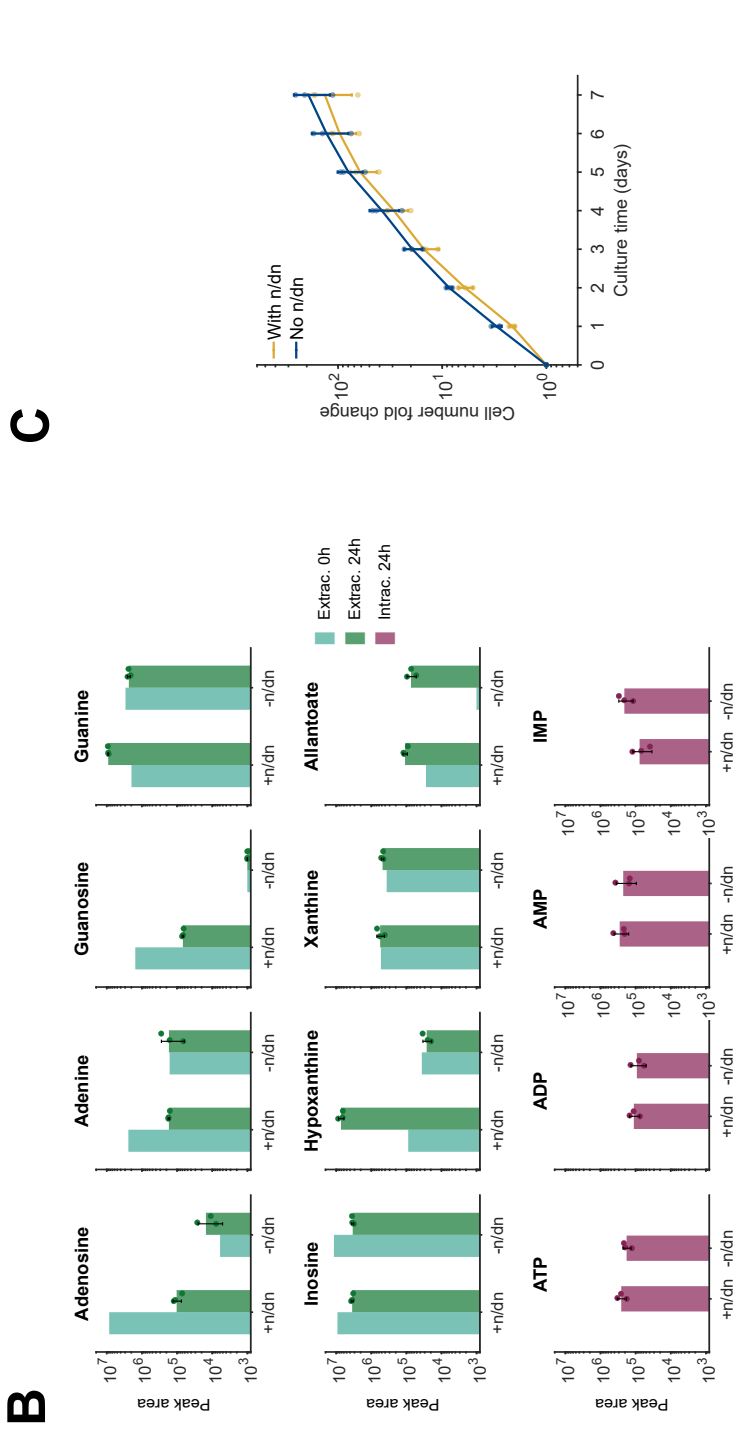

Figure 6.
(See caption on next page)

3.3.7. Indications for oxidative stress conditions in erythroblast cultures

The accumulation of allantoate suggests a high activity of the ROS-producing purine degradation pathway. A state of oxidative stress in the cells may also be caused by the culture at atmospheric oxygen levels (hyperoxic, compared to *in vivo* conditions), or due to the high metabolic activity required to support rapid erythroblast proliferation. Thus, the activity of antioxidant pathways is likely an important parameter in erythroblast cultures. Specifically, control of oxidative stress by ascorbic acid and glutathione is crucial in erythropoiesis [53]. The intracellular measurements show depletion of the glutathione pool. Glutathione disulfide (GSSG) and ascorbate steadily decreased during 36 h. The reduced counterparts, GSH and dehydroascorbate increased at 12 h but then rapidly decreased well below starting levels (Figure 7A). Such decrease of the expected conserved moiety of the glutathione pool suggests an insufficient glutathione synthesis flux. Glutathione or ɣ-l-glutamyl-l-cysteinyl glycine is synthesized from the ɣ-glutamyl cycle by ɣ-glutamyl-cysteine ligase and glutathione synthetase from glycine, glutamate and cysteine. While glutamate was accumulating extracellularly over the whole experiment, the other precursor glycine and the intermediate ɣ-glutamyl-cysteine first increased till 24 h, followed by a decline well below starting levels. (Figure 7B).

The rate-limiting step of glutathione synthesis is catalyzed by ɣ-glutamyl-cysteine ligase, with cysteine often being the limiting substrate [54,55]. Cysteine is supplemented to media, but can also be synthesized from methionine via transsulfuration pathway. All measured metabolites from both the transsulfuration pathway and the methionine cycle displayed a continuous decrease of concentration during 36 h. Furthermore,

Figure 6. Cultured erythroblasts show high activity of the purine degradation pathway. (A) Extracellular (**green**) and intracellular (**red**) levels of purine degradation pathway intermediates for erythroblast (day 11) cultured at a starting cell concentration of 2.0×10^6 cells/mL for 36 h in fresh proliferation medium. Although human cells do not have the enzymes required for the conversion of urate into allantoin and allantoate (dotted arrows), non-enzymatic processes can lead to those conversions. Some metabolites were only detected intra- or extracellularly. **(B)** To evaluate the effect of eliminating nucleosides (n) and deoxynucleosides (dn) from the medium formulation on the metabolism of cultured erythroblasts metabolism, cells were cultured for 24h in medium with (+n/dn) and without (-n/dn) (deoxy-)nucleosides. Extracellular and intracellular levels of purine degradation pathway intermediates are displayed. **(C)** Medium without (deoxy-) nucleosides was further tested on long-term erythroblast cultures. Medium was refreshed daily, reseeding cells at 1×10^6 cells/mL. All data are displayed as mean ± SD (error bars; $n=3$ donors, except for 0 h extracellular data of panel B, for which only 1 sample was measured). One-tailed paired Student's t-test was used for the comparisons of panel C ($H_0: C_{-\mathrm{n,dn}} = C_{+\mathrm{n,dn}}$, $H_1: C_{-\mathrm{n,dn}} > C_{+\mathrm{n,dn}}$; ns for non-significant, * for $p<0.05$, ** for $p<0.01$).

byproducts of the methionine salvage pathway accumulated. Particularly, degradation products of the intermediate 5-methylthioadenosine (MTA), the polyamines spermine and spermidine, accumulated extracellularly (Figure 7C).

With these results, we hypothesize that exhaustion of erythroblast culture medium impacts the control of oxidative stress levels intracellularly through a decrease in glutathione pools and glutathione synthesis capacity.

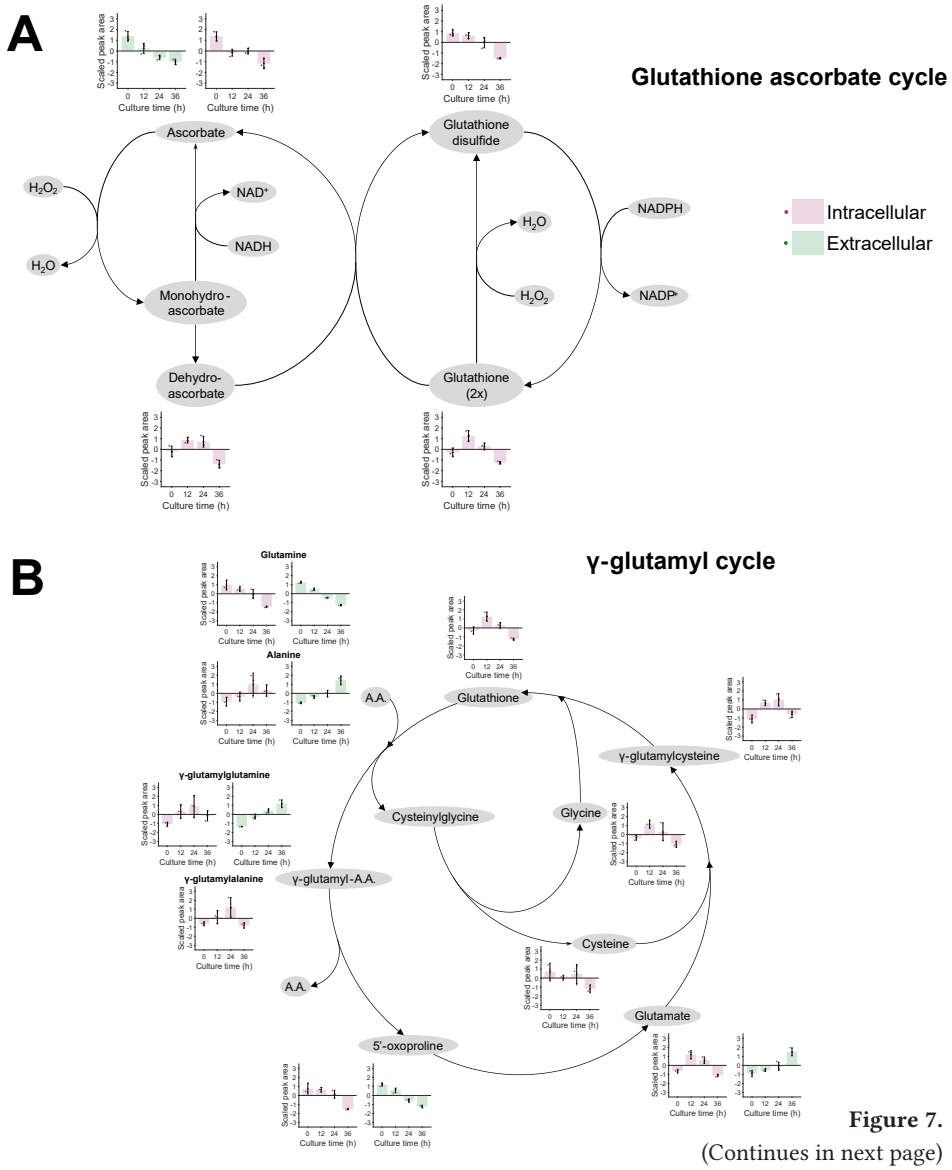

Figure 7.
(Continues in next page)

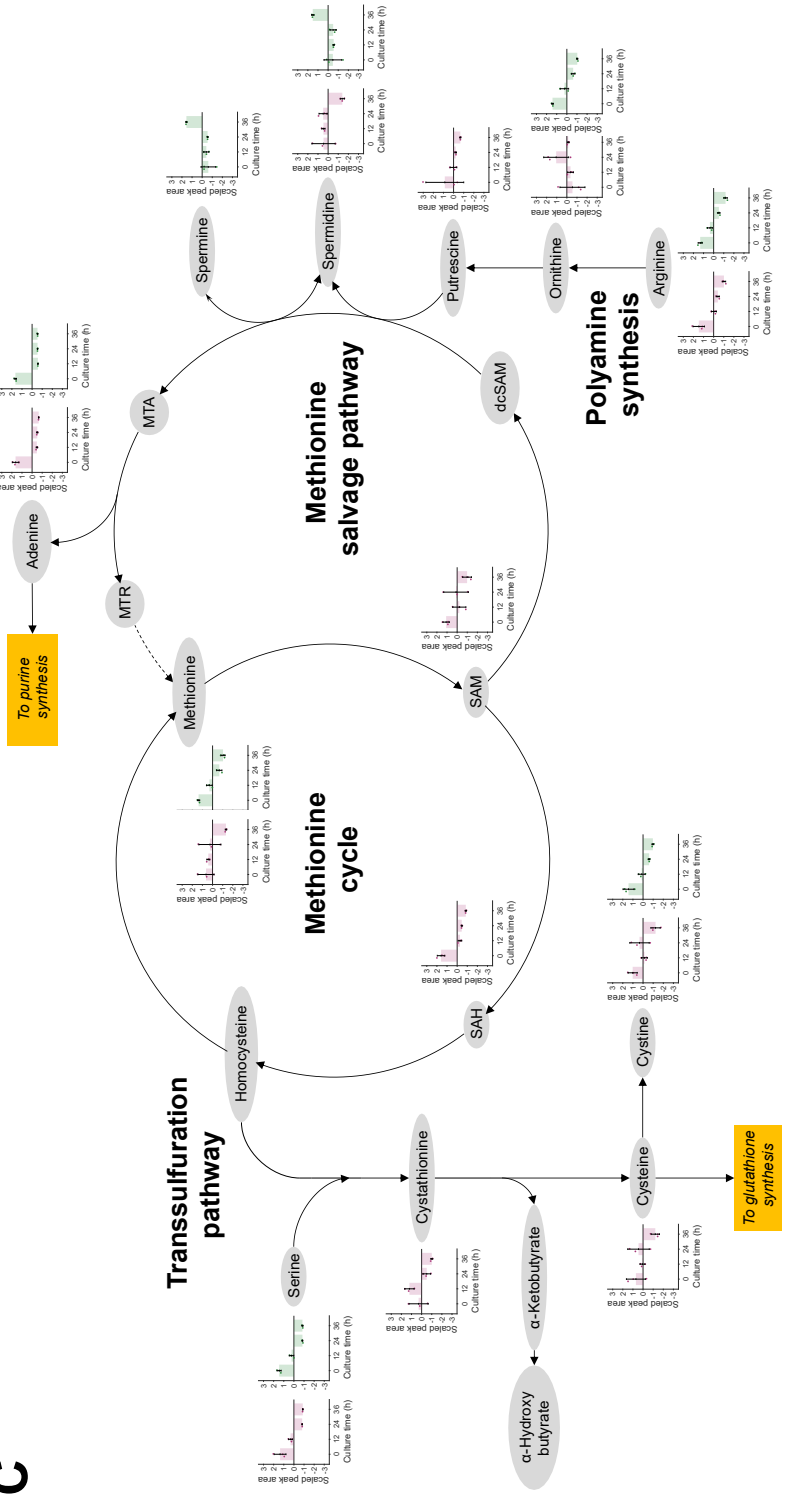

Figure 7.
(See caption on next page)

3.4. Discussion

Economically feasible production of cRBCs for transfusion purposes requires efficient erythroblast expansion and differentiation, significant media cost reduction, and large-scale bioreactor cultivation [14]. Cell density limitations in erythroblast expansion represent a clear challenge for the scale up of cRBC production. At a maximum erythroblast cell density of 2×10^6 cells/mL, the production of a single transfusion unit (2×10^{12} cells) would require a 1000 L culture. The current study shows that exhaustion of low molecular weight medium components (<3 kDa) rather than the accumulation of toxic components limits cell density during the expansion phase of erythroblast cultures. Untargeted metabolism gives a lead to metabolic processes that are affected by medium exhaustion.

3.4.1. Metabolite depletion or accumulation of toxic byproduct?

Supplementation of depleted supernatants with fresh medium suggested that lack of nutrients rather than accumulation of toxic byproducts (metabolites or cytokines) likely caused the observed growth inhibition of erythroblast cultures. Nevertheless, supplementation with components from the medium did not lead to a significant recovery in growth. Bayley et al. observed similar results for cultures of umbilical cord-derived erythroid cultures supplemented with extra glucose, amino acids, and vitamins [12]. It is possible that the observed erythroblast growth limitations are caused by the combined effect of multiple simultaneous nutrient limitations, as observed in other bioprocesses [56].

Thus, feeding strategies must be designed to replenish depleted nutrients, and to remove or reduce the production of toxic metabolites that can become growth inhibiting at higher cell densities. We showed that continuous perfusion with fresh medium allows to overcome the observed cell density limitations in erythroblast cultures, albeit leading to large fresh medium requirements. Of note, we observed lower cell concentrations in the perfusion run compared to the predictions of the kinetic model. This may be

Figure 7. Depletion of glutathione and glutathione synthesis intermediates during erythroblast expansion cultures. Extracellular (**green**) and intracellular (**red**) levels of the glutathione-ascorbate cycle **(A)**, γ-glutamyl cycle **(B)**, and methionine cycle + salvage pathway **(C)** for erythroblast (day 11) cultured at a starting cell concentration of 2.0×10^6 cells/mL for 36 h in fresh proliferation medium. Some metabolites were only detected intra- or extracellularly. All data are displayed as mean ± SD (error bars; $n = 3$ donors). Abbreviations: A.A., amino acid; SAH, S-adenosyl homocysteine; SAM, S-adenosyl methionine; dcSAM: decarboxylated S-adenosyl methionine; MTA: 5'-methylthioadenosine; MTR: 5'-methylthioribose.

explained by the culture conditions used by Glen et al. (i.e. lack of glucocorticoids), which allow for fast cell divisions typical of terminal differentiation, while our experimental model maintains cells in a transient renewal phase.

Determination of an optimal perfusion profile for erythroblast cultures can be done experimentally, but our results show that this can be achieved faster using *in silico* methods with growth models fitted to experimental data. This will be sensitive to the hypothesized inhibition production mechanism. Although similar results were obtained using the kinetic model proposed by Glen et al. and the simplified model proposed in this study, significantly more medium is required for a situation in which there is no inhibition decay. Although it is difficult to assert whether this mechanism takes place without knowing which is the set of metabolites that is being depleted during culture, the kinetic model without inhibition decay appears to fit better the limitations in cell productivity observed in batch cultures (Figure 1E; Supplementary Figure S4).

3.4.2. Metabolic requirements of proliferating erythroblasts

Erythroblast proliferation cultures require massive expansion levels to produce the number of RBCs of a single transfusion unit, and consequently, high uptake rates of amino acids to support the protein synthesis for new biomass production. The amino acid concentrations in Cellquin medium are ~2-fold higher than what is required to produce the 3.5-4.0 million erythroblasts that can be generated per mL of the current medium. The metabolomics results confirm a generalized decrease of the amino acid pool in the medium during erythroblast growth, with glutamine having the largest cells-specific consumption rate. Glutamine, often the most abundant amino acid in cell culture medium, is quickly consumed and used for synthesis of TCA cycle intermediates, nucleotides, and non-essential amino acids [57,58]. Glutamine availability has also been shown to be critical for the commitment of hematopoietic stem cells to the erythroid lineage, being mainly used as direct precursor for nucleotide synthesis [59].

Serine is the only amino acid that was fully depleted, similarly to what was previously observed in cultures of an immortalized erythroblast cell line [60]. This could be explained by the high heme synthesis activity in erythroblasts, which is required for hemoglobin (Hb) production: serine can be converted to glycine (Gly), a direct substrate for heme synthesis, by the activity of serine hydroxymethyltransferase (E.C. 2.1.2.1). A total of 8 Gly molecules are required for a single heme unit, or 1.2 pg Gly per single fully hemoglobinized RBC containing ~300 million Hb molecules. Interestingly, we observed that only 25% of the medium glycine was depleted after 2 days in cultures seeded at 2×10^6 cells/mL. The maintenance of glycine levels, and the common interconversion of glycin and serine, may imply that the low serine levels are not limiting. Low levels may

also indicate rapid turnover rather than low availability.

Alanine and glutamate were the only amino acids that displayed extracellular accumulation during erythroblast proliferation. Alanine can be produced as alternative to lactate from pyruvate (Pyr) via transamination, and its accumulation can inhibit the activity of pyruvate kinase, restricting the glycolytic flux towards the TCA cycle [61]. It has been hypothesized that alanine production via the activity of alanine aminotransferase (ALT; Pyr + Glu ⟶ Ala + αKG, with αKG = α-ketoglutarate or 2-oxoglutarate) coupled with the regeneration of glutamate via glutamate dehydrogenase (GDH; αKG + NH_4^+ ⟶ Glu) may be a way to capture excess ammonia produced during culture [62,63].

Conversion of glutamine to the TCA cycle intermediate 2-oxoglutarate via glutamate is the main source of ammonia production [21]. We have recently reported production rates of ammonia of 0.1 pmol/cell/day in erythroblast bioreactor and dish cultures, corresponding to ~30% of the total glutamine uptake rates reported here [26]. Although ammonia levels were <0.6 mM, below typical growth-inhibiting concentrations for other cells lines, higher concentrations are expected in cultures at higher cell densities. To minimize wasteful utilization of glutamine and glucose in erythroblast cultures, improved feeding strategies in which glucose and glutamine concentrations are maintained at low levels could be used [64].

We suggest optimization of the medium to be done by balancing amino acid concentrations according to the uptake rates reported in this work. Following this, an optimal perfusion rate that is sufficient to supply enough amino acids for erythroblast growth could be implemented in the process. This perfusion profile should also ensure the removal toxic metabolites, while avoiding the excessive accumulation of metabolites that can be precursors to those metabolic byproducts (e.g. glucose and amino acids). This could allow for the reduction of the total medium requirements and the overall costs of the process.

3.4.3. Towards integration of -omics data for the optimization of erythroid cultures

Metabolite set enrichment analysis (MSEA) and pathway enrichment analysis (PEA) incorporate biological-relevant information (set of metabolites involved in the same pathway) missing in purely statistical methods such as PCA or clustering analysis. Following this approach, we could identify a high activity of the purine degradation pathway, causing transient accumulation of hypoxanthine and allantoate. The accumulation of allantoate was observed even when nucleosides are not supplemented

in the medium, implying that allantoate is naturally produced in proliferating erythroblasts, possibly due to a high flux of the purine salvage pathway in cells that extensively change their transcriptome.

Imbalances in oxidative stress control were also observed. Interestingly, although levels of ascorbate, a potent antioxidant present in culture media, show a large decrease simultaneous with an increase of its oxidized form (dehydroascorbate) in high cell density erythroblast cultures, intracellular levels of both metabolites were more stable (Figure 8). The observed larger dispersion between samples in the PCA for intracellular data (Figure 5A) compared to extracellular data also suggests that intracellular metabolite levels show less time-dependency compared to concentrations in the supernatant, indicating homeostasis in intracellular metabolism.

It is important to note that MSEA and PEA are strongly influenced by the selection of the pathway and metabolite set databases, as those libraries show differences in coverage of reactions in the human metabolic network. However, the choice of analytical platform foremost defines the pool of identifiable metabolites and the areas of the metabolome that are probed [49]. We used a rapid UHPLC-MS assay that covers the central carbon and nitrogen metabolism, bile acids and oxylipids, and that is robust to different biological matrices [36,65]. However, vitamins and heme metabolism intermediates, which are especially relevant in erythropoiesis, are generally poorly covered areas in metabolomic analysis [66]. To fill these gaps in our metabolomic data, assays targeting these pathways could be performed and combined with the metabolomic dataset reported here.

We hope this erythroblast metabolomics dataset can be used for a more rational development of erythroblast culture medium and culture feeding profiles that considers the dynamic metabolic requirements of cultured erythroblasts. Currently we are extending the approach showed in this study to the analysis of erythroid differentiation, in which drastic morphological changes take place, including organelle clearance and changes in membrane structural organization.

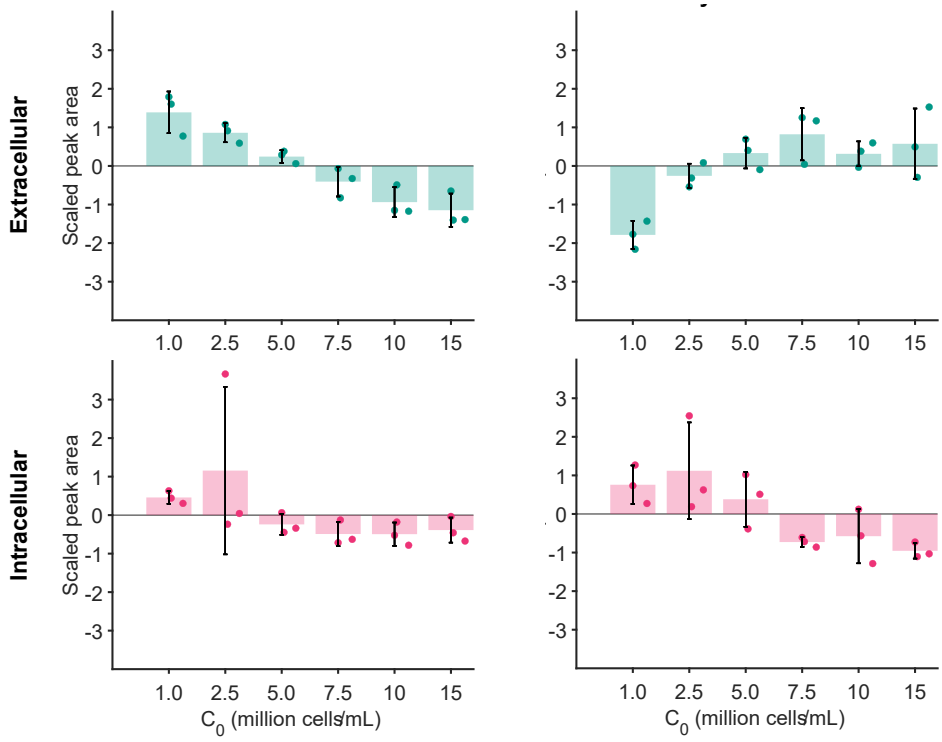

Figure 8. Increased oxidative levels in high cell density erythroblast cultures. Spent medium samples and cell pellets from erythroblasts cultured for 16 h at different starting cell concentrations (1-15×10^6 cells/mL) were analyzed by untargeted metabolomics. Extracellular (**green**) and intracellular (**red**) levels of ascorbate and dehydroascorbate are displayed. Data for other metabolites is available in Supplementary Figure S8. All data are displayed as mean ± SD (error bars; $n = 3$ donors).

3.5. Acknowledgements

We thank Arjan Hoogendijk and John van Dam (Bioinformatics, Sanquin Research) for technical help and advice on the analysis and visualization of metabolomics data. This work was supported by the ZonMW TAS program (project 116003004; https://www.zonmw.nl/nl/over-zonmw/innovatie-in-de-zorg/programmas/programma-detail/translationeel-adult-stamcelonderzoek/), by the Landsteiner Foundation for Bloodtransfusion Research (LSBR project 1239; https://lsbr.nl/), and by Sanquin Blood Supply grants PPOC17-28 and PPOC119-14 (https://www.sanquin.org/research).

3.6. Author contribution

Conceptualization, JSGM, MvL, AW, and EvdA; methodology, JSGM, NY, MvL, and AW; software, JSGM and IvL; formal analysis, JSGM, IvL, JR, and AD; investigation, JSGM, NY, and JR; resources, JR, AD; data curation, JSGM; writing—original draft preparation, JSGM, MvL, and AW; writing—review and editing, EvdA, LvdW, AD; visualization, JSGM, MvL, and AW.; supervision, MvL, AW, EvdA, and AD; project administration, MvL; funding acquisition, MvL, EvdA, and AW.

3.7. References

1. Lee, E.; Sivalingam, J.; Lim, Z.R.; Chia, G.; Shi, L.G.; Roberts, M.; Loh, Y.-H.; Reuveny, S.; Oh, S.K.-W. Review: In Vitro Generation of Red Blood Cells for Transfusion Medicine: Progress, Prospects and Challenges. *Biotechnol. Adv.* **2018**, *36*, 2118–2128, doi:10.1016/j.biotechadv.2018.09.006.

2. Peyrard, T.; Bardiaux, L.; Krause, C.; Kobari, L.; Lapillonne, H.; Andreu, G.; Douay, L. Banking of Pluripotent Adult Stem Cells as an Unlimited Source for Red Blood Cell Production: Potential Applications for Alloimmunized Patients and Rare Blood Challenges. *Transfus. Med. Rev.* **2011**, *25*, 206–216, doi:10.1016/j.tmrv.2011.01.002.

3. Rousseau, G.F.; Mazurier, C.; Douay, L. Culturing Red Blood Cells from Stem Cells: A Solution to Present and Future Challenges of Transfusion Medicine? *ISBT Sci. Ser.* **2016**, *11*, 111–117, doi:10.1111/voxs.12235.

4. Pellegrin, S.; Severn, C.E.; Toye, A.M. Towards Manufactured Red Blood Cells for the Treatment of Inherited Anemia. *Haematologica* **2021**, doi:10.3324/haematol.2020.268847.

5. Shah, S.; Huang, X.; Cheng, L. Concise Review: Stem Cell-Based Approaches to Red Blood Cell Production for Transfusion. *Stem Cells Transl. Med.* **2014**, *3*, 346–355, doi:10.5966/sctm.2013-0054.

6. Leberbauer, C.; Boulmé, F.; Unfried, G.; Huber, J.; Beug, H.; Müllner, E.W. Different Steroids Co-Regulate Long-Term Expansion versus Terminal Differentiation in Primary Human Erythroid Progenitors. *Blood* **2005**, *105*, 85–94, doi:10.1182/blood-2004-03-1002.

7. von Lindern, M.; Zauner, W.; Mellitzer, G.; Steinlein, P.; Fritsch, G.; Huber, K.; Löwenberg, B.; Beug, H. The Glucocorticoid Receptor Cooperates with the Erythropoietin Receptor and C-Kit to Enhance and Sustain Proliferation of Erythroid Progenitors in Vitro. *Blood* **1999**, *94*, 550–559, doi:10.1182/blood.V94.2.550.

8. Migliaccio, G.; Di Pietro, R.; di Giacomo, V.; Di Baldassarre, A.; Migliaccio, A.R.; Maccioni, L.; Galanello, R.; Papayannopoulou, T. In Vitro Mass Production of Human Erythroid Cells from the Blood of Normal Donors and of Thalassemic Patients. *Blood Cells. Mol. Dis.* **2002**, *28*, 169–180, doi:10.1006/bcmd.2002.0502.

9. Dorn, I.; Lazar-Karsten, P.; Boie, S.; Ribbat, J.; Hartwig, D.; Driller, B.; Kirchner, H.; Schlenke, P. In Vitro Proliferation and Differentiation of Human CD34+ Cells from Peripheral Blood into Mature Red Blood Cells with Two Different Cell Culture Systems. *Transfusion (Paris)* **2008**, *48*, 1122–1132, doi:10.1111/j.1537-2995.2008.01653.x.

10. Migliaccio, G.; Sanchez, M.; Masiello, F.; Tirelli, V.; Varricchio, L.; Whitsett, C.; Migliaccio, A.R. Humanized Culture Medium for Clinical Expansion of Human Erythroblasts. *Cell Transplant.* **2010**, *19*, 453–469, doi:10.3727/096368909X485049.

11. Lee, E.; Han, S.Y.; Choi, H.S.; Chun, B.; Hwang, B.; Baek, E.J. Red Blood Cell Generation by Three-Dimensional Aggregate Cultivation of Late Erythroblasts. *Tissue Eng. Part A* **2015**, *21*, 817–828, doi:10.1089/ten.tea.2014.0325.

12. Bayley, R.; Ahmed, F.; Glen, K.; McCall, M.; Stacey, A.; Thomas, R. The Productivity Limit of Manufacturing Blood Cell Therapy in Scalable Stirred Bioreactors. *J. Tissue Eng. Regen. Med.* **2017**, doi:10.1002/term.2337.

13. Glen, K.E.; Stacey, A.; Thomas, R. Modelling Productivity to Optimise Red Blood Cell Manufacture from Haematopoietic Stem Cells. *Cytotherapy* **2017**, *19*, S76, doi:10.1016/j.jcyt.2017.02.118.

14. Timmins, N.E.; Nielsen, L.K. Manufactured RBC — Rivers of Blood, or an Oasis in the Desert? *Biotechnol. Adv.* **2011**, *29*, 661–666, doi:10.1016/j.biotechadv.2011.05.002.

15. Rousseau, G.F.; Giarratana, M.-C.; Douay, L. Large-Scale Production of Red Blood Cells from Stem Cells: What Are the Technical Challenges Ahead? *Biotechnol. J.* **2014**, *9*, 28–38, doi:10.1002/biot.201200368.

16. Hassell, T.; Gleave, S.; Butler, M. Growth Inhibition in Animal Cell Culture. The Effect of Lactate and Ammonia. *Appl. Biochem. Biotechnol.* **1991**, *30*, 29–41, doi:10.1007/BF02922022.

17. Lao, M.-S.; Toth, D. Effects of Ammonium and Lactate on Growth and Metabolism of a Recombinant Chinese Hamster Ovary Cell Culture. *Biotechnol. Prog.* **1997**, *13*, 688–691, doi:10.1021/bp9602360.

18. Cruz, H.J.; Freitas, C.M.; Alves, P.M.; Moreira, J.L.; Carrondo, M.J.T. Effects of Ammonia and Lactate on Growth, Metabolism, and Productivity of BHK Cells. *Enzyme Microb. Technol.* **2000**, *27*, 43–52, doi:10.1016/S0141-0229(00)00151-4.

19. Ozturk, S.S.; Riley, M.R.; Palsson, B.O. Effects of Ammonia and Lactate on Hybridoma Growth, Metabolism, and Antibody Production. *Biotechnol. Bioeng.* **1992**, *39*, 418–431, doi:10.1002/bit.260390408.

20. Michl, J.; Park, K.C.; Swietach, P. Evidence-Based Guidelines for Controlling PH in Mammalian Live-Cell Culture Systems. *Commun. Biol.* **2019**, *2*, 1–12, doi:10.1038/s42003-019-0393-7.

21. Schneider, M.; Marison, I.W.; von Stockar, U. The Importance of Ammonia in Mammalian Cell Culture. *J. Biotechnol.* **1996**, *46*, 161–185, doi:10.1016/0168-1656(95)00196-4.

22. Han, S.Y.; Lee, E.M.; Lee, J.; Lee, H.; Kwon, A.M.; Ryu, K.Y.; Choi, W.-S.; Baek, E.J. Red Cell Manufacturing Using Parallel Stirred-Tank Bioreactors at the Final Stages of Differentiation Enhances Reticulocyte Maturation. *Biotechnol. Bioeng.* **2021**, *118*, doi:https://doi.org/10.1002/bit.27691.

23. Ratcliffe, E.; Glen, K.E.; Workman, V.L.; Stacey, A.J.; Thomas, R.J. A Novel Automated Bioreactor for Scalable Process Optimisation of Haematopoietic Stem Cell Culture. *J. Biotechnol.* **2012**, *161*, 387–390, doi:10.1016/j.jbiotec.2012.06.025.

24. Sivalingam, J.; SuE, Y.; Lim, Z.R.; Lam, A.T.L.; Lee, A.P.; Lim, H.L.; Chen, H.Y.; Tan, H.K.; Warrier, T.; Hang, J.W.; et al. A Scalable Suspension Platform for Generating High-Density Cultures of Universal Red Blood Cells from Human Induced Pluripotent Stem Cells. *Stem Cell Rep.* **2020**, *16*, 182–197, doi:10.1016/j.stemcr.2020.11.008.

25. Patel, S.D.; Papoutsakis, E.T.; Winter, J.N.; Miller, W.M. The Lactate Issue Revisited: Novel Feeding Protocols To Examine Inhibition of Cell Proliferation and Glucose Metabolism in Hematopoietic Cell Cultures. *Biotechnol. Prog.* **2000**, *16*, 885–892, doi:10.1021/bp000080a.

26. Gallego-Murillo, J.S.; Iacono, G.; van der Wielen, L.A.M.; van den Akker, E.; von Lindern, M.; Wahl, S.A. Expansion and Differentiation of Ex Vivo Cultured Erythroblasts in Scalable Stirred Bioreactors. *Biotechnol. Bioeng.* **2022**, *119*, 3096–3116, doi:10.1002/bit.28193.

27. Pereira, S.; Kildegaard, H.F.; Andersen, M.R. Impact of CHO Metabolism on Cell Growth and Protein Production: An Overview of Toxic and Inhibiting Metabolites and Nutrients. *Biotechnol. J.* **2018**, *13*, e1700499, doi:10.1002/biot.201700499.

28. Kuang, B.; Dhara, V.G.; Hoang, D.; Jenkins, J.; Ladiwala, P.; Tan, Y.; Shaffer, S.A.; Galbraith, S.C.; Betenbaugh, M.J.; Yoon, S. Identification of Novel Inhibitory Metabolites and Impact Verification on Growth and Protein Synthesis in Mammalian Cells. *Metab. Eng. Commun.* **2021**, *13*, e00182, doi:10.1016/j.mec.2021.e00182.

29. Alden, N.; Raju, R.; McElearney, K.; Lambropoulos, J.; Kshirsagar, R.; Gilbert, A.; Lee, K. Using Metabolomics to Identify Cell Line-Independent Indicators of Growth Inhibition for Chinese Hamster Ovary Cell-Based Bioprocesses. *Metabolites* **2020**, *10*, E199, doi:10.3390/metabo10050199.

30. Mulukutla, B.C.; Kale, J.; Kalomeris, T.; Jacobs, M.; Hiller, G.W. Identification and Control of Novel Growth Inhibitors in Fed-Batch Cultures of Chinese Hamster Ovary Cells. *Biotechnol. Bioeng.* **2017**, *114*, 1779–1790, doi:10.1002/bit.26313.

31. Mulukutla, B.C.; Mitchell, J.; Geoffroy, P.; Harrington, C.; Krishnan, M.; Kalomeris, T.; Morris, C.; Zhang, L.; Pegman, P.; Hiller, G.W. Metabolic Engineering of Chinese Hamster Ovary Cells towards Reduced Biosynthesis and Accumulation of Novel Growth Inhibitors in Fed-Batch Cultures. *Metab. Eng.* **2019**, *54*, 54–68, doi:10.1016/j.ymben.2019.03.001.

32. Brunner, M.; Kolb, K.; Keitel, A.; Stiefel, F.; Wucherpfennig, T.; Bechmann, J.; Unsoeld, A.; Schaub, J. Application of Metabolic Modeling for Targeted Optimization of High Seeding Density Processes. *Biotechnol. Bioeng.* **2021**, *118*, 1793–1804, doi:10.1002/bit.27693.

33. de Jonge, L.P.; Buijs, N.A.A.; ten Pierick, A.; Deshmukh, A.; Zhao, Z.; Kiel, J.A.K.W.; Heijnen, J.J.; van Gulik, W.M. Scale-down of Penicillin Production in Penicillium Chrysogenum. *Biotechnol. J.* **2011**, *6*, 944–958, doi:10.1002/biot.201000409.

34. Gorenflo, V.M.; Ritter, J.B.; Aeschliman, D.S.; Drouin, H.; Bowen, B.D.; Piret, J.M. Characterization and Optimization of Acoustic Filter Performance by Experimental Design Methodology. *Biotechnol. Bioeng.* **2005**, *90*, 746–753, doi:10.1002/bit.20476.

35. Gorenflo, V.M.; Angepat, S.; Bowen, B.D.; Piret, J.M. Optimization of an Acoustic Cell Filter with a Novel Air-Backflush System. *Biotechnol. Prog.* **2003**, *19*, 30–36, doi:10.1021/bp025625a.

36. Nemkov, T.; Hansen, K.C.; D'Alessandro, A. A Three-Minute Method for High-Throughput Quantitative Metabolomics and Quantitative Tracing Experiments of Central Carbon and Nitrogen Pathways. *Rapid Commun. Mass Spectrom. RCM* **2017**, *31*, 663–673, doi:10.1002/rcm.7834.

37. Melamud, E.; Vastag, L.; Rabinowitz, J.D. Metabolomic Analysis and Visualization Engine for LC–MS Data. *Anal. Chem.* **2010**, *82*, 9818–9826, doi:10.1021/ac1021166.

38. Gu, Z.; Eils, R.; Schlesner, M. Complex Heatmaps Reveal Patterns and Correlations in Multidimensional Genomic Data. *Bioinformatics* **2016**, *32*, 2847–2849, doi:10.1093/bioinformatics/btw313.

39. Zappia, L.; Oshlack, A. Clustering Trees: A Visualization for Evaluating Clusterings at Multiple Resolutions. *GigaScience* **2018**, *7*, giy083, doi:10.1093/gigascience/giy083.

40. Chong, J.; Wishart, D.S.; Xia, J. Using MetaboAnalyst 4.0 for Comprehensive and Integrative Metabolomics Data Analysis. *Curr. Protoc. Bioinforma.* **2019**, *68*, e86, doi:https://doi.org/10.1002/cpbi.86.

41. Pang, Z.; Chong, J.; Li, S.; Xia, J. MetaboAnalystR 3.0: Toward an Optimized Workflow for Global Metabolomics. *Metabolites* **2020**, *10*, 186, doi:10.3390/metabo10050186.

42. Frolkis, A.; Knox, C.; Lim, E.; Jewison, T.; Law, V.; Hau, D.D.; Liu, P.; Gautam, B.; Ly, S.; Guo, A.C.; et al. SMPDB: The Small Molecule Pathway Database. *Nucleic Acids Res.* **2010**, *38*, D480-487, doi:10.1093/nar/gkp1002.

43. Jewison, T.; Su, Y.; Disfany, F.M.; Liang, Y.; Knox, C.; Maciejewski, A.; Poelzer, J.; Huynh, J.; Zhou, Y.; Arndt, D.; et al. SMPDB 2.0: Big Improvements to the Small Molecule Pathway Database. *Nucleic Acids Res.* **2014**, *42*, D478-484, doi:10.1093/nar/gkt1067.

44. Jagschies, G.; Lindskog, E.; Łącki, K.; Galliher, P. *Biopharmaceutical Processing: Development, Design, and Implementation of Manufacturing Processes*; Elsevier, **2018**; ISBN 978-0-08-100623-8.

45. Glen, K.E.; Cheeseman, E.A.; Stacey, A.J.; Thomas, R.J. A Mechanistic Model of Erythroblast Growth Inhibition Providing a Framework for Optimisation of Cell Therapy Manufacturing. *Biochem. Eng. J.* **2018**, *133*, 28–38, doi:10.1016/j.bej.2018.01.033.

46. Hosios, A.M.; Hecht, V.C.; Danai, L.V.; Johnson, M.O.; Rathmell, J.C.; Steinhauser, M.L.; Manalis, S.R.; Vander Heiden, M.G. Amino Acids Rather than Glucose Account for the Majority of Cell Mass in Proliferating Mammalian Cells. *Dev. Cell* **2016**, *36*, 540–549, doi:10.1016/j.devcel.2016.02.012.

47. Marco-Ramell, A.; Palau-Rodriguez, M.; Alay, A.; Tulipani, S.; Urpi-Sarda, M.; Sanchez-Pla, A.; Andres-Lacueva, C. Evaluation and Comparison of Bioinformatic Tools for the Enrichment Analysis of Metabolomics Data. *BMC Bioinformatics* **2018**, *19*, 1–11, doi:10.1186/s12859-017-2006-0.

48. Xia, J.; Wishart, D.S. MSEA: A Web-Based Tool to Identify Biologically Meaningful Patterns in Quantitative Metabolomic Data. *Nucleic Acids Res.* **2010**, *38*, W71–W77, doi:10.1093/nar/gkq329.

49. Wieder, C.; Frainay, C.; Poupin, N.; Rodríguez-Mier, P.; Vinson, F.; Cooke, J.; Lai, R.P.; Bundy, J.G.; Jourdan, F.; Ebbels, T. Pathway Analysis in Metabolomics: Recommendations for the Use of over-Representation Analysis. *PLoS Comput. Biol.* **2021**, *17*, e1009105, doi:10.1371/journal.pcbi.1009105.

50. Pareek, V.; Pedley, A.M.; Benkovic, S.J. Human de Novo Purine Biosynthesis. *Crit. Rev. Biochem. Mol. Biol.* **2021**, *56*, 1–16, doi:10.1080/10409238.2020.1832438.

51. Furuhashi, M. New Insights into Purine Metabolism in Metabolic Diseases: Role of Xanthine Oxidoreductase Activity. *Am. J. Physiol.-Endocrinol. Metab.* **2020**, *319*, E827–E834, doi:10.1152/ajpendo.00378.2020.

52. Cantu-Medellin, N.; Kelley, E.E. Xanthine Oxidoreductase-Catalyzed Reactive Species Generation: A Process in Critical Need of Reevaluation. *Redox Biol.* **2013**, *1*, 353–358, doi:10.1016/j.redox.2013.05.002.

53. Gonzalez-Menendez, P.; Romano, M.; Yan, H.; Deshmukh, R.; Papoin, J.; Oburoglu, L.; Daumur, M.; Dumé, A.-S.; Phadke, I.; Mongellaz, C.; et al. An IDH1-Vitamin C Crosstalk Drives Human Erythroid Development by Inhibiting pro-Oxidant Mitochondrial Metabolism. *Cell Rep.* **2021**, *34*, 108723, doi:10.1016/j.celrep.2021.108723.

54. Griffith, O.W.; Mulcahy, R.T. The Enzymes of Glutathione Synthesis: Gamma-Glutamylcysteine Synthetase. *Adv. Enzymol. Relat. Areas Mol. Biol.* **1999**, *73*, 209–267, xii, doi:10.1002/9780470123195.ch7.

55. Griffith, O.W. Biologic and Pharmacologic Regulation of Mammalian Glutathione Synthesis. *Free Radic. Biol. Med.* **1999**, *27*, 922–935, doi:10.1016/S0891-5849(99)00176-8.

56. Egli, T.; Zinn, M. The Concept of Multiple-Nutrient-Limited Growth of Microorganisms and Its Application in Biotechnological Processes. *Biotechnol. Adv.* **2003**, *22*, 35–43, doi:10.1016/j.biotechadv.2003.08.006.

57. Yoo, H.C.; Yu, Y.C.; Sung, Y.; Han, J.M. Glutamine Reliance in Cell Metabolism. *Exp. Mol. Med.* **2020**, *52*, 1496–1516, doi:10.1038/s12276-020-00504-8.

58. Kirsch, B.J.; Bennun, S.V.; Mendez, A.; Johnson, A.S.; Wang, H.; Qiu, H.; Li, N.; Lawrence, S.M.; Bak, H.; Betenbaugh, M.J. Metabolic Analysis of the Asparagine and Glutamine Dynamics in an Industrial Chinese Hamster Ovary Fed-Batch Process. *Biotechnol. Bioeng.* **2022**, *119*, 807–819, doi:10.1002/bit.27993.

59. Oburoglu, L.; Tardito, S.; Fritz, V.; de Barros, S.C.; Merida, P.; Craveiro, M.; Mamede, J.; Cretenet, G.; Mongellaz, C.; An, X.; et al. Glucose and Glutamine Metabolism Regulate Human Hematopoietic Stem Cell Lineage Specification. *Cell Stem Cell* **2014**, *15*, 169–184, doi:10.1016/j.stem.2014.06.002.

60. Lee, E.; Lim, Z.R.; Chen, H.-Y.; Yang, B.X.; Lam, A.T.-L.; Chen, A.K.-L.; Sivalingam, J.; Reuveny, S.; Loh, Y.-H.; Oh, S.K.-W. Defined Serum-Free Medium for Bioreactor Culture of an Immortalized Human Erythroblast Cell Line. *Biotechnol. J.* **2018**, *13*, e1700567, doi:10.1002/biot.201700567.

61. Yuan, M.; McNae, I.W.; Chen, Y.; Blackburn, E.A.; Wear, M.A.; Michels, P.A.M.; Fothergill-Gilmore, L.A.; Hupp, T.; Walkinshaw, M.D. An Allostatic Mechanism for M2 Pyruvate Kinase as an Amino-Acid Sensor. *Biochem. J.* **2018**, *475*, 1821–1837, doi:10.1042/BCJ20180171.

62. Synoground, B.F.; McGraw, C.E.; Elliott, K.S.; Leuze, C.; Roth, J.R.; Harcum, S.W.; Sandoval, N.R. Transient Ammonia Stress on Chinese Hamster Ovary (CHO) Cells Yield Alterations to Alanine Metabolism and IgG Glycosylation Profiles. *Biotechnol. J.* **2021**, *16*, e2100098, doi:10.1002/biot.202100098.

63. Dadsetan, S.; Kukolj, E.; Bak, L.K.; Sørensen, M.; Ott, P.; Vilstrup, H.; Schousboe, A.; Keiding, S.; Waagepetersen, H.S. Brain Alanine Formation as an Ammonia-Scavenging Pathway during Hyperammonemia: Effects of Glutamine Synthetase Inhibition in Rats and Astrocyte–Neuron Co-Cultures. *J. Cereb. Blood Flow Metab.* **2013**, *33*, 1235–1241, doi:10.1038/jcbfm.2013.73.

64. Glacken, M.W.; Fleischaker, R.J.; Sinskey, A.J. Reduction of Waste Product Excretion via Nutrient Control: Possible Strategies for Maximizing Product and Cell Yields on Serum in Cultures of Mammalian Cells. *Biotechnol. Bioeng.* **1986**, *28*, 1376–1389, doi:10.1002/bit.260280912.

65. Reisz, J.A.; Zheng, C.; D'Alessandro, A.; Nemkov, T. Untargeted and Semi-Targeted Lipid Analysis of Biological Samples Using Mass Spectrometry-Based Metabolomics. In *High-Throughput Metabolomics: Methods and Protocols*; D'Alessandro, A., Ed.; Methods in Molecular Biology; Springer: New York, NY, **2019**; pp. 121–135 ISBN 978-1-4939-9236-2.

66. Frainay, C.; Schymanski, E.L.; Neumann, S.; Merlet, B.; Salek, R.M.; Jourdan, F.; Yanes, O. Mind the Gap: Mapping Mass Spectral Databases in Genome-Scale Metabolic Networks Reveals Poorly Covered Areas. *Metabolites* **2018**, *8*, 51, doi:10.3390/metabo8030051.

3.8. Supplementary materials

3.8.1. Supplementary methods

Kinetic models for erythroblast growth

The kinetic growth model proposed by Glen et al. [45] was considered for the numerical simulations of erythroblast cultures under different feeding regimes. Briefly, this model assumes that erythroblasts (cell concentration = C_X) can proliferate under exponential growth with a maximum growth rate $\mu_{\max}$. Accumulation of an inhibitory factor (non-dimensionalized concentration = C_I^*; arbitrary concentration units), which can be interpreted as either the accumulation of a toxic metabolite or the depletion of a growth-limiting metabolite, leads to a decrease in the growth rate. The dose-response curve for this inhibition is described by a sigmoidal function with two parameters: the inhibition threshold k_c^* and the inhibitor sensitivity k_s^* (Equation A1).

$$\mu = \mu_{\max} \cdot (1 + \exp(-k_s^*(k_c^* - C_I^*))^{-1} \qquad \text{Equation (A1)}$$

The inhibitor I is produced in a growth-dependent manner. An inhibition decay term (first order kinetics) is included, with an inhibitor decay rate r_d. Equations A2 and A3 describe the concentration of cells and inhibitory factor for a batch culture.

$$\frac{d\,C_X}{dt} = \mu\,C_X \qquad \text{Equation (A2)}$$

$$\frac{d\,C_I^*}{dt} = \frac{d\,C_X}{dt} - r_d C_I^* = \mu C_X - r_d C_I^* \qquad \text{Equation (A3)}$$

After fitting of this model to experimental data from erythroblast cultures under different treatments (batch growth; reset of cell concentration by removing all cells from a batch culture and inoculating the spent medium with fresh proliferating cells; medium dilution by harvesting cells and reinoculation in a defined ratio of spent and fresh medium), Glen et al. obtained the following best fit parameters: $\mu_{\max} = 0.0541$ 1/h, $k_c^* = 3.4$ 1/h, $k_s^* = 5.6$ 1/h, $r_d = 0.014$ 1/h.

A simplified kinetic model was developed for this study in which: (1) the inhibitory factor is produced in a growth-dependent manner, (2) the inhibitor affects growth following a Hill dose-response curve, and (3) no inhibition decay is considered. Equation A4 describes the effect of the inhibitor in cell growth. The parameters of this model are the maximum growth rate $\mu_{\max}$, the half-saturation concentration K_I, the Hill coefficient n_I, and the yield of inhibitor on cells $Y_{I/X}$. Equations A5 and A6 describe the concentrations of cells and inhibitory factor in a batch culture.

$$\mu = \mu_{\max} \cdot \left(1 - \frac{1}{1 + (K_I/C_I)^{n_I}}\right) \qquad \text{Equation (A4)}$$

$$\frac{d\,C_X}{dt} = \mu\,C_X \qquad \text{Equation (A5)}$$

$$\frac{d\,C_I}{dt} = Y_{I/X}\,\frac{d\,C_X}{dt} = Y_{I/X}\,\mu\,C_X \qquad \text{Equation (A6)}$$

In a similar manner as in Glen et al.' approach, the concentration of the inhibitory factor can be non-dimensionalized using the half-saturation constant ($C_I^* = C_I/K_I$), reducing the number of parameters of the model. A new parameter $\alpha_I^* = Y_{I/X}/K_I$ can be defined, resulting in Equations A7 and A8 describing the growth inhibition dose-response curve and the inhibitor concentration over time in a batch process, respectively:

$$\mu = \mu_{\max} \cdot \left(1 - \frac{1}{1 + (1/C_I^*)^{n_I}}\right) \qquad \text{Equation (A7)}$$

$$\frac{d\,C_I^*}{dt} = \alpha_I^*\,\mu\,C_X \qquad \text{Equation (A8)}$$

This model was fitted to the experimental dataset obtained by Glen et al. [45]. The fitting was performed minimizing the total sum of squared relative errors of cell concentrations for all treatments reported by Glen et al., weighted by the number of measurements of each treatment. A global optimization strategy was used as initial step (genetic algorithm), followed by local optimization using the Nelder-Mead simplex algorithm (MATLAB ver. R2018b; Mathworks; USA). Fitted parameters were: $\mu_{\max} = 0.04$ 1/h, $\alpha_I^* = 0.32 \times 10^{-6}$ mL/cell, $n_I = 9.5$. Note that the non-dimensionalized inhibitor concentrations in both models are not equivalent, as the non-dimensionalization is performed using parameters from different dose-response inhibition models. Supplementary Figure S4 displays the predicted growth inhibition and volumetric productivity limits in batch erythroblast cultures for both models.

Numerical simulations of erythroblast bioreactor cultures

Bioreactor cultures under different feeding regimes were simulated solving numerically the differential equations describing the concentration of cells and (non-dimensionalized) inhibitor factor. Equations A9 and A10 show the generic mass balance for cells and inhibitory factor that were used for all feeding regimes. Equation A11 describes the change in liquid volume in the reactor,

$$\frac{d\,C_X}{dt} = \frac{1}{V}\left(-F_{\text{out}}C_{X,\text{out}} + \mu\,C_X\,V - C_X\frac{dV}{dt}\right) \qquad \text{Equation (A9)}$$

$$\frac{d\,C_I^*}{dt} = \frac{1}{V}\left(-F_{\text{out}}C_{I,\text{out}}^* + \alpha_I^*\,\mu\,C_X\,V - C_I^*\frac{dV}{dt}\right) \qquad \text{Equation (A10)}$$

$$\frac{dV}{dt} = F_{\text{in}} - F_{\text{out}} \qquad \text{Equation (A11)}$$

where F_{in} and F_{out} are the volumetric inflow and outflow rates, and V is the working volume of the bioreactor at any specific timepoint. Cell growth rate is calculated at each timepoint using Equation A4 or A7, depending on the growth inhibition model being evaluated. The value of α_I^* is equal to 1 for Glen et al. model.

The inflow and outflow terms are defined depending on the feeding regime. For batch mode, $F_{\text{in}} = F_{\text{out}} = 0$, resulting in $\frac{dV}{dt} = 0$, and Equations A5 and A8. For both fed batch regimes (FB_{const} and FB_{exp}), $F_{\text{out}} = 0$, and the feeding rate was normalized by the initial working volume of the reactor $D = F_{\text{in}}/V_0$, resulting in Equations A12, A13 and A14. For FB_{const}, the value of D is constant, while for FB_{exp} it is described by $D = D_0\exp(\theta \cdot t)$.

$$\frac{d\,C_X}{dt} = \frac{1}{V}\left(\mu\,C_X\,V - C_X\frac{dV}{dt}\right) \qquad \text{Equation (A12)}$$

$$\frac{d\,C_I^*}{dt} = \frac{1}{V}\left(\alpha_I^*\,\mu\,C_X\,V - C_I^*\frac{dV}{dt}\right) \qquad \text{Equation (A13)}$$

$$\frac{dV}{dt} = D\,V_0 \qquad \text{Equation (A14)}$$

For both perfusion regimes (P_{const} and P_{CSPR}), it is assumed that the working volume in the reactor is constant ($F_{\text{out}} = F_{\text{in}}$), that no cells are lost in the permeate ($C_{X,\text{out}} = 0$), and that the reactor is well-mixed for the inhibitory factor ($C^*_{I,\text{out}} = C^*_I$). The perfusion rate is expressed normalized by the working volume of the reactor $P = F_{\text{out}}/V$, resulting in Equations (A15), (A16) and (A17). For P_{const}, the value of P is constant, while for P_{CSPR} it is a function of the cell-specific perfusion rate CSPR and the cell concentration in the reactor ($P = CSPR \cdot C_X$).

$$\frac{d\,C_X}{dt} = \frac{1}{V}\left(\mu\,C_X\,V - C_X\frac{dV}{dt}\right) \qquad \text{Equation (A15)}$$

$$\frac{d\,C^*_I}{dt} = \frac{1}{V}\left(-P\,V\,C^*_I + \alpha^*_I\,\mu\,C_X\,V - C^*_I\frac{dV}{dt}\right) \qquad \text{Equation (A16)}$$

$$\frac{dV}{dt} = 0 \qquad \text{Equation (A17)}$$

To be able to compare different feeding regimes, the feeding parameters of each feeding regime were optimized under the same constraints: production of 30×10^9 cells in 4 days in a 1 L bioreactor inoculated at a starting cell concentration of 1×10^6 cells/mL in fresh medium free of the inhibitory factor. The objective function of the minimization problem was the total volume of medium required during the process.

3.9. Supplementary figures

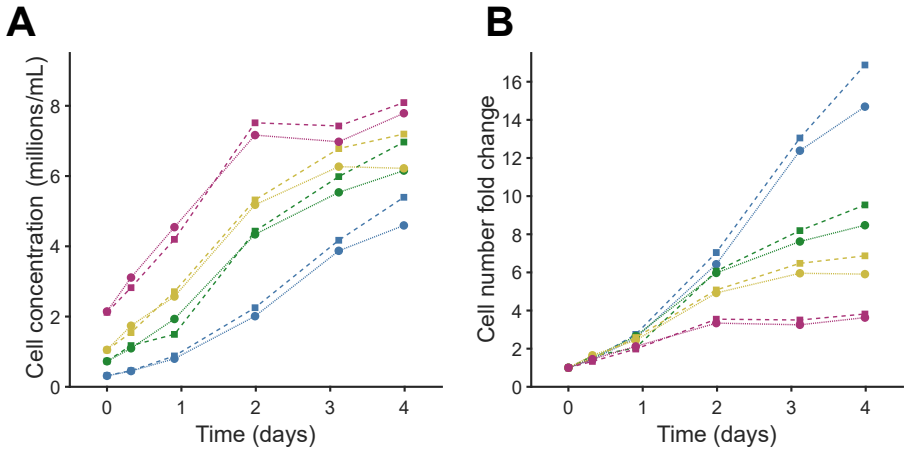

Supplementary Figure S1. Growth in erythroblast cultures without medium refreshment. PBMC-derived day 10 erythroblasts from two independent donors (donor 1: dashed line; donor 2: solid lined) were inoculated in fresh proliferation medium at different starting cell densities (0.3, 0.7, 1 and 2×10^6 cells/mL; indicated by colors). Cell concentration **(A)** and cell number fold change relative to the start of the culture **(B)** are displayed.

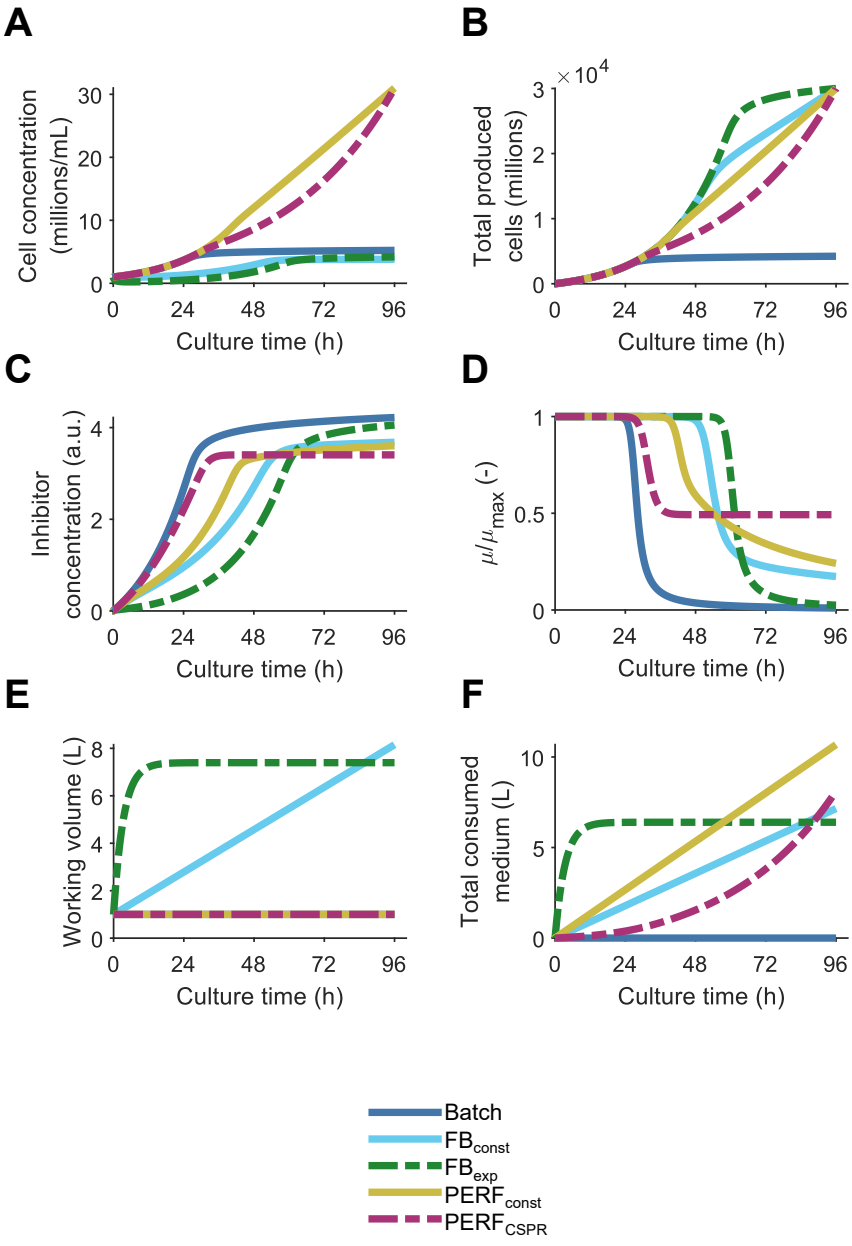

Supplementary Figure S2.
(See caption on next page)

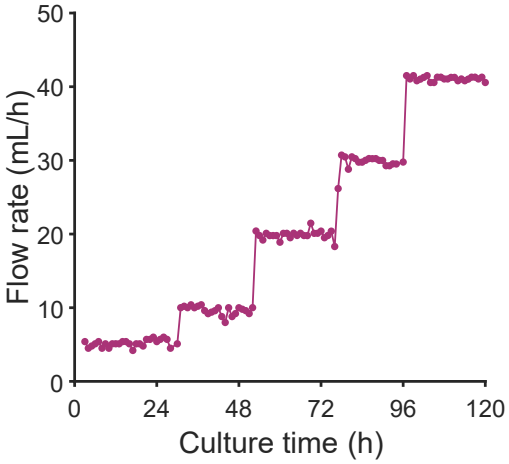

Supplementary Figure S3. Perfusion rate in bioreactor with acoustic cell retention. Erythroblasts were cultured for 5 days in a 0.5 L stirred tank bioreactor (working volume = 250 mL), using an Applikon BioSep for cell retention. The permeate flow rate was increased sequentially according to the daily measurements of cell concentration, targeting an average daily cell-specific perfusion rate (CSPR) of 500 pL/cell/day.

Supplementary Figure S2. Evaluation of feeding strategies in erythroblast bioreactor cultures with alternative growth inhibition model. Bioreactor cultures with different feeding strategies (batch, fed batch with constant feed rate FB_{const}, fed batch with exponentially increasing feed FB_{exp}, perfusion at a constant rate $PERF_{const}$, perfusion at a constant cell-specific perfusion rate $PERF_{CSPR}$) were simulated, using the kinetic growth model for erythroblast proliferation proposed by Glen et al. Similar to the model used for Figure 2, this model includes the production of a putative inhibitor in a growth-dependent manner. However, the dose-response curve to this inhibitor is described using a sigmoidal equation. Furthermore, inhibition decay is also considered (first order kinetics). Except for batch mode, the feeding parameters of each feeding regime were optimized to achieve a production of 30×10^9 cells in 4 days in a 1 L bioreactor inoculated at a starting cell concentration of 1×10^6 cells/mL, minimizing the medium volume requirement. Cell concentration **(A)**, total produced cells **(B)**, concentration of the putative inhibitor (arbitrary units; **C**), magnitude of the growth inhibition calculated as the ratio of the instantaneous growth rate μ and the maximum growth rate μ_{max} **(D)**, total volume of medium consumed **(E)**, and reactor working volume **(F)** are displayed for all evaluated feeding regimes. Equations used for the growth model and for the bioreactor simulations are available in Supplementary Methods. Optimized parameters for each feeding regime are included in Supplementary Table S1.

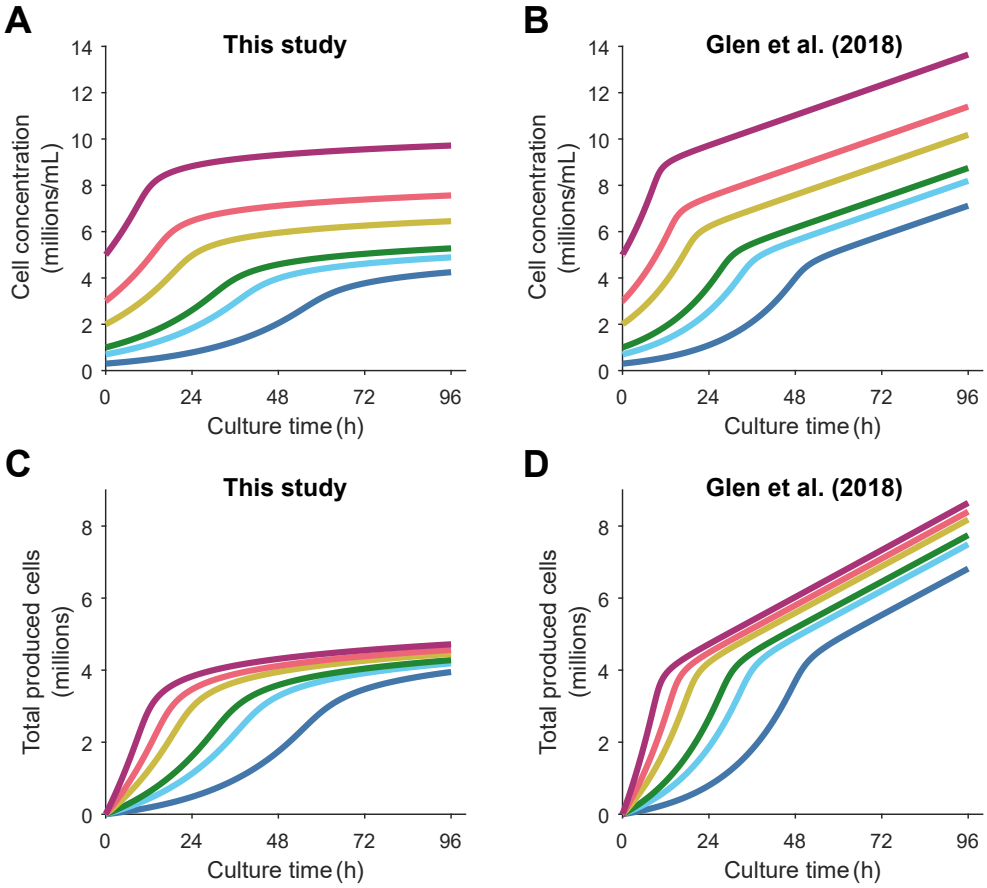

Supplementary Figure S4. Predicted growth inhibition and volumetric productivity limits in batch erythroblast cultures. Simulations of batch erythroblast cultures (no medium refreshment) for different initial cell densities. Two different growth inhibition models were used for the predictions: the growth inhibition model proposed by Glen et al. including inhibition decay (panels **B** and **D**), and a simplified model without inhibition decay (This study; panels **A** and **C**) fitted to the same dataset. Cell concentration and total produced cells (C-C_0) are displayed. Equations used for the growth model and for the bioreactor simulations are available in Supplementary Methods.

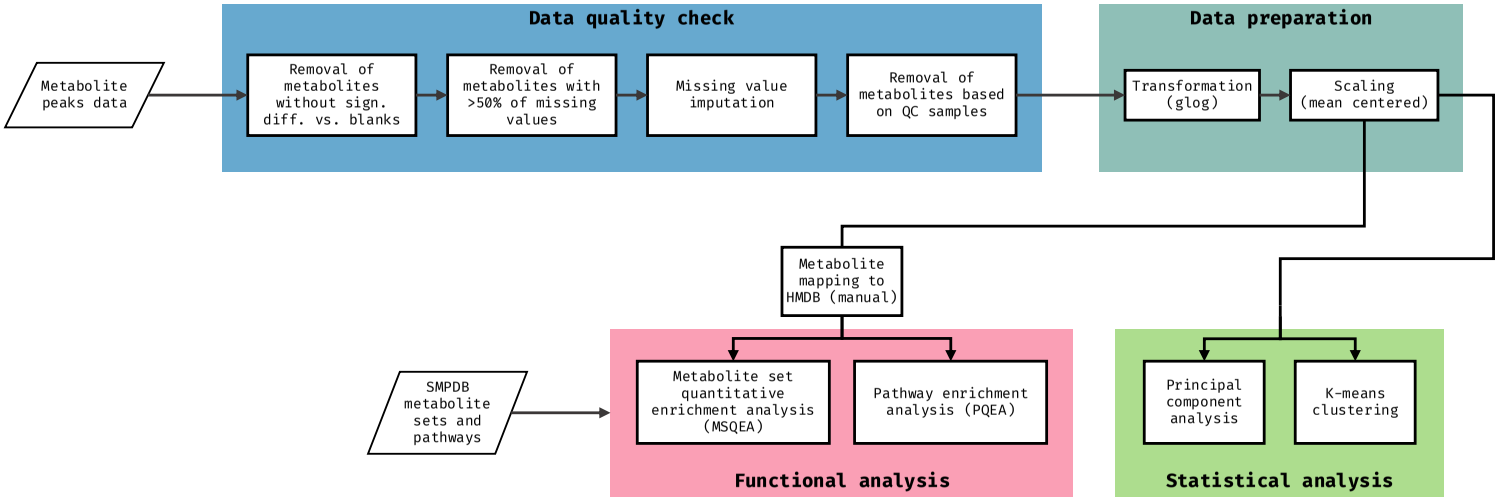

Supplementary Figure S5. Workflow for analysis of untargeted metabolomic data. Metabolite peak data obtained after acquisition (using a UHPLC-MS Vanquish coupled online to a Q Exactive mass spectrometer; Thermo Fischer Scientific; USA), validation, and annotation (using MAVEN), was used as input for the metabolomics analysis workflow. Data cleaning was performed in three stages: (i) pre-filtering of metabolites with peak areas not significantly different to blank samples (Student t-test; $p<0.05$), (ii) missing value imputation (missing values replaced by 1/5 of the smallest positive value in the original dataset), and (iii) filtering based on the quality control (QC) samples (if a metabolite showed a relative standard deviation > 25% in the QC samples, it is not considered for further analysis). Following this, peak data was transformed (glog method) and scaled (mean centered). Processed peak data was used for statistical analysis (principal component analysis and *k*-means clustering). For functional analysis, metabolites were first mapped to the Human Metabolome Database (HMDB). Metabolic set quantitative enrichment analysis (MSQEA) and pathway quantitative enrichment analysis (PQEA) was performed using MetaboAnalystR using a database of metabolite sets and pathways from the Small Molecule Pathway Database (SMPDB).

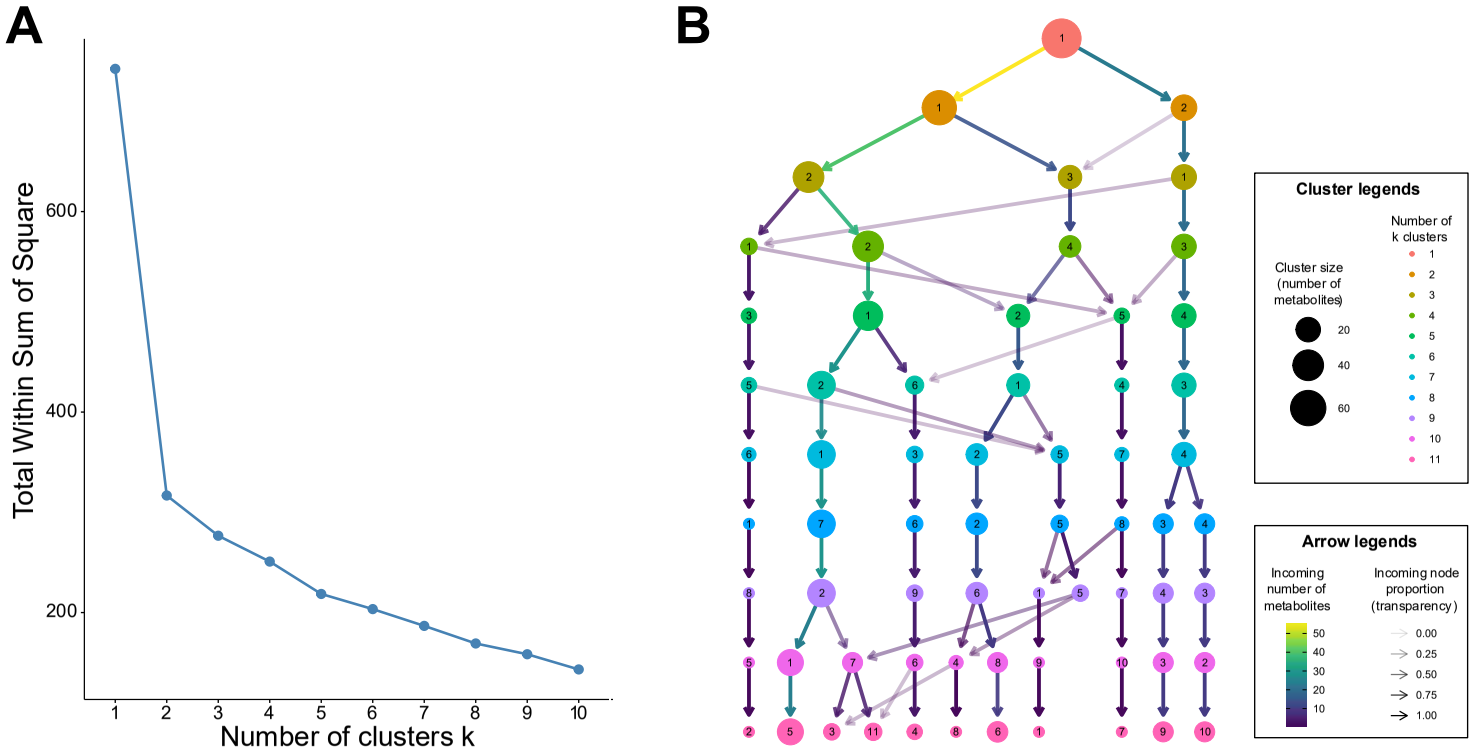

Supplementary Figure S6.
(Continues in next page)

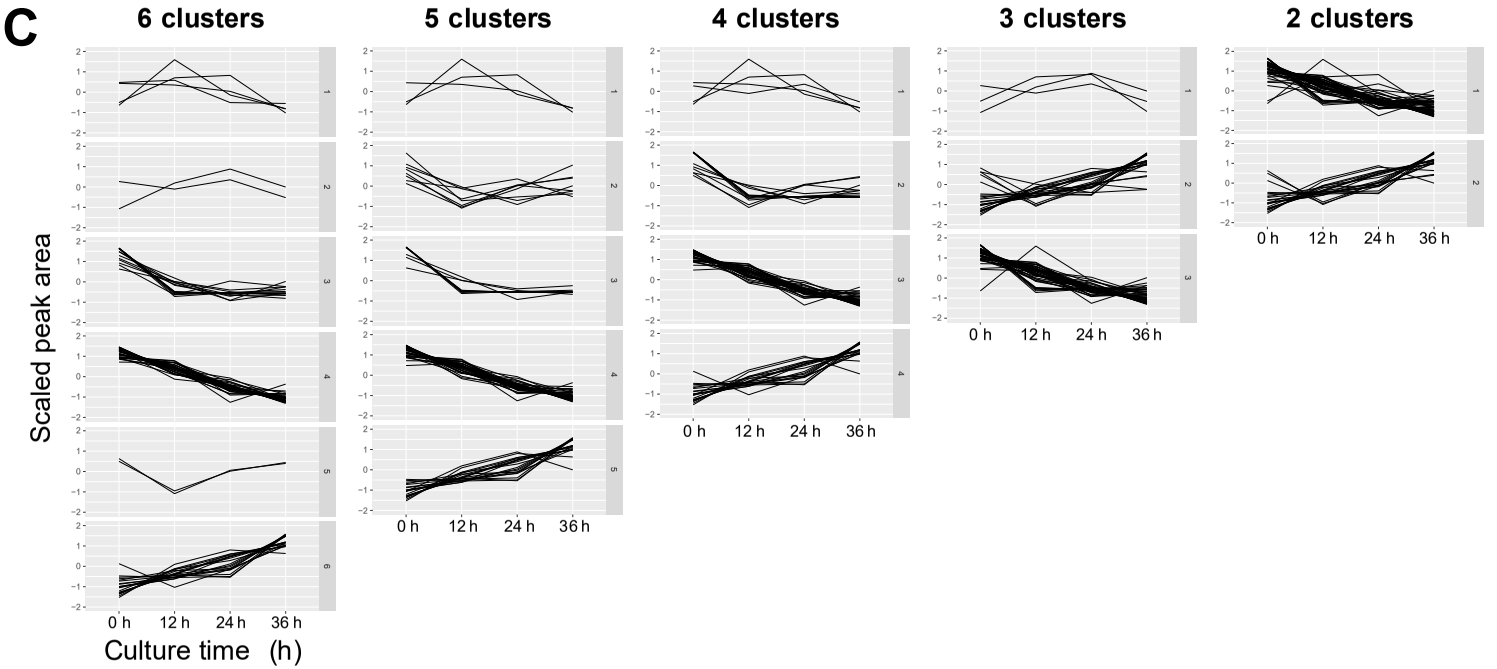

Supplementary Figure S6. Determination of optimal number of *k*-clusters for exo-metabolomics data of high cell concentration erythroblast cultures. (A) Effect of number of *k*-clusters on the total explained variation. Increasing the number of clusters leads to a higher percentage of the total variation explained by the clusters, here measured as a decrease in the total sum of squares. **(B)** Effect of increasing cluster number on the distribution of metabolites in the *k*-clusters. Over-clustering of data can be seen as an increase in incoming arrows to a newly generated clusters, representing a reassignment of metabolites previously in other clusters in the new cluster. An example of this can be seen when going from 6 to 7 clusters, with cluster 5 receiving metabolites from three different clusters. **(C)** Trends of scaled peak area for each cluster as cluster number increases from 2 to 6. Results from all panels were generated using the function *fviz_nbclust* from the R package *factoextra*.

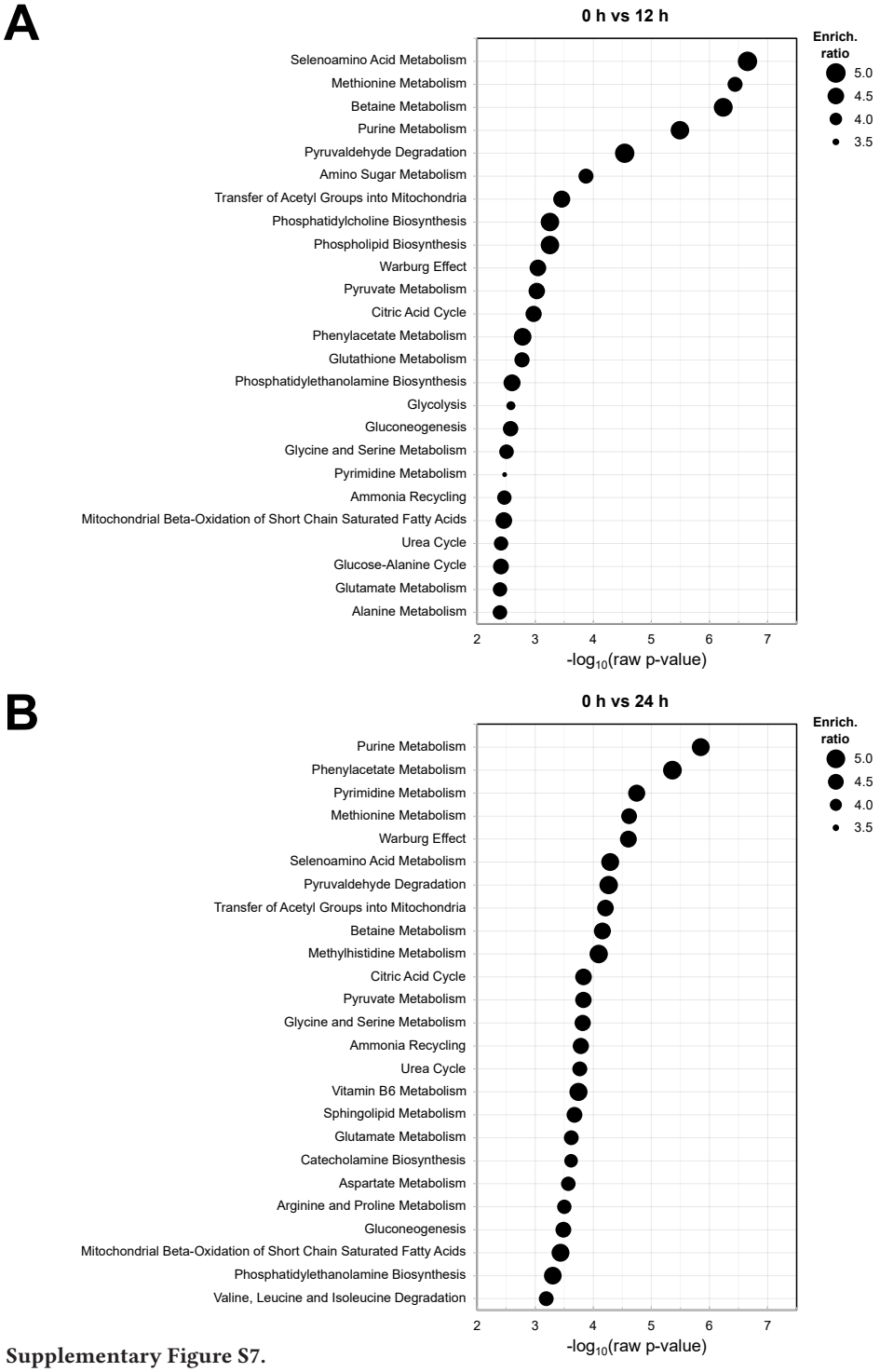

Supplementary Figure S7.
(Continues in next page)

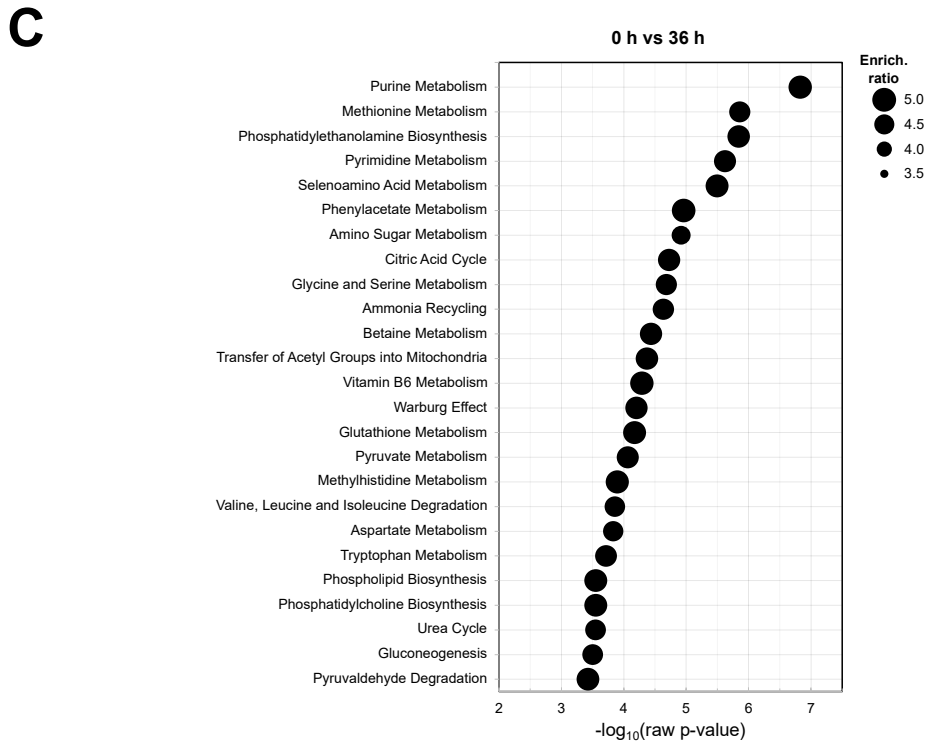

Supplementary Figure S7. Metabolite set quantitative enrichment analysis (MSQEA) of extracellular metabolome data of proliferating erythroblast cultures. After mapping the identified metabolites to the Human Metabolome Database (HMDB), metabolite-set quantitative enrichment analysis (MSQEA) was performed. Supernatant untargeted metabolomics data for cultures started at a high cell concentration (2.0×10^6 cells/mL) was used for this analysis. Results for the pairwise comparisons of 12 h **(A)**, 24 h **(B)**, and 36 h **(C)** relative to the start of the culture (0 h) are displayed. MSQEA was performed using the Small Molecule Pathway Database (SMPDB) available in MetaboAnalystR v3. For each metabolite set or pathway, the enrichment level and *p*-value are displayed (x-axis and size of the circle, respectively). Only the top 25 most enriched metabolite sets are displayed.

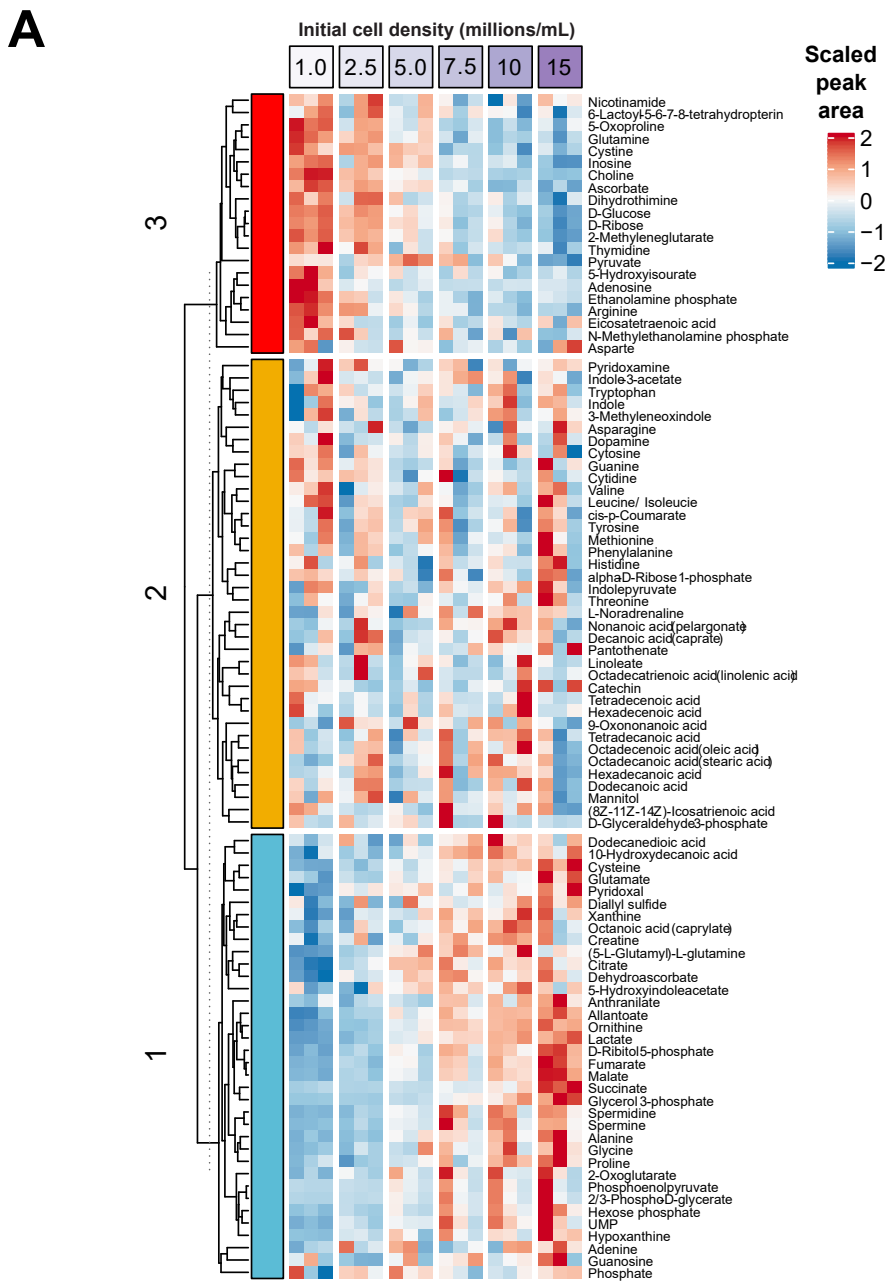

Supplementary Figure S8.
(Continues in next page)

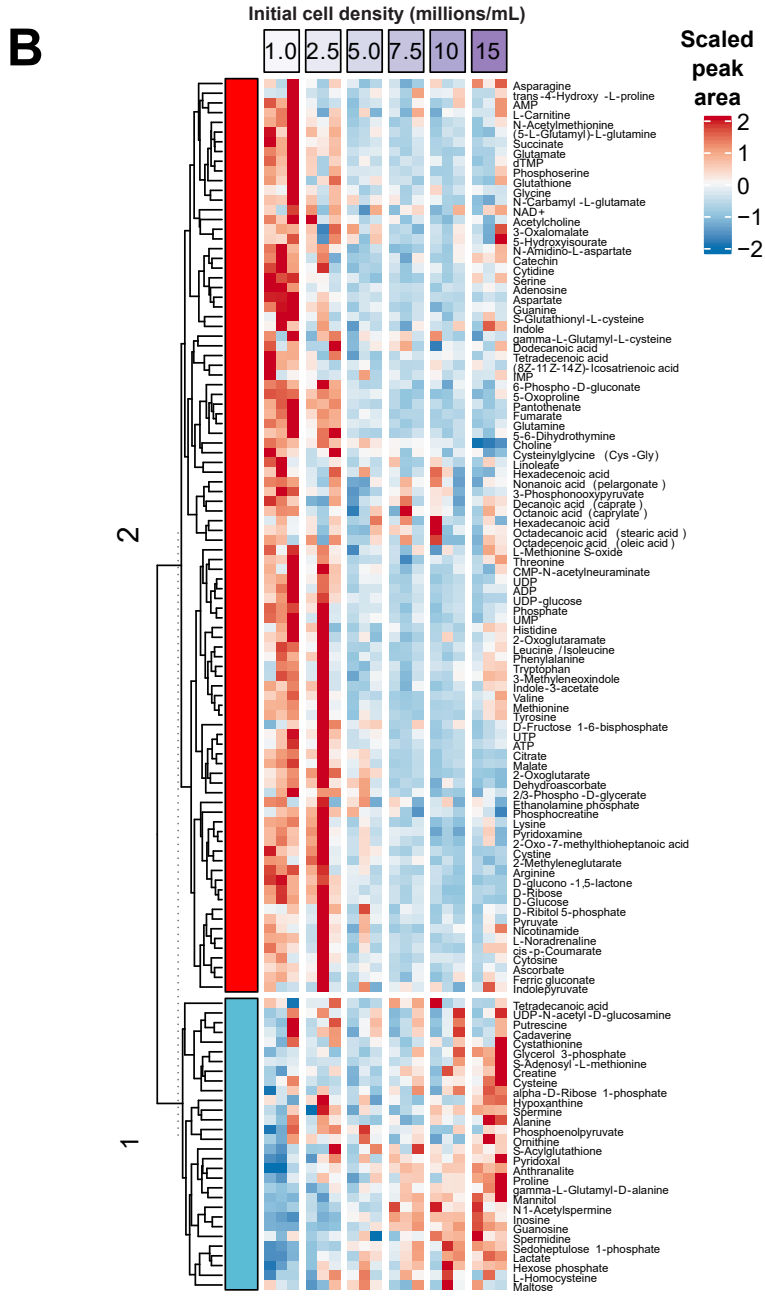

Supplementary Figure S8. Untargeted metabolomics analysis of erythroblast cultures at varying cell concentrations. Spent medium samples and cell pellets from erythroblasts cultured for 16 h at different starting cell concentrations (1-15×10^6 cells/mL) were analyzed by untargeted metabolomics. Heatmaps (including *k*-clusters) for extracellular (**A**) and intracellular (**B**) measurements are included ($n = 3$ donors).

3.10. Supplementary tables

Supplementary Table S1. Optimized operating parameters for evaluated feeding profiles. Parameters for fed-batch and perfusion feeding strategies were optimized to achieve a production of 30×10^9 cells in 4 days in a 1 L bioreactor inoculated at a starting cell concentration of 1×10^6 cells/mL, minimizing total medium consumption. Optimized parameters were as follow: feeding rate normalized by initial culture volume ($F/V_0 = D$; 1/h) for the fed batch culture using constant feed rate FB_{const}; initial feeding rate normalized by initial culture volume ($F_0/V_0 = D_0$; 1/h) and exponential increase rate of the feeding rate (θ; 1/h) for the fed batch culture with exponentially increasing feed FB_{exp}; perfusion rate normalized by culture volume ($F/V_0 = P$; 1/h) for the perfusion culture at a constant perfusion rate $PERF_{const}$; cell-specific perfusion rate (CSPR; pL/cell/day) for the perfusion at a constant CSPR $PERF_{CSPR}$. Two different growth inhibition models were used for the bioreactor simulations: the growth inhibition model proposed by Glen et al. including inhibition decay, and a simplified model without inhibition decay (This study) fitted to the same dataset. Equations used for the growth model and for the bioreactor simulations are available in Supplementary Methods.

Feeding strategy	Optimized feeding parameters	This study	Glen et al. (2018)
FB_{const}	D (1/h)	0.086	0.075
FB_{exp}	D_0 (1/h) θ (1/h)	0.49 -0.064	1.89 -0.30
$PERF_{const}$	P (1/h)	0.19	0.11
$PERF_{CSPR}$	$CSPR$ (pL/cell/day)	297	187

Supplementary Table S2. Quantification of amino acid concentrations in erythroblast proliferation cultures. Erythroblast from two donors were cultured from PBMCs for 10 days, seeded in fresh medium for 2 days at a starting cell density of 1.0×10^6 cells/mL, and cultured for 2 days. Supernatant amino acid concentrations at days 0 and 2 of culture were measured by GC-MS and IDMS. Control samples in medium without cells were also measured. Data not available (n.a.) for arginine, as it could not be measured with the used method.

		Concentration (µmol/L)																		
Condition	**Day**	**Ala**	**Arg**	**Asn**	**Asp**	**Cys**	**Gln**	**Glu**	**Gly**	**His**	**Ile**	**Leu**	**Lys**	**Met**	**Phe**	**Pro**	**Ser**	**Thr**	**Trp**	**Tyr**
No cells	0	296	n.a.	265	240	144	2454	547	436	264	797	764	890	181	395	339	366	841	91	467
No cells	2	303	n.a.	238	235	202	2129	563	397	280	835	784	909	186	412	362	395	930	84	479
Donor 1	0	285	n.a.	239	235	137	2346	503	406	233	785	739	868	175	390	339	349	771	85	444
Donor 1	2	520	n.a.	192	244	135	796	721	328	155	530	420	643	130	310	328	10	728	56	397
Donor 2	0	303	n.a.	224	231	224	2410	529	417	247	806	770	910	175	399	352	364	806	91	452
Donor 2	2	432	n.a.	172	254	111	752	679	292	145	547	429	646	129	306	316	17	718	61	392

Supplementary Table S3. Cell-specific consumption and production rates of amino acids in erythroblast proliferation cultures. Erythroblast from two donors were cultured from PBMCs for 10 days, seeded in fresh medium for 2 days at a starting cell density of 1.0×10^6 cells/mL, and cultured for 2 days. Supernatant amino acid concentrations at days 0 and 2 of culture were measured by GC-MS and IDMS (concentrations available in Supplementary Table S2). The cell specific consumption/production rate (q_i; <0 if consumed, >0 if produced) for each amino acid was determined using the average growth rate between day 0 and 2 (Equation 2), and the initial and final concentration of the amino acid in the supernatant (Equation 1). Data not available (n.a.) for arginine, as its concentration could not be quantified with the used method.

	q_i (nmol/million cells/day)																		
Donor	**Ala**	**Arg**	**Asn**	**Asp**	**Cys**	**Gln**	**Glu**	**Gly**	**His**	**Ile**	**Leu**	**Lys**	**Met**	**Phe**	**Pro**	**Ser**	**Thr**	**Trp**	**Tyr**	**Val**
1	43.0	n.a.	-8.5	1.6	-0.4	-283	39.9	-14.2	-14.2	-46.6	-58.3	-41.2	-8.3	-14.7	-2.0	-61.8	-7.8	-5.4	-8.7	-46.8
2	24.4	n.a.	-10.0	4.2	-21.3	-314	28.4	-23.8	-19.4	-49.2	-64.7	-50.0	-8.7	-17.6	-6.8	-65.9	-16.8	-5.7	-11.4	-53.6
Average	33.7	n.a.	-9.2	2.9	-10.9	-299	34.1	-19.0	-16.8	-47.9	-61.5	-45.6	-8.5	-16.1	-4.4	-63.8	-12.3	-5.5	-10.1	-50.2

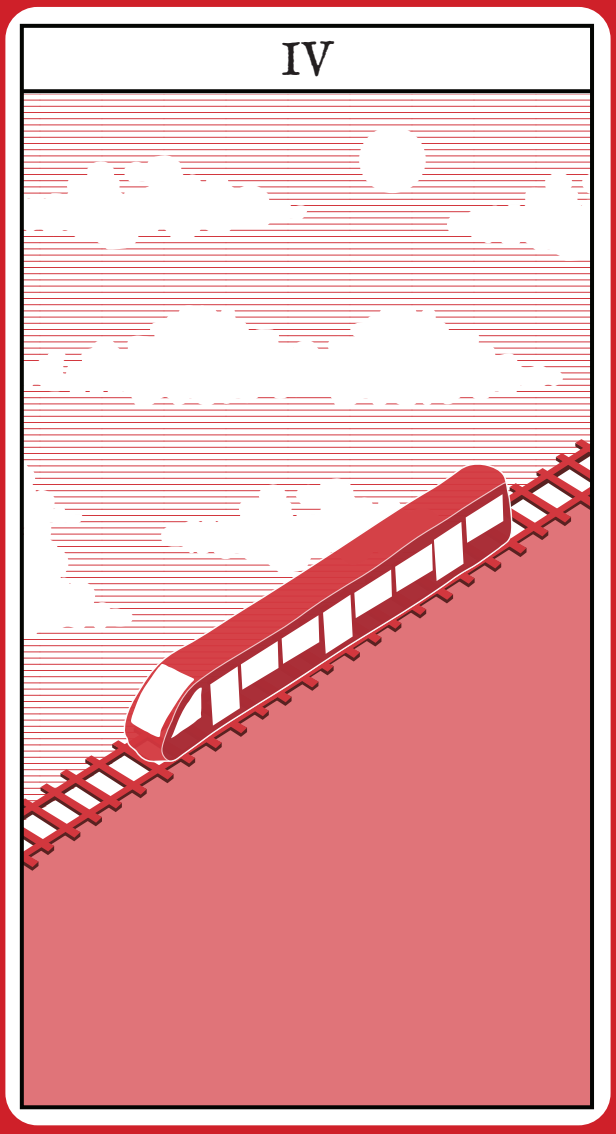
IV

Chapter 4

Iron-loaded deferiprone can support full hemoglobinization of cultured red blood cells

This chapter has been published in Scientific Reports:
Sci Rep 13, 6960 (2023). DOI: https://doi.org/10.1038/s41598-023-32706-1

Joan Sebastián Gallego Murillo | Nurcan Yağcı | Eduardo Machado Pinho | Sebastian Aljoscha Wahl | Emile van den Akker | Marieke von Lindern

Abstract

Iron, supplemented as iron-loaded transferrin (holotransferrin), is an essential nutrient in mammalian cell cultures, particularly for erythroid cultures. The high cost of human transferrin represents a challenge for large scale production of cultured red blood cells (cRBCs) and for cell therapies in general. We evaluated the use of deferiprone, a cell membrane-permeable drug for iron chelation therapy, as an iron carrier for erythroid cultures. Iron-loaded deferiprone ($Def_3 \cdot Fe^{3+}$, at 52 µmol/L) could eliminate the need for holotransferrin supplementation during *in vitro* expansion and differentiation of erythroblast cultures to produce large numbers of enucleated cRBCs. Only the first stage, when hematopoietic stem cells committed to erythroblasts, required holotransferrin supplementation. RBCs cultured in presence of $Def_3 \cdot Fe^{3+}$ or holotransferrin (1000 µg/mL) were similar with respect to differentiation kinetics, expression of cell-surface markers CD235a and CD49d, hemoglobin content, and oxygen association/dissociation. Replacement of holotransferrin supplementation by $Def_3 \cdot Fe^{3+}$ was also successful in cultures of myeloid cell lines (MOLM13, NB4, EOL1, K562, HL60, ML2). Thus, iron-loaded deferiprone can partially replace holotransferrin as a supplement in chemically defined cell culture medium. This holds promise for a significant decrease in medium cost and improved economic perspectives of the large scale production of red blood cells for transfusion purposes.

4.1. Introduction

Iron is an essential nutrient for all eukaryotic microorganisms. Erythroid precursors, however, have exceptionally high iron requirements to facilitate hemoglobin synthesis during the generation of red blood cells (RBCs). A single RBC contains approximately 300 million molecules of hemoglobin (≈30 pg), associated with 1.2×10^9 Fe^{3+} ions [1]. In healthy humans, 65-75% of all body iron is present as hemoglobin in RBCs [2]. Free ferrous iron Fe^{2+} can lead to the production of toxic radicals via the Fenton reaction [3]. Therefore, plasma iron is transported bound to e.g. transferrin (Tf). Human transferrin is a single chain glycoprotein with a molecular weight of ~80 kDa. It has two distinct iron-binding lobes (N- and C-lobe). The binding of Fe^{3+} to Tf is sequential, resulting in four possible Tf species: iron-free Tf (aTf: apotransferrin), diferric Tf (hTf: holotransferrin), and two monoferric Tf forms depending on which lobe contains the Fe^{3+} ion (mTf_N and mTf_C for the species with the iron ion in the N- or C-lobe, respectively) [4].

High expression of the transferrin receptor 1 (TFR1; CD71) on erythroblasts facilitates their increased uptake of hTf for heme synthesis. Iron deficiency reduces the yield of burst-forming erythroid-units in early stages of *ex vivo* erythropoiesis [5], and of reticulocytes during terminal erythroid differentiation [6]. Assuming that hTf is the sole source of iron, ~80 pg of hTf need to be internalized for a single fully-hemoglobinized RBC, corresponding to ~160 g hTf for a single transfusion unit of RBCs (2×10^{12} RBCs). Transferrin is endocytosed upon binding to TFR1. Fe^{3+} ions are released at the low endocytic pH, reduced to Fe^{2+} by STEAP3, transported to mitochondria by direct endosome-mitochondria association, and ultimately incorporated into heme [7]. Excess iron is bound to cytosolic ferritin [8]. Vesicles containing aTf still bound to TFR1 recycle to the cell surface where aTf is released. In the body, the released aTf can bind new Fe^{3+} ions via direct transfer from ceruloplasmin ferroxidase [9]. In addition to TFR1, erythroblasts also express TFR2 which associates with the erythropoietin receptor (EpoR) [10,11]. Transferrin-dependent internalization of TFR2 modulates the Epo response, particularly at suboptimal Epo levels [12,13].

The expression level of key regulatory proteins involved in iron uptake, storage and export is controlled by the RNA-binding proteins Iron regulatory protein-1 and -2 (IRP1/2) [14]. IRP1 binding to Fe-S clusters changes its conformation, and inhibits binding to iron-responsive elements (IREs) in the untranslated regions of mRNAs. For iron uptake proteins such as TFR1 and DMT1, IRP1 binding to IREs in the 3' UTR of respective mRNAs increases mRNA stability [15]. By contrast, IRP1 binding to the IREs in the 5' UTR of mRNAs encoding proteins involved in iron storage and export (e.g. ferritin and ferroportin) decreases their translation [16,17]. Iron deficiency decreases heme levels, which activates Heme-regulated eIF2α kinase (HRI), resulting

in phosphorylation of eIF2 and a global inhibition of protein translation [18–20]. At the level of erythropoiesis, lack of iron causes microcytic anemia *in vivo* [21], and decreases the proliferation and differentiation of erythroblast cultures *ex vivo* [6].

In serum-free cell culture systems, high levels of hTf (1000 µg/mL) are added during terminal differentiation [22,23]. Currently, most of the Tf used in cultures is purified from human plasma. However, there is a growing need to transition towards animal-free media components to ensure safety of the final product. Production of recombinant Tf in *Escherichia coli*, insects, yeast, rice and BHK cells represents an alternative, but is still not cost-effective for the *ex vivo* production of RBCs [24].

Several small molecules have been reported to chelate and deliver iron into the cells. Iron-loaded PIH (pyridoxal isonicotinoyl hydrazone) restored proliferation and differentiation in several cell lines in absence of hTf by directly crossing the cellular membrane [25–27]. Supplementation of iron-loaded hinokitiol was also shown to restore proliferation and hemoglobinization in DMT1-deficient cells in transferrin-free medium, although its effectiveness seems to depend on the presence of large iron gradients across the cellular membrane [28]. More recently, a low Tf culture medium for cRBC production has been reported, in which supplementation with Fe^{3+}-EDTA supports reloading of Tf (aTf ⟶ hTf), which can then be re-utilized by the cells [29].

Chelators used to treat iron overload *in vivo* can have a high affinity for iron that is lower than transferrin, which allows them to scavenge all non-transferrin-bound iron (NTBI) to prevent oxidative damage [30,31]. Among them is deferiprone (1,2-dimethyl-3-hydroxypyridin-4-one), a bidentate alpha-keto hydroxypyridine molecule that binds iron with a stoichiometry of 3:1 ($Def_3{\cdot}Fe^{3+}$) at physiological conditions [32]. Its ability to cross the cell membrane and mobilize intracellular iron is the principle of combined chelation therapy, in which deferiprone scavenges intracellular iron and transfers it to a second non-permeable chelator such as deferoxamine [33,34].

In this study, we evaluated the potential of iron-loaded deferiprone ($Def_3{\cdot}Fe^{3+}$) to replace the supplementation with high levels of hTf in cultures of erythroid precursors for the *ex vivo* production of RBCs. We demonstrated that $Def_3{\cdot}Fe^{3+}$ can recharge aTf to hTf. Medium supplementation with $Def_3{\cdot}Fe^{3+}$ alone was sufficient to sustain efficient *ex vivo* production of fully hemoglobinized RBCs with an oxygen binding capacity comparable to peripheral blood RBCs. Excess $Def_3{\cdot}Fe^{3+}$ showed no sign of toxicity in erythroblast proliferation and differentiation. Additionally, the use of $Def_3{\cdot}Fe^{3+}$ as the only iron source in serum-free medium was sufficient to sustain the proliferation of other transferrin-dependent mammalian cell lines.

4.2. Methods

4.2.1. Cell culture

Donor-derived buffy coats are a Sanquin not-for-transfusion product from which human peripheral blood mononuclear cells (PBMCs) are purified by density centrifugation. Informed written consent was given by donors to give approval for the use of waste material for research purposes, and was checked by Sanquin's NVT Committee (approval file number NVT0258; 2012) in accordance with the Declaration of Helsinki and the Sanquin Ethical Advisory Board. Erythroid cells were cultured from PBMCs in serum-free medium as previously described [22] with minor modifications to Cellquin medium, which lacked nucleosides, and contained a defined lipid mix (Sigma-Aldrich; USA; 1:1000) replacing cholesterol, oleic acid, and L-α-phosphatidylcholine. Transferrin concentrations varied as indicated. hTf (Sanquin; Netherlands) or aTf (Sigma-Aldrich) were added as indicated. In the first phase, erythroblast cultures are established from PBMC in presence of erythropoietin (Epo, 2 U/mL; EPREX®, Janssen-Cilag, Netherlands), hSCF (100 ng/mL, produced in HEK293T cells), dexamethasone (1 µmol/L; Sigma-Aldrich), and IL-3 (1 ng/mL first day only; Stemcell Technologies; Canada). From day 6, erythroblast cultures were expanded and the cell density was maintained between 0.7-2×10^6 cells/mL (CASY Model TCC; OLS OMNI Life Science; Germany). To induce differentiation, cells were washed and reseeded at 1-2×10^6 cells/mL in presence of Epo (10 U/mL), 5% Omniplasma (Octapharma GmbH; Germany), and heparin (5 U/mL; LEO Pharma A/S; Denmark). During this differentiation phase the cells undergo 3-4 divisions before they mature to enucleated reticulocytes. AML-derived cell lines MOLM13 [35], NB4 [36], EOL1 [37], K562 [38], HL60 [39] and ML2 [40] were seeded at a concentration of 0.3×10^6 cells/mL in Cellquin, supplemented with hTf and $Def_3{\cdot}Fe^{3+}$ as indicated.

4.2.2. Iron chelators

Deferiprone (Def; Sigma-Aldrich), deferoxamine mesylate (DFOA; Sigma-Aldrich), deferasirox (DFO; Sigma-Aldrich) and hinokitiol (HINO; Sigma-Aldrich) were dissolved as indicated by the manufacturer and mixed at stoichiometric ratio with an iron(III) chloride solution (Sigma-Aldrich; 16 h, 20 °C), to obtain a concentration of 26 mmol/L chelated Fe^{3+} ($Def_3{\cdot}Fe^{3+}$, $DFOA{\cdot}Fe^{3+}$, $DFO_2{\cdot}Fe^{3+}$, $HINO_3{\cdot}Fe^{3+}$), equivalent to the iron content of 1000 mg/mL hTf.

4.2.3. Flow cytometry

Cells were stained in HEPES buffer + 0.5% BSA (25-30 min, 4 °C), measured using a BD FACSCanto™ II flow cytometer (BD Biosciences), gated against specific isotypes, and analyzed using FlowJo™ (version 10.3; USA). Antibodies or reagents used were: (i) CD235a-PE (1:2500 dilution; OriGene cat#DM066R), CD49d-BV421 (1:100 dilution;

BD-Biosciences cat#565277), DRAQ7 (live/dead stain; 1:200 dilution; ThermoFischer Scientific cat#D15106); (ii) CD235a-PE (1:2500 dilution; OriGene cat#DM066R), CD71-APC (1:200 dilution; Miltenyi cat#130-099-219); (iii) CD71-VioBlue (1:200 dilution; Miltenyi cat#130-101-631); (iv) DRAQ5 (nuclear stain; 1:2500 dilution; abcam cat#ab108410); (v) PI (live/dead stain; 1:2000 dilution; Invitrogen cat#P3566).

4.2.4. Western blots

Iron saturation of transferrin was measured on 6% TBE-urea gels as previously described [41]. Gels were stained with InstantBlue Coomassie protein stain (abcam).

For the determination of the expression level of proteins involved in iron metabolism, whole cell lysates harvested during differentiation were prepared in RIPA buffer (10 min, 4 °C). For Epo induction experiments, erythroblasts cultured in expansion medium supplemented with 300 µg hTf or 52 µM $Def_3{\cdot}Fe^{3+}$ and Epo (2 U/mL) were washed twice in PBS and reseeded in expansion medium with hTf and $Def_3{\cdot}Fe^{3+}$ but without Epo. After 3 hours, cells were stimulated with Epo as indicated for 20 min at 37 °C, washed in ice-cold PBS and harvested in RIPA buffer.

Protein concentration was determined by colorimetry (DC™ Protein Assay; Bio-Rad; USA). Lysates were diluted 1:4 with Laemmli sample buffer (Bio-Rad), incubated for 95 °C (5 min), subjected to SDS-polyacrylamide gel electrophoresis (4–20% Criterion™ Tris-HCl Protein Gel, Bio-Rad), transferred to nitrocellulose membranes (iBlot2 system; ThermoFischer Scientific), and stained. Membranes were cut after protein transfer to reduce the volume of antibodies needed for staining. Primary antibodies included actin (Sigma cat#A3853), transferrin receptor (Merck cat#SAB4200398), ferritin (abcam cat#ab75973), p-eIF2 (CellSignaling cat#3597L), total eIF2 (CellSignaling cat#9722S), p-STAT5 (Millipore; USA; cat#05-495), and total STAT5 (Santa Cruz; USA; cat#SC-835). Western blots were analyzed using GelAnalyzer 19.1. Original uncropped blot images are deposited in the publicly available data repository Zenodo under the link https://doi.org/10.5281/zenodo.6350135.

4.2.5. Hemoglobin quantification and oxygenation

Hemoglobin content was determined using *o*-phenylenediamine as described [42]. Intracellular hemoglobin concentration was calculated using the mean of technical triplicates, and the measured cell volume (CASY Model TCC). Oxygen association/dissociation curves for RBCs were determined by continuous dual wavelength spectrophotometric measurement with a HEMOX Analyzer (TCS Scientific Corp.; USA), using RBCs that were washed and resuspended at 20×10^6 cells/mL in analysis buffer (PBS + 0.5% BSA + 0.005% Y-30 antifoam). P_{50} values were calculated as the oxygen partial pressure that leads to a 50% saturation of hemoglobin.

4.2.6. Statistical analysis

Statistical analyses were performed using the two-tailed two sample Student's *t*-test. For comparison of fold change (FC) data, log(FC) values were first calculated and then used for the statistical test. When indicated, *p*-values were corrected for multiple comparisons with the Holm-Bonferroni method. All data in figures is displayed as mean ± the standard deviation of the measurements. The number of replicates is n≥3 for all experiments. Significance is expressed as: ns for not significant differences, * for $p<0.05$, ** for $p<0.01$, *** for $p<0.001$.

4.3. Results

4.3.1. Iron-loaded deferiprone supports erythroid differentiation at low holotransferrin concentrations

As reference for the different iron supplementation strategies, we first tested different holotransferrin concentrations during erythroblast differentiation, the culture stage in which cells have the highest iron requirements. Twelve days post-seeding PBMCs in expansion medium, erythroblasts were cultured in differentiation medium supplemented with decreasing concentrations of hTf (1000, 200, 100, 50 and 0 µg/mL; equivalent to 26, 5.2, 1.3 and 0 µmol/L of chelated Fe^{3+} respectively). At 1000 µg/mL hTf, erythroblasts proliferated for 3-4 days followed by cell growth arrest at the final stage of differentiation [22]. A gradual decrease of hTf concentrations resulted in a gradual decrease in cell yields, in accordance with previously described data (Figure 1A) [6]. Erythroblast differentiation is accompanied by a progressive loss of cell volume to reach the cell size of erythrocytes. Suboptimal hTf concentrations led to a faster decrease in cell size during the first 4 days compared with 1000 µg/mL hTf, and a consistently lower cell volume that was still present after 8 days of culture (Supplementary Figure S1A). This seems to be in accordance with microcytic anemia associated with iron deficiency. However, cultured reticulocytes are generally larger compared to primary erythrocytes, and also reticulocytes cultured at low iron concentrations remain larger compared to primary erythrocytes. Thus, it is not clear how low or high concentrations of iron result in aberrantly sized cultured reticulocytes. Hemoglobin (Hb) levels per cell were low at the start of differentiation, and rapidly increased dependent on the hTf concentration (Supplementary Figure S1B).

hTf is internalized upon binding to TFR1. After releasing Fe^{3+}, iron-depleted transferrin (apotransferrin; aTf) is recycled back to the cell membrane together with the TFR1. We tested whether supplementation of culture medium with an iron-loaded chelator can sustain differentiation of erythroblasts at low hTf concentrations. Four chelators loaded

with iron (52 µmol/L chelated Fe^{3+}) were added to medium with a growth-limiting hTf concentration (100 µg/mL). Supplementation with iron-loaded deferiprone ($Def_3 \cdot Fe^{3+}$) or deferoxamine (DFOA·Fe^{3+}) enabled proliferation similar to 1000 µg/mL of hTf. To a lesser extent also deferasirox ($DFO_2 \cdot Fe^{3+}$) and hinokitiol ($HINO_3 \cdot Fe^{3+}$) rescued growth recovery (Figure 1B).

To test the ability of these chelators to reload aTf, 1000 µg/mL aTf was incubated with 52 µmol/L of chelated iron at 37 °C overnight and subjected to urea-PAGE gel electrophoresis. The mobility of aTf is lower compared to hTf, while the monoferric transferrin forms (mTf_C, mTf_N) have an intermediate migration speed. Deferasirox and hinokitiol showed a low Tf saturation level, while both deferiprone and deferoxamine could reload most aTf (Figure 1C). Soluble iron, added as $FeCl_3$, was also able to reload the majority of aTf, with minor amounts of both mTf forms present. Although deferiprone resulted in more mTf compared to deferoxamine, the former was favored for stability [43] and cost-effectiveness.

Decreasing deferiprone concentrations reduced the final saturation level of Tf (Figure 1C). To further test the effect of iron-loaded deferiprone supplementation ($Def_3 \cdot Fe^{3+}$) on iron-limited erythroid differentiation, erythroblasts were seeded in differentiation medium supplemented with 100 µg/mL hTf and $Def_3 \cdot Fe^{3+}$ at concentrations between 3.2 and 52 µmol/L (equivalent to 125 and 2000 µg/mL hTf, respectively). $Def_3 \cdot Fe^{3+}$ improved cell growth dependent on the $Def_3 \cdot Fe^{3+}$ concentration (Figure 1D).

In differentiation cultures, most of the hemoglobin is synthesized in the first 2-4 days of culture, and hemoglobin content per cell is strongly dependent on the hTf concentration in the medium (Supplementary Figure S1B). At day 4, the hemoglobin content of cultured cells showed saturation kinetics (hyperbolic) as a function of the media iron content. Of note, cells cultured in absence of hTf had a 10-fold decrease in hemoglobin (Hb) mass per cell compared to the highest hTf dose tested (Figure 1E). This dose-response behavior was also observed when using 100 µg/mL hTf with increasing deferiprone concentrations, with a maximal response using >13 µmol/L $Def_3 \cdot Fe^{3+}$. The same iron-dependent response was seen for hemoglobin accumulation (Hb intracellular concentration; Supplementary Figure S1C-D), with no difference observed between $Def_3 \cdot Fe^{3+}$ concentrations >13 µmol/L and medium containing 1000 µg/mL hTf.

The data suggests that $Def_3 \cdot Fe^{3+}$ supplementation can reload apotransferrin generated during culture. To validate this assumption, we calculated the concentrations

of transferrin and deferiprone species assuming equilibria at culture conditions (pH = 7.4, 3.5 mmol/L HCO_3^-; Supplementary Figure S2). For transferrin, the association equilibrium constants of 7.0×10^{22} L/mol and 3.6×10^{21} L/mol for the binding of the first and second Fe^{3+} ion were assumed, respectively [44]. For deferiprone, the global stability constants (log β) for the Def·Fe^{3+}, Def_2·Fe^{3+} and Def_3·Fe^{3+} complexes were assumed to be 15.01, 27.30 and 37.43, respectively [32]. It was assumed that iron association and dissociation kinetics with Tf and Def dominate iron concentration in the extracellular space, and that this is faster than the net utilization rate of iron in the intracellular space. As a model condition, a constant net average iron uptake rate (inflow + iron export from the cells) of 1.7×10^{-7} mol Fe^{3+}/L·h was assumed, corresponding to the production of 10×10^6 hemoglobinized cells per mL of culture (1 cell = 300×10^6 Hb molecules) in the first 4 days of culture, as observed in Supplementary Figure S1B. The calculated time profiles for the concentrations of the different transferrin and deferiprone species indicated that the addition of 26 or 52 μmol/L Def_3·Fe^{3+} to 100 mg/L hTf at the start of differentiation results in higher holotransferrin availability (percentage of total Tf) and lower apotransferrin levels, and thereby to a potentially better iron delivery compared to the addition of 1000 mg/L hTf alone (Supplementary Figure S2C). Although this simplified model does not consider direct transfer of Fe^{3+} from Def_3·Fe^{3+} to transferrin, the chemical equilibria simulations support the observation that Def_3·Fe^{3+} can reload iron-depleted transferrin, even by assuming the leaching of Fe^{3+} as the sole mechanism of iron transfer between the two chelators.

Figure 1. Deferiprone supplementation restores efficient differentiation of erythroblasts in transferrin-limited medium. Erythroblasts were expanded from PBMCs for 10-12 days, and subsequently seeded in differentiation medium at a starting cell concentration of $1.5\text{-}2.0\times10^6$ cells/mL. (**A)** Cells were seeded with decreasing holotransferrin concentrations (1000, 200, 100, 50 and 0 μg/mL). Cell number was determined at indicated days. **(B)** Cell concentration at day 7 days of differentiation in medium with low hTf (100 μg/mL), with or without 52 μmol/L Fe^{3+} associated with one of four iron-loaded chelators (deferiprone=Def; deferoxamine=DFOA; deferasirox=DFO; hinokitiol=HINO). **(C)** 1000 μg/mL apotransferrin was incubated for 16 h with iron-loaded chelators (52 μmol/L of chelated Fe^{3+}, unless indicated). All samples were incubated overnight in PBS at 37 °C (pH = 7.4). All samples were mixed 1:1 with Novex™ TBE-Urea gel sample buffer, loaded in a Novex™ 6% TBE-urea gel (3.0 μg of Tf per well; Invitrogen; Waltham, MA), and run for 2.25 h at 150 V. Gels were stained with Coomassie. Full uncropped gel image is displayed. Purified holo-transferrin (first lane) and apo-transferrin (second lane) function as size markers **(D)** Cell concentration after 6 days of differentiation in medium with hTf (values in μg/mL) and Def_3·Fe^{3+} (values in μmol/L) as indicated. **(E)** Hemoglobin content per cell after 4 days of differentiation at increasing iron concentration in cells cultured using hTf as sole iron source (●), or Def_3·Fe^{3+} plus 100 μg/mL hTf (■). A hyperbolic dose-response curve is fitted on the data ($Hb = Hb_{max} \times [Fe^{3+}] \times (EC_{50} + [Fe^{3+}])^{-1}$). All data is displayed as mean ± SD (error bars; n≥3). Significance is shown for the comparison with 1000 μg/mL hTf (unpaired two-tailed two-sample Student's *t*-test).

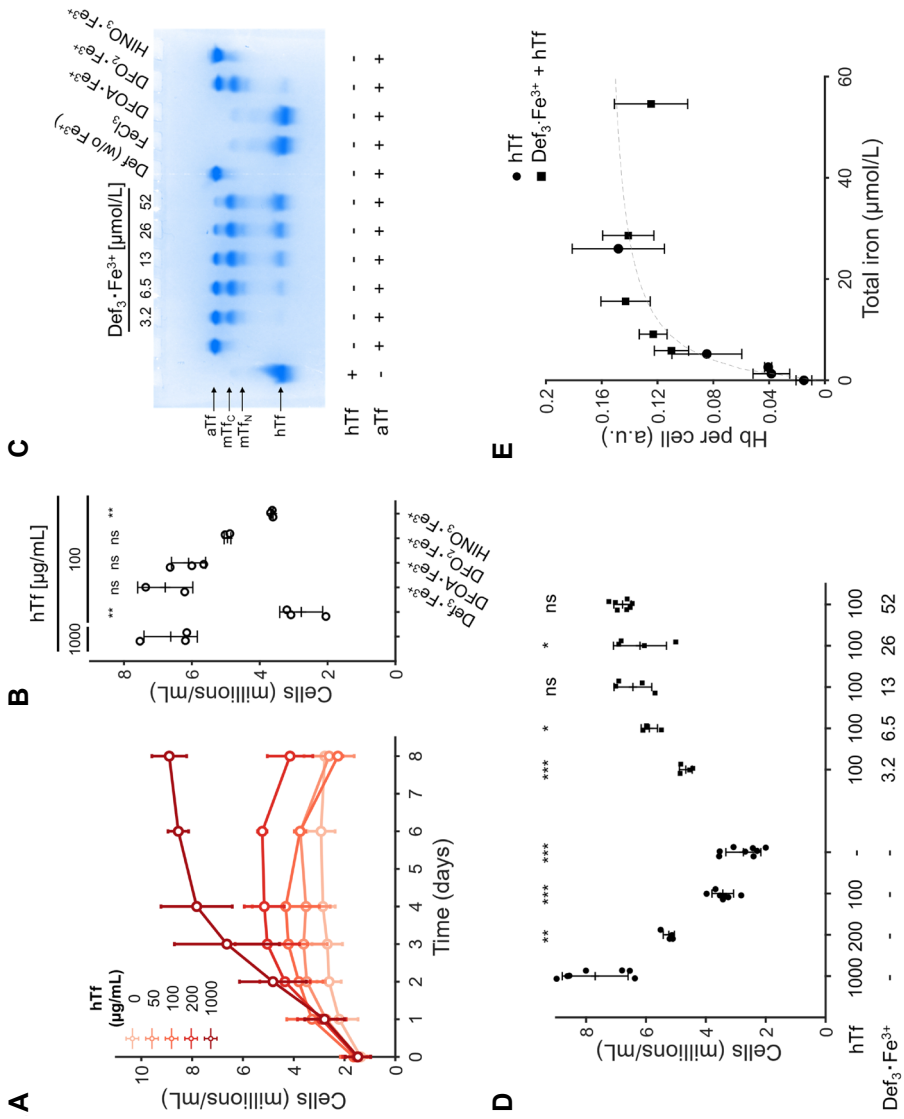

Figure 1.
(See caption on previous page)

4.3.2. Iron-loaded deferiprone can replace holotransferrin supplementation in differentiation

Due to its lipophilic nature and small size, deferiprone is expected to be cell permeable and able to redistribute iron between cell types, independent of ferroportin and transferrin [45,46]. We tested whether the larger $Def_3 \cdot Fe^{3+}$ complex can support erythroid differentiation in absence of transferrin supplementation (Tf concentration <0.2 µg/mL due to the 5% plasma used in differentiation medium [47]). Expanded erythroblast cultures (day 12) were reseeded at 1.5×10^6 cells/mL in differentiation medium with increasing concentrations of $Def_3 \cdot Fe^{3+}$ as sole iron source. At day 6 of differentiation, 3 times higher cell numbers were obtained using >13 µmol/L $Def_3 \cdot Fe^{3+}$ compared with no hTf supplementation and no $Def_3 \cdot Fe^{3+}$ cultures (Figure 2A). Similar dose-response curves were obtained for total hemoglobin per cell (Figure 2B). The addition of increasing hTf concentrations to optimal concentrations of $Def_3 \cdot Fe^{3+}$ (52 µmol/L) did not further increase cell number or hemoglobin content (Figure 2B-C). Interestingly, the combination of high levels $Def_3 \cdot Fe^{3+}$ together with a high concentration hTf did not lower cell numbers, suggesting that $Def_3 \cdot Fe^{3+}$ is not toxic to erythroblasts.

Oxygen association and dissociation are crucial for RBC function. Reticulocytes obtained from differentiation cultures supplemented with 52 µmol/L $Def_3 \cdot Fe^{3+}$ as had similar hemoglobin oxygen dissociation and association curves compared to peripheral blood RBCs and reticulocytes obtained in medium supplemented with hTf, with a slightly higher P_{50} (blood = 26.8 mmHg, hTf = 24.2 mmHg, deferiprone = 28.0 mmHg; calculated from oxygenation profile; Figure 2D).

Flow cytometry studies were performed to evaluate the effect of hTf and $Def_3 \cdot Fe^{3+}$ on the erythroblast maturation level. During *ex vivo* differentiation cultures, erythroblast acquire CD235 (Glycophorin A), and eventually lose CD71 (TFR1) expression [22]. Expression of CD71 may not be a reliable differentiation marker when evaluating the effect of hTf and $Def_3 \cdot Fe^{3+}$ supplementation, as it is upregulated at low iron availability [48]. At day 10 of differentiation, cells had a high expression of CD235 under all tested conditions (gating strategy in Supplementary Figure S3A). In contrast, CD71 expression levels decreased with increasing iron availability, independent of whether iron is presented as hTf or $Def_3 \cdot Fe^{3+}$ (Figure 2E; Supplementary Figure S3B). CD49d (integrin alpha 4) is an early differentiation marker [49], expressed independent of iron metabolism regulation. Regardless of the hTf or $Def_3 \cdot Fe^{3+}$ concentration, 30%-40% of all cells had a $CD235^+$ $CD49d^+$ phenotype, suggesting that deferiprone supplementation did not delay erythroid differentiation (Figure 2F).

The availability of chelated iron has been reported to affect erythroblast enucleation [50]. Enucleation efficiency of the cultures was evaluated using the nuclear stain DRAQ5 and cell size by flow cytometry (Supplementary Figure S3A). The ratio between enucleated (R) and total cells (R+E) indicates the enucleation ratio. High hTf concentrations led to a higher enucleation efficiency (65%) compared with suboptimal hTf concentrations (0 µg/mL hTf: 46%; 50 µg/mL hTf: 35%; 200 µg/mL hTf: 50%). Addition of 52 µmol/L $Def_3 \cdot Fe^{3+}$ increased terminal enucleation to 80% in the absence of hTf (Figure 2G). In addition, $Def_3 \cdot Fe^{3+}$ increased the ratio of reticulocytes over nuclei, indicating a positive effect on reticulocyte stability (Figure 2H). Collectively, these results suggest that $Def_3 \cdot Fe^{3+}$ can replace hTf as medium supplement in differentiation cultures, maintaining high cell yields and enucleation efficiency, hemoglobin content and oxygen carrying capacity.

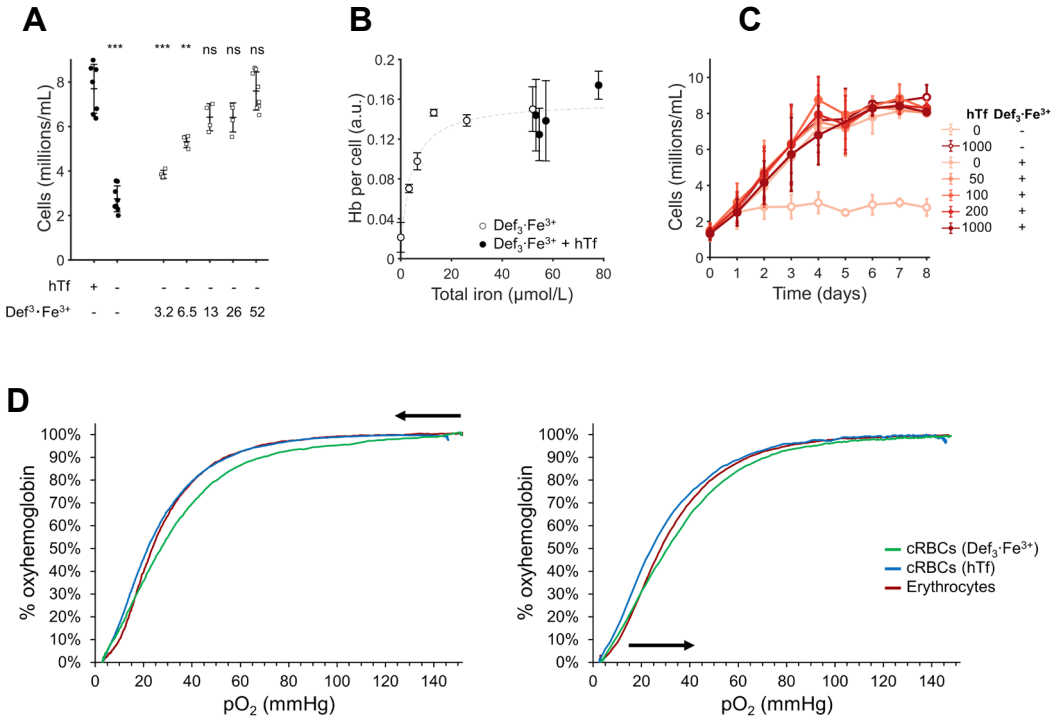

Figure 2.

(Continues in next page)

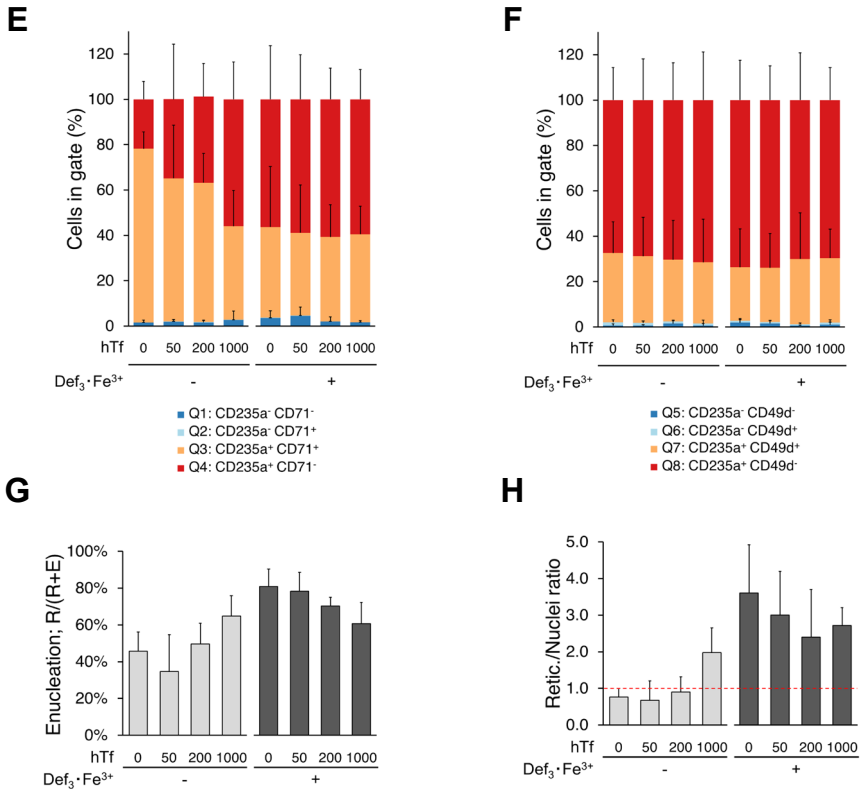

Figure 2. Deferiprone can replace holotransferrin supplementation in erythroblast differentiation cultures. Erythroblast were expanded from PBMCs for 10-12 days, and subsequently seeded in differentiation medium. **(A)** Cell concentration after 6 days of differentiation in medium without hTf supplementation, with varying levels of $Def_3{\cdot}Fe^{3+}$ (concentrations indicated in µmol/L). **(B)** Hemoglobin content of cells after 4 days in differentiation in medium using $Def_3{\cdot}Fe^{3+}$ as sole iron source (○), or with varying hTf concentrations (1000, 500, 200, 100, 50 µg/mL) in the presence of 52 µmol/L $Def_3{\cdot}Fe^{3+}$ (●). **(C)** Cell concentration of erythroblasts seeded in medium with or without 52 µmol/L $Def_3{\cdot}Fe^{3+}$ (filled and empty symbols, respectively), plus a decreasing concentration of hTf (values in µg/mL). **(D)** Oxygen dissociation (left) and association (right) curves measured by a HEMOX analyzer for peripheral blood erythrocytes (red), and reticulocytes cultured using either 1000 µg/mL hTf (blue) or 52 µmol/L $Def_3{\cdot}Fe^{3+}$ (green) as iron supplement. **(E-H)** Cells, differentiated for 10 days in presence of hTf and/or $Def_3{\cdot}Fe^{3+}$ as indicated, were stained with CD235 plus CD71 **(E)**, CD235a plus CD49d **(F)**, or DRAQ5 (cell permeable DNA stain; **G, H**). Relative cell numbers per quadrant were calculated (gating strategy available in Supplementary Figure S3A). **(G)** Enucleation percentage of erythroid cells, and **(H)** ratio of reticulocytes versus pyrenocytes (extruded nuclei) were calculated from the forward scatter and DRAQ5 staining. A retic./nuclei ratio > 1 means more reticulocytes than nuclei. Conditions labeled as 0 µg/mL hTf correspond to differentiation medium without hTf supplementation. Trace levels of hTf are present (<0.2 µg/mL) due to the plasma used in the differentiation medium (5%). All data is displayed as mean ± SD (error bars; n≥3). Significance is shown for the comparison with the 1000 µg/mL hTf condition (unpaired two-tailed two-sample Student's *t*-test).

4.3.3. $Def_3 \cdot Fe^{3+}$ supplementation prevents molecular responses to iron deficiency

Next, we studied whether iron supplementation by $Def_3 \cdot Fe^{3+}$ and hTf similarly controlled cellular iron metabolism in erythroblasts. The IRP1/2-dependent expression of ferritin and TFR1, and HRI-dependent phosphorylation of eIF2 was measured during the first 2 days of differentiation in presence of high and low levels of hTf or $Def_3 \cdot Fe^{3+}$ (Figure 3A). The expression of TFR1 was upregulated in presence of apotransterrin. This is in accordance with IRP stabilizing TFR1 mRNA in iron-limiting conditions (as shown in Figure 2E). Low iron concentrations did not significantly affect TFR1 expression, possibly due to the stability and recycling of the TFR1 (quantification: Figure 3B).

Ferritin synthesis, in contrast, is inhibited upon IRP binding to ferritin mRNA [17]. Ferritin levels remained high in presence of high total iron concentrations (1000 µg/mL hTf, or 52 µmol/L $Def_3 \cdot Fe^{3+}$), but were reduced at low or absent iron levels (100 µg/mL hTf, or apotransferrin) (Figure 3C). Finally, high levels of p-eIF2 were observed in cultures with iron limitation (Figure 3D; day 2). $Def_3 \cdot Fe^{3+}$ supplementation restored the low phosphorylation levels of eIF2 detected in cultures with high hTf concentration. Together, our results suggest that iron supplementation to erythroblast differentiation cultures either by $Def_3 \cdot Fe^{3+}$ or hTf is fully interchangeable at the molecular level.

Figure 3. Recovery of iron regulation metabolism using deferiprone in differentiation. Erythroblasts were expanded from PBMCs for 10-12 days, and subsequently seeded in differentiation medium supplemented with hTf or aTf (values µg/mL) or $Def_3 \cdot Fe^{3+}$ (52 µmol/L). Cells were harvested at seeding (Day 0) and after 1 and 2 days of culture. **(A)** Western blots of one representative donor showing the expression level of proteins involved in iron metabolism regulation. Actin was used as housekeeping protein for relative quantification of protein abundance. Position of size markers is indicated in kDa at the left. Membrane images were cropped by timepoint for clarity of the presentation, indicated by the dividing black lines and white space in between. Blots were cut in separate size intervals. The processing of blots and raw scans are available in https://doi.org/10.5281/zenodo.6350135. **(B-C)** Relative abundance (r.a.) of transferrin receptor (TFR1) and ferritin. Relative protein levels were calculated using actin signal, followed by normalization using the average of each donor at the start of the culture (day 0). **(D)** Level of the phosphorylated form of eIF2 (p-eIF2) relative to the total levels of eIF2. In order to compare different experiments, the relative p-eIF2/eIF2 ratio was normalized using the average of each donor at the start of the culture (day 0). Conditions labeled as 0 µg/mL hTf correspond to differentiation medium without hTf supplementation. Data is displayed as mean ± SD (error bars; n=3). Significance is shown for the comparison with 1000 µg/mL hTf (unpaired two-tailed two-sample Student's *t*-test with Helm-Bonferrin correction for multiple comparisons).

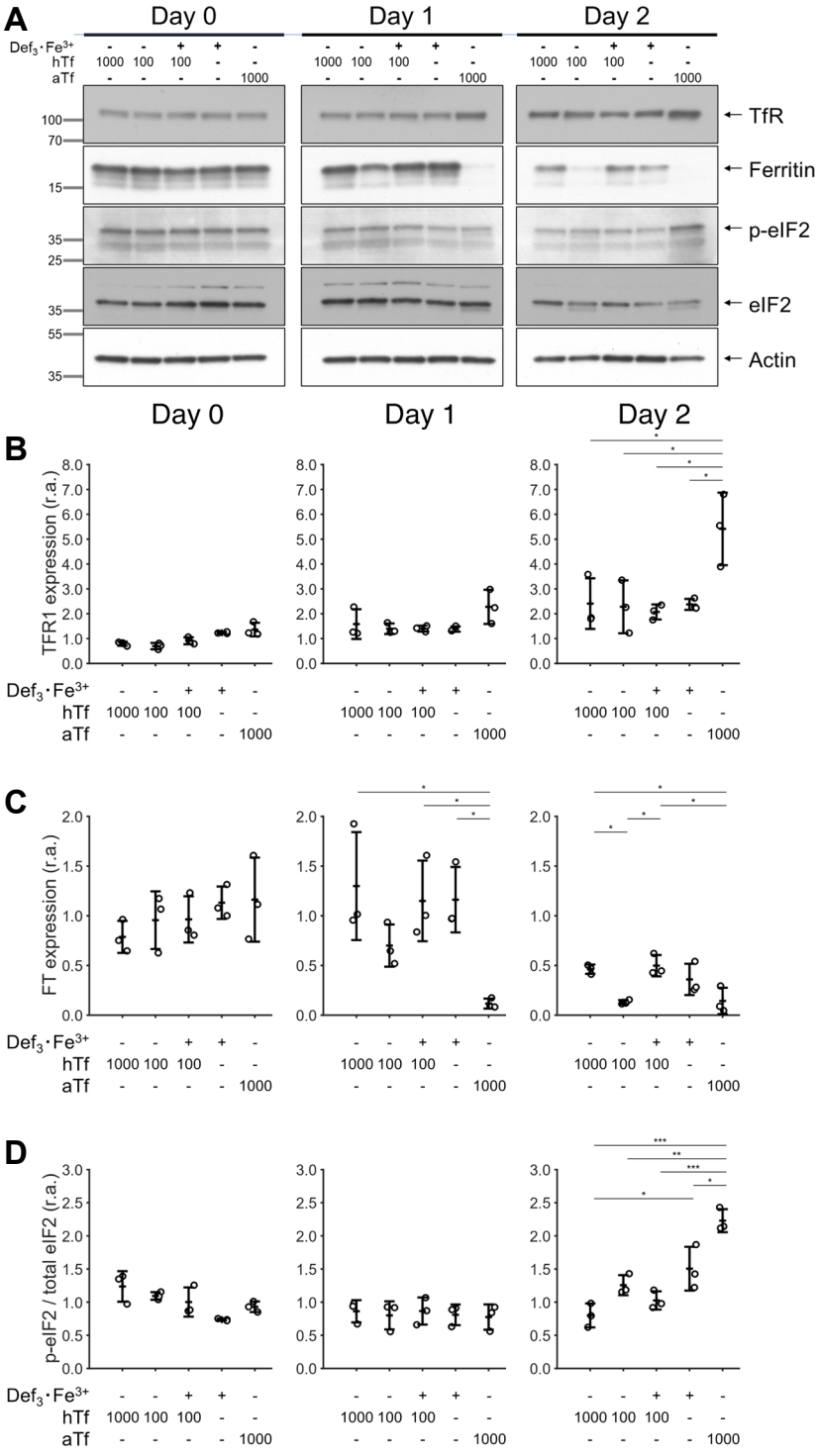

Figure 3.
(See caption on previous page)

4.3.4. Medium containing iron-loaded deferiprone can sustain expansion of erythroblasts

Iron requirements are especially high during erythroblast differentiation when hemoglobin is synthesized. However, cells do require iron as constituent of essential metalloproteins, such as cytochromes and some peroxidases [51]. We tested if deferiprone could also replace hTf supplementation during the first phase of our culture protocol, when hematopoietic stem and progenitor cells commit to the erythroid lineage, and subsequently when committed erythroblasts proliferate but hemoglobin production remain low. Erythroid cultures were established from peripheral blood mononuclear cells (PBMCs) in serum-free medium supplemented with the standard hTf concentration for culturing of non-hemoglobinized cells (300 µg/mL hTf), or with a 10× lower hTf concentration, in presence or absence of $Def_3{\cdot}Fe^{3+}$ (52 µmol/L). The presence of hTf (300 µg/mL) was required to obtain a culture of $CD71^+$ cells from PBMCs (Figure 4A; Supplementary Figure S3A-B), while deferiprone alone was not sufficient to establish an erythroid culture in the absence of hTf supplementation. At a lower hTf concentration (30 µg/mL) cultures yielded less $CD71^+$ erythroblasts, which was unaffected if deferiprone was supplemented. As shown previously, $CD71^+$ cells cultured in absence of hTf expressed CD71 at increased levels. In these early stages, deferiprone did not reduce CD71 levels to those observed with hTf (Supplementary Figure S4). Upon prolonged expansion of committed erythroblasts $Def_3{\cdot}Fe^{3+}$, alone or supplemented to low hTf levels, resulted in the same erythroblast growth rate as when 300 µg/mL hTf was used (Figure 4B).

To determine the optimal $Def_3{\cdot}Fe^{3+}$ concentration to sustain proerythroblast proliferation once erythroid cultures are established, PBMCs were first expanded for 6 days in medium with hTf, followed by culture in medium with a suboptimal hTf level supplemented with $Def_3{\cdot}Fe^{3+}$ at concentrations between 0.8 and 52 µmol/L (Figure 4C). Maximum recovery required at least 6.5 µmol/L $Def_3{\cdot}Fe^{3+}$ (Figure 4D). Lack of iron, or low levels of iron (30 µg/mL hTf) increased the number of non-viable cells as detected by DRAQ7. Supplementation with $Def_3{\cdot}Fe^{3+}$ recovered viability of the expansion cultures (Figure 4E).

High CD71 (TfR) expression characterizes erythroblasts. During the expansion phase of erythroblast cultures, the $CD71^{high}$ erythroblast population slowly gains CD235 expression from day 10 onwards [22]. A $CD71^{mid}$ $CD235^-$ subpopulation, that was observed under iron-limited conditions (0 and 30 µg/mL hTf) and less prominently under low $Def_3{\cdot}Fe^{3+}$ concentrations (1.6 and 0.8 µmol/L), indicates a non-erythroid cell population that remains due to the failure of erythroblast outgrowth (Supplementary Figure S5). The presence of these seemingly non-erythroid cells was also observed

when following the expression of CD49d (Figure 4F). High levels of $Def_3 \cdot Fe^{3+}$ enhanced the gain of CD235 and loss of CD49d to levels observed with 300 µg/mL hTf.

Because TFR2 associates with the EpoR, reduced internalization and recycling of TFR2/EpoR complex to the membrane was shown to modulate EpoR signaling [12,13]. To investigate whether $Def_3 \cdot Fe^{3+}$ supplementation interferes with EpoR signaling, erythroblasts were cultured in presence of hTf or $Def_3 \cdot Fe^{3+}$, deprived of Epo and restimulated (0.2 or 1.0 U/mL), all in presence of hTf or $Def_3 \cdot Fe^{3+}$. In accordance with previous reports, Epo-induced STAT5 phosphorylation was reduced in absence of hTf, and $Def_3 \cdot Fe^{3+}$ did not restore STAT5 phosphorylation (Figure 4G).

Figure 4. Deferiprone supplementations sustains erythroblast expansion. Adult PBMCs were isolated (day 0) and cultured in expansion medium at a starting cell concentration of 1×10^6 cells/mL using hTf (values in µg/mL) in the presence or absence of $Def_3 \cdot Fe^{3+}$ (52 µmol/L). **(A)** Total number of $CD71^+$ cells was determined on day 6 after PBMC isolation (combining cell count and CD71+ frequency by flow cytometry; data available in Supplementary Figure S4). **(B)** Erythroblast cell concentration was monitored for additional 9 days of culture, with daily medium refreshment. Fold change in cell number was calculated using the measured number of erythroblasts at day 6. Significance indicated for comparison of end (day 15) values. **(C-F)** Erythroblasts were expanded from PBMCs in expansion medium with hTf as iron source (300 µg/mL) for 7 days, and subsequently reseeded in medium with varying hTf concentrations (300, 30, 0 µg/mL) in the presence of $Def_3 \cdot Fe^{3+}$ (0.8 – 52 µmol/L $Def_3 \cdot Fe^{3+}$). Cultures were maintained for 8 days (15 days since PBMC isolation) during which daily medium refreshments were performed **(C)**. After 8 days of culture, cell number fold change was calculated relative to the start of treatment **(D)**. Cells were stained with DRAQ7 (cell impermeable DNA stain; **E**), and CD235a plus CD49d **(F)**. Relative cell numbers per quadrant were calculated (representative density plots available in Supplementary Figure S5). **(G)** Analysis of the effect of $Def_3 \cdot Fe^{3+}$ on Epo signaling. Erythroblasts were cultured with hTf (300 µg/mL), $Def_3 \cdot Fe^{3+}$ (52 µM) or no iron, withdrawn from Epo for 3 h, and restimulated (0.2 or 1.0 U/mL EPO). Lysates were subjected to western blot analysis using phospho-STAT5 and total-STAT5 antibodies. All 9 samples (3 Epo concentrations × 3 iron supplementation treatments) were run in the same gel. Original uncropped membrane images for both donors are available in https://doi.org/10.5281/zenodo.6350135. Data in panels **(A-F)** is displayed as mean ± SD (error bars; n=3). Significance is shown for the comparison with 300 µg/mL hTf (unpaired two-tailed two-sample Student's *t*-test). Data for panels **(B-E)** available in Supplementary Table S1.

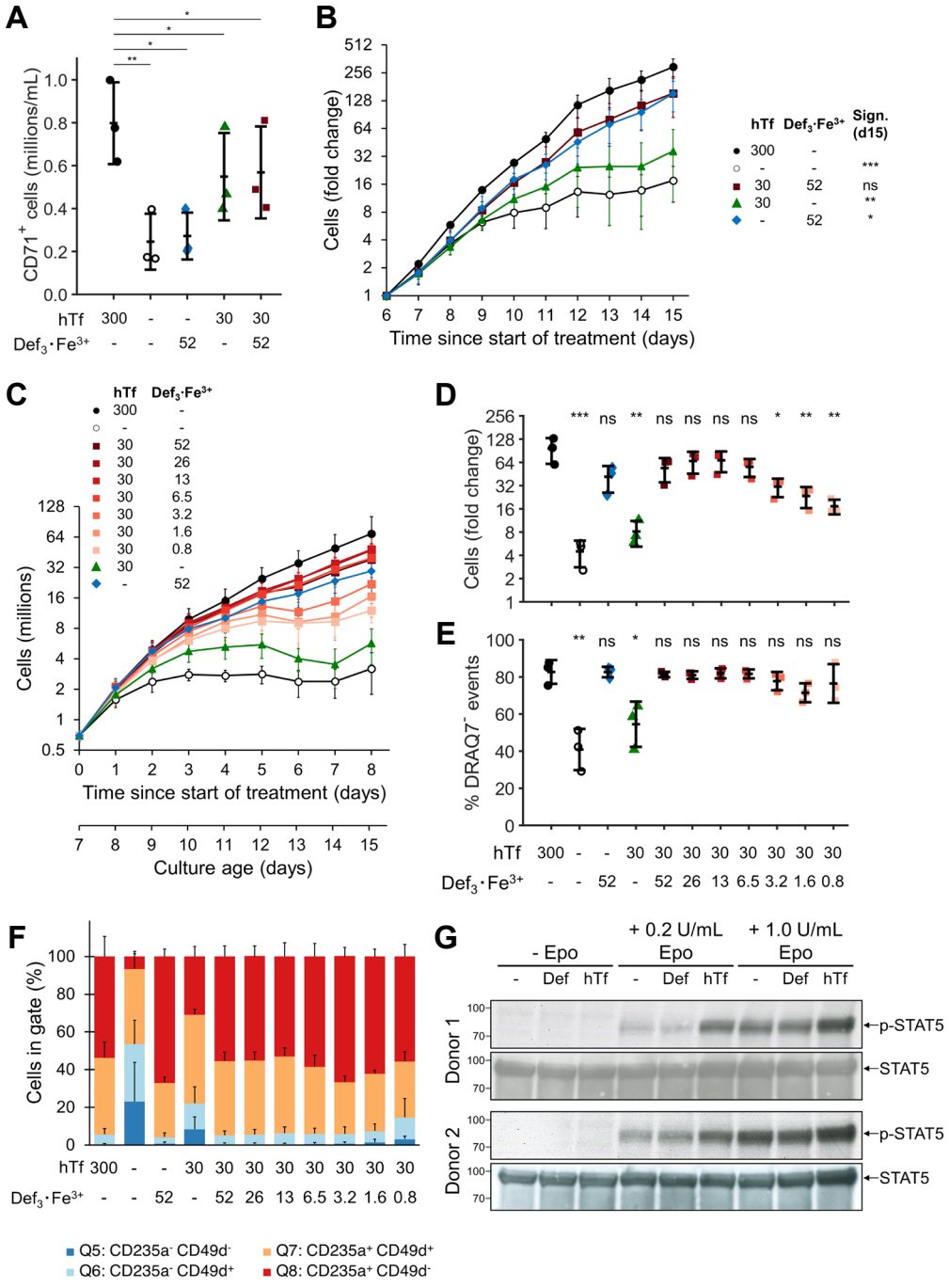

Figure 4.
(See caption on previous page)

4.3.5. Iron-loaded deferiprone can replace holotransferrin for other myeloid cell lines

As a limited number of cell lines are able to produce Tf, it is commonly used as supplement in chemically defined media (i.e serum-free) for most mammalian cell cultures [52]. Thus, we evaluated the potential of $Def_3 \cdot Fe^{3+}$ to fully replace holotransferrin in cultures of the myeloid cell lines MOLM13, NB4, EOL1, K562, HL-60, and ML-2. Cells were seeded in media containing no iron, 300 µg/mL hTf or 52 µmol/L $Def_3 \cdot Fe^{3+}$. All cell lines could be expanded in our serum-free medium supplemented with hTf (Figure 5A; Supplementary Figure S6). Lack of iron decreased the growth rate, with MOLM13 and NB4 cells showing a decrease of 4 orders of magnitude in cell numbers after 16 days of culture. EOL1 cultures seemed less sensitive to lack of hTf, but proliferation in presence of hTf was also low. $Def_3 \cdot Fe^{3+}$ recovered growth to levels comparable with only-hTf conditions. As observed in *ex vivo* erythroblast expansion and differentiation cultures, lack of hTf led to an upregulation of CD71 expression in all cell lines (Figure 5B). $Def_3 \cdot Fe^{3+}$ supplementation restored CD71 expression levels and viability (Figure 5C) comparable to that in hTf-only cultures.

Figure 5. Deferiprone sustains expansion of selected myeloid cell lines. Myeloid cell lines were cultured in Cellquin medium supplemented or not with 300 µg/mL hTf or 52 µmol/L $Def_3 \cdot Fe^{3+}$ for 16 days. **(A)** Total cell number fold change relative to day 0. **(B)** Expression level of the transferrin receptor (CD71) determined by flow cytometry. MFI for corresponding isotypes is between 1×10^2 - 3×10^2. **(C)** Cells were stained with DRAQ7 (cell impermeable DNA stain) to quantify the viability of the cultures. Data is displayed as mean ± SD (error bars; individual datapoints are indicated; n=3). Significance is shown for the comparison with 300 µg/mL hTf (unpaired two-tailed two-sample Student's *t*-test).

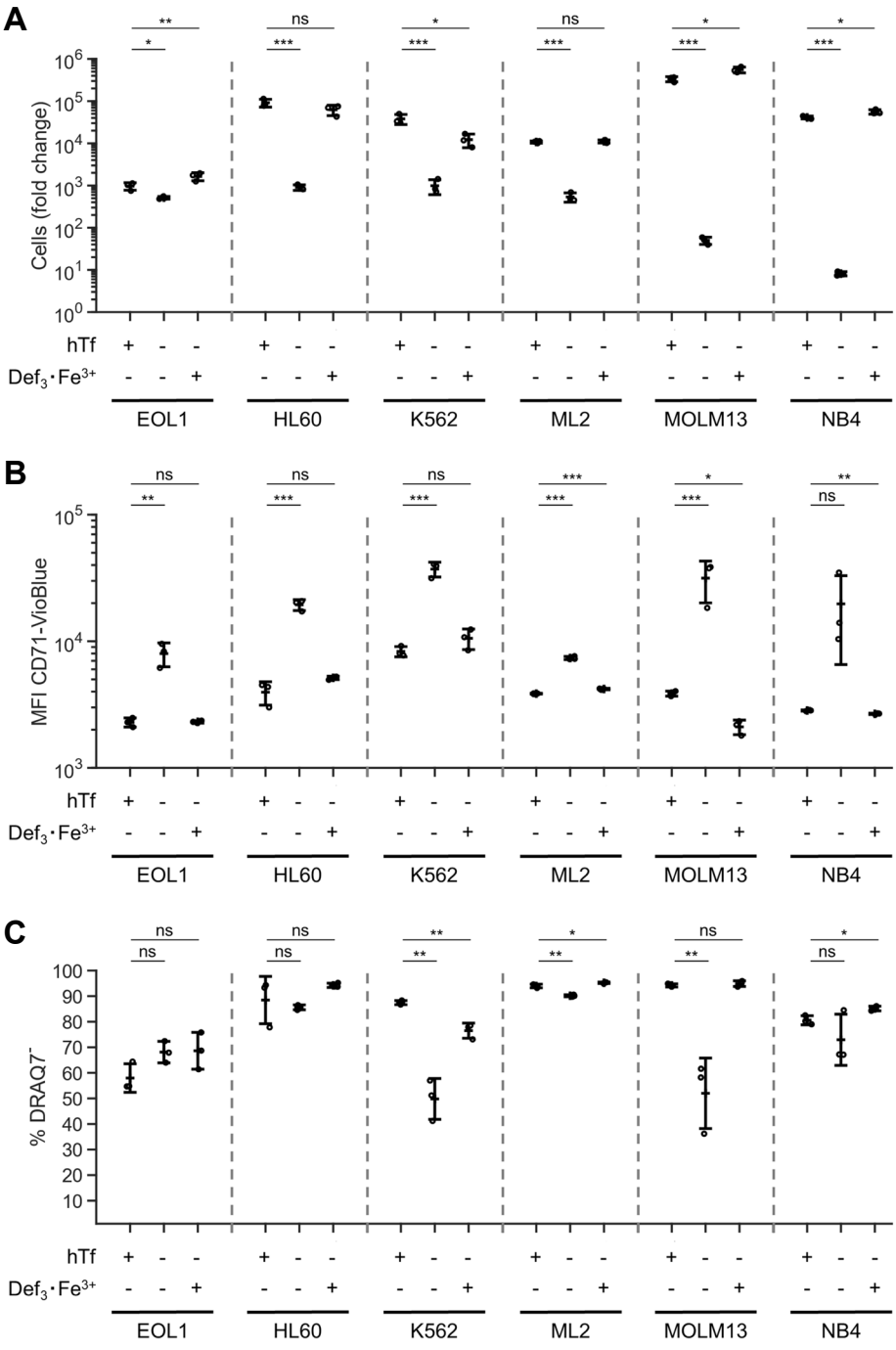

Figure 5.
(See caption on previous page)

4.4. Discussion

Hemoglobin production requires a high uptake of iron in differentiating erythroblasts, which is supplied as hTf. We evaluated whether iron-loaded chelators can be a low-cost alternative for the high hTf supplementation levels required in *ex vivo* erythroid cultures. Our data show that deferiprone, a bidentate α-ketohydroxypyridine iron-specific chelator, could replace holotransferrin supplementation to produce large numbers of enucleated hemoglobinized cultured RBCs at concentrations as low as 26 μmol/L ($Def_3 \cdot Fe^{3+}$). Hemoglobin content and oxyhemoglobin dissociation dynamics of cultured RBCs (cRBCs) derived with $Def_3 \cdot Fe^{3+}$ or with hTf as sole iron source were similar.

We show that hemoglobin is expressed at similar levels, and is equally functional in reticulocytes cultured in presence of hTf or $Def_3 \cdot Fe^{3+}$. Iron-loaded chelators can serve as an iron pool to low amounts of transferrin still present in our cultures dependent on their affinity for iron. Chelators with a relatively low affinity for iron such as deferiprone (pFe^{3+}: 19.3) will transfer Fe^{3+} to aTf (pFe^{3+}: 22.3; pFe^{3+} value is defined as $-\log_{10}[Fe^{3+}]$ with 1 μM total iron and 10 μM total ligand at pH 7.4). Instead, chelators with a pFe^{3+} larger than aTf such as deferoxamine mesylate (DFOA) and deferasirox (DFO; $pFe^{3+} > 26$) will deplete hTf from iron. By consequence, deferiprone is very well suited to stabilize Fe^{3+} in cell culture media and to transfer Fe^{3+} to aTF to enable uptake via TfR1 and TfR2.

Tf may still be present due to, for instance, the use of plasma in differentiation cultures, or due to intracellular pools of transferrin from the preculture stage. Deferiprone, however, is able to permeate the cell and access labile iron pools in subcellular compartments possibly due to its low molecular weight (139.1 g/mol) and mild lipophilic nature (distribution coefficient $D_{7.4}$ = 0.17, octanol/water at pH 7.4), as previously reported [53,54]. Deferiprone's ability to enter cells is not clearly required to enable iron transfer to Tf. However, we speculate that this known characteristic of deferiprone may enable a more robust redistribution of iron between cells in culture. Deferiprone can mobilize intracellular iron and render it available for hemoglobin synthesis [34]. Other iron-loaded chelators such as $DFOA \cdot Fe^{3+}$ can also function as substrate for heme synthesis instead of holotransferrin [55]. Excessive iron availability, however, may also cause oxidative damage [56,57]. High levels of $Def_3 \cdot Fe^{3+}$ (26-52 μmol/L) did not have a detrimental effect on the expansion or differentiation of erythroid cultures. This may indicate that the iron-binding affinity of deferiprone is just right to prevent toxicity of free iron, while simultaneously releasing iron to either intracellular

proteins or to transferrin molecules. Alternatively, erythroid cells may be protected against high iron levels because of the expression of anti-oxidant proteins [58].

The recommended dosage of deferiprone for iron-chelation therapy is 75 mg/kg/day to attain deferiprone plasma levels ranging between 10 and 40 mg/L [59–61]. Differentiation medium contains 21.7 mg/L Def (52 μM $Def_3 \cdot Fe^{3+}$). Assuming an equal distribution of deferiprone in the extra- and intracellular space, and a cell volume of 200 pL (Supplementary Figure S1A), 1 unit packed reticulocytes (2×10^{12} cells) would contain 87 mg deferiprone. For an average human adult (62 kg), the transfusion of a single unit of packed red blood cells would correspond to 0.14 mg Def/kg, two orders of magnitude lower than the recommended deferiprone dosage in a single day of treatment. Even if it is assumed that all deferiprone in the medium is accumulated inside the cultured reticulocytes, the deferiprone dosage would be 70 mg/kg, still lower than the recommended daily dosage of deferiprone. We expected these values to be lower, as cultured reticulocytes must be washed to remove medium components and pyrenocytes before being used for therapeutic purposes.

The use of deferiprone is not without potential side effects. Neutropenia has been observed for deferiprone treatment of thalassemia patients at much higher dosages (75 mg/kg/day) and an incidence of ~2 per 100 patient years [62]. We expect, however, a low risk for side effects after transfusion of cRBCs cultured with iron-loaded deferiprone as iron source. Deferiprone is able to redistribute iron among cells, but half of it still contains iron. The deferiprone load in cRBCs is low, it will rapidly diffuse out of the cRBC, and be eliminated from the body via degradation in the liver and excretion via the kidneys with a half-life of 2-3 hours [45].

We hypothesize that $Def_3 \cdot Fe^{3+}$ may act independent of Tf and the TFR1, but only deletion of TFR1/TFR2 will confirm this. Compared to addition of aTf, both $Def_3 \cdot Fe^{3+}$ and hTf treatment of cultured erythroblasts increased ferritin expression and decreased CD71 (TFR1) surface expression, indicating that $Def_3 \cdot Fe^{3+}$ increased intracellular iron concentration. Recently, modulation of Epo-mediated signaling via transferrin and TFR2 was reported, in which the binding of hTf or mTf_C to TFR2 increased Epo sensitivity, enhancing the survival, proliferation and differentiation of erythroid progenitor cells, specially at low Epo concentrations (0.1 U/mL) [13,63]. Notably, Epo-induced STAT5 phosphorylation is reduced in absence of hTF, which is not rescued by $Def_3 \cdot Fe^{3+}$. Thus, supplementation of media with $Def_3 \cdot Fe^{3+}$ instead of hTf may shift the Epo dose-response of erythroblasts. The observation that expansion of erythroblast cultures supplemented with only $Def_3 \cdot Fe^{3+}$ is not as high as expansion in presence of hTf plus $Def_3 \cdot Fe^{3+}$ (ca. 50-fold instead of 100-fold in 8 days) may be due to reduced EpoR signaling.

Phosphorylation levels of eIF2α in cells cultured with $Def_3 \cdot Fe^{3+}$ were increased compared to addition of hTf, but lower than in presence of aTf. eIF2α can be phosphorylated by the heme-regulated eIF2α-kinase (HRI), which is activated under heme-limited conditions in erythroid cells [18]. As hemoglobin levels were maintained in $Def_3 \cdot Fe^{3+}$-treated cells, it is possible that the observed increase in p-eIF2α is due to other mechanisms, such as an increase in intracellular oxidative stress levels due to iron overload.

$Def_3 \cdot Fe^{3+}$ in serum-free expansion medium without hTf supplementation supported erythroblast proliferation during the second stage of our culture system. However, $Def_3 \cdot Fe^{3+}$ was unable to support the establishment of erythroblast-enriched cultures from PBMCs. The addition of suboptimal concentrations of hTf to these cultures allows for limited outgrowth of erythroblasts, which was not altered by the presence of $Def_3 \cdot Fe^{3+}$. Possibly, toxicity by iron overload is causing the lower yield. Once cells were committed to the erythroid lineage, $Def_3 \cdot Fe^{3+}$ could fully substitute hTf supplementation.

It is also possible that in the first days of culture, precursor cells not yet committed to the erythroid lineage may lack the molecular machinery to incorporate iron ions provided by $Def_3 \cdot Fe^{3+}$. It becomes relevant to understand how $Def_3 \cdot Fe^{3+}$ complexes are processed by the cells and their interaction with intracellular iron pools, as the data suggests a differential ability between hematopoietic progenitors and erythroblasts to utilize this source of iron. Of note, these early cultures are small scale and the use of hTf is not yet an important cost factor. Thus, cultures could be started in presence of hTf, and be continued in medium supplemented with $Def_3 \cdot Fe^{3+}$ once an erythroblast-enriched population is established.

Holotransferrin is the main iron source in mammalian cell culture medium, and is typically included in culture media by supplementation with serum. However, serum-containing media have an unclear chemical composition, typically show batch-to-batch variation, and have a risk of contamination; for example, by viruses. Defined serum-free formulations have been developed, and require purified hTf [64]. Use of purified Tf from plasma, or of recombinant Tf from rice or yeast, can potentially introduce contaminants. $Def_3 \cdot Fe^{3+}$, however, is chemically produced, which can be an advantage with respect to purity in the production of chemically-defined protein-free medium.

Migliaccio et al. [5] proposed the first serum-free medium formulation for erythroid culture, and showed that transferrin levels have a direct impact on the yields of erythroid progenitor cells. Erythroblast expansion and differentiation can be achieved using 300 and 1000 μg/mL hTf, respectively [22]. Olivier et al. developed chemically defined culture media for cRBC production in which supplemented Fe^{3+}-

EDTA reloads the used Tf, allowing for lower Tf concentrations [29]. Nevertheless, 50 µg/mL Tf are still needed in this strategy to reach growth and enucleation levels like those of cultures using Tf-only medium. The results of our study indicate that although transferrin supplementation of serum-free medium is currently essential for the establishment of erythroid cultures from PBMCs, it can be fully replaced by $Def_3 \cdot Fe^{3+}$ supplementation during erythroblast expansion, differentiation and maturation. In the medium described in Heshusius et al. [22], holotransferrin constitute 65% of the costs of the differentiation medium, including the cost of Epo. Iron-loaded deferiprone at the concentration described in our manuscript (52 µmol/L $Def_3 \cdot Fe^{3+}$) is at least 400-fold less expensive than recombinant transferrin and thus reduces the medium price by 64% [65]. At 50 µg/ml as proposed by Olivier et al. [29], hTf would constitute 8% of the costs, still considerably more than ~0.5% of the costs using only $Def_3 \cdot Fe^{3+}$. Although hTf concentrations are significantly lower in culture media for other primary cells and for cell lines typically used in biopharmaceutical processes (e.g. hybridoma, CHO, Vero; ranging between 5 and 100 µg/mL), its replacement with $Def_3 \cdot Fe^{3+}$ may be a significant cost-saver at an industrial production scale. Furthermore, replacing transferrin by a small iron chelator could help towards protein-free culture medium formulations, which could speed up translations of stem cell cultures to conditions compliant with good manufacturing practices (GMP).

4.5. Acknowledgments

We thank Paul Kaijen and Jan Voorberg (Molecular Hematology, Sanquin Research) for technical help and advice on iron loading of transferrin, and Dorine Swinkels (Sanquin Research) for critical reading of the manuscript.

4.6. Autorship

J.S.G.M., E.v.d.A., and M.v.L. planned experiments; J.S.G.M., N.Y., and E.M.P. performed experiments; J.S.G.M., S.A.W., E.v.d.A. and M.v.L. analyzed data; J.S.G.M., S.A.W., and M.v.L. wrote the manuscript.

4.7. References

1. Malka, R.; Delgado, F.F.; Manalis, S.R.; Higgins, J.M. In Vivo Volume and Hemoglobin Dynamics of Human Red Blood Cells. *PLoS Comput. Biol.* **2014**, *10*, e1003839, doi:10.1371/journal.pcbi.1003839.

2. Ganz, T. Systemic Iron Homeostasis. *Physiol. Rev.* **2013**, *93*, 1721–1741, doi:10.1152/physrev.00008.2013.

3. Agil, A.; Fuller, C.; Jialal, I. Susceptibility of Plasma to Ferrous Iron/Hydrogen Peroxide-Mediated Oxidation: Demonstration of a Possible Fenton Reaction. *Clin. Chem.* **1995**, *41*, 220–225, doi:10.1093/CLINCHEM/41.2.220.

4. Huebers, H.; Josephson, B.; Huebers, E.; Csiba, E.; Finch, C. Uptake and Release of Iron from Human Transferrin. *Proc. Natl. Acad. Sci. U. S. A.* **1981**, *78*, 2572–2576, doi:10.1073/pnas.78.4.2572.

5. Migliaccio, G.; Migliaccio, A.R. Cloning of Human Erythroid Progenitors (BFU-E) in the Absence of Fetal Bovine Serum. *Br. J. Haematol.* **1987**, *67*, 129–133, doi:10.1111/j.1365-2141.1987.00129.x.

6. Byrnes, C.; Lee, Y.T.; Meier, E.R.; Rabel, A.; Sacks, D.B.; Miller, J.L. Iron Dose-Dependent Differentiation and Enucleation of Human Erythroblasts in Serum-Free Medium. *J. Tissue Eng. Regen. Med.* **2016**, *10*, E84–E89, doi:10.1002/term.1743.

7. Hamdi, A.; Roshan, T.M.; Kahawita, T.M.; Mason, A.B.; Sheftel, A.D.; Ponka, P. Erythroid Cell Mitochondria Receive Endosomal Iron by a "Kiss-and-Run" Mechanism. *Biochim. Biophys. Acta BBA - Mol. Cell Res.* **2016**, *1863*, 2859–2867, doi:10.1016/j.bbamcr.2016.09.008.

8. Shi, H.; Bencze, K.Z.; Stemmler, T.L.; Philpott, C.C. A Cytosolic Iron Chaperone That Delivers Iron to Ferritin. *Science* **2008**, *320*, 1207–1210, doi:10.1126/science.1157643.

9. Eid, C.; Hémadi, M.; Ha-Duong, N.-T.; El Hage Chahine, J.-M. Iron Uptake and Transfer from Ceruloplasmin to Transferrin. *Biochim. Biophys. Acta BBA - Gen. Subj.* **2014**, *1840*, 1771–1781, doi:10.1016/j.bbagen.2014.01.011.

10. Forejtnikovà, H.; Vieillevoye, M.; Zermati, Y.; Lambert, M.; Pellegrino, R.M.; Guihard, S.; Gaudry, M.; Camaschella, C.; Lacombe, C.; Roetto, A.; et al. Transferrin Receptor 2 Is a Component of the Erythropoietin Receptor Complex and Is Required for Efficient Erythropoiesis. *Blood* **2010**, *116*, 5357–5367, doi:10.1182/blood-2010-04-281360.

11. Silvestri, L.; Nai, A.; Pagani, A.; Camaschella, C. The Extrahepatic Role of TFR2 in Iron Homeostasis. *Front. Pharmacol.* **2014**, *5*, 93, doi:10.3389/fphar.2014.00093.

12. Nai, A.; Lidonnici, M.R.; Rausa, M.; Mandelli, G.; Pagani, A.; Silvestri, L.; Ferrari, G.; Camaschella, C. The Second Transferrin Receptor Regulates Red Blood Cell Production in Mice. *Blood* **2015**, *125*, 1170–1179, doi:10.1182/blood-2014-08-596254.

13. Fouquet, G.; Thongsa-ad, U.; Lefevre, C.; Rousseau, A.; Tanhuad, N.; Khongkla, E.; Saengsawang, W.; Anurathapan, U.; Hongeng, S.; Maciel, T.T.; et al. Iron-Loaded Transferrin Potentiates Erythropoietin Effects on Erythroblast Proliferation and Survival: A Novel Role through Transferrin Receptors. *Exp. Hematol.* **2021**, *99*, 12-20.e3, doi:10.1016/j.exphem.2021.05.005.

14. Muckenthaler, M.U.; Rivella, S.; Hentze, M.W.; Galy, B. A Red Carpet for Iron Metabolism. *Cell* **2017**, *168*, 344–361, doi:10.1016/j.cell.2016.12.034.

15. Erlitzki, R.; Long, J.C.; Theil, E.C. Multiple, Conserved Iron-Responsive Elements in the 3'-Untranslated Region of Transferrin Receptor MRNA Enhance Binding of Iron Regulatory Protein 2. *J. Biol. Chem.* **2002**, *277*, 42579–42587, doi:10.1074/jbc.M207918200.

16. Kim, H.Y.; Klausner, R.D.; Rouault, T.A. Translational Repressor Activity Is Equivalent and Is Quantitatively Predicted by in Vitro RNA Binding for Two Iron-Responsive Element-Binding Proteins, IRP1 and IRP2. *J. Biol. Chem.* **1995**, *270*, 4983–4986, doi:10.1074/jbc.270.10.4983.

17. Muckenthaler, M.; Gray, N.K.; Hentze, M.W. IRP-1 Binding to Ferritin MRNA Prevents the Recruitment of the Small Ribosomal Subunit by the Cap-Binding Complex EIF4F. *Mol. Cell* **1998**, *2*, 383–388, doi:10.1016/S1097-2765(00)80282-8.

18. Han, A.-P.; Yu, C.; Lu, L.; Fujiwara, Y.; Browne, C.; Chin, G.; Fleming, M.; Leboulch, P.; Orkin, S.H.; Chen, J.-J. Heme-Regulated EIF2α Kinase (HRI) Is Required for Translational Regulation and Survival of Erythroid Precursors in Iron Deficiency. *EMBO J.* **2001**, *20*, 6909–6918, doi:10.1093/emboj/20.23.6909.

19. Paolini, N.A.; Moore, K.S.; Summa, F.M. di; Fokkema, I.F.A.C.; Hoen, P.A.C. 't; Lindern, M. von Ribosome Profiling Uncovers Selective MRNA Translation Associated with EIF2 Phosphorylation in Erythroid Progenitors. *PLOS ONE* **2018**, *13*, e0193790, doi:10.1371/journal.pone.0193790.

20. Zhang, S.; Macias-Garcia, A.; Ulirsch, J.C.; Velazquez, J.; Butty, V.L.; Levine, S.S.; Sankaran, V.G.; Chen, J.-J. HRI Coordinates Translation Necessary for Protein Homeostasis and Mitochondrial Function in Erythropoiesis. *eLife* **2019**, *8*, e46976, doi:10.7554/eLife.46976.

21. Iolascon, A.; De Falco, L.; Beaumont, C. Molecular Basis of Inherited Microcytic Anemia Due to Defects in Iron Acquisition or Heme Synthesis. *Haematologica* **2009**, *94*, 395–408, doi:10.3324/haematol.13619.

22. Heshusius, S.; Heideveld, E.; Burger, P.; Thiel-Valkhof, M.; Sellink, E.; Varga, E.; Ovchynnikova, E.; Visser, A.; Martens, J.H.A.; von Lindern, M.; et al. Large-Scale in Vitro Production of Red Blood Cells from Human Peripheral Blood Mononuclear Cells. *Blood Adv.* **2019**, *3*, 3337–3350, doi:10.1182/bloodadvances.2019000689.

23. Migliaccio, G.; Sanchez, M.; Masiello, F.; Tirelli, V.; Varricchio, L.; Whitsett, C.; Migliaccio, A.R. Humanized Culture Medium for Clinical Expansion of Human Erythroblasts. *Cell Transplant.* **2010**, *19*, 453–469, doi:10.3727/096368909X485049.

24. Brandsma, M.E.; Jevnikar, A.M.; Ma, S. Recombinant Human Transferrin: Beyond Iron Binding and Transport. *Biotechnol. Adv.* **2011**, *29*, 230–238, doi:10.1016/j.biotechadv.2010.11.007.

25. Brock, J.H.; Stevenson, J. Replacement of Transferrin in Serum-Free Cultures of Mitogen-Stimulated Mouse Lymphocytes by a Lipophilic Iron Chelator. *Immunol. Lett.* **1987**, *15*, 23–25, doi:10.1016/0165-2478(87)90071-x.

26. Landschulz, W.; Thesleff, I.; Ekblom, P. A Lipophilic Iron Chelator Can Replace Transferrin as a Stimulator of Cell Proliferation and Differentiation. *J. Cell Biol.* **1984**, *98*, 596–601, doi:10.1083/jcb.98.2.596.

27. Ponka, P.; Schulman, H.M.; Wilczynska, A. Ferric Pyridoxal Isonicotinol Hydrazone Can Provide Iron for Heme Synthesis in Reticulocytes. *Biochim. Biophys. Acta BBA - Gen. Subj.* **1982**, *718*, 151–156, doi:10.1016/0304-4165(82)90213-6.

28. Grillo, A.S.; SantaMaria, A.M.; Kafina, M.D.; Cioffi, A.G.; Huston, N.C.; Han, M.; Seo, Y.A.; Yien, Y.Y.; Nardone, C.; Menon, A.V.; et al. Restored Iron Transport by a Small Molecule Promotes Absorption and Hemoglobinization in Animals. *Science* **2017**, *356*, 608–616, doi:10.1126/science.aah3862.

29. Olivier, E.N.; Zhang, S.; Yan, Z.; Suzuka, S.; Roberts, K.; Wang, K.; Bouhassira, E.E. PSC-RED and MNC-RED: Albumin-Free and Low-Transferrin Robust Erythroid Differentiation Protocols to Produce Human Enucleated Red Blood Cells. *Exp. Hematol.* **2019**, *75*, 31-52.e15, doi:10.1016/j.exphem.2019.05.006.

30. Crisponi, G.; Nurchi, V.M.; Crespo-Alonso, M.; Sanna, G.; Zoroddu, M.A.; Alberti, G.; Biesuz, R. A Speciation Study on the Perturbing Effects of Iron Chelators on the Homeostasis of Essential Metal Ions. *PLOS ONE* **2015**, *10*, e0133050, doi:10.1371/journal.pone.0133050.

31. Evans, R.W.; Kong, X.; Hider, R.C. Iron Mobilization from Transferrin by Therapeutic Iron Chelating Agents. *Biochim. Biophys. Acta BBA - Gen. Subj.* **2012**, *1820*, 282–290, doi:10.1016/j.bbagen.2011.11.007.

32. Nurchi, V.M.; Crisponi, G.; Pivetta, T.; Donatoni, M.; Remelli, M. Potentiometric, Spectrophotometric and Calorimetric Study on Iron(III) and Copper(II) Complexes with 1,2-Dimethyl-3-Hydroxy-4-Pyridinone. *J. Inorg. Biochem.* **2008**, *102*, 684–692, doi:10.1016/j.jinorgbio.2007.10.012.

33. Devanur, L.D.; Evans, R.W.; Evans, P.J.; Hider, R.C. Chelator-Facilitated Removal of Iron from Transferrin: Relevance to Combined Chelation Therapy. *Biochem. J.* **2008**, *409*, 439–447, doi:10.1042/BJ20070823.

34. Sohn, Y.-S.; Breuer, W.; Munnich, A.; Cabantchik, Z.I. Redistribution of Accumulated Cell Iron: A Modality of Chelation with Therapeutic Implications. *Blood* **2008**, *111*, 1690–1699, doi:10.1182/blood-2007-07-102335.

35. Matsuo, Y.; MacLeod, R.A.; Uphoff, C.C.; Drexler, H.G.; Nishizaki, C.; Katayama, Y.; Kimura, G.; Fujii, N.; Omoto, E.; Harada, M.; et al. Two Acute Monocytic Leukemia (AML-M5a) Cell Lines (MOLM-13 and MOLM-14) with Interclonal Phenotypic Heterogeneity Showing MLL-AF9 Fusion Resulting from an Occult Chromosome Insertion, Ins(11;9)(Q23;P22p23). *Leukemia* **1997**, *11*, 1469–1477, doi:10.1038/sj.leu.2400768.

36. Lanotte, M.; Martin-Thouvenin, V.; Najman, S.; Balerini, P.; Valensi, F.; Berger, R. NB4, a Maturation Inducible Cell Line with t(15;17) Marker Isolated from a Human Acute Promyelocytic Leukemia (M3). *Blood* **1991**, *77*, 1080–1086, doi:10.1182/blood.V77.5.1080.1080.

37. Saito, H.; Bourinbaiar, A.; Ginsburg, M.; Minato, K.; Ceresi, E.; Yamada, K.; Machover, D.; Bréard, J.; Mathé, G. Establishment and Characterization of a New Human Eosinophilic Leukemia Cell Line. *Blood* **1985**, *66*, 1233–1240, doi:10.1182/blood.V66.6.1233.1233

38. Lozzio, C.B.; Lozzio, B.B. Human Chronic Myelogenous Leukemia Cell-Line with Positive Philadelphia Chromosome. *Blood* **1975**, *45*, 321–334, doi:10.1182/blood.V45.3.321.321.

39. Collins, S.J.; Ruscetti, F.W.; Gallagher, R.E.; Gallo, R.C. Terminal Differentiation of Human Promyelocytic Leukemia Cells Induced by Dimethyl Sulfoxide and Other Polar Compounds. *Proc. Natl. Acad. Sci. U. S. A.* **1978**, *75*, 2458–2462, doi:10.1073/pnas.75.5.2458.

40. Palumbo, A.; Minowada, J.; Erikson, J.; Croce, C.M.; Rovera, G. Lineage Infidelity of a Human Myelogenous Leukemia Cell Line. *Blood* **1984**, *64*, 1059–1063, doi:10.1182/blood.v64.5.1059.1059.

41. Hu, J.; Liu, J.; Xue, F.; Halverson, G.; Reid, M.; Guo, A.; Chen, L.; Raza, A.; Galili, N.; Jaffray, Evans, R.W.; Williams, J. The Electrophoresis of Transferrins in Urea/Polyacrylamide Gels. *Biochem. J.* **1980**, *189*, 541–546, doi:10.1042/bj1890541.

42. Bakker, W.J.; Blázquez-Domingo, M.; Kolbus, A.; Besooyen, J.; Steinlein, P.; Beug, H.; Coffer, P.J.; Löwenberg, B.; von Lindern, M.; van Dijk, T.B. FoxO3a Regulates Erythroid Differentiation and Induces BTG1, an Activator of Protein Arginine Methyl Transferase 1. *J. Cell Biol.* **2004**, *164*, 175–184, doi:10.1083/jcb.200307056.

43. Hayes, D.M.; Reilly, R.M.; Lee, M.M.C. The Pharmaceutical Stability of Deferoxamine Mesylate. *Can. J. Hosp. Pharm.* **1994**, *47*, 9–14, doi:10.4212/cjhp.v47i1.2355.

44. Aisen, P.; Leibman, A. Thermodynamic and Accessibility Factors in the Specific Binding of Iron to Human Transferrin. In *Transport by Proteins: Proceedings of a Symposium held at the University of Konstanz, West Germany, July 9-15, 1978.*; FEBS Symposium; Walter de Gruyter, **1978**; pp. 277–291 ISBN 3-11-007694-2.

45. Galanello, R. Deferiprone in the Treatment of Transfusion-Dependent Thalassemia: A Review and Perspective. *Ther. Clin. Risk Manag.* **2007**, *3*, 795–805.

46. Sohn, Y.-S.; Mitterstiller, A.-M.; Breuer, W.; Weiss, G.; Cabantchik, Z.I. Rescuing Iron-Overloaded Macrophages by Conservative Relocation of the Accumulated Metal. *Br. J. Pharmacol.* **2011**, *164*, 406–418, doi:10.1111/j.1476-5381.2010.01120.x.

47. Bhagavan, N.V.; Ha, C.-E. Chapter 27 - Metabolism of Iron and Heme. In *Essentials of Medical Biochemistry (Second Edition)*; Bhagavan, N.V., Ha, C.-E., Eds.; Academic Press: San Diego, **2015**; pp. 511–529 ISBN 978-0-12-416687-5.

48. Miyazawa, M.; Bogdan, A.R.; Hashimoto, K.; Tsuji, Y. Regulation of Transferrin Receptor-1 MRNA by the Interplay between IRE-Binding Proteins and MiR-7/MiR-141 in the 3′-IRE Stem–Loops. *RNA* **2018**, *24*, 468–479, doi:10.1261/rna.063941.117.

49. Hu, J.; Liu, J.; Xue, F.; Halverson, G.; Reid, M.; Guo, A.; Chen, L.; Raza, A.; Galili, N.; Jaffray, J.; et al. Isolation and Functional Characterization of Human Erythroblasts at Distinct Stages: Implications for Understanding of Normal and Disordered Erythropoiesis in Vivo. *Blood* **2013**, *121*, 3246–3253, doi:10.1182/blood-2013-01-476390.

50. Aoto, M.; Iwashita, A.; Mita, K.; Ohkubo, N.; Tsujimoto, Y.; Mitsuda, N. Transferrin Receptor 1 Is Required for Enucleation of Mouse Erythroblasts during Terminal Differentiation. *FEBS Open Bio* **2019**, *9*, 291–303, doi:10.1002/2211-5463.12573.

51. Dlouhy, A.C.; Outten, C.E. The Iron Metallome in Eukaryotic Organisms. In *Metallomics and the Cell*; Banci, L., Ed.; Metal Ions in Life Sciences; Springer Netherlands: Dordrecht, **2013**; pp. 241–278 ISBN 978-94-007-5561-1.

52. Barnes, D.; Sato, G. Serum-Free Cell Culture: A Unifying Approach. *Cell* **1980**, *22*, 649–655, doi:10.1016/0092-8674(80)90540-1.

53. Glickstein, H.; El, R.B.; Link, G.; Breuer, W.; Konijn, A.M.; Hershko, C.; Nick, H.; Cabantchik, Z.I. Action of Chelators in Iron-Loaded Cardiac Cells: Accessibility to Intracellular Labile Iron and Functional Consequences. *Blood* **2006**, *108*, 3195–3203, doi:10.1182/blood-2006-05-020867.

54. Hider, R.C.; Liu, Z.D.; Piyamongkol, S. The Design and Properties of 3-Hydroxypyridin-4-One Iron Chelators with High PFe3+ Values. *Transfus. Sci.* **2000**, *23*, 201–209, doi:10.1016/S0955-3886(00)00090-4.

55. Barnekow, A.; Winkelmann, G. Use of Iron from Transferrin and Microbial Chelates as Substrate for Heme Synthetase in Transformed and Primary Erythroid Cell Cultures. *Biochim. Biophys. Acta BBA - Gen. Subj.* **1978**, *543*, 530–535, doi:10.1016/0304-4165(78)90307-0.

56. Chai, X.; Li, D.; Cao, X.; Zhang, Y.; Mu, J.; Lu, W.; Xiao, X.; Li, C.; Meng, J.; Chen, J.; et al. ROS-Mediated Iron Overload Injures the Hematopoiesis of Bone Marrow by Damaging Hematopoietic Stem/Progenitor Cells in Mice. *Sci. Rep.* **2015**, *5*, 10181, doi:10.1038/srep10181.

57. Zhang, Y.; Zhai, W.; Zhao, M.; Li, D.; Chai, X.; Cao, X.; Meng, J.; Chen, J.; Xiao, X.; Li, Q.; et al. Effects of Iron Overload on the Bone Marrow Microenvironment in Mice. *PLoS ONE* **2015**, *10*, e0120219, doi:10.1371/journal.pone.0120219.

58. Matte, A.; De Franceschi, L. Oxidation and Erythropoiesis. *Curr. Opin. Hematol.* **2019**, *26*, 145–151, doi:10.1097/MOH.0000000000000495.

59. Bellanti, F.; Danhof, M.; Della Pasqua, O. Population Pharmacokinetics of Deferiprone in Healthy Subjects. *Br. J. Clin. Pharmacol.* **2014**, *78*, 1397–1406, doi:10.1111/bcp.12473.

60. Spino, M.; Connelly, J.; Tsang, Y.-C.; Fradette, C.; Tricta, F. Deferiprone Pharmacokinetics with and without Iron Overload and in Special Patient Populations. *Blood* **2015**, *126*, 3365, doi:10.1182/blood.V126.23.3365.3365.

61. Barman Balfour, J.A.; Foster, R.H. Deferiprone: A Review of Its Clinical Potential in Iron Overload in Beta-Thalassaemia Major and Other Transfusion-Dependent Diseases. *Drugs* **1999**, *58*, 553–578, doi:10.2165/00003495-199958030-00021.

62. Cohen, A.R.; Galanello, R.; Piga, A.; De Sanctis, V.; Tricta, F. Safety and Effectiveness of Long-Term Therapy with the Oral Iron Chelator Deferiprone. *Blood* **2003**, *102*, 1583–1587, doi:10.1182/blood-2002-10-3280.

63. Parrow, N.L.; Li, Y.; Feola, M.; Guerra, A.; Casu, C.; Prasad, P.; Mammen, L.; Ali, F.; Vaicikauskas, E.; Rivella, S.; et al. Lobe Specificity of Iron Binding to Transferrin Modulates Murine Erythropoiesis and Iron Homeostasis. *Blood* **2019**, *134*, 1373–1384, doi:10.1182/blood.2018893099.

64. Yao, T.; Asayama, Y. Animal-cell Culture Media: History, Characteristics, and Current Issues. *Reprod. Med. Biol.* **2017**, *16*, 99–117, doi:10.1002/rmb2.12024.

65. Pepe, A.; Rossi, G.; Bentley, A.; Putti, M.C.; Frizziero, L.; D'Ascola, D.G.; Cuccia, L.; Spasiano, A.; Filosa, A.; Caruso, V.; et al. Cost-Utility Analysis of Three Iron Chelators Used in Monotherapy for the Treatment of Chronic Iron Overload in β-Thalassaemia Major Patients: An Italian Perspective. *Clin. Drug Investig.* **2017**, *37*, 453–464, doi:10.1007/s40261-017-0496-1.

4.8. Supplementary materials

4.8.1. Supplementary figures

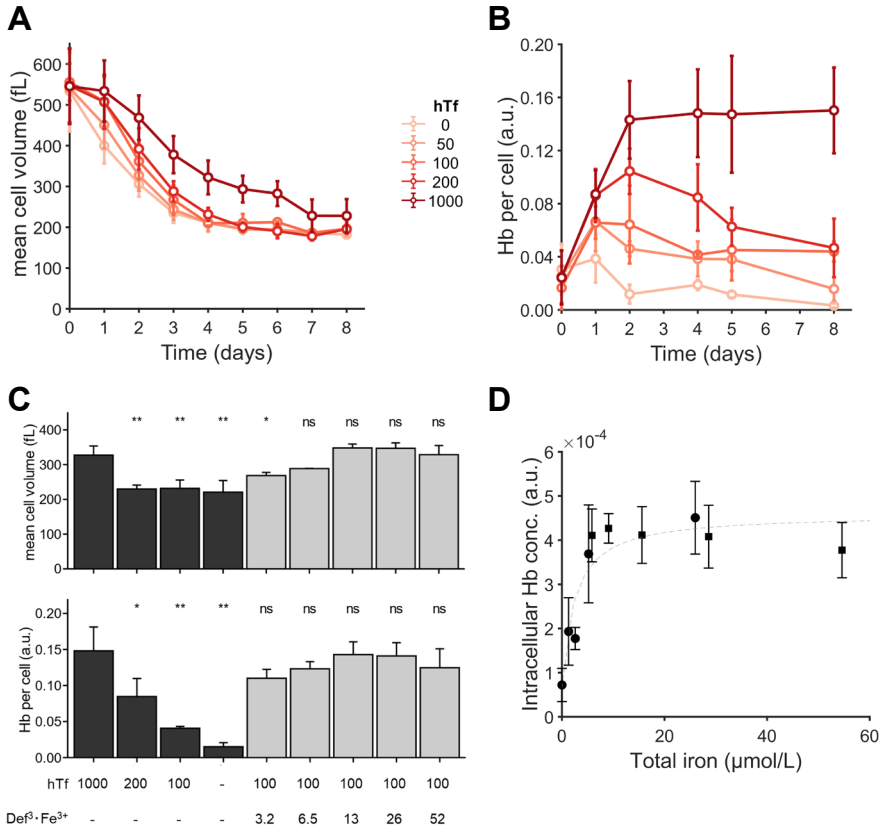

Supplementary Figure S1. Intracellular hemoglobin concentration of differentiating erythroblasts using holotransferrin and iron-loaded deferiprone as iron source. Erythroblasts were expanded from PBMCs for 10-12 days, and subsequently seeded in differentiation medium at a starting cell concentration of 1.5 – 2.0×10^6 cells. **(A)** Cells were seeded with decreasing holotransferrin concentrations (1000, 200, 100, 50 and 0 µg/mL). Evolution of mean cell diameter is depicted. **(B)** Hemoglobin cell content (i.e. mass of hemoglobin per cell; displayed as arbitrary units = absorbance at 420 nm per million cells) was determined at indicated days. The effect of deferiprone supplementation with sub-optimal hTf concentrations on erythroblast cell volume **(C)** and hemoglobin content **(C,D)** in differentiation cultures was also evaluated. For this, erythroblast expanded from PBMCs were seeded in medium using hTf as sole iron source (dark grey; ●), or in hTf-limited conditions (100 µg/mL hTf) in the presence of $Def_3{\cdot}Fe^{3+}$ in concentrations ranging between 3.2 and 52 µmol/L (light grey; ■). Intracellular hemoglobin concentration was calculated using the cell volume and Hb per cell values (day 4 of treatment), and is depicted in arbitrary units (a.u.) of absorbance per fL of cell volume. Mean ± SD (error bars; n≥3). Significance is shown for the comparison with 1000 µg/mL hTf (unpaired two-tailed two-sample Student's *t*-test).

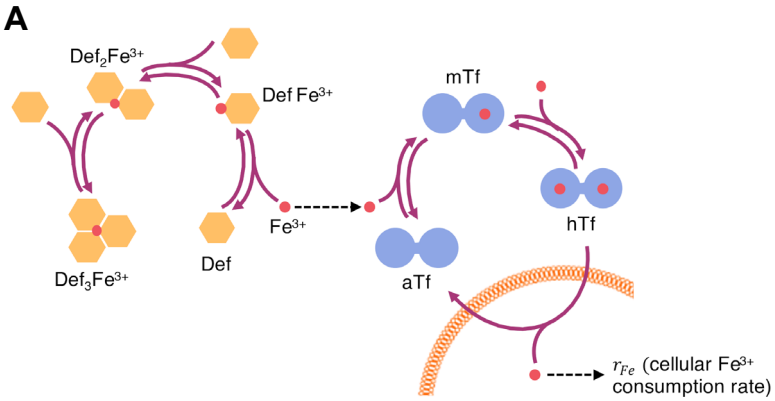

B

$$aTf + Fe^{3+} \underset{}{\overset{K_{Tf,1}}{\rightleftharpoons}} mTf \qquad K_{Tf,1} = \frac{[mTf]}{[aTf][Fe^{3+}]} = 7.0 \times 10^{22}\ M^{-1}$$

$$mTf + Fe^{3+} \underset{}{\overset{K_{Tf,2}}{\rightleftharpoons}} hTf \qquad K_{Tf,2} = \frac{[hTf]}{[mTf][Fe^{3+}]} = 3.6 \times 10^{21}\ M^{-1}$$

$$Def + Fe^{3+} \underset{}{\overset{\beta_{Def,1}}{\rightleftharpoons}} Def \cdot Fe^{3+} \qquad \beta_{Def,1} = \frac{[Def{\cdot}Fe^{3+}]}{[Def][Fe^{3+}]} = 10^{15.01}\ M^{-1}$$

$$Def \cdot Fe^{3+} + Fe^{3+} \underset{\beta_{Def,1}}{\overset{\beta_{Def,2}}{\rightleftharpoons}} Def_2 \cdot Fe^{3+} \qquad \beta_{Def,2} = \frac{[Def_2{\cdot}Fe^{3+}]}{[Def]^2[Fe^{3+}]} = 10^{27.30}\ M^{-2}$$

$$Def_2 \cdot Fe^{3+} + Fe^{3+} \underset{\beta_{Def,2}}{\overset{\beta_{Def,3}}{\rightleftharpoons}} Def_3 \cdot Fe^{3+} \qquad \beta_{Def,3} = \frac{[Def_3{\cdot}Fe^{3+}]}{[Def]^3[Fe^{3+}]} = 10^{37.43}\ M^{-3}$$

Supplementary Figure S2. Modeling of iron saturation in transferrin and deferiprone solutions. (A) Iron shuttling mathematical model proposed for the reloading of apotransferrin in culture using iron-loaded deferiprone. Leaching of Fe^{3+} ions from deferiprone or transferrin was the only mechanism considered for the transfer of iron between the two chelators. **(B)** Concentrations of transferrin and deferiprone species were calculated assuming equilibria at culture conditions (pH = 7.4, 3.5 mmol/L HCO_3^-). For transferrin, the association equilibrium constants of 7.0×10^{22} L/mol and 3.6×10^{21} L/mol for the binding of the first and second Fe^{3+} ion were assumed, respectively [44]. No difference in the association of iron to the N- and C-lobes of transferrin was considered. For deferiprone, the global stability constants (log β) for the Def·Fe^{3+}, Def_2·Fe^{3+} and Def_3·Fe^{3+} complexes were assumed to be 15.01, 27.30 and 37.43, respectively [32].

(Figure and caption continue on next page)

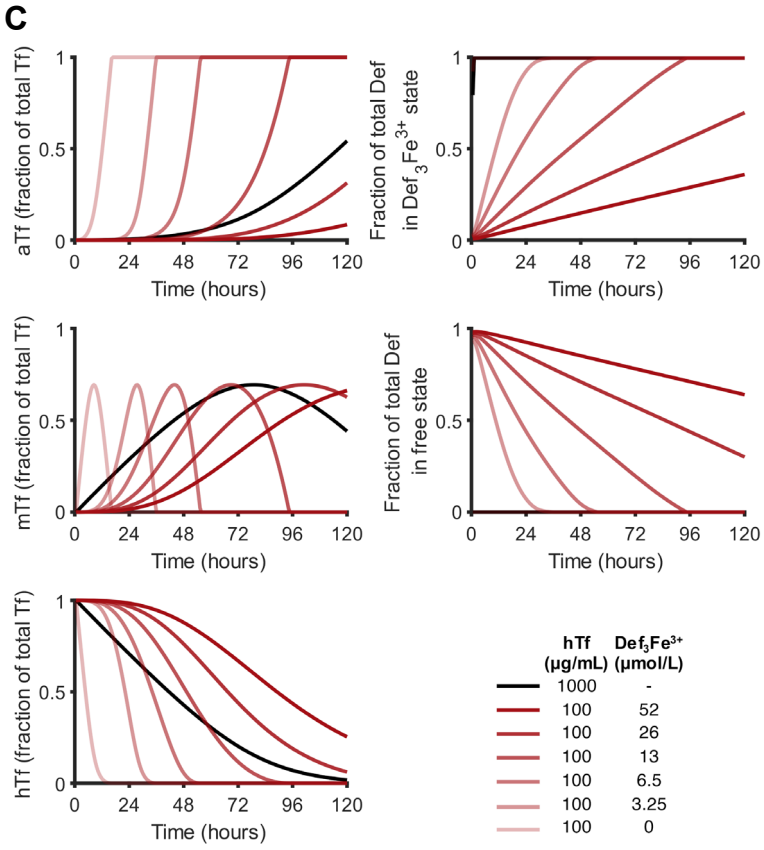

For simplicity purposes, a constant net average iron uptake rate (inflow + iron export from the cells) of 1.7×10^{-7} mol Fe^{3+}/L·h was assumed, corresponding to the production of 10×10^{6} hemoglobinized cells per mL of culture (1 cell = 300 million Hb molecules) in 4 days. It was assumed that iron association and dissociation kinetics with Tf and Def dominate iron concentration in the extracellular space, and that this is faster than the net utilization rate of iron in the intracellular space. Calculation of transferrin and deferiprone concentrations for each timepoint was performed solving the system of nonlinear chemical equilibrium equations with MATLAB ver. R2019b. **(C)** Calculated time profiles for the concentrations of the different transferrin and deferiprone species for cultures with either 1000 or 100 µg/mL of hTf, in presence or absence of $Def_3{\cdot}Fe^{3+}$. Under low hTf conditions, supplementation with $Def_3{\cdot}Fe^{3+}$ leads to a delay on the depletion of hTf.

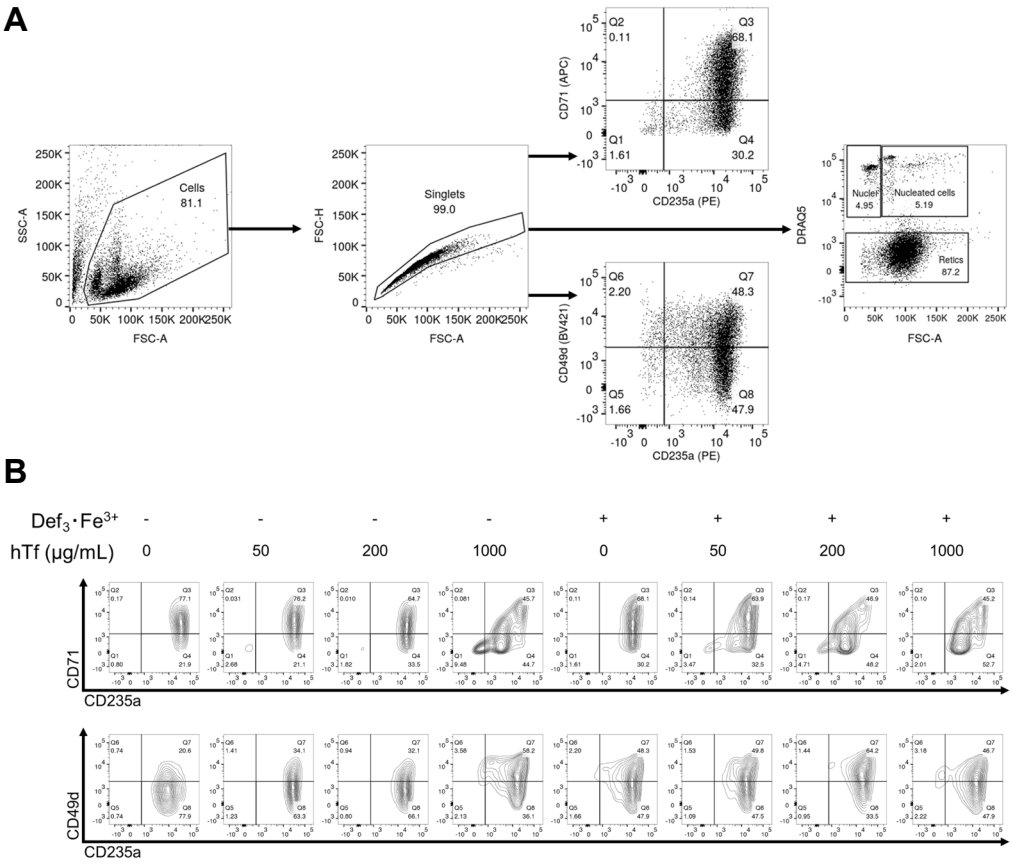

Supplementary Figure S3. Expression of erythroid cell surface markers in differentiation cultures supplemented with deferiprone. Erythroblasts were differentiated for 10 days in medium at different hTf concentrations, in the presence or absence of $Def_3 \cdot Fe^{3+}$ (52 µmol/L). **(A)** Gating strategy to evaluate the differentiation level of cultured erythroblasts. Cells were gated (FSC/SSC), followed by gating of single cells (FSC-A/FSC-H). Cells are depicted in a CD235a/CD71 or a CD235a/CD49d dot plot. To evaluate enucleation levels, erythroblasts ($DRAQ5^+$ FSC^{high}), pyrenocytes (extruded nuclei; $DRAQ5^+$ FSC^{low}) and reticulocytes ($DRAQ5^-$) were gated. **(B)** Representative density plots indicating the expression of the cell surface markers CD71, CD235 and CD49d after 10 days of culture.

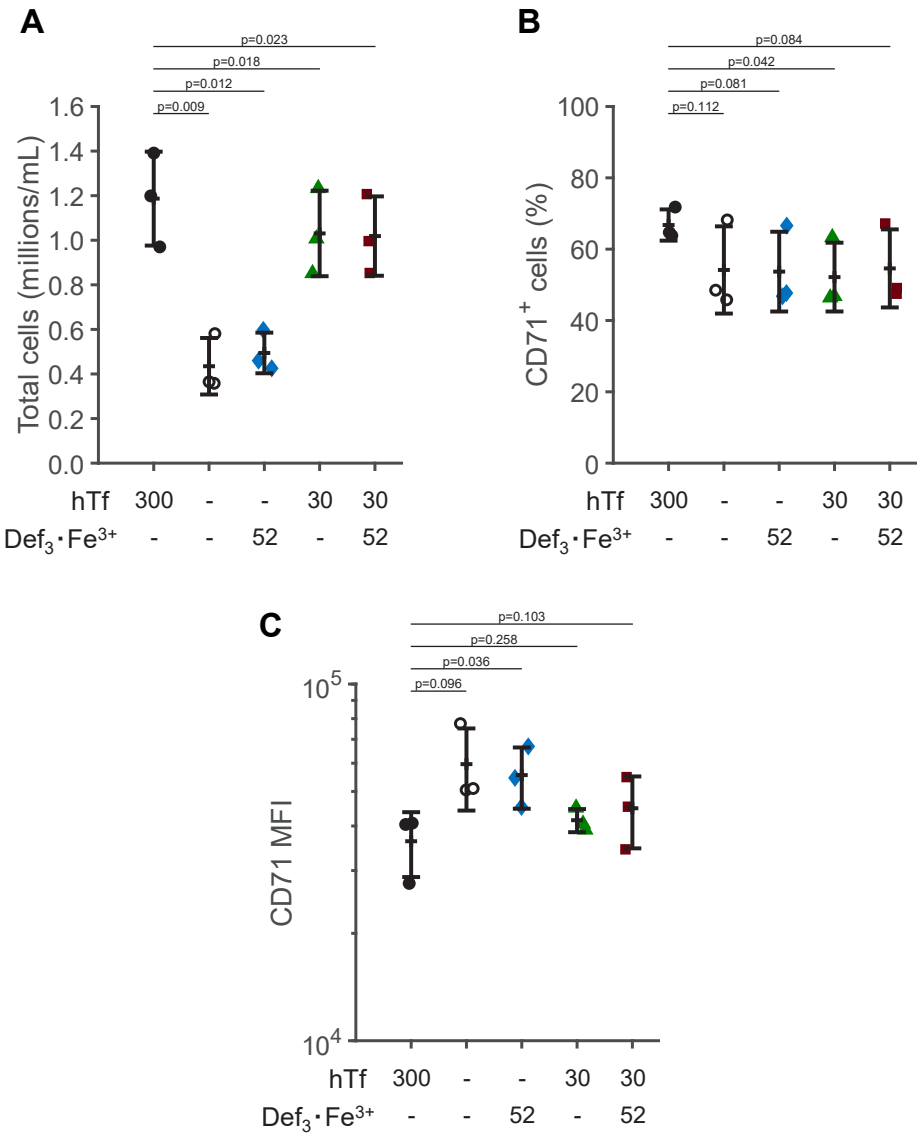

Supplementary Figure S4. Cell yields and expression of transferrin receptor TFR1 (CD71) on erythroid cultures stablished under deferiprone supplementation. PBMCs were cultured in expansion medium without iron, or supplemented with holotransferrin (30 µg/mL or 300 µg/mL) and $Def_3{\cdot}Fe^{3+}$ (52 µmol/L), as indicated. After 6 days of culture, the typical time for the establishment of erythroid cultures, total cell concentration was measured **(A)**. Percentage of $CD71^+$ cells **(B)** and the mean fluorescence intensity of CD71 **(C)** were determined by flow cytometry. Cultures were kept for 9 days more, as shown in Figure 4B. Mean ± SD (error bar; n=3). Significance is shown for the comparison with the 300 µg/mL hTf condition (paired two-tailed two-sample Student's *t*-test).

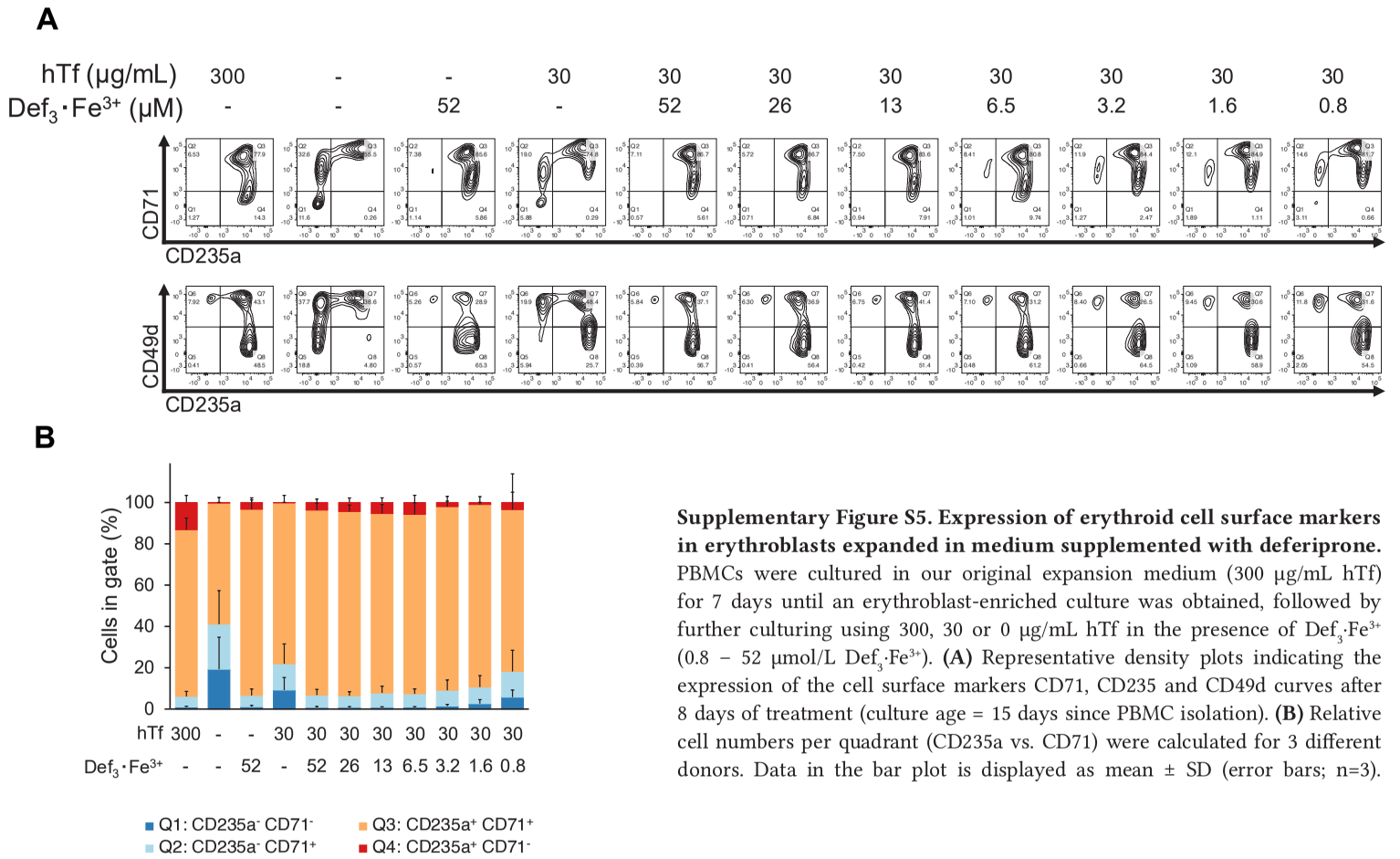

Supplementary Figure S5. Expression of erythroid cell surface markers in erythroblasts expanded in medium supplemented with deferiprone. PBMCs were cultured in our original expansion medium (300 µg/mL hTf) for 7 days until an erythroblast-enriched culture was obtained, followed by further culturing using 300, 30 or 0 µg/mL hTf in the presence of $Def_3 \cdot Fe^{3+}$ (0.8 – 52 µmol/L $Def_3 \cdot Fe^{3+}$). **(A)** Representative density plots indicating the expression of the cell surface markers CD71, CD235 and CD49d curves after 8 days of treatment (culture age = 15 days since PBMC isolation). **(B)** Relative cell numbers per quadrant (CD235a vs. CD71) were calculated for 3 different donors. Data in the bar plot is displayed as mean ± SD (error bars; n=3).

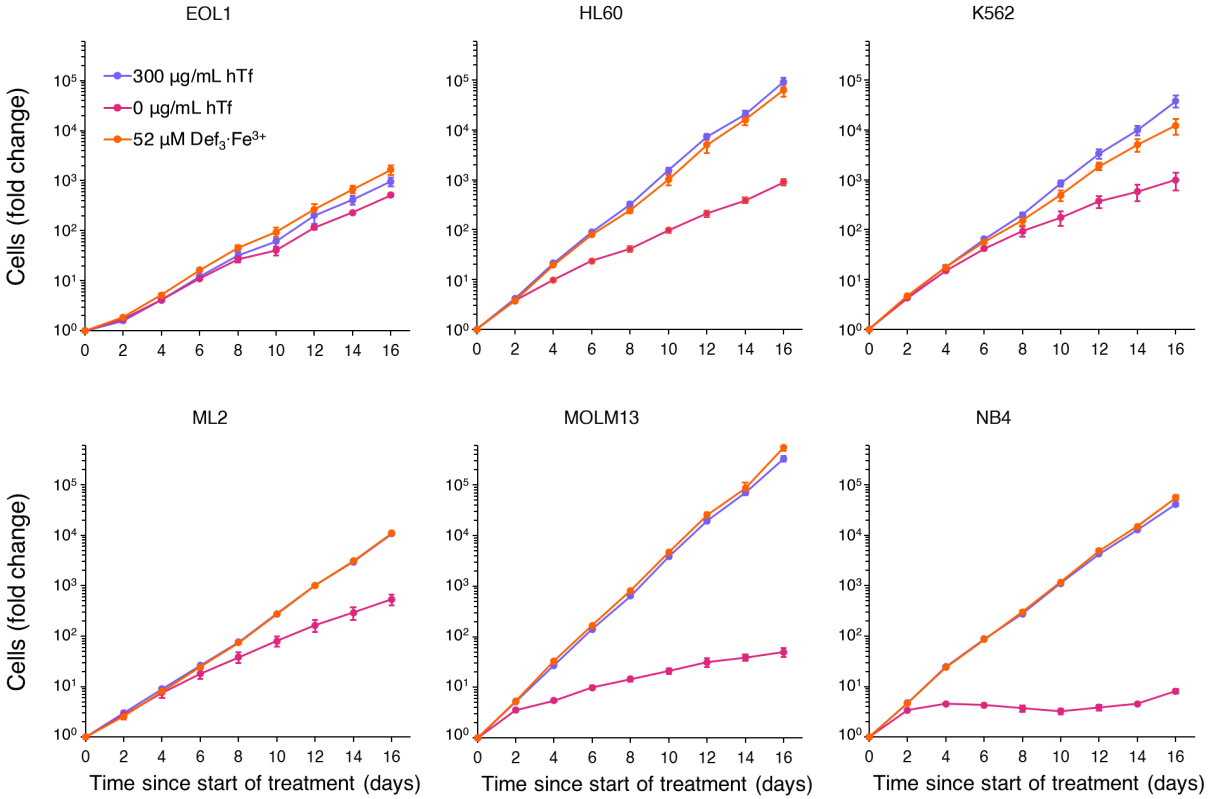

Supplementary Figure S6. Deferiprone sustains expansion of selected myeloid cell lines. Six myeloid cell lines were cultured in serum-free expansion medium supplemented with 300 µg/mL hTf or 52 µmol/L $Def_3 \cdot Fe^{3+}$ for 16 days. Cells were cultured under static conditions at a concentration of 0.3×10^6 cells/mL, with changing of medium every 2 days. Final cell number fold change relative to day 0 is depicted. Data is displayed as mean ± SD (error bar; n=3).

4.8.2. Supplementary tables

Supplementary Table S1A. Analysis of the effect of deferiprone supplementation from day 0 of the culture protocol on erythroblast cell numbers.

Condition		Cell number fold change (FC) at day 15 (relative to day 6) (n=3)		log_{10}(FC) (n=3)		
hTf (µg/mL)	$Def_3 \cdot Fe^{3+}$ (µmol/L)	Mean	(Range)	Mean	(Range)	*p*-value*
300	0	296.6	(227.4 – 357.9)	2.46	(2.36 – 2.55)	
0	0	17.5	(10.4 – 24.9)	1.22	(1.02 – 1.40)	0.0018
30	52	153.5	(106.4 – 233.0)	2.16	(2.03 – 2.37)	0.0399
30	0	36.4	(15.9 – 65.8)	1.49	(1.20 – 1.82)	0.0162
0	52	152.4	(117.3 – 216.1)	2.17	(2.07 – 2.33)	0.0367

Data corresponding to Figure 4B.

* *p*-values were calculated using the log_{10}(fold change) data and an unpaired 2-tail Student t-test, with the condition "300 µg/mL hTf + no $Def_3 \cdot Fe^{3+}$" (first row) as reference.

Supplementary Table S1B. Analysis of the effect of deferiprone supplementation from day 7 of the culture protocol on erythroblast cell numbers.

Condition		Cell number fold change (FC) at day 15 (relative to day 7) (n=3)		log_{10}(FC) (n=3)		
hTf (µg/mL)	$Def_3 \cdot Fe^{3+}$ (µmol/L)	Mean	(Range)	Mean	(Range)	*p*-value*
300	0	96.5	(60.1 – 130.7)	1.96	(1.78 – 2.12)	
0	0	4.5	(2.6 – 5.7)	0.63	(0.41 – 0.76)	0.0008
0	52	41.7	(24.1 – 54.6)	1.59	(1.38 – 1.74)	0.0657
30	0	8.2	(5.8 – 11.5)	0.89	(0.76 – 1.06)	0.0013
30	52	54.0	(32.4 – 65.2)	1.71	(1.51 – 1.81)	0.1479
30	26	66.7	(42.7 – 82.2)	1.81	(1.63 – 1.91)	0.3047
30	13	68.1	(44.6 – 81.3)	1.82	(1.65 – 1.91)	0.3262
30	6.5	56.1	(39.1 – 66.0)	1.74	(1.59 – 1.82)	0.1393
30	3.2	31.0	(21.4 – 36.2)	1.48	(1.33 – 1.56)	0.0174
30	1.6	23.5	(15.3 – 28.1)	1.36	(1.18 – 1.45)	0.0097
30	0.8	17.3	(14.8 – 21.6)	1.23	(1.17 – 1.33)	0.0028

Data corresponding to Figure 4C and D.

* *p*-values were calculated using the log_{10}(fold change) data and an unpaired 2-tail Student t-test, with the condition "300 µg/mL hTf + no $Def_3 \cdot Fe^{3+}$" (first row) as reference.

Supplementary Table S1C. Analysis of the effect of deferiprone supplementation from day 7 of the culture protocol on erythroblast viability.

Condition		% of DRAQ7$^-$ cells at day 15 (n=3)		
hTf (µg/mL)	$Def_3{\cdot}Fe^{3+}$ (µmol/L)	Mean	(Range)	*p*-value*
300	0	82.7	(75.4 – 87.5)	
0	0	40.9	(29.1 – 51.2)	0.0049
0	52	82.6	(79.4 – 84.6)	0.9938
30	0	54.5	(40.8 – 64.2)	0.0240
30	52	81.3	(80.0 – 82.9)	0.7370
30	26	81.0	(78.6 – 82.2)	0.6842
30	13	81.9	(79.1 – 84.5)	0.8640
30	6.5	81.6	(78.9 – 83.4)	0.8065
30	3.2	77.7	(72.1 – 81.4)	0.3508
30	1.6	71.5	(66.3 – 76.5)	0.0769
30	0.8	76.5	(67.2 – 87.8)	0.4306

Data corresponding to Figure 4E.

* *p*-values were calculated using the $\log_{10}$(fold change) data and an unpaired 2-tail Student t-test, with the condition "300 µg/mL hTf + no $Def_3{\cdot}Fe^{3+}$" (first row) as reference.

V

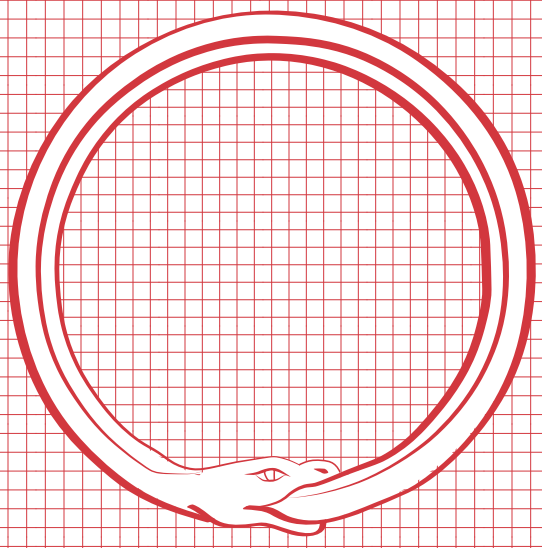

Chapter 5

General discussion

Cultured red blood cells (cRBCs) are a promising new source of erythrocytes for transfusion purposes, not only to cover the shortcomings of the current fully-donor-dependent system, but also for novel cellular therapies using RBCs as carriers of therapeutics. The research described in this thesis is part of the larger global aim to develop an efficient and cost-effective protocol to produce cRBC for transfusion purposes. To tackle current challenges in the large scale production of cRBC, a culture protocol for the production of cRBCs using stirred tank bioreactors was developed. The culture system was used to investigate the effect of relevant parameters for further scale-up, such as oxygen availability and turbulence due to agitation. Furthermore, we studied the potential sources of the observed cell density limitations in erythroblast proliferation cultures, and we proposed medium modifications to improve the productivity and cost-effectiveness of the process. Challenges that were identified during this thesis study are discussed in this chapter.

5.1. Towards a defined safe erythroid culture medium

The development of serum-free medium for erythroid cultures represented an important milestone for the production of safe clinical grade cRBCs, as serum is a poorly defined component that can carry contaminants such as viral agents or prions [1–3]. In those media formulations, serum is replaced by a defined mix of lipids, small molecules, and proteins. Although these media can be compliant with Good Manufacturing Practices (GMP) quality standards, issues with batch-to-batch variations and presence of contaminants in the supplemented proteins can lead to safety concerns. Thus, a clear next step for the development of erythroid culture medium is the reduction or full replacement of such components.

Albumin, an essential component in serum-free erythroid culture media, often displays batch-to-batch variations with putative contaminants [4–6]. Albumin purity level has been shown to have a direct impact on the efficiency of erythroid cultures [7]. Full replacement of albumin would represent a step towards a more consistent process and a safer final product. However, replacement of albumin in media for mammalian cell culture processes is challenging, as it can fulfill different roles: (i) carrier of hormones, lipids, trace elements, and other small molecules; (ii) scavenger of toxic byproducts (e.g. reactive oxygen species ROS, inhibitory metabolic byproducts); (iii) shear protectant in agitated reactors; and (iv) direct nutrient source as it can be internalized and degraded, releasing amino acids and small peptides [8]. Polyvinyl alcohol (PVA), a non-toxic polymer has been applied as albumin replacement in erythroid cultures with promising results in static cultures, sustaining the proliferation capacity of HSCs and erythroid progenitor cells [9,10]. Further testing of PVA in agitated culture systems is needed to assess whether the shear protection as provided by albumin is functional with PVA as well.

In differentiation, albumin can be eliminated from the culture if supplementation with plasma is maintained (data not shown). In the culture protocol developed by Heshusius et al., plasma is supplemented to differentiation medium at a final concentration of 5% v/v [7]. Removal from plasma led to impaired terminal differentiation and low enucleation levels (<25%). Lot-to-lot variation for plasma can be a large source of variability in the process. This effect has been minimized in this thesis by using pooled plasma from 600-1200 donors (Omniplasma; Octopharm, Austria). Although the composition of Omniplasma regarding coagulation factors and other plasma proteins has been described, it is still an undefined mixture with unknow full composition, as it carries lipids, hormones and other small molecules for which exact concentrations are not reported. This limits the determination of the set of molecules that makes plasma necessary for an efficient differentiation process. To elucidate the role of plasma on erythroblast differentiation, a design-of-experiments approach could be followed to test multiple combinations of replacement molecules at varying concentrations. This could be supported by a characterization of plasma composition before and after culture to identify depleted molecules during differentiation.

Transferrin purified from human plasma is also supplemented to erythroid culture medium. Although recombinant transferrin is commercially available, it is prohibitively expensive for large scale cRBC production. We developed a strategy to reduce transferrin requirements in all erythroid culture stages, using an iron-loaded chelator (deferiprone, **Chapter 4**). Deferiprone is already used in chelation therapy, and data is available regarding uptake mechanisms, safety levels, potential side effects, and interactions with other drugs. We estimate that even under a worst-case scenario (assuming the unlikely scenario that all deferiprone supplemented to the medium remains in the cytosol), the equivalent dosage of deferiprone after transfusing a packed unit of cRBC would still be lower than the maximum recommended dosage of deferiprone for chelation therapy. However, the described ability of deferiprone to cross the cell membrane and redistribute iron between cellular compartments suggests that no intracellular accumulation of deferiprone would take place. Washing steps could be performed on the cRBCs after the differentiation process, significantly reducing deferiprone levels in the final product.

5.2. Media cost reduction

The high cost of medium, for both proliferation and differentiation phases, leads to non-competitive cRBCs compared to the current source of RBCs for transfusion purposes (donations), even considering the more expensive cryopreserved units from rare donors. The main cost drivers are the growth factors and other proteins added to the medium (Table 1). Although transferrin only contributes to 17% of proliferation medium costs, it is the major cost driver in differentiation medium (65% of total cost

per liter of differentiation medium). The elimination of transferrin requirements in differentiation and the reduction in concentration in proliferation medium from 300 µg/L to 30 µg/L (**Chapter 4**) massively reduces the cost of the process (Table 1). However, the need for holotransferrin in the process could not be fully eliminated. We observed that holotransferrin is needed in the first stage of erythroid cultures in which HSCs commit to the erythroid lineage. It is known that hTf potentiates EpoR signaling required for efficient erythroid proliferation and differentiation [11]. We hypothesize that a recovery in growth in HSC cultures under absence of hTf could be achieved by adjusting Epo levels in the medium. If still low concentrations of transferrin are required in that culture stage, further reduction in transferrin costs could be achieved by using low-cost transferrin alternatives, such as recombinant transferrin produced in rice or yeast. However, as with any other medium modification in the process, the safety of these recombinant proteins must be fully assessed.

EXPANSION MEDIUM	Original formulation	This thesis	Replacement of hSCF	Replacement of albumin
Cellquin	100 € (19%)	100 € (22%)	100 € (29%)	55 € (19%)
Holotransferrin	92 € (17%)	9.2 € (2%)	9.2 € (3%)	9.2 € (3%)
hSCF	323 € (61%)	323 € (72%)		
Epo	13.3 € (3%)	13.3 € (3%)	13.3 € (4%)	13.3 € (5%)
$Def_3{\cdot}Fe^{3+}$ *		0.9 € (<1%)	0.9 € (<1%)	0.9 € (<1%)
740Y-P *			216 € (64%)	216 € (73%)
Polyvinyl alcohol				0.3 € (<1%)
Total cost per L	528 €	446 €	339 €	295 €
Total cost reduction		-15%	-36%	-44%

DIFFERENTIATION MEDIUM	Original formulation	This thesis	Replacement of albumin
Cellquin	100 € (21%)	100 € (60%)	55 € (45%)
Holotransferrin	307 € (65%)		
Epo	67 € (14%)	67 € (40%)	67 € (54%)
$Def_3{\cdot}Fe^{3+}$ *		0.9 € (<1%)	0.9 € (<1%)
Polyvinyl alcohol			0.3 € (<1%)
Total cost per L	474 €	168 €	123 €
Total cost reduction		-64%	-74%

* Research-grade reagents

Table 1.

(See caption on next page)

Stem cell factor (hSCF; h for human) is a clear target to continue with media cost reduction, as it contributes to 61% of the current proliferation medium cost. hSCF is required for the survival and proliferation of HSCs and proerythroblasts. Upon binding to its cognate receptor (c-Kit), triggering signal transduction pathways associated to the regulation of cell proliferation and survival, hSCF is internalized together with c-Kit, and is then degraded. Thus, a net decrease in hSCF concentration takes place in erythroid cultures (**Chapter 2**). However, this internalization process is not required to trigger the signaling cascades relevant to maintain erythroblast proliferation, as membrane-associated SCF can also trigger signaling transduction pathways, though with different intensity compared to soluble SCF [13,14]. Magnetic microparticles with immobilized hSCF that can be retained and reused between media refreshments have been developed [15]. Although this form of immobilized hSCF could support the proliferation of an erythroblast cell line, it was less active than soluble hSCF. Compatibility with GMP requirements and the safety of the final product are critical points for the use of any immobilized form of hSCF. To achieve this, full recovery of the particles containing the immobilized growth factor from the final product would be required.

An alternative approach to reduce hSCF costs in the process is the use of short synthetic "mimetic" peptides that can trigger the same signaling pathways as full soluble hSCF. This strategy has been used to replace other growth factors, such as fibroblast growth factor (FGF-2) and hepatocyte growth factor (HGF) [16,17]. The design of these peptides must consider the intracellular signaling cascades linked to hSCF. Sakurai et al. have recently reported that 740Y-P, a 25-residue peptide, can fully replace hSCF in HSC cultures [12]. 740Y-P stimulates the proliferation of $CD34^+$ cells by activating PIK3, one of the major signaling pathways associated to hSCF. Replacement of hSCF by 740Y-P would result in further media cost reduction (see Table 1), but it must be validated in erythroblast cultures.

Table 1. Cost of components within proliferation and differentiation medium for erythroid cultures. Cost per liter of proliferation (top) and differentiation (bottom) medium for erythroblast cultures was estimated using currently reported prices for all components. The effects of full replacement of human serum albumin by polyvinyl alcohol (PVA; 0.1% w/w), and of hSCF by a PIK-3 agonist (740Y-P; 1 μM) recently reported by Sakurai et al. [12] were also analyzed. Prices of research-grade components were used when no available data for GMP-compliant reagents was available (Epo: EPREX®, Janssen-Cilag, cat#13953729; hSCF: R&D Systemscat#255-GMP-01M; Def_3·Fe^{3+}: Sigma cat#379409 and 451649; 740Y-P: AbMole cat#M9389; PVA: Sigma cat#141350). The cost of Cellquin medium includes the costs of the basal medium (IMDM) and all supplements previously described by Heshusius et al. [7] (i.e. albumin, lipids, insulin, nucleosides, trace elements, L-glutamine, and sodium pyruvate).

5.3. Understanding erythroblast metabolism for medium optimization

Decreasing the media costs is only one of the many steps needed for efficient production of competitively priced cRBCs. Due to observed limitations in cell concentrations in erythroblast proliferation cultures (1-2×10^6 cells/mL), a culture volume of 1000-2000 L is needed to produce 2×10^{12} RBCs for a transfusion unit. Even with a 10× reduction in the cost of the medium, the production cost of a single transfusion unit would still be in the range of 40 000-50 000 EUR considering just the proliferation medium, still significantly higher than the current hospital cost of donor RBCs (~200 EUR per unit for common blood groups, 700-1200 EUR for frozen blood with rare phenotypes; [18,19]). Larger bioreactor vessels would also bring high operating costs, due to the energy requirements for mixing and heating. Thus, there is a clear need for the optimization of medium composition to support higher cell densities.

5.3.1. Identifying and overcoming nutrient limitations in erythroid cultures

Experimental data shown in **Chapter 3** indicate that exhaustion of nutrients with small molecular weight (<3 kDa) hampers proliferation of erythroblasts in high cell density cultures. Rapidly proliferating mammalian cells demand high uptake rates of amino acids to support the protein synthesis for new biomass production [20]. A high demand for other essential nutrients directly related to biomass synthesis, including essential lipids, vitamins and trace elements, can also be expected in erythroblast proliferation cultures [21–23]. Of the 13 vitamins considered essential for humans (vitamins A, C, D, E, K, B1, B2, B3, B5, B6, B7, B9, and B12), only B vitamins are included in IMDM. Although supplementation of spent medium with the vitamins already present in IMDM did not show an increase in growth, vitamins not included in IMDM may be limiting. Some of the remaining vitamins might already be present in the medium, as the plasma-derived human albumin included in the current medium formulations can carry hydrophobic ligands, such as fat-soluble vitamins. Measuring the concentration of all essential vitamins during culture can reveal hidden limitations that could not be identified by the untargeted metabolomics approach followed in this thesis, or potential limitations when reaching even higher cell densities. A similar approach can also be followed for trace elements, determining the concentration of each species by techniques such as ICP-MS, or supplementing cell culture medium with other trace elements (e.g. commercially available pharma-grade trace element mixes) than those already included in the current medium formulation (Mn^{2+}, Ni^{2+}, Sn^{2+}, MoO_4^{2+}, VO_4^{3-}, SO_4^{2+}), such as zinc and copper.

The observed decrease in growth could be caused by the combined effect of multiple simultaneous nutrient limitations, or by bottlenecks in important pathways for biomass synthesis that are not easy to identify using untargeted or targeted metabolomic approaches. Metabolic flux analysis of small scale metabolic networks has already been used for industrially relevant mammalian cells (CHO, hybridoma), and had allowed to identify hidden limitations for cell growth or for the production of the molecules of interest, typically monoclonal antibodies [24–26]. By considering the complete set of reactions taking place inside the cell, genome-scale metabolic models (GEMs) can be even more successful. GEMs have already been used in combination with constraint-based metabolic modelling to drive culture media optimization [27,28]. This has allowed to reduce the experimental time required compared to conventional media optimization methods based on statistical design of experiments (DoE), which are challenging for mammalian cell culture medium typically containing >50 components.

It is important to consider that the reconstruction process of a cell-specific GEM (i.e. defining the full set of metabolic reactions) is a time-consuming process, requiring different types of omics data and extensive manual curation. An erythroblast-specific GEM should be developed using existing proteomics and transcriptomics data of proliferating erythroblasts. Quantitative data on fluxes going in and out of the cells can also be used to constrain the model, although alternative methods that allow to use untargeted semiquantitative metabolomics measurements (such as those presented in **Chapter 3**) are also available [29]. Although not included in this thesis, flux balance analysis of an erythroblast-specific GEM extracted from the human metabolic reconstruction model Human1 suggest limitations in biomass synthesis caused by bottlenecks in lipid metabolism. However, it is important to note that those results are highly dependent on the biomass reaction, which should accurately represent the biomass composition of a proliferating erythroblast. The determination of this erythroblast biomass equation should be derived from experimental measurements of the macromolecule composition of the cells.

Although in this thesis we focused on proliferation cultures, profiling the metabolism of erythroblasts in differentiation will also be required to further optimize medium composition in that culture stage. Differentiation is a challenging stage because metabolic requirements of the cells will change over time as erythroblasts go through the maturation process from proerythroblasts to basophilic, polychromatophilic, and orthochromatic erythroblasts, and finally to enucleated reticulocytes. Hemoglobin synthesis is a clear example of the dynamic metabolic requirements during differentiation, as it takes place mainly during the first days of differentiation culture (**Chapter 4**). In this period, cultured cells need to cover the massive heme and globin synthesis requirements, increasing the consumption rates of specific nutrients, such as glycine.

5.3.2. Addressing toxic byproduct accumulations

Rapidly proliferating mammalian cells often display "wasteful" metabolism of glucose, characterized by high activity of the glycolytic pathway and elevated lactate production, even under sufficient oxygen availability [30]. Furthermore, a large fraction of the nitrogen of the consumed glutamine is secreted as ammonia and alanine [31]. Accumulation of lactate and ammonium is the common cause of growth inhibition in mammalian cell cultures. However, inhibition due to lactate and ammonium alone or in combination does not explain the decrease in growth rate in erythroblast proliferation cultures [32]. Other inhibitory metabolite byproducts have been recently described in animal cell cultures, including side products and intermediates of amino acid catabolism pathways [33–35]. Nevertheless, significant levels of those metabolites were not detected in the metabolic profiling of erythroblast cultures (**Chapter 3**).

It is possible that accumulation of lactate, ammonia, and these recently described toxic metabolites could reach toxic levels if the potential nutrient limitations in the current culture protocol are overcome, and higher cell densities are achieved. These metabolites can display a superadditive inhibitory effect, in which the total impact in growth is larger than the sum of the individual toxic effects of each individually. This synergistic effect on cell expansion of molecules which individually are below inhibitory threshold levels has been observed for hematopoietic stem cell cultures [36].

Control of glucose and glutamine concentrations have been used to minimize lactate and ammonium accumulation, and similar strategies have been proposed for the reduction of amino acid metabolism toxic byproducts [34,37,38]. Metabolic engineering to reduce the production of such toxic metabolites has also been used to reduce the accumulation of such metabolites. This can become an attractive strategy when transitioning from using donor-derived HSCs to stable iPSC cell lines as source of cells for cRBC production.

5.4. Bioprocess scale-up

High erythroblast cell densities are required for large scale production of cRBCs. If maximum cell densities of 100-200×10^6 cells/mL reached in CHO cell cultures [39] can be also obtained for erythroblasts, a 10-20 L bioreactor would be sufficient to produce a single cRBC transfusion unit. However, cultured blood with a specific rare blood group phenotype may not be in demand just as a single unit to alleviate anaemia or an acute vaso-occlusive crisis in a sickle cell disease patient. The urgent need is also in multiple units required for surgery or in obstetrics. If a single transfusion unit can be cultured with a bioreactor end-volume of 20 L, we could culture 10 units in 200 L.

In **Chapter 2**, the scale-up of erythroblast proliferation and differentiation cultures was evaluated, using 0.5 L and 3 L stirred tank bioreactors. For the larger bioreactors required to produce full cRBC transfusion units, mixing and aeration challenges will become more relevant than in the lab-scale bioreactors used in this thesis. Additionally, efficient cell retention systems for such culture volumes will be required, not only for perfusion of the cultures but also for the final harvest of the produced cRBCs.

5.4.1. Gas-liquid mass transfer for large scale erythroblast cultures

The effect of mixing and dissolved oxygen levels on erythroblast proliferation cultures described in this thesis suggest a high tolerance of erythroblasts to conditions typically considered harsh for mammalian cell cultures: sparging and high stirring speeds. It is important to note that bioreactor culture results include an overlap of both sparging and stirring speed effects (**Chapter 2**). To compare the effect of different agitation rates or dissolved oxygen levels on erythroblast cultures we need to consider that lower gas flow rates are needed at low dissolved oxygen levels to maintain the oxygen concentration at the desired setpoint, which in turn results in less contribution of bubble rise and burst to the overall shear stress and turbulent conditions to which cells are exposed. In a similar manner, at high agitation rates mass transfer is improved, resulting in lower gas flow rates needed to maintain dissolved oxygen concentration at the same level. Evaluation of the individual effect of both variables on the performance of the culture and quality of the cells would require other aeration systems.

Membrane aeration offers an alternative that would allow to decuple aeration from the mechanical stress caused by sparging. Although it is not a widely used aeration system for cell cultures, membrane aeration is a technique used in other bioprocesses in which efficient gas mass transfer is required, such as in wastewater treatment (membrane-aerated biofilm reactors; MABR). In these systems, gas flows through a membrane system in contact with the culture, either inside the reactor or in an external circulation loop. Oxygen diffuses from the gas to the liquid phase, passing through the membrane material. This bubbleless gas transfer using membranes would thus partially mimic the *in vivo* gas exchange taking place in the bone marrow, in which an oxygen rich phase circulates through the vascular system, transporting oxygen to the erythroblastic islands, and removing excess CO_2. Preliminary results of erythroblast proliferation cultures in 0.5 L bioreactors in which sparging was replaced by aeration using a submerged silicone (PDMS) module did not show a significant improvement in cell growth (data not shown), suggesting that the mechanical stress caused by sparging does not have a detrimental effect on the culture at this scale.

Accumulation of carbon dioxide is a commonly reported challenge in large scale mammalian cell cultures [40]. High CO_2 levels are expected in larger reactors: as hydrostatic pressure rises due to the increase in liquid height when scaling up, the solubility of CO_2 increases. An increase in the dissolved CO_2 levels caused by the metabolism of the cultured cells leads to the acidification of the medium, which must be compensated by addition of base to keep the pH of the culture constant, resulting in an increase in osmolarity. Hyperosmolar conditions lead to cell shrinkage, decreased cell growth, and increase cell apoptosis [41–43]. Negative effects of elevated CO_2 levels (>150 mmHg, equivalent to ~5 mM dissolved CO_2) on cell growth when controlling for osmolarity has also been described [44–46]. In the erythroblast bioreactor cultures of this study, CO_2 accumulation was not an issue (<40 mmHg), and dissolved CO_2 levels were similar to those *in vivo*. However, at this scale (AppliFlex 0.5 L, liquid height <8 cm; AppliFlex 3 L, liquid height <18 cm), the increase in CO_2 solubility due to the hydrostatic pressure at the bottom of the reactor is negligible (<2%). Furthermore, we used a base-free pH control system for erythroblast bioreactor cultures in which CO_2 was sparged when pH was above the setpoint, accompanied by stripping of excess of CO_2 by a continuous headspace flow of air. CO_2 stripping by headspace aeration becomes increasingly challenging at larger reactor volumes, as the top liquid surface scales by area. Excess CO_2 could be stripped by sparging air into the culture and ensuring sufficient gas residence time to saturate gas bubbles with CO_2 [47].

5.4.2. Mixing challenges

Mixing cultures at large scale is a common problem when scaling up bioprocesses. Scale-up of the bioreactors while maintaining a constant mixing time would lead to an increase in shear rate to which cells would be exposed in the bioreactor, and very large power requirements[1]. Additionally, the aspect ratio of the reactors is not usually maintained when scaling up, as tall reactor vessels are favored at larger scales. In those systems, ensuring good mixing is also a challenge [48].

Although high shear rates have traditionally been considered as the cause of decreased growth and viability in mammalian cell cultures in stirred tank bioreactors, recent research suggests that the local turbulent energy dissipation rate (EDR) is better

[1] If constant mixing time between scales is chosen to be the scaling parameter, and the bioreactor is scaled-up with a geometric factor k (equal to d_2/d_1; where d_1 and d_2 are the bioreactor diameters at the two scales) while maintaining geometric similarity (i.e. constant h/d, where h is the reactor height), the power per volume input required to mix the reactor (P/V; W/m^3) would scale with a factor of k^2, and the impeller tip speed with a factor of k. As it is assumed that impeller tip speed is proportional to maximum shear rate, the scale-up would lead to higher shear rates.

correlated to the effect of hydrodynamic conditions on cell cultures [49–52]. EDR is a scalar value (units = W/m^3) that quantifies the rate at which the kinetic energy of a fluid is converted to heat through eddy formation and viscous forces. Computational fluid dynamics (CFD) can facilitate a successful scale up of the system regarding mixing and exposure of the cells to hydrodynamic forces (e.g. EDR), by predicting the hydrodynamic conditions through the culture volume at the different scales and operating conditions (stirring speeds). It also allows to design scale-down experiments in which the maximum shear rates and EDR are mimicked in smaller culture systems. We followed this approach to chose the agitation conditions in shake flask cell cultures that would mimic the shear conditions of the 0.5 L bioreactors used in this thesis [53].

In addition to the determination of the velocity profiles and shear stress distribution through the culture volume, more detailed analysis could be performed, tracking the hydrodynamic conditions to which individual cells would be exposed while traveling through the liquid volume. The use of this "lifeline" analysis has been previously used to evaluate the exposure of cells to nutrient concentrations in stirred bioreactors with nutrient gradients [54]. Preliminary results of following this approach using CFD simulations of the 0.5 L and 3 L bioreactors used in this thesis allowed us to quantify not only the magnitude of the shear stress or EDR to which individual cells would be exposed at each bioreactor scale, but also the frequency and duration of those events (Figure 1). We expect this data can be used to design scale-down experimental set-ups that allow to study the physiological effects of intermittent exposure to high EDR values that erythroblast would experience at large scale bioreactors.

Figure 1. CFD-driven analysis of the hydrodynamic conditions to which erythroblast are exposed during culture. (A) Liquid velocity profiles in the bioreactor are obtained from CFD simulations at defined operating conditions (e.g. agitation speed). The shear rate tensor (τ) and the energy dissipation rates (EDR) can be calculated at each point in the bioreactor. Using the velocity profiles, individual particles mimicking single cells are tracked. **(B)** The effect of agitation speed on the range of EDR values in the liquid can be predicted. **(C)** The EDR values to which each particle is exposed can be recorded along the particle trajectory, resulting in a lifeline. Regime analysis can be performed using lifeline data. For this example, a EDR threshold of 10 W/m^3 is used to define a high EDR regime. **(D-E)** With sufficient tracked particles and simulation time, statistical analysis can be applied to lifeline data to, for example, determine the frequency at which cells are exposed to high EDR values **(D)**, and the exposure time to high EDR conditions **(E)**.

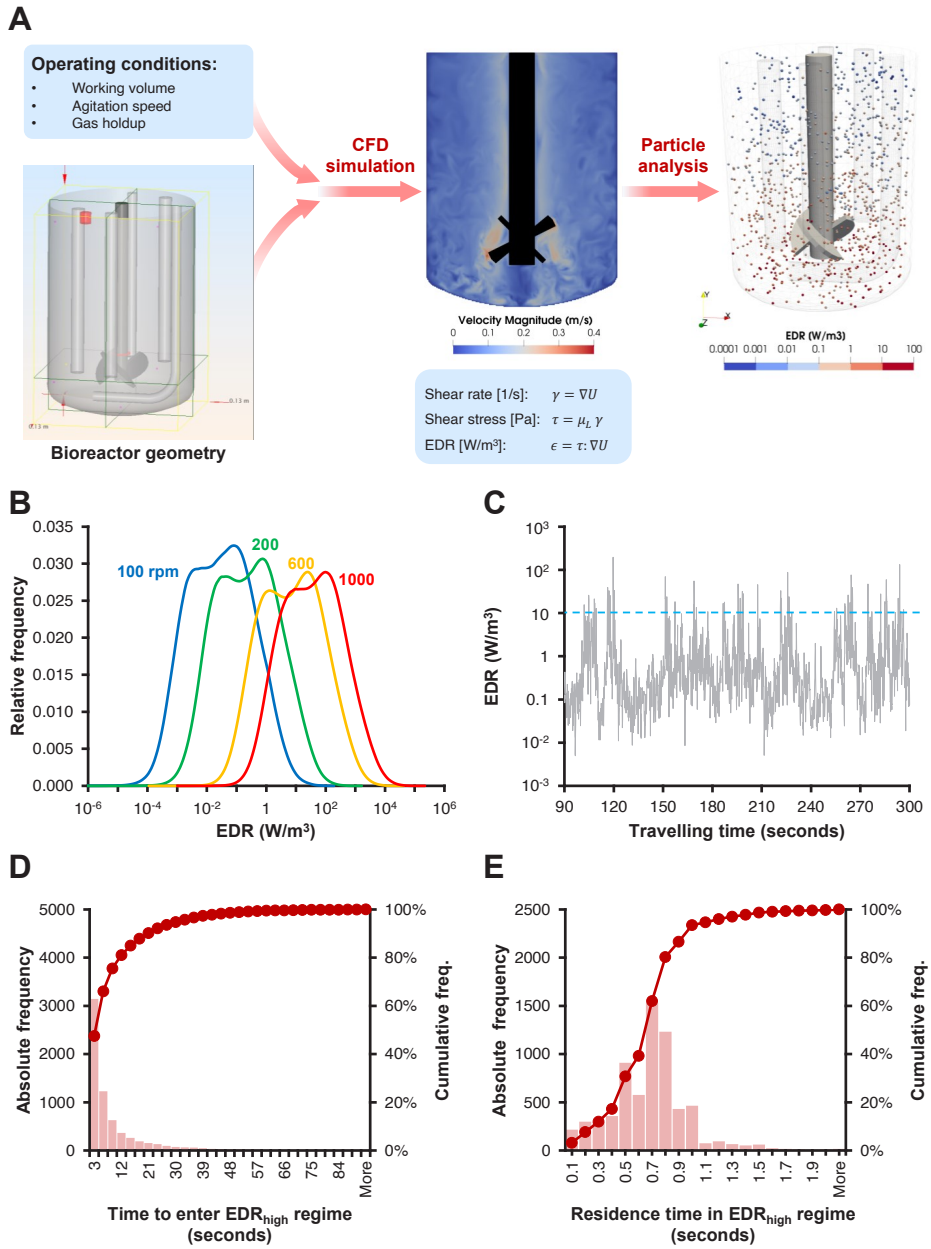

Figure 1.
(See caption on previous page)

5.4.3. Intensifying process productivity

Perfusion approaches allow for high cell densities and productivities, while opening the door to continuous manufacturing bioprocesses [39,55,56]. Furthermore, it allows for a more stable extracellular environment for the cells [57–59]. In this thesis we developed a perfusion process using an acoustic cell retention device and a constant cell-specific perfusion rate (CSPR; 500 pL/cell/day) approach (**Chapter 2**). For the target 20 L culture with a cell concentration of 100×10^6 cells/mL, this would result in a maximum perfusion rate of 1000 L/day, corresponding to 50 full media vessel refreshments daily. However, this large perfusion rate is consequence of the conservative CSPR value chosen for the perfusion culture (mimicking the same ratio of media refreshment that is performed in repeated batch cultures in dishes), and could be significantly decreased: CSPRs of 50-80 pL/cell/day are often used in high cell density CHO perfusion cultures. With such CSPR values, a maximum perfusion rate of 100-160 L/day (5-8 full refreshments per day) would be required. As depletion of essential nutrients seems to be the main cause for the decrease in erythroblast growth, further reduction of the perfusion rates could be achieved by increasing the concentration of limiting nutrients in the feed medium.

Increase of the overall productivity of the cRBC production process will also require the implementation of perfusion in the differentiation culture stage: with the current cell concentration used in batch differentiation cultures (10×10^6 cells/mL), a 10 L proliferation perfusion culture reaching cell densities of 100×10^6 cells/mL would require a 100 L differentiation bioreactor. In this study we did not evaluate the use of perfusion for differentiation. Implementation of perfusion in differentiation will also require the determination of optimal perfusion rates. Due to the expected changes in metabolic requirements during erythroblast maturation, further optimization could be achieved using variable perfusion rates during the differentiation culture. Preliminary metabolomics data of erythroblast differentiation cultures indicate that most changes in the exometabolome take place in the first 2 days of culture (data not shown), suggesting that high perfusion rates would only be required in that time interval, potentially followed by batch or fed-batch for the remaining 8-10 days of culture. The use of inline cell density and metabolite measurements to actively control the perfusion rate maintaining a constant CSPR will be key to develop robust erythroblast perfusion cultures.

In this study, an acoustic filter for cell retention was used for erythroblast perfusion cultures. Although similar systems have been used in 100 L perfusion bioreactors with permeate flows of up to 400 L/day, reaching high separation efficiencies (>95%) with flow rates >200 L/day is challenging [60]. Furthermore, cells can be exposed to large temperature gradients (>7 °C) when circulating through the separation chamber, which could lead to a decline in viability [61]. Thus, other cell retention devices should be

considered for further scale up of erythroid perfusion cultures. External microfiltration system through which the cell culture is circulated could be used, in either a tangential flow filtration (TFF) or alternating flow filtration (ATF) configuration. Very high cell densities (>200×10^6 cells/mL) have been reached with both set-ups [62]. Implementation of TFF or ATF systems in erythroblast cultures would first require an evaluation of the effect of the hydrodynamic stresses caused by pumping and the circulation through the hollow fiber filters.

By using a perfusion system with a microfiltration membrane of small pore size (e.g. 0.2 μm) for cell retention, it would be possible to obtain a cell-free permeate stream that could be further processed to recover unused components in the medium. For example, remaining proteins like growth factors or albumin could be recovered and reused for the preparation of fresh feed medium. Alternatively, the complete permeate could be further processed to remove inhibitory metabolic byproducts (e.g. lactate and ammonia using zeolites as adsorbents; [63,64]), supplemented with nutrients that were depleted or degraded during culture, and recirculated back to the reactor to be used as feed. Bleeding of the perfusion culture would be necessary to avoid excessive accumulation of cell debris and inhibitors not removed in the external media processing loop.

5.4.4. Intermediate and final harvest of cultured cells

In current erythroid protocols, two cell harvesting steps are needed: (i) a first intermediate harvest in which immature erythroblasts cultured under expansion conditions are harvested, washed, and resuspended in differentiation medium, and (ii) a final harvest in which reticulocytes are collected, and separated from pyrenocytes (egressed membrane-wrapped nuclei) and any remaining nucleated cells. For both stages, a scalable harvesting system with low cell losses is required.

For efficient erythroblast differentiation, erythroblasts must be washed to remove growth factors present in proliferation medium. Traces of dexamethasone (Dex) and hSCF negatively affect the enucleation efficiency of the differentiation culture. A potential advantage of using perfusion for the differentiation culture is that it could eliminate this first harvesting step: by continuous perfusion of differentiation medium, hSCF and Dex would be washed out (at a perfusion rate of 1 working volume per day, the concentration of both growth factors should have decreased by 63% and 95% after 24h and 72h, respectively).

Use of cRBCs for therapeutic purposes requires the removal of pyrenocytes, especially for the case of allogeneic cRBC transfusion. Thus, the final cell harvesting step must ensure a high selectivity of reticulocytes over pyrenocytes. Although pyrenocytes are more dense (typical relative density of cytoplasm vs. nuclei in mammalian cells

is ~0.9; [65]), smaller (reticulocytes: 7.0-8.0 µm; pyrenocytes: and 5.5-6.5 µm;[66]), and less flexible than reticulocytes, neither centrifugation nor microfiltration techniques resulted in sufficient levels of pyrenocyte removal while maintaining high reticulocyte recovery yields. Leukocyte depletion filters reduce reticulocyte numbers in fresh blood and result in large losses of reticulocytes during purification of cRBC [7]. Thus, other reticulocyte purification strategies are needed. Inertial microfluidic devices have been recently developed to separate nuclei from reticulocytes, taking advantage of the deformability differences between both particles [67]. Scale-out approaches, dividing the total culture broth in multiple microfluidic chips operated in parallel, could offer a solution for the large liquid throughput required when scaling up cRBC production [68].

5.4.5. HSC cultures in stirred bioreactors: the missing piece

Although this research focused on the scale-up of erythroblast proliferation and differentiation cultures, the first culture stage of all erythroid cultures in which HSCs are expanded and committed to the erythroid lineage must also be scaled-up. For this thesis, HSC cultures for all experiments were performed under static conditions in culture dishes using PBMCs as starting material, with a single 300 mL erythroblast proliferation bioreactor culture often requiring more than twenty 10 cm culture dishes as inoculum source. Transferring HSC cultures to stirred bioreactors will be challenging due to potential effects on proliferation and fate determination caused by the hydrodynamic stresses of agitation [69]. If PBMCs are maintained as source of HSCs, the effect of turbulence on the different cell populations in the PBMC pool must be also considered, as erythroid-supporting macrophages known to increase the erythroid yield in this first culture stage may show a different sensitivity to turbulent conditions than that reported for erythroblasts in this thesis.

Induced pluripotent stem cells (iPSCs) or immortalized erythroid progenitor cell lines have been proposed as alternative cell source for cRBC production, opening the opportunity to move away from cell sources limited by donor availability, such as peripheral blood or cord blood [70]. Novel bioreactor designs with reduced shear stress and turbulence have been proposed for iPSC cultures, including vertical-wheel stirred bioreactors or fluidized bed systems using microcarriers to which stem cells can attach [71,72]. The scalability of such systems to support the efficient proliferation of iPSCs, the formation of embryoid bodies from the cultured iPSCs, and the subsequent commitment to the erythroid lineage must be evaluated. It is important to note that protocols for the establishment of erythroid cultures using cell lines, including iPSCs, require extra culture stages, including the culture of somatic cells, their reprogramming to a pluripotent state, the proliferation of the iPSCS, and the differentiation to HSCs. Extra growth factors and cytokines will be required for these protocols, adding to the cost of the process.

5.5. Conclusion

Production of transfusion-ready cRBCs at scale can help to address some of the limitations of current donation-dependent systems, especially for cases in which RBCs with specific or rare blood groups difficult to find in the donor pool are required. In this research, we have developed solutions that tackle some of the key challenges in the scaling up of cRBC manufacture. This was achieved through experimental and computational approaches, in different culture systems, from culture dishes to stirred bioreactors, and at multiple culture scales. Further scale-up of the process will require more research in the areas highlighted in this chapter. For this, a multidisciplinary approach will be required, in which cell biology and bioprocess engineering knowledge is used to define optimal operating parameters for the scaled-up process, further reduce media costs, and improve the productivity of the culture.

5.6. References

1. Iscove, N.N.; Guilbert, L.J.; Weyman, C. Complete Replacement of Serum in Primary Cultures of Erythropoietin-Dependent Red Cell Precursors (CFU-E) by Albumin, Transferrin, Iron, Unsaturated Fatty Acid, Lecithin and Cholesterol. *Exp. Cell Res.* **1980**, *126*, 121–126, doi:10.1016/0014-4827(80)90476-0.

2. Stewart, S.; Zhu, B.; Axelrad, A. A "Serum-Free" Medium for the Production of Erythropoietic Bursts by Murine Bone Marrow Cells. *Exp. Hematol.* **1984**, *12*, 309–318, PMID:6723823.

3. Migliaccio, G.; Migliaccio, A.R. Cloning of Human Erythroid Progenitors (BFU-E) in the Absence of Fetal Bovine Serum. *Br. J. Haematol.* **1987**, *67*, 129–133, doi:10.1111/j.1365-2141.1987.00129.x.

4. Darcel, C.L.; Kaldy, M.S. Further Evidence for the Heterogeneity of Serum Albumin. *Comp. Biochem. Physiol. B* **1986**, *85*, 15–22, doi:10.1016/0305-0491(86)90215-4.

5. Hanson, R.W.; Ballard, F.J. Citrate, Pyruvate, and Lactate Contaminants of Commercial Serum Albumin. *J. Lipid Res.* **1968**, *9*, 667–668, doi:10.1016/S0022-2275(20)42716-6.

6. Quinlan, G.J.; Coudray, C.; Hubbard, A.; Gutteridge, J.M.C. Vanadium and Copper in Clinical Solutions of Albumin and Their Potential To Damage Protein Structure. *J. Pharm. Sci.* **1992**, *81*, 611–614, doi:10.1002/jps.2600810703.

7. Heshusius, S.; Heideveld, E.; Burger, P.; Thiel-Valkhof, M.; Sellink, E.; Varga, E.; Ovchynnikova, E.; Visser, A.; Martens, J.H.A.; von Lindern, M.; et al. Large-Scale in Vitro Production of Red Blood Cells from Human Peripheral Blood Mononuclear Cells. *Blood Adv.* **2019**, *3*, 3337–3350, doi:10.1182/bloodadvances.2019000689.

8. Mishra, V.; Heath, R.J. Structural and Biochemical Features of Human Serum Albumin Essential for Eukaryotic Cell Culture. *Int. J. Mol. Sci.* **2021**, *22*, 8411, doi:10.3390/ijms22168411.

9. Wilkinson, A.C.; Ishida, R.; Kikuchi, M.; Sudo, K.; Morita, M.; Crisostomo, R.V.; Yamamoto, R.; Loh, K.M.; Nakamura, Y.; Watanabe, M.; et al. Long-Term Ex Vivo Haematopoietic-Stem-Cell Expansion Allows Nonconditioned Transplantation. *Nature* **2019**, *571*, 117–121, doi:10.1038/s41586-019-1244-x.

10. Sudo, K.; Yamazaki, S.; Wilkinson, A.C.; Nakauchi, H.; Nakamura, Y. Polyvinyl Alcohol Hydrolysis Rate and Molecular Weight Influence Human and Murine HSC Activity Ex Vivo. *Stem Cell Res.* **2021**, *56*, 102531, doi:10.1016/j.scr.2021.102531.

11. Fouquet, G.; Thongsa-ad, U.; Lefevre, C.; Rousseau, A.; Tanhuad, N.; Khongkla, E.; Saengsawang, W.; Anurathapan, U.; Hongeng, S.; Maciel, T.T.; et al. Iron-Loaded Transferrin Potentiates Erythropoietin Effects on Erythroblast Proliferation and Survival: A Novel Role through Transferrin Receptors. *Exp. Hematol.* **2021**, *99*, 12-20.e3, doi:10.1016/j.exphem.2021.05.005.

12. Sakurai, M.; Ishitsuka, K.; Ito, R.; Wilkinson, A.C.; Kimura, T.; Mizutani, E.; Nishikii, H.; Sudo, K.; Becker, H.J.; Takemoto, H.; et al. Chemically Defined Cytokine-Free Expansion of Human Haematopoietic Stem Cells. *Nature* **2023**, *615*, 127–133, doi:10.1038/s41586-023-05739-9.

13. Toksoz, D.; Zsebo, K.M.; Smith, K.A.; Hu, S.; Brankow, D.; Suggs, S.V.; Martin, F.H.; Williams, D.A. Support of Human Hematopoiesis in Long-Term Bone Marrow Cultures by Murine Stromal Cells Selectively Expressing the Membrane-Bound and Secreted Forms of the Human Homolog of the Steel Gene Product, Stem Cell Factor. *Proc. Natl. Acad. Sci. U. S. A.* **1992**, *89*, 7350–7354, doi:10.1073/pnas.89.16.7350.

14. Kapur, R.; Majumdar, M.; Xiao, X.; McAndrews-Hill, M.; Schindler, K.; Williams, D.A. Signaling Through the Interaction of Membrane-Restricted Stem Cell Factor and c-Kit Receptor Tyrosine Kinase: Genetic Evidence for a Differential Role in Erythropoiesis. *Blood* **1998**, *91*, 879–889, doi:10.1182/blood.V91.3.879.

15. Worrallo, M.J.; Moore, R.L.L.; Glen, K.E.; Thomas, R.J. Immobilized Hematopoietic Growth Factors onto Magnetic Particles Offer a Scalable Strategy for Cell Therapy Manufacturing in Suspension Cultures. *Biotechnol. J.* **2017**, *12*, doi:10.1002/biot.201600493.

16. Rubert Pérez, C.M.; Álvarez, Z.; Chen, F.; Aytun, T.; Stupp, S.I. Mimicking the Bioactivity of Fibroblast Growth Factor-2 Using Supramolecular Nanoribbons. *ACS Biomater. Sci. Eng.* **2017**, *3*, 2166–2175, doi:10.1021/acsbiomaterials.7b00347.

17. Miao, W.; Sakai, K.; Ozawa, N.; Nishiuchi, T.; Suzuki, Y.; Ito, K.; Morioka, T.; Umitsu, M.; Takagi, J.; Suga, H.; et al. Cellular Signaling and Gene Expression Profiles Evoked by a Bivalent Macrocyclic Peptide That Serves as an Artificial MET Receptor Agonist. *Sci. Rep.* **2018**, *8*, 16492, doi:10.1038/s41598-018-34835-4.

18. Toner, R.W.; Pizzi, L.; Leas, B.; Ballas, S.K.; Quigley, A.; Goldfarb, N.I. Costs to Hospitals of Acquiring and Processing Blood in the US: A Survey of Hospital-Based Blood Banks and Transfusion Services. *Appl. Health Econ. Health Policy.* **2011**, *9*, 29–37, doi:10.2165/11530740-000000000-00000.

19. Zeuner, A.; Martelli, F.; Vaglio, S.; Federici, G.; Whitsett, C.; Migliaccio, A.R. Concise Review: Stem Cell-Derived Erythrocytes as Upcoming Players in Blood Transfusion. *Stem Cells* **2012**, *30*, 1587–1596, doi:10.1002/stem.1136.

20. Hosios, A.M.; Hecht, V.C.; Danai, L.V.; Johnson, M.O.; Rathmell, J.C.; Steinhauser, M.L.; Manalis, S.R.; Vander Heiden, M.G. Amino Acids Rather than Glucose Account for the Majority of Cell Mass in Proliferating Mammalian Cells. *Dev. Cell* **2016**, *36*, 540–549, doi:10.1016/j.devcel.2016.02.012.

21. Arigony, A.L.V.; de Oliveira, I.M.; Machado, M.; Bordin, D.L.; Bergter, L.; Prá, D.; Pêgas Henriques, J.A. The Influence of Micronutrients in Cell Culture: A Reflection on Viability and Genomic Stability. *BioMed Res. Int.* **2013**, *2013*, 597282, doi:10.1155/2013/597282.

22. Das, U.N. Essential Fatty Acids: Biochemistry, Physiology and Pathology. *Biotechnol. J.* **2006**, *1*, 420–439, doi:10.1002/biot.200600012.

23. Else, P.L. The Highly Unnatural Fatty Acid Profile of Cells in Culture. *Prog. Lipid Res.* **2020**, *77*, 101017, doi:10.1016/j.plipres.2019.101017.

24. Dorka, P.; Fischer, C.; Budman, H.; Scharer, J.M. Metabolic Flux-Based Modeling of MAb Production during Batch and Fed-Batch Operations. *Bioprocess Biosyst. Eng.* **2009**, *32*, 183–196, doi:10.1007/s00449-008-0236-2.

25. Xing, Z.; Kenty, B.; Koyrakh, I.; Borys, M.; Pan, S.-H.; Li, Z.J. Optimizing Amino Acid Composition of CHO Cell Culture Media for a Fusion Protein Production. *Process Biochem.* **2011**, *46*, 1423–1429, doi:10.1016/j.procbio.2011.03.014.

26. Robitaille, J.; Chen, J.; Jolicoeur, M. A Single Dynamic Metabolic Model Can Describe MAb Producing CHO Cell Batch and Fed-Batch Cultures on Different Culture Media. *PLOS ONE* **2015**, *10*, e0136815, doi:10.1371/journal.pone.0136815.

27. Branco dos Santos, F.; Olivier, B.G.; Boele, J.; Smessaert, V.; De Rop, P.; Krumpochova, P.; Klau, G.W.; Giera, M.; Dehottay, P.; Teusink, B.; et al. Probing the Genome-Scale Metabolic Landscape of Bordetella Pertussis, the Causative Agent of Whooping Cough. *Appl. Environ. Microbiol.* **2017**, *83*, e01528-17, doi:10.1128/AEM.01528-17.

28. Huang, Z.; Xu, J.; Yongky, A.; Morris, C.S.; Polanco, A.L.; Reily, M.; Borys, M.C.; Li, Z.J.; Yoon, S. CHO Cell Productivity Improvement by Genome-Scale Modeling and Pathway Analysis: Application to Feed Supplements. *Biochem. Eng. J.* **2020**, *160*, 107638, doi:10.1016/j.bej.2020.107638.

29. Aurich, M.K.; Fleming, R.M.T.; Thiele, I. MetaboTools: A Comprehensive Toolbox for Analysis of Genome-Scale Metabolic Models. *Front. Physiol.* **2016**, *7*, doi:10.3389/fphys.2016.00327.

30. Young, J.D. Metabolic Flux Rewiring in Mammalian Cell Cultures. *Curr. Opin. Biotechnol.* **2013**, *24*, doi:10.1016/j.copbio.2013.04.016.

31. DeBerardinis, R.J.; Mancuso, A.; Daikhin, E.; Nissim, I.; Yudkoff, M.; Wehrli, S.; Thompson, C.B. Beyond Aerobic Glycolysis: Transformed Cells Can Engage in Glutamine Metabolism That Exceeds the Requirement for Protein and Nucleotide Synthesis. *Proc. Natl. Acad. Sci.* **2007**, *104*, 19345–19350, doi:10.1073/pnas.0709747104.

32. Bayley, R.; Ahmed, F.; Glen, K.; McCall, M.; Stacey, A.; Thomas, R. The Productivity Limit of Manufacturing Blood Cell Therapy in Scalable Stirred Bioreactors. *J. Tissue Eng. Regen. Med.* **2017**, doi:10.1002/term.2337.

33. Pereira, S.; Kildegaard, H.F.; Andersen, M.R. Impact of CHO Metabolism on Cell Growth and Protein Production: An Overview of Toxic and Inhibiting Metabolites and Nutrients. *Biotechnol. J.* **2018**, *13*, e1700499, doi:10.1002/biot.201700499.

34. Mulukutla, B.C.; Kale, J.; Kalomeris, T.; Jacobs, M.; Hiller, G.W. Identification and Control of Novel Growth Inhibitors in Fed-Batch Cultures of Chinese Hamster Ovary Cells. *Biotechnol. Bioeng.* **2017**, *114*, 1779–1790, doi:10.1002/bit.26313.

35. Coulet, M.; Kepp, O.; Kroemer, G.; Basmaciogullari, S. Metabolic Profiling of CHO Cells during the Production of Biotherapeutics. *Cells* **2022**, *11*, 1929, doi:10.3390/cells11121929.

36. Csaszar, E.; Kirouac, D.C.; Yu, M.; Wang, W.; Qiao, W.; Cooke, M.P.; Boitano, A.E.; Ito, C.; Zandstra, P.W. Rapid Expansion of Human Hematopoietic Stem Cells by Automated Control of Inhibitory Feedback Signaling. *Cell Stem Cell* **2012**, *10*, 218–229, doi:10.1016/j.stem.2012.01.003.

37. Konakovsky, V.; Clemens, C.; Müller, M.M.; Bechmann, J.; Berger, M.; Schlatter, S.; Herwig, C. Metabolic Control in Mammalian Fed-Batch Cell Cultures for Reduced Lactic Acid Accumulation and Improved Process Robustness. *Bioengineering* **2016**, *3*, 5, doi:10.3390/bioengineering3010005.

38. Glacken, M.W.; Fleischaker, R.J.; Sinskey, A.J. Reduction of Waste Product Excretion via Nutrient Control: Possible Strategies for Maximizing Product and Cell Yields on Serum in Cultures of Mammalian Cells. *Biotechnol. Bioeng.* **1986**, *28*, 1376–1389, doi:10.1002/bit.260280912.

39. Clincke, M.-F.; Mölleryd, C.; Zhang, Y.; Lindskog, E.; Walsh, K.; Chotteau, V. Very High Density of CHO Cells in Perfusion by ATF or TFF in WAVE Bioreactor™. Part I. Effect of the Cell Density on the Process. *Biotechnol. Prog.* **2013**, *29*, 754–767, doi:10.1002/btpr.1704.

40. Hu, W.-S.; Aunins, J.G. Large-Scale Mammalian Cell Culture. *Curr. Opin. Biotechnol.* **1997**, *8*, 148–153, doi:10.1016/S0958-1669(97)80093-6.

41. Ozturk, S.S.; Palsson, B.O. Effect of Medium Osmolarity on Hybridoma Growth, Metabolism, and Antibody Production. *Biotechnol. Bioeng.* **1991**, *37*, 989–993, doi:10.1002/bit.260371015.

42. Thiemicke, A.; Neuert, G. Kinetics of Osmotic Stress Regulate a Cell Fate Switch of Cell Survival. *Sci. Adv.* **2021**, *7*, eabe1122, doi:10.1126/sciadv.abe1122.

43. Alhuthali, S.; Kotidis, P.; Kontoravdi, C. Osmolality Effects on CHO Cell Growth, Cell Volume, Antibody Productivity and Glycosylation. *Int. J. Mol. Sci.* **2021**, *22*, 3290, doi:10.3390/ijms22073290.

44. deZengotita, V.M.; Kimura, R.; Miller, W.M. Effects of CO2 and Osmolality on Hybridoma Cells: Growth, Metabolism and Monoclonal Antibody Production. *Cytotechnology* **1998**, *28*, 213–227, doi:10.1023/A:1008010605287.

45. Zhu, M.M.; Goyal, A.; Rank, D.L.; Gupta, S.K.; Vanden Boom, T.; Lee, S.S. Effects of Elevated PCO2 and Osmolality on Growth of CHO Cells and Production of Antibody-Fusion Protein B1: A Case Study. *Biotechnol. Prog.* **2005**, *21*, 70–77, doi:10.1021/bp049815s.

46. Xing, Z.; Li, Z.; Chow, V.; Lee, S.S. Identifying Inhibitory Threshold Values of Repressing Metabolites in CHO Cell Culture Using Multivariate Analysis Methods. *Biotechnol. Prog.* **2008**, *24*, 675–683, doi:10.1021/bp070466m.

47. Xing, Z.; Lewis, A.M.; Borys, M.C.; Li, Z.J. A Carbon Dioxide Stripping Model for Mammalian Cell Culture in Manufacturing Scale Bioreactors. *Biotechnol. Bioeng.* **2017**, *114*, 1184–1194, doi:10.1002/bit.26232.

48. Rodgers, T.L.; Gangolf, L.; Vannier, C.; Parriaud, M.; Cooke, M. Mixing Times for Process Vessels with Aspect Ratios Greater than One. *Chem. Eng. Sci.* **2011**, *66*, 2935–2944, doi:10.1016/j.ces.2011.03.036.

49. Mollet, M.; Godoy-Silva, R.; Berdugo, C.; Chalmers, J.J. Acute Hydrodynamic Forces and Apoptosis: A Complex Question. *Biotechnol. Bioeng.* **2007**, *98*, 772–788, doi:10.1002/bit.21476.

50. Hu, W.; Berdugo, C.; Chalmers, J.J. The Potential of Hydrodynamic Damage to Animal Cells of Industrial Relevance: Current Understanding. *Cytotechnology* **2011**, *63*, 445–460, doi:10.1007/s10616-011-9368-3.

51. Godoy-Silva, R.; Chalmers, J.J.; Casnocha, S.A.; Bass, L.A.; Ma, N. Physiological Responses of CHO Cells to Repetitive Hydrodynamic Stress. *Biotechnol. Bioeng.* **2009**, *103*, 1103–1117, doi:10.1002/bit.22339.

52. Walls, P.L.L.; McRae, O.; Natarajan, V.; Johnson, C.; Antoniou, C.; Bird, J.C. Quantifying the Potential for Bursting Bubbles to Damage Suspended Cells. *Sci. Rep.* **2017**, *7*, 1–9, doi:10.1038/s41598-017-14531-5.

53. Aglialoro, F.; Abay, A.; Yagci, N.; Rab, M.A.E.; Kaestner, L.; van Wijk, R.; von Lindern, M.; van den Akker, E. Mechanical Stress Induces Ca2+-Dependent Signal Transduction in Erythroblasts and Modulates Erythropoiesis. *Int. J. Mol. Sci.* **2021**, *22*, doi:10.3390/ijms22020955.

54. Haringa, C.; Tang, W.; Deshmukh, A.T.; Xia, J.; Reuss, M.; Heijnen, J.J.; Mudde, R.F.; Noorman, H.J. Euler-Lagrange Computational Fluid Dynamics for (Bio)Reactor Scale down: An Analysis of Organism Lifelines. *Eng. Life Sci.* **2016**, *16*, 652–663, doi:10.1002/elsc.201600061.

55. Zhang, Y.; Stobbe, P.; Silvander, C.O.; Chotteau, V. Very High Cell Density Perfusion of CHO Cells Anchored in a Non-Woven Matrix-Based Bioreactor. *J. Biotechnol.* **2015**, *213*, 28–41, doi:10.1016/j.jbiotec.2015.07.006.

56. Bielser, J.-M.; Wolf, M.; Souquet, J.; Broly, H.; Morbidelli, M. Perfusion Mammalian Cell Culture for Recombinant Protein Manufacturing – A Critical Review. *Biotechnol. Adv.* **2018**, *36*, 1328–1340, doi:10.1016/j.biotechadv.2018.04.011.

57. Kropp, C.; Kempf, H.; Halloin, C.; Robles-Diaz, D.; Franke, A.; Scheper, T.; Kinast, K.; Knorpp, T.; Joos, T.O.; Haverich, A.; et al. Impact of Feeding Strategies on the Scalable Expansion of Human Pluripotent Stem Cells in Single-Use Stirred Tank Bioreactors. *Stem Cells Transl. Med.* **2016**, *5*, 1289–1301, doi:10.5966/sctm.2015-0253.

58. Ozturk, S.S.; Thrift, J.C.; Blackie, J.D.; Naveh, D. Real-Time Monitoring and Control of Glucose and Lactate Concentrations in a Mammalian Cell Perfusion Reactor. *Biotechnol. Bioeng.* **1997**, *53*, 372–378, doi:10.1002/(SICI)1097-0290(19970220)53:4<372::AID-BIT3>3.0.CO;2-K.

59. Zamani, L.; Lundqvist, M.; Zhang, Y.; Aberg, M.; Edfors, F.; Bidkhori, G.; Lindahl, A.; Mie, A.; Mardinoglu, A.; Field, R.; et al. High Cell Density Perfusion Culture Has a Maintained Exoproteome and Metabolome. *Biotechnol. J.* **2018**, doi:10.1002/biot.201800036.

60. Gorenflo, V.M.; Smith, L.; Dedinsky, B.; Persson, B.; Piret, J.M. Scale-up and Optimization of an Acoustic Filter for 200 L/Day Perfusion of a CHO Cell Culture. *Biotechnol. Bioeng.* **2002**, *80*, 438–444, doi:10.1002/bit.10386.

61. Drouin, H.; Ritter, J.B.; Gorenflo, V.M.; Bowen, B.D.; Piret, J.M. Cell Separator Operation within Temperature Ranges to Minimize Effects on Chinese Hamster Ovary Cell Perfusion Culture. *Biotechnol. Prog.* **2007**, *23*, 1473–1484, doi:10.1021/bp070276b.

62. Clincke, M.-F.; Mölleryd, C.; Zhang, Y.; Lindskog, E.; Walsh, K.; Chotteau, V. Very High Density of CHO Cells in Perfusion by ATF or TFF in WAVE Bioreactor™. Part I. Effect of the Cell Density on the Process. *Biotechnol. Prog.* **2013**, *29*, 754–767, doi:10.1002/btpr.1704.

63. Aljundi, I.H.; Belovich, J.M.; Talu, O. Adsorption of Lactic Acid from Fermentation Broth and Aqueous Solutions on Zeolite Molecular Sieves. *Chem. Eng. Sci.* **2005**, *60*, 5004–5009, doi:10.1016/j.ces.2005.04.034.

64. Jorgensen, T.C.; Weatherley, L.R. Ammonia Removal from Wastewater by Ion Exchange in the Presence of Organic Contaminants. *Water Res.* **2003**, *37*, 1723–1728, doi:10.1016/S0043-1354(02)00571-7.

65. Kim, K.; Guck, J. The Relative Densities of Cytoplasm and Nuclear Compartments Are Robust against Strong Perturbation. *Biophys. J.* **2020**, *119*, 1946–1957, doi:10.1016/j.bpj.2020.08.044.

66. Gautier, E.-F.; Ducamp, S.; Leduc, M.; Salnot, V.; Guillonneau, F.; Dussiot, M.; Hale, J.; Giarratana, M.-C.; Raimbault, A.; Douay, L.; et al. Comprehensive Proteomic Analysis of Human Erythropoiesis. *Cell Rep.* **2016**, *16*, 1470–1484, doi:10.1016/j.celrep.2016.06.085.

67. Zeming, K.K.; Sato, Y.; Yin, L.; Huang, N.-J.; Wong, L.H.; Loo, H.L.; Lim, Y.B.; Lim, C.T.; Chen, J.; Preiser, P.R.; et al. Microfluidic Label-Free Bioprocessing of Human Reticulocytes from Erythroid Culture. *Lab. Chip* **2020**, *20*, 3445–3460, doi:10.1039/C9LC01128E.

68. Miller, B.; Jimenez, M.; Bridle, H. Cascading and Parallelising Curvilinear Inertial Focusing Systems for High Volume, Wide Size Distribution, Separation and Concentration of Particles. *Sci. Rep.* **2016**, *6*, 36386, doi:10.1038/srep36386.

69. Leung, H.W.; Chen, A.; Choo, A.B.H.; Reuveny, S.; Oh, S.K.W. Agitation Can Induce Differentiation of Human Pluripotent Stem Cells in Microcarrier Cultures. *Tissue Eng. Part C Methods* **2011**, *17*, 165–172, doi:10.1089/ten.TEC.2010.0320.

70. Lim, Z.R.; Vassilev, S.; Leong, Y.W.; Hang, J.W.; Rénia, L.; Malleret, B.; Oh, S.K.-W. Industrially Compatible Transfusable IPSC-Derived RBCs: Progress, Challenges and Prospective Solutions. *Int. J. Mol. Sci.* **2021**, *22*, 9808, doi:10.3390/ijms22189808.

71. Borys, B.S.; Dang, T.; So, T.; Rohani, L.; Revay, T.; Walsh, T.; Thompson, M.; Argiropoulos, B.; Rancourt, D.E.; Jung, S.; et al. Overcoming Bioprocess Bottlenecks in the Large-Scale Expansion of High-Quality HiPSC Aggregates in Vertical-Wheel Stirred Suspension Bioreactors. *Stem Cell Res. Ther.* **2021**, *12*, 55, doi:10.1186/s13287-020-02109-4.

72. Odeleye, A.O.O.; Baudequin, T.; Chui, C.-Y.; Cui, Z.; Ye, H. An Additive Manufacturing Approach to Bioreactor Design for Mesenchymal Stem Cell Culture. *Biochem. Eng. J.* **2020**, *156*, 107515, doi:10.1016/j.bej.2020.107515.

Acknowledgements

One of the big advantages of working in a multidisciplinary project such as this one is that you end up meeting a lot of people that contribute, in one way or another, to its success. Of course, the disadvantage is that, if you lack the skill of compact writing (as in my case, as clearly seen in this thesis), you end up writing a research-article-length text trying to thank everyone for their help and support. So, buckle up, grab a cup of lapsang souchong[1], and enjoy the read.

First and foremost, I would like to thank my supervisors for all their support during this project. **Marieke**, I could not have finished this project without all your guidance and understanding. Your motivation and scientific curiosity were always an example for me, especially when I felt that results were not looking good or that progress was slow. Thank you not only for the supervision during the project, but also for your help in the lab handling of >500 culture dishes (estimate) and for the cross-country door-to-door delivery of cells. Thank you also for our weekend writing sessions and Leiden and Krimpen in the last year, which helped me a lot to not lose the momentum to finish the thesis.

Aljoscha, thank you for all the discussions and advice during the project. You always helped me to realize the scientific value of my results, especially for the parts of the project where building the storyline was challenging. Thank you also for all the help supervising the students I had during my project. I learned a lot from your approach to lead students and let them thrive.

To **Luuk**, thank you for all your contributions to the project. You always brought critical and relevant questions to the table, which made the thesis much sharper than what it would have been without your feedback. Thanks also for your pragmatic mindset that definitively helped this book to transition from the world of ideas to the physical world.

Emile, thanks for all your feedback and supervision during the project, your critical questions during the HEP weekly meetings, and for the motivation you brought to try new things in the bioreactors. Thank you also for the endless patience when teaching me how to do flow cytometry, although I never managed to be as fast as you.

I also want to thank **Maria**, for trusting me with this project and for supervising me in the first 9 months. From the first weeks you helped me to find a balance between Sanquin and TU Delft in this complex multi-disciplinary and multi-location project.

[1] Favourite tea of the author.

I learned from you that a "cowboy" approach to research and not being afraid of testing the limits are very often needed to put the wheels in motion.

Nurcan, I think I owe you around half of my thesis. Thanks for all the help in the lab, from the planning of the experiments to performing them while I was running bioreactors at Delft. Thanks also for bearing with my crazy experiment ideas. I always felt supported by you, not only for the completion of the project, but also for reminding me that taking care of myself is more important than any lab result.

Song, thank you for teaching me so much in the lab and for all your support in my experiments at Delft. When I started this PhD project, I had zero experience with bioreactors, and it was thanks to you that I could learn how to work with them. Thanks for all the troubleshooting sessions of my set-ups, finding solutions to the crazy problems that I had, and your "it will be fine" words that always gave me confidence in the lab. I also enjoyed a lot working with you during the practical courses with the bachelor students. I am sure we will have more hotpot and dim sum sessions together.

I owe another big part of this thesis to the invaluable contributions of the students I had the opportunity to work with. **Ainhoa** and **Queralt**, you can proudly say that you run the first bioreactor experiments of this thesis, both at Sanquin and Delft, respectively. **Judith** and **Victor**, I ended up learning a lot about fluid dynamics from all your work with the CFD simulations of the reactors. **Eduardo** and **Adrián**, your wet lab work was essential for many of the results with the transferrin and deferiprone experiments. **Ingeborg**, thanks to your methodic way of working we could combine a lot of experimental data to understand better the limitations of our cultures. I am very grateful for everything that I learned from all of you, and I know that you will see your contributions, in one way or another, in this book.

I would also like to express my gratitude to all the other contributors to the chapters of this thesis. **Cristian**, I appreciated a lot talking with you about how to use mathematical models during the project, and I am grateful for all the support I received from you during some of the Master end projects. I would be extremely happy to reach even 1% of your expertise on numerical modelling. **Cees**, although I had to leave our results from the CFD simulations out of this book, I enjoyed and learned a lot during the time we worked together in the last months of my PhD. **Victoria** and **Jurgen**, thank you for all the work during our collaboration, putting a bit of systems biology on erythropoiesis.

To all the support that I received in the lab: **Dirk** and **Rob**, thanks for helping me so much in the CSE labs. Your hacking skills with bioreactors always left me in awe. **Stef**, **Max** and **Christiaan**, thanks for your help in the BPE labs. **Marcel L.**, thank you for your help and patience with the custom pieces that you made for my bioreactor set-ups. I knew that if I had an extravagant idea, you would make it real for me to test in the lab. **Patricia** and **Cor**, thank you for all the help with my samples.

Apilena, **Astrid** and **Jannie**, without your organization skills and your hard work, no experiment at BT would be possible. To the **Sanquin Central Facility**, thank you for all the help with the flow cytometry. Thanks also to **Tom** and **Cristina** from Applikon for the bioreactor set-ups I used in this thesis, both at Delft and at Sanquin, and for the opportunity to present our results in several international conferences.

To my amazing paranymphs, **Mariana** and **Oriol**. **Mariana**, queen of BPE, to say that I admire you is quite an understatement. Your pragmatism, get-things-done mentality, efficacy, and assertiveness motivated me immensely during my project, especially in this last year. I loved our gossip sessions, either during coffee breaks or at your place, that helped me feel connected even after weeks of absence due to experiments at Amsterdam. I always think that having a friend that is so fan of things is amazing, because then I don't have to hide how I am (also a great fan of things).

Oriol, estaré siempre muy agradecido de poder llamarte amigo. Aprecio mucho todas las veces que compartiste conmigo las cosas que te apasionan. Aunque a veces no coincidíamos (yo paso un paco de Brandon Sanderson, y tú pasas de Cecilia Giménez), cada vez que hablo contigo siento la pasión genuina y contagiosa que tienes por lo que te gusta hacer. Admiro tu fortaleza estos últimos años, y agradezco tu interés constante en escuchar, apoyar y ayudar a los que te rodean y te quieren. No puedo esperar para que nuestra banda se deje de llamar Los Nuncatocanjuntos.

Marina, we learned together, we struggled together, we laughed together. I admire a lot your resilience, and your passion for doing innovative science. Thank you for putting up with me, for the brainstorming sessions, and for the emotional support in these years. I am sure that, in the future, we can win a second round of the plantain plant caring competition.

Tiago and **Marijn**, my favourite metalheads: thank you for all the fun you brought to my life in the last years. **Tiago**, me encantó conocerte y charlar con alguien que fuera tan crítico de nuestro sistema económico actual. Espero que no me guardes rencor por haber sido un poco Voldemort en las clases de NMMST. Pero bueno, mejor ser Voldemort que Bezos, ¿no? El amor que tú y **Raquel** tienen por tus mascotas me inspira a poder ser así cuando tenga las mías (ojalá pronto). **Marijn**, thank you for your unselfish friendship and your big heart. I always felt your genuine care for me and everyone at BPE. I am very happy that you also are taking time to take care of yourself.

I am very grateful to my office partners, **Rita**, **Lars** and **Clara**. You made my day-to-day work much better. Thank you for the support during our time together in C0.240. To the "old" BPE generation, **Mónica**, **Chema**, **Debbie**, **Silvia**, **Joana**, **Bianca**, and **Marcelo**, thanks for being so welcoming when I arrived, and your experienced comments when I was setting up my project. **Daphne**, **Roxana**, **Tim**, **Marteen**, and **Zulhaj**, thank you for the energy you brought to BPE, I admire the tenacity and dedication that you have.

Héctor, **Ramón**, and **Brenda**, I am sure you will do great research and have fun in your projects. I also want to thank **Marcel**, **Adrie**, **Ludo** and **Marieke** for your constructive feedback during our BPE meetings. And **Kawieta**, your dedication and hard work is invaluable to BPE.

Apart from the BPE group, I also want to thank people in other groups at the Biotechnology department with whom I could work and chill during the last years. **Walter, Martin**, **Flo**, **Yaya**, **Mariana**, **Koen**, **Carla**, **Maxime**, and **Hugo**, I enjoyed a lot our time working together in CSE. **Sergio**, let's keep being fans of Eurovision. **David**, thank you for your incredible hospitality, your amazing cooking skills, and all the laughs.

I also had the luck to work with a lot of amazing people at Sanquin. **Francesca**, you guided me through the Ery group when I started my PhD, and you gave me a great advice that I tried to take with me during my project: collaboration makes a PhD much better and easier to finish. I will always be grateful for that. **Asena**, your motivation and hard work inspires me a lot. It was great to have our engineering conversations at Sanquin, and to collaborate in the shear experiments.

Marea, **Steven**, and **Esther**, thank you for adopting me at U2. Although in the first years of my project I was most of the time at Delft, every time I went to Sanquin I had good times with you all. **Roos** and **Marie-José**, your incredible resilience and hard-work with cultures and flow cytometry were always an example to me. **Giulia,** I enjoyed a lot working with you in our bioreactor collaboration. I hope you have a lot of fun in your project too. **Huan**, we only met in the last years of my PhD, but I know that you will do (and are doing) great work. Big thanks to **Eszter**, **Marten**, **Greta**, **Han**, **Eelke**, **Kerly**, **Max**, **Arthur**, and **Zoltan** too.

I am very grateful to **Derk**, **Micha**, **Robin**, **Ellen**, **Gestur**, **Carlijn**, and **Monika** for their challenging but always constructive questions. Although in the first months of my project I was scared of the "big" IHEP Friday presentations at Sanquin's auditorium, I ended up enjoying them a lot because of your feedback and not-engineering perspective about the project. **Arjan** and **John**, thanks for helping me to make sense of the humongous metabolomics dataset that we generated. I learned a lot from the bioinformatic sessions you organized. **Erica** and **Marijke**, thank you for your patience when taking me along in the first weeks of my project to teach me how you did things at the LCT.

Every day after finishing work I knew that I would arrive home, I could stop thinking about experiments, and just enjoy time with my RolaHola people. *Ayaya*, **Fred**: thanks for supporting me pretty much during my whole PhD. Thanks for sharing with me your seasonal obsessions (some of them even turned into my own obsessions!), your hypercriticisms about everything, and for always listening when I just had to vent out after a long day of work. **Klest**, your great sense of humour always made me laugh.

Thank you for your great PPP (pasta pesto pomodori) recipe. I am excited to celebrate the end of your PhD project in the near future. **Elisabeth**, RolaHola sadly lost its ladybugs after you left. I enjoyed a lot our time together during Covid madness. I wish that you could see all the skills and abilities that you have. **Fede Ra**, I saw you "grow" from Master to now PhD candidate, and I can only think that with your hard work you will succeed in anything you want to do. Thanks for your generosity and for sharing your beautiful heart with me. **Ioanna**, *la pana*, thanks for sharing your stories, dreams, cultural discoveries and adventures with me. Every time I see you smile (many times per day), I smile too. And **Fede Ru**, an honorary member, thank you for bringing more Colombia, more *catolicismo*, and Quincitosan to this house.

A mi comadre **Ena**, creo que compartimos cierto nivel de desvarío, porque ¿cómo se puede explicar que nos hayamos metido casi al mismo tiempo en esta vaca loca del doctorado, y más en este continente olvidado por Dios, de inviernos fríos, lejos de nuestro trópico guamuno? Pero bueno, hemos sobrevivido. Muchas gracias por las invitaciones a la Suiza, que siempre fue un oasis de tranquilidad cuando necesitaba dejar de pensar en el trabajo, o cuando necesitaba descansar de la planitud tierrabajuna.

A mi familia de sangre, gracias por todo el apoyo estos 9 años que llevo lejos de casa. A mi mamá **Elizabeth** y a mi papá **Ramiro**, muchas gracias por todo el sacrificio que hicieron para que yo llegara a este momento. Gracias por enseñarme que la generosidad, la honestidad y la disciplina son lo que hacen que al final del día uno pueda estar plenamente satisfecho con lo que uno hace, independientemente de lo que uno tenga o le haga falta. A mis hermanos **Fabián**, **Paula** y **Esteban**, gracias por escucharme, por seguirme la corriente, y por aguantar mis desapariciones por meses. Y a mi abuela, **Maria Elvia**, gracias por siempre darme voces de aliento y de motivación.

Cuando pienso en la palabra "casa", una imagen en la que se superponen todos los lugares en los que he vivido viene a mi mente, como un pastiche de muros, cuartos y puertas. Pero sobre esa imagen borrosa que ya casi que no responde a un lugar existente, una imagen mucho más fuerte y vívida viene, y es la de **Daniela**. Ajita, eres un lugar, y ese lugar es casa. Y como en casa, me sentí abrazado, protegido y seguro contigo durante todo este PhD, y lo sigo sintiendo más y más. Tus palabras han sido como bálsamo para mi corazón, siempre dándome ánimo para seguir adelante y terminar este PhD, especialmente en esos días en los que quería dejar todo botado. Gracias por la paciencia para este amor transatlántico que tantas toneladas de CO_2 ha generado. Y gracias también por ser la jefe editorial de este proyecto, y por convertir este libro en algo de lo que me siento feliz de imprimir. Además de lugar, eres ilusión: la ilusión de que seguiremos creciendo juntos, ojalá con una montaña a nuestro lado, compartiendo nuestras felicidades, y dividiendo nuestras penas. Amén.

ACK

Curriculum vitæ

Joan Sebastián Gallego Murillo was born in Bogotá, Colombia, on 21 September 1992. He grew up in the *Magdalena* River Valley and in the *Altiplano Cundiboyacense*, always surrounded by the Andes mountains.

Although initially interested on studying Petroleum engineering, he discovered his passion for biology in the last year of high school. Thus, after receiving the *Quiero estudiar* scholarship from Universidad de los Andes (Bogotá, Colombia) in 2008, he decided to follow an undergraduate program in Environmental engineering. As part of his studies, he worked with prof. Juan Manuel Cordovez Álvarez on the mathematical modelling of the sylvatic cycle of *Trypanosoma cruzi*, the parasite that causes Chagas disease, a neglected tropical disease endemic in most countries in the Americas. In parallel, Joan also followed the Chemical engineering program, which he started in 2009. During his Chemical engineering studies, he discovered the world of biochemical engineering and environmental biotechnology. Joan worked under the supervision of prof. Johanna Husserl Orjuela and prof. Andrés Fernando González Barrios on the bioprospecting potential of High Andean Forest soil metagenomes for remediation purposes.

CV

Between January and June 2012, Joan joined the Civil and Environmental Engineering department at Carnegie Mellon University (Pittsburgh, USA) as visiting scholar. There, he worked with prof. Kelvin Gregory on the environmental effect of nanotechnology, focusing on the interactions between nanoparticles and organic matter. After going to back to Colombia, Joan finished his studies in Chemical engineering, and graduated in 2013. Then, he worked as Graduate Research Assistant at the Environmental and Civil Engineering Department of Universidad de Los Andes with prof. Sergio Fernando Barrera Tapias on the analysis of atmospheric data.

After deciding to focus on biotechnology, Joan moved to the Netherlands to pursue a MSc. in Life Sciences and Technology at Delft University of Technology. During his master thesis, he worked on the characterization of sugar transporters in *Saccharomyces*

yeasts under the supervision of prof. Jean-Marc Daran. This was the first time he had hands-on experience with molecular biology techniques. As part of his master studies, Joan also did an internship at BioscienZ (Breda, the Netherlands), where he did his first bioreactor experiments. He completed his Master's degree in 2017.

Wanting to focus on upstream bioprocess development, Joan started a PhD project on the scaling up of the production of cultured red blood cells for transfusion purposes. This project was a collaboration between the Bioprocess Engineering group at Delft University of Technology, and the Department of Hematopoiesis at Sanquin Research (Amsterdam, the Netherlands). Under the supervision of Dr. Marieke von Lindern, Prof. Sebastian Aljoscha Wahl, Dr. Emile van den Akker, and Prof. Luuk A.M. van der Wielen, Joan focused his work on combining experimental and modelling approaches to address the challenges in the scaling of cultured red blood cell manufacturing. Most of the results of his research are presented in this thesis.

Since 2022, Joan is working as a Bioprocess Scientist at Meatable (Leiden, the Netherlands), a startup in the cultivated meat field. He continues to be driven by the idea of building bridges connecting lab work to modeling and simulations, cell biology knowledge to biochemical engineering, and fundamental research to process optimization.

List of publications

Journal articles

- **Gallego-Murillo, J.S.**; Yağcı, N.; Pinho, E.M.; Wahl, S.A.; van den Akker, E.; von Lindern, M. Iron-Loaded Deferiprone Can Support Full Hemoglobinization of Cultured Red Blood Cells. *Scientific Reports* **2023**, 13, 6960, doi:10.1038/s41598-023-32706-1.
- **Gallego-Murillo, J.S.**; Iacono, G.; van der Wielen, L.A.M.; van den Akker, E.; von Lindern, M.; Wahl, S.A. Expansion and Differentiation of Ex Vivo Cultured Erythroblasts in Scalable Stirred Bioreactors. *Biotechnolgy and Bioengineering* **2022**, 119, 3096–3116, doi:10.1002/bit.28193.
- Simionato, G.; Rabe, A.; **Gallego-Murillo, J.S.**; van der Zwaan, C.; Hoogendijk, A.J.; van den Biggelaar, M.; Minetti, G.; Bogdanova, A.; Mairbäurl, H.; Wagner, C.; et al. In Vitro Erythropoiesis at Different pO_2 Induces Adaptations That Are Independent of Prior Systemic Exposure to Hypoxia. *Cells* **2022**, 11, 1082, doi:10.3390/cells11071082.

Conference contributions

Presenting author is indicated underlined.

- Gallego-Murillo, J.S.; van Valderen, R.D.; Cohen, J.; Bernal-Martínez, C.; van Arragon, T.; von Lindern, M.; Picioreanu, C.; Wahl, S.A. To mix effectively and not to kill: fluid dynamics and energy dissipation rate distribution in single-use stirred tank bioreactors. **14th European Congress of Chemical Engineering and 7th European Congress of Applied Biotechnology**. Berlin, Germany (September 2023). Oral presentation.
- Gallego-Murillo, J.S.; Bernal-Martínez, C.; van Arragon, T.; van der Wielen, L.A.M.; van den Akker, E.; von Lindern, M.; Wahl, S.A. Raining fresh red blood cells: scale-up of *ex vivo* erythroblast expansion for transfusion purposes. **14th European Congress of Chemical Engineering and 7th European Congress of Applied Biotechnology**. Berlin, Germany (September 2023). Oral presentation.
- Gallego-Murillo, J.S.; Bernal-Martínez, C.; van Arragon, T.; van der Wielen, L.A.M.; van den Akker, E.; von Lindern, M.; Wahl, S.A. *Ex vivo* expansion and differentiation of erythroblasts: from culture dishes to stirred bioreactors for the production of red blood cells. **Cell Culture Engineering XVIII Conference**. Cancun, Mexico (April 2023). Poster.

LP

- Gallego-Murillo, J.S.; van den Akker, E.; von Lindern, M.; Wahl, S.A. Identification of putative inhibitors during erythroblast cultivation using metabolomics. **Himmelfahrtstagung 2023 - Novel production routes and processes for bio-pharmaceuticals and industrial bioeconomy**. Weimar, Germany (May 2023). Oral presentation.

- Gallego-Murillo, J.S.; Abay, A.; Aglialoro, F.; Claessen, M.J.; Iacono, G.; Yağcı, N.; van der Wielen, L.A.M.; van den Akker, E.; Wahl, S.A.; von Lindern, M. Escalamiento del cultivo de glóbulos rojos para transfusión. **19th Mexican Congress of Biotechnology and Bioengineering**. Virtual (October 2021). Oral presentation.

- Gallego-Murillo, J.S.; Abay, A.; Aglialoro, F.; Claessen, M.J.; Iacono, G.; Yağcı, N.; van der Wielen, L.A.M.; van den Akker, E.; Wahl, S.A.; von Lindern, M. Scale-up of the *ex vivo* production of red blood cells for transfusion purposes. **13th European Congress of Chemical Engineering and 6th European Congress of Applied Biotechnology**. Virtual (September 2021). Oral presentation.

- Gallego-Murillo, J.S.; Yağcı, N.; D'Alessandro, A.; van der Wielen, L.A.M.; van den Akker, E.; von Lindern, M.; Wahl, S.A. Metabolic profiling of cultured erythroblasts for the large scale production of red blood cells. **8th Conference on Metabolic Pathway Analysis**. Virtual (August 2021). Oral presentation.

- Gallego-Murillo, J.S.; Abay, A.; Aglialoro, F.; Claessen, M.J.; Iacono, G.; Yağcı, N.; van der Wielen, L.A.M.; van den Akker, E.; Wahl, S.A.; von Lindern, M. Upscaling of *ex vivo* production of red blood cells for transfusion purposes. **International Society for Stem Cell Resarch (ISSCR) Annual Meeting**. Virtual (June 2021). Poster.

- Gallego-Murillo, J.S.; Yağcı, N.; Burger, P.; D'Alessandro, A.; Wahl, S.A.; van den Akker, E.; von Lindern, M. Metabolomics analysis reveals depletion of key intermediates in oxidative stress-related pathways in high cell density erythroblast cultures. **15th Annual Conference of the Metabolomics Society**. The Hague, the Netherlands (June 2019). Poster.

- Gallego-Murillo, J.S.; Yağcı, N.; Burger, P.; D'Alessandro, A.; Wahl, S.A.; van den Akker, E.; von Lindern, M. Metabolomics analysis reveals depletion of key intermediates in oxidative stress-related pathways in high cell density erythroblast cultures. **Bioinformatics and Systems Biology (BioSB) Conference**. Lunteren, the Netherlands (April 2019). Poster.

- Uribarren, A.; Gallego-Murillo, J.S.; von Lindern, M.; Cuellar, M.C. Predicting the effect of shear stress during cultivation of erythroblasts in suspension bioreactors for scale-up optimization. **Netherlands Biotechnology Congress (NBC-18)**. Ede, the Netherlands (May 2018). Poster.

Invited talks

- Gallego-Murillo, J.S.; Claessen, M.J.; Yağcı, N.; van der Wielen, L.A.M.; van den Akker, E.; Wahl, S.A.; von Lindern, M. *Ex vivo* expansion of erythroblasts: Media and culture condition optimization using untargeted metabolomics. **Advanced Course - Integrated Multi-Omics approaches for Improvement of Industrial Microbes**. Delft, the Netherlands (November 2021).
- Gallego-Murillo, J.S.; van den Akker, E.; Wahl, S.A.; von Lindern, M. From cell biology and modelling technology for high cell densiltivations of erythroblasts. **Applikon Webinar Series**. Virtual (September 2021).

This book was printed in the Netherlands on October 2023,
37 years after the release of the song *Raining Blood* by Slayer.